

UNIVERSITY OF SHEFFIELD

DOCTORAL THESIS

---

# Layout Optimization of Aerospace Components with Minimum Frequency Constraints Suitable for Additive Manufacturing

---

*Author:*

Stephen John SALT

*Supervisor:*

Prof. Matthew GILBERT

*A thesis submitted in fulfilment of the requirements  
for the degree of Doctor of Philosophy*

*in the*

Computational Mechanics and Design Group  
Department of Civil and Structural Engineering

July 2024



University of  
Sheffield

# Declaration of Authorship

I, Stephen John SALT, declare that this thesis titled, ‘Layout Optimization of Aerospace Components with Minimum Frequency Constraints Suitable for Additive Manufacturing’ and the work presented in it are my own. I confirm that:

- This work was done wholly or mainly while in candidature for a research degree at this University.
- Where any part of this thesis has previously been submitted for a degree or any other qualification at this University or any other institution, this has been clearly stated.
- Where I have consulted the published work of others, this is always clearly attributed.
- Where I have quoted from the work of others, the source is always given. With the exception of such quotations, this thesis is entirely my own work.
- I have acknowledged all main sources of help.
- Where the thesis is based on work done by myself jointly with others, I have made clear exactly what was done by others and what I have contributed myself.

Signed:

---

*“I don’t know what I may seem to the world, but as to myself, I seem to have been only like a boy playing on the sea-shore and diverting myself in now and then finding a smoother pebble or a prettier shell than ordinary, whilst the great ocean of truth lay all undiscovered before me.”*

Sir Isaac Newton, 1727

UNIVERSITY OF SHEFFIELD

# *Abstract*

Faculty of Engineering

Department of Civil and Structural Engineering

Doctor of Philosophy

## **Layout Optimization of Aerospace Components with Minimum Frequency Constraints Suitable for Additive Manufacturing**

by Stephen John SALT

The art of aerospace engineering is producing the highest performing component whilst meeting: stringent rules on safety; material strength and temperature capabilities; component and product weight; frequency requirements; and meeting cost targets. Automated optimization techniques are necessary to ensure that the best product can be achieved to meet these criteria. Optimization tools have long been used, these have tended towards size and shape optimization, however the advent of high powered computing and modern manufacturing techniques has allowed generative design methods to come to the fore. Topology optimization is widely employed in the demonstration of optimization for engineering design, though it is not without its detractors. Truss layout optimization, familiar in the field of civil engineering, has been little used in aerospace.

This thesis looks at the optimization methods used in aerospace. A comparison is drawn between topology and truss layout optimization, following the end-to-end design process for each before drawing conclusions that both offer substantial weight savings but truss layout optimization does so in shorter timescales. A new bespoke tool for optimizing components using truss based layout optimization with constraints on natural frequency has been developed and its success is demonstrated via a diverse range of numerical examples. This is then extended to frame structures, which contain rigid joints and more closely represent an additively manufactured component. A second bespoke tool is presented to treat frame structures with frequency constraints and its capability is once again demonstrated via numerical examples.



# *Acknowledgements*

My immense gratitude goes to my supervisor Prof. Matthew Gilbert for his support over the last 8 years, his guidance, patience and depth of knowledge. He has guided me through this journey in all aspects of the research and taught me to write for an academic audience.

A big thank you to Rolls-Royce Plc. for providing the financial support for this work, providing a huge body of knowledge to draw on, and allowing me time away from work to study when needed.

I would also like to thank my work colleague Dr John Marshall for the support given to me over the course of this study and being an invaluable sounding board when I was faced with difficult problems.

I must say thank you to my daughter, Blythe, for being so understanding while Daddy spent a lot of evenings working and writing, when he could have been playing Lego.

Last but by no means least, I want to thank my wife, Ruth, who has supported me through this journey, celebrated the highs with me and been there for me through the lows. I could not have managed this without her by my side.

# Contents

<b>Declaration of Authorship</b>	<b>i</b>
<b>Abstract</b>	<b>iii</b>
<b>Acknowledgements</b>	<b>iv</b>
<b>Contents</b>	<b>v</b>
<b>List of Figures</b>	<b>ix</b>
<b>List of Tables</b>	<b>xi</b>
<b>Abbreviations</b>	<b>xii</b>
<b>Symbols</b>	<b>xiii</b>
<b>1 Introduction</b>	<b>1</b>
1.1 The design process: concept to manufacture . . . . .	3
1.2 Motivation and objectives . . . . .	5
1.3 Structure of the thesis . . . . .	6
<b>2 Literature review and background to study</b>	<b>8</b>
2.1 Design optimization . . . . .	8
2.2 Structural elements . . . . .	10
2.2.1 Trusses . . . . .	10
2.2.2 Beams . . . . .	14
2.2.3 Frames . . . . .	14
2.2.4 Eigenvalue analysis . . . . .	16
2.3 Mathematical optimization . . . . .	18
2.3.1 Convexity and local/global optima . . . . .	18
2.4 Linear programming . . . . .	20
2.4.1 Duality theory . . . . .	21
2.5 Nonlinear programming . . . . .	21
2.5.1 Semidefinite programming . . . . .	23
2.6 Elastic & plastic design . . . . .	25

2.7	Continuum & discrete representations . . . . .	26
2.8	Programming applied to structural optimization . . . . .	27
2.9	Geometry optimization . . . . .	28
2.10	Layout optimization . . . . .	29
2.10.1	Ground-structure method . . . . .	30
2.10.2	Hemp's theory . . . . .	31
2.10.3	Efficiency improvement . . . . .	33
2.10.4	Geometry rationalisation . . . . .	34
2.11	Topology optimization . . . . .	35
2.11.1	Evolutionary structural optimization . . . . .	35
2.11.2	Solid isotropic material with penalisation . . . . .	36
2.11.3	Applications of topology optimization . . . . .	38
2.12	Additive manufacturing . . . . .	39
2.12.1	Additive manufacturing benefits . . . . .	42
2.12.2	Additive manufacturing challenges . . . . .	43
2.13	Aerospace design . . . . .	45
2.13.1	Design for weight and CO <sub>2</sub> reduction . . . . .	47
2.13.2	Frequency analysis for damage prevention . . . . .	48
2.14	Conclusions . . . . .	49
<b>3</b>	<b>A comparison of truss and topology optimization as effective tools for reducing mass and CO<sub>2</sub> emissions of aerospace components for production by AM</b>	<b>51</b>
3.1	Introduction . . . . .	52
3.2	Optimization techniques . . . . .	54
3.2.1	Layout optimization . . . . .	54
3.2.2	Topology optimization . . . . .	57
3.3	Remodelling of optimization results and workflow . . . . .	58
3.3.1	Remodelling truss layout optimization results . . . . .	58
3.3.2	Remodelling topology optimization results . . . . .	59
3.3.3	Workflow comparison . . . . .	60
3.4	Aerospace optimization case studies . . . . .	61
3.4.1	Case Study 1 - Gear Box Bracket . . . . .	63
3.4.1.1	Topology optimization workflow . . . . .	64
3.4.1.2	Truss layout optimization workflow . . . . .	65
3.4.2	Case Study 2 - Inlet Mounting . . . . .	66
3.4.2.1	Topology optimization workflow . . . . .	66
3.4.2.2	Truss layout optimization workflow . . . . .	69
3.5	Comparison of topology optimization and truss layout optimization workflows . . . . .	71
3.5.1	Required engineering time . . . . .	71
3.5.2	Quality of results obtained . . . . .	72
3.5.3	Assessment of optimized load path . . . . .	72
3.6	Impact on CO <sub>2</sub> emissions . . . . .	73
3.7	Conclusions . . . . .	75

<b>4</b>	<b>Layout optimization of pin-jointed truss structures with minimum frequency constraints</b>	<b>77</b>
4.1	Introduction . . . . .	77
4.2	Basic formulations . . . . .	80
4.2.1	Truss layout optimization formulation . . . . .	80
4.2.2	General eigenvalue equation . . . . .	82
4.2.3	Frequency formulation . . . . .	83
4.2.3.1	Determine the reference frequencies . . . . .	83
4.2.3.2	Semidefinite constraint . . . . .	83
4.2.4	Short cantilever example . . . . .	84
4.2.4.1	Two phase optimization approach . . . . .	85
4.2.4.2	Holistic optimization . . . . .	87
4.3	Semidefinite programming formulation with member-adding . . . . .	88
4.3.1	Details of the SDP member-adding algorithm . . . . .	89
4.3.2	Revisiting the short cantilever and half-wheel examples . . . . .	90
4.3.3	Influence of initial member arrangement on computation . . . . .	91
4.4	Numerical examples . . . . .	94
4.4.1	Hemp cantilever example . . . . .	94
4.4.2	MBB beam example . . . . .	95
4.4.3	3D cantilever example . . . . .	97
4.5	Conclusions . . . . .	98
<b>5</b>	<b>Layout optimization of rigid frame structures with semidefinite frequency constraints</b>	<b>101</b>
5.1	Introduction . . . . .	101
5.2	Truss layout optimization . . . . .	104
5.2.1	Minimum volume with stress constraints formulation . . . . .	104
5.2.2	Semidefinite frequency constraint . . . . .	105
5.3	Frame layout optimization . . . . .	106
5.3.1	Stiffness and mass matrices for frames . . . . .	107
5.3.2	Relationship between cross-sectional area & second moment of area	108
5.3.2.1	Solid rectangular cross-section of fixed height . . . . .	109
5.3.2.2	I-section beam with fixed height . . . . .	110
5.3.3	Iterative solution procedure for frame layout optimization with frequency constraints . . . . .	111
5.3.3.1	Overview . . . . .	111
5.3.3.2	Frame layout optimization . . . . .	111
5.3.3.3	Frequency solver . . . . .	114
5.3.3.4	Solution refinement . . . . .	114
5.4	Numerical examples . . . . .	116
5.4.1	Simply-supported cantilever . . . . .	117
5.4.1.1	Optimize frame frequency whilst maintaining section depth	117
5.4.1.2	Refinement by modifying section depth . . . . .	118
5.4.1.3	Increasing nodal density . . . . .	119
5.4.2	L-shaped bracket . . . . .	120
5.5	Discussion . . . . .	122
5.6	Conclusions . . . . .	123

---

<b>6</b>	<b>Discussion and potential applications</b>	<b>126</b>
6.1	Application of generative design in aerospace . . . . .	127
6.1.1	Topology optimization . . . . .	127
6.1.2	Opportunities for layout optimization . . . . .	128
6.2	Methods for geometry rationalisation of truss and frame structures . . . . .	130
6.2.1	Reducing the number of elements . . . . .	131
6.2.2	Collinear and intersecting elements . . . . .	132
6.3	Element transitions for 3D trusses and frames . . . . .	134
6.4	AM build of optimized structures . . . . .	135
6.5	An outline for a frame structure with frequency toolkit . . . . .	137
6.5.1	Further linearisation of $I$ for frame analysis . . . . .	138
6.5.2	SDP frame solver . . . . .	140
<b>7</b>	<b>Conclusions</b>	<b>142</b>
<b>8</b>	<b>Recommended future work</b>	<b>145</b>
<b>A</b>	<b>Second Moment of Area</b>	<b>147</b>
A.1	Second moment of area formulae for various bar forms . . . . .	147
<b>B</b>	<b>Bespoke MATLAB codes</b>	<b>148</b>
B.1	Identify member intersections and add new nodes . . . . .	148
<b>C</b>	<b>Poster presentation of research into frequency constrained truss structures</b>	<b>150</b>
<b>D</b>	<b>Layout optimization of pin-jointed truss structures with minimum frequency constraints</b>	<b>152</b>
	<b>References</b>	<b>172</b>

# List of Figures

1.1	The Pont du Gard in southern France . . . . .	1
1.2	The design spiral . . . . .	3
1.3	Decisions impact on design process progression . . . . .	4
2.1	Definition of robust design . . . . .	9
2.2	Typical truss element and example structure . . . . .	11
2.3	Beam and frame elements . . . . .	15
2.4	Examples of convex and non-convex problems . . . . .	19
2.5	Example graphical approach to solve a linear program . . . . .	21
2.6	6 Bar SDP Numerical Example . . . . .	24
2.7	Stress-strain relationship for elastic vs. plastic analysis . . . . .	25
2.8	Types of optimization with examples . . . . .	28
2.9	Michell cantilever problem definition . . . . .	28
2.10	Layout optimized Michell cantilever . . . . .	30
2.11	Steps in layout optimization . . . . .	31
2.12	BESO optimized Michell cantilever . . . . .	36
2.13	Comparison of density values in BESO and SIMP algorithms . . . . .	37
2.14	SIMP optimized Michell cantilever . . . . .	38
2.15	Additive manufacturing process . . . . .	40
2.16	Example of where AM has been used for advanced cooling holes . . . . .	43
2.17	Example Campbell Diagram . . . . .	49
3.1	Example topology optimized aerospace component . . . . .	52
3.2	The steps in layout optimization and geometry rationalisation . . . . .	56
3.3	A comparison of how BESO and SIMP treat element densities . . . . .	58
3.4	Translation of layout optimization results to NURBS surfaces . . . . .	59
3.5	Examples workflows for truss and topology optimization . . . . .	62
3.6	Gear box bracket case study problem definition . . . . .	64
3.7	Gear box bracket case study results . . . . .	67
3.8	Inlet mounting case study problem definition . . . . .	68
3.9	Inlet mounting case study results . . . . .	70
3.10	Comparison of times taken on study workflow . . . . .	71
3.11	FEA results for case studies . . . . .	73
3.12	Optimized load path assessment . . . . .	74
4.1	The steps in layout optimization . . . . .	82
4.2	Short cantilever example problem definition . . . . .	85
4.3	Results for short cantilever LP and SDP optimization . . . . .	86

4.4	Half wheel example definition and optimal structure . . . . .	87
4.5	Short cantilever example, SDP w. member-adding results . . . . .	91
4.6	Half wheel example SDP w. member-adding results . . . . .	92
4.7	Variations on minimally-connected ground-structures . . . . .	94
4.8	Hemp cantilever frequency optimization results . . . . .	96
4.9	MBB beam frequency optimization results . . . . .	97
4.10	3D cantilever frequency optimization results . . . . .	99
5.1	Steps in truss layout optimization . . . . .	105
5.2	Degrees of freedom in truss, beam and frame elements . . . . .	107
5.3	Plot showing linear relationship between $a$ and $I$ for selection of bar forms . . . . .	110
5.4	Example I-section beam with fixed height . . . . .	111
5.5	10 bar frame example domain and results . . . . .	112
5.6	Frame analysis tool: Layout optimization . . . . .	113
5.7	Frame analysis tool: Frequency solver . . . . .	115
5.8	Frame analysis tool: Solution refinement . . . . .	116
5.9	Simply supported cantilever definition and LP results . . . . .	117
5.10	Simply supported cantilever example SDP results . . . . .	118
5.11	Simply supported cantilever iterative refinement . . . . .	119
5.12	Simply supported cantilever increasing nodal density . . . . .	120
5.13	L-shaped bracket definition, LP and SDP results . . . . .	121
5.14	Representation of manufactured L-shaped bracket . . . . .	122
5.15	Square domain density study structural layouts . . . . .	124
6.1	Opportunities for layout optimization in aerospace . . . . .	129
6.2	Geometry rationalisation for truss and frame structures . . . . .	131
6.3	Layout optimization geometry rationalisation . . . . .	133
6.4	High stresses at element transitions . . . . .	134
6.5	AM build preparation of the aerospace case studies . . . . .	136
6.6	SDP frame solver algorithm proposal . . . . .	137

# List of Tables

2.1	Geometric properties of the example truss structure . . . . .	11
2.2	Results for 6 bar SDP example . . . . .	24
2.3	Computation time for layout optimization w. full ground-structures . . . . .	32
3.1	Material properties applied to each case study . . . . .	63
3.2	Inlet mounting case study: Load cases applied . . . . .	68
3.3	Numerical case study results . . . . .	71
4.1	Short cantilever example LP and SDP results . . . . .	88
4.2	Short cantilever fully-connected ground-structure results . . . . .	90
4.3	Short cantilever SDP w. member-adding results . . . . .	91
4.4	Influence of initial member connectivity on efficiency . . . . .	93
4.5	Hemp cantilever SDP w. member-adding results . . . . .	95
4.6	MBB beam SDP w. member-adding results . . . . .	97
4.7	3D cantilever SDP w. member-adding results . . . . .	98
5.1	Values for second moment of area $I$ for various bar forms . . . . .	109
5.2	Cross-sectional area results for the 10-bar frame example . . . . .	115
5.3	Second moment of area for the 10-bar frame example . . . . .	115
5.4	Square domain density study definition and results . . . . .	123
6.1	AM build preparation of the aerospace case studies . . . . .	136
A.1	Method for calculating second moment of area $I_x$ for various bar forms . . . . .	147



# Abbreviations

<b>ALARP</b>	<b>A</b> s <b>L</b> ow <b>A</b> s <b>R</b> easoably <b>P</b> racticable
<b>ALM</b>	<b>A</b> dditive <b>L</b> ayer <b>M</b> anufacturing
<b>AM</b>	<b>A</b> dditive <b>M</b> anufacturing
<b>BESO</b>	<b>B</b> idirectional <b>E</b> volutionary <b>S</b> tructural <b>O</b> ptimization
<b>CAD</b>	<b>C</b> omputer <b>A</b> ided <b>D</b> esign
<b>CPU</b>	<b>C</b> entral <b>P</b> rocessing <b>U</b> nit
<b>DLD</b>	<b>D</b> irect <b>L</b> aser <b>D</b> eposition
<b>DoF</b>	<b>D</b> egree <b>o</b> f <b>F</b> reedom
<b>EASA</b>	<b>E</b> uropean <b>U</b> nion <b>A</b> viation <b>S</b> afety <b>A</b> gency
<b>EBM</b>	<b>E</b> lectron <b>B</b> eam <b>M</b> elting
<b>EO</b>	<b>E</b> ngine <b>O</b> rders
<b>ESO</b>	<b>E</b> volutionary <b>S</b> tructural <b>O</b> ptimization
<b>FAA</b>	<b>F</b> ederal <b>A</b> viation <b>A</b> uthority
<b>FDM</b>	<b>F</b> used <b>D</b> eposition <b>M</b> odelling
<b>FEA</b>	<b>F</b> inite <b>E</b> lement <b>A</b> nalysis
<b>FOD</b>	<b>F</b> oreign <b>O</b> bject <b>D</b> amage
<b>HCF</b>	<b>H</b> igh <b>C</b> ycle <b>F</b> atigue
<b>IT</b>	<b>I</b> nformation <b>T</b> echnology
<b>LCF</b>	<b>L</b> ow <b>C</b> ycle <b>F</b> atigue
<b>LP</b>	<b>L</b> inear <b>P</b> rogramming
<b>LPBF</b>	<b>L</b> aser <b>P</b> owder <b>B</b> ed <b>F</b> usion
<b>NLP</b>	<b>N</b> on <b>L</b> inear <b>P</b> rogramming
<b>NURBS</b>	<b>N</b> on- <b>U</b> niform <b>R</b> ational <b>B</b> - <b>S</b> pline
<b>OC</b>	<b>O</b> ptimality <b>C</b> riterion
<b>OEM</b>	<b>O</b> riginal <b>E</b> quipment <b>M</b> anufacturer
<b>SDP</b>	<b>S</b> emi <b>D</b> efinite <b>P</b> rogramming
<b>SIMP</b>	<b>S</b> olid <b>I</b> sotropic <b>M</b> aterial with <b>P</b> enalization
<b>SLA</b>	<b>S</b> tereo <b>L</b> ithogr <b>A</b> phy
<b>SLS</b>	<b>S</b> elective <b>L</b> aser <b>S</b> intering
<b>STL</b>	<b>S</b> tandard <b>T</b> riangle <b>L</b> anguage
<b>UTS</b>	<b>U</b> ltimate <b>T</b> ensile <b>S</b> trength

# Symbols

This section lists the symbols used in this thesis. The symbols are divided by alphabet (Latin/Greek); Latin letters are further divided by case, then by style.

## **Latin**, Upper Case, Italic

	Description	Units
$B$	Base width of a beam	$L$
$E$	Young's Modulus	$\text{N m}^{-2}$
$F_T$	Total fuel consumed	kg
$H$	Height of a beam	$L$
$I$	Second moment of area	$L^4$
$L$	Unit of measure	
$P$	Applied point load	N
$V$	Volume	$L^3$
$W$	Virtual work	N

## **Latin**, Upper Case, Bold

	Description	Units
$\mathbf{B}$	Equilibrium matrix	
$\mathbf{K}_i$	Element stiffness matrix in global coordinates	
$\bar{\mathbf{K}}_i$	Element stiffness coefficient matrix in global coordinates	
$\mathbf{M}_i$	Element mass matrix in global coordinates	
$\bar{\mathbf{M}}_i$	Element mass coefficient matrix in global coordinates	
$\mathbf{T}$	Transposition matrix	

## **Latin**, Lower Case, Italic

	Description	Units
$a_E$	Empty area of I-section beam	$L^2$
$a_i$	Area of an individual element	$L^2$
$a_T$	Total area of I-section beam	$L^2$
$b$	Width of I-section beam minus web thickness ( $b = B - t$ )	$L$
$c$	Cosine directional vector	
$f$	Frequency for a given mode	Hz
$f_{min}$	Minimum frequency	Hz
$f_F$	Frequency of a frame structure	Hz
$f_T$	Frequency of a truss structure	Hz

$h$	Height between I-section flanges	$L$
$i$	Identifier for an individual element	
$k$	Ratio between occupied and empty space in an Isection beam	
$l_i$	Length of an individual element	$L$
$m$	Number of elements within a design domain	
$n$	Number of nodes within a design domain	
$q_i$	Force within an individual element	N
$s$	Sine directional vector	
$t$	Thickness of I-section beam web	$L$
$u$	Element force in axial direction	N
$v$	Element force perpendicular to its axis	N

**Latin, Lower Case, Bold**

	Description	Units
<b>a</b>	Vector of element areas	$L^2$
<b>d</b>	Vector of element displacements	$L$
<b>k<sub>i</sub></b>	Element stiffness matrix in local coordinates	
<b>l</b>	Vector of element lengths	$L$
<b>m<sub>i</sub></b>	Element mass matrix in local coordinates	
<b>p</b>	Vector of applied forces	N
<b>q</b>	Vector of element forces	N

**Greek**

	Description	Units
$\beta$	Coefficient for fuel consumption vs CO <sub>2</sub> emissions	
$\delta$	Delta of two scalars	
$\epsilon$	Virtual strain	
$\theta$	Angle of elements from major axis	°
$\lambda$	Frequency	Hz
$\nu$	Poisson's ratio	
$\rho$	Density	kg m <sup>-2</sup>
$\sigma$	Stress	MPa
$\Phi$	Mode of vibration	
$\phi$	Moment rotation	N m
$\omega$	Angular frequency	rad s <sup>-1</sup>

*Dedicated to my wife and daughter, without their support and encouragement I would not have made so many wonderful discoveries.*

# Chapter 1

## Introduction

There is a spark of creativity & ingenuity of design evident even in the earliest human activity and oldest remaining structures. From the first humble shelters to more advanced infrastructure such as roads and bridges, the field of engineering was born, enabling the growth of civilisations & empires. In ancient times there was not the available modern computing power that we as engineers enjoy today; instead the methods of verifying and validating a design were largely to build it and see if it worked. Many did, and there are a number of impressive structures from the ancient world, such as the Pont du Gard, Figure 1.1, still standing today due to the ingenuity and skill in design of those engineers. To support ever-growing & increasingly sophisticated societies, engineering evolved into the highly complex field it is today, as did the rigour required to ensure that the products, objects, and structures performed as designed.



FIGURE 1.1: The Pont du Gard in southern France, completed in 40-60 AD, is 48.8 m tall and carried 200 000 m<sup>3</sup> of water per day over its 275 m length, it is largely built of limestone and is predominantly mortar-less ([Song, 2014](#), Accessed June 2016).

Material utilisation costs and the economic climate no longer allow the luxury of a ‘trial and error’ approach, meaning that design and verification activities need to happen

virtually, in a low cost electronic environment. Since the middle of the twentieth century, ongoing developments in the fields of Information Technology (IT) and software have allowed engineers unprecedented access to the power and resources required to repeatedly design and test structures and components before any material needs to be cut. This gives today's engineers access to structural and mechanical optimization tools that enable them to repeatedly analyse a system to yield the desired results (whether it be stress, compliance or response), whilst utilising the minimum amount of material possible, thereby costing the least amount of money.

There are a multitude of different methods for optimizing a structure or a component. Many of these are based on the same basic principle: that the material utilized must be capable of withstanding the applied loading. The approaches that different methods take, however, can vary wildly by application. For example, a tool that is designed to aid an architect to determine the most appropriate positions for load-bearing members in a building may only take this as a frame of reference, and then design the structure around this framework to achieve the customer's visual requirements. Conversely, a mechanical engineer may use a more visual Computer Aided Design (CAD) geometry to fully conceptualize the optimum component and the stresses within the part down to a resolution of only a few microns to verify the part meets its capability criterion. Both will give an optimized solution based upon the customer's requirements, but because there may be aesthetic considerations or manufacturing constraints to be applied, it may be the case that the true optimum cannot be achieved in the real world.

It is important to ensure that though there may be process or aesthetic requirements to consider, it is crucial that the starting point be as optimal as possible before any variation is made. In addition, the resulting design should have sufficient capacity such that variances in the manufacturing process or the applied loading will not lead to failure, this is referred to a 'robust design'. There have been many different tools created to assist in the design and optimization of mechanical components, usually embedded within proprietary software packages. These generally rely on a pre-determined knowledge of the component's form and operate on continuum structures and geometry based optimization tools.

The field of aeronautical engineering, and more specifically, the components of aerospace gas turbines are chosen in this study to demonstrate real-world applications of these new tools and design methods. The environment of a gas turbine is challenging from a design perspective: there is a constant drive to ensure a component's mass is at the minimum to reduce fuel burn; the engine has a wide variation in temperature from  $-65^{\circ}\text{C}$  to  $1800^{\circ}\text{C}$ ; and there are constant sources of vibration to be considered in the design of the part for longevity in service. There is also a need for components installed in a gas turbine engine

to be designed to avoid excitation by ground sources of vibration, i.e. the component itself should not amplify any vibration it experiences. It is therefore necessary to ensure that this factor can be incorporated into a design during optimization with other factors such as component weight and cost.

## 1.1 The design process: concept to manufacture

Most commonly represented as a spiral, Figure 1.2, the design engineering process continually revisits a number of specific areas to develop an idea into a final design. At its outset the idea is in the concept stage where a number of potential designs will be considered and once a viable design has been found, it will be progressed to preliminary design. The concept is now refined, and may be redesigned to solve certain problems, prior to moving forwards to the detailed design stage where all the work to make the part ready for manufacture is completed. A number of iterations may take place in the design process due to the highly complex nature of many mechanical, automotive or aeronautical design requirements. Though computational analysis is fairly common in modern design organisations, it should be noted that in the majority of cases the analysis has no direct effect on the geometry of parts (Keane and Nair, 2005); instead, experienced designers are generally required to interpret the results and adapt the design accordingly.

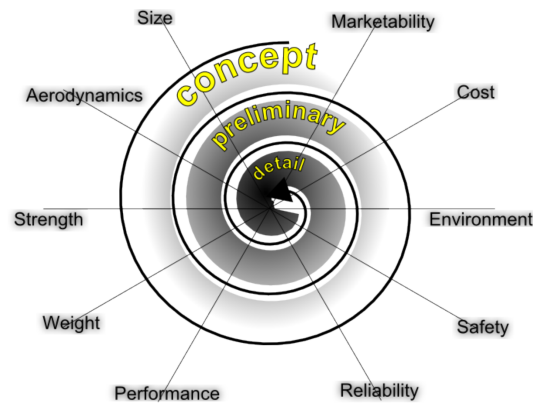


FIGURE 1.2: The design spiral.

The same experienced designers will dominate the decision making process in the early design phase, using their knowledge of previous designs and evidence to indicate success or failure. In the early design stages, few analysis tools will be used; instead previous designs will be assessed and traded on a variety of variables to formulate the requirements for the new product. The most advanced analytical tool that may be employed at this stage is a spreadsheet.

Once the preliminary design phase is reached, the design tasks may be split between different teams. Computational analyses start to be utilized at this point to further develop the concepts, and it is generally here that they will have the biggest impact. Due to the effort required to set-up, run, and interpret the results of the analysis it may be the case that the design gets frozen early in the process. This is to avoid the additional cost and resource that would be consumed through re-analysis, which may outweigh the benefit of the re-design. It is generally considered that the decisions made in this early design phase have a much bigger impact on the overall product than all the decisions that come in later stages, Figure 1.3.

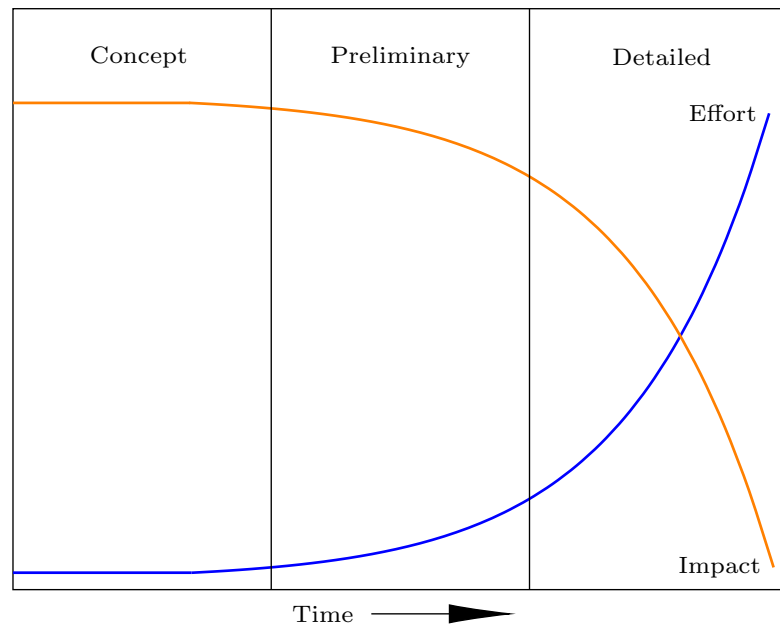


FIGURE 1.3: The impact that decisions have on the product reduces as the design progresses through the spiral.

A number of analysis tools are available for preliminary structural design, the most dominant being Finite Element Analysis (FEA). In preparation for FEA, the structure or component is broken up into many nodes and connecting elements, referred to as a mesh, and has a number of loads and boundary conditions applied. When submitted to the solver, the FEA uses a set of governing equations to determine the displacement of each nodal point in the domain, based on the deformation of each element. FEA can be performed at varying levels of fidelity; simple structures may be represented by 1D elements, such as an aircraft wing represented by a cantilever, or a full discretized 3D model which is assessed for strength, impact resistance, or excitation frequency. The level of fidelity utilized during preliminary design must be selected in order to sufficiently model the situation within an acceptable time frame.

Finally, the detailed design stage is reached. At this stage the design is finalised and prepared for manufacture and entry into service. The component(s) will be fully detailed



in Computer Aided Design (CAD) to ensure that they can be produced and inspected to ensure product compliance. To ensure safety the final design must once again be verified by FEA; however because the CAD models are now more complex there may be some idealisation required to be able to perform the FEA in a reasonable timescale. Iterations arising from the analysis results will usually be small in comparison with those made at earlier design stages, as there can be significant impact on other components within the product if one component's design is significantly altered; this correlates with Figure 1.3, where decisions made in the detailed design stage have lesser impact on the product.

The concept of taking decisive action earlier in the design phase is a major motivation to ensure that any preliminary work done is both efficient and effective at making these major decisions which will influence the success of the product. It is for this reason that it is essential that tools which facilitate multiple, efficient iterations, performed automatically, be investigated and made available to engineers.

## 1.2 Motivation and objectives

This study will determine the suitability of automated optimization techniques to design components which can be both capable of reacting any structural loading placed upon them, and also reside outside of certain frequencies to avoid failures due to excitation. These two criteria must be met by structures which exhibit the least possible component weight in order to reduce fuel burn and resulting CO<sub>2</sub> emissions whilst in service in an aircraft. A comparison will be drawn between the capability of both topology optimization and layout optimization techniques in achieving the preconceived requirements for mass, whilst also proving to be computationally efficient, before moving on to vibration analysis. Up to now there has been no capability for directly optimizing for vibration with truss optimization, and therefore an efficient method to augment layout optimization with frequency constraints is developed in this study to fill this capability gap.

In summary the content of this thesis shall cover:

- a) The determination, through literature review, of the available capabilities of mathematical optimization and its application to automated optimization tools and techniques. These shall be reviewed for their suitability for use in aerospace design. Areas for improvement shall be identified.
- b) A comparison shall be drawn of the effectiveness of both topology optimization and layout optimization in achieving the structural requirements for specific aerospace

case study examples. The focus of these studies shall be on quantifiable achievements made in the reduction of both component mass and CO<sub>2</sub> emissions, additionally the increase in computational efficiency and subsequent reduction of the burden on the analyst shall be discussed.

- c) A method shall be proposed for existing layout optimization tools to be augmented with constraints on natural frequency. This will initially be focused on pin-jointed truss structures ensuring that a defined component is outside of any ranges of vibratory excitation. Any such tool should be computationally efficient enough to run on a standard engineering desktop PC.
- d) Further develop the techniques created for pin-jointed truss structures and apply them to rigid frames with the same loading and vibrational constraints, the results should be representative of a continuum component which may be produced by Additive Manufacturing (AM).

### 1.3 Structure of the thesis

This thesis is structured around three papers which have been produced for publication in appropriate journals. Their content is underpinned by a preceding Literature Review and further developed with relevant critique and potential applications in the final three chapters.

- a) Chapter 1: Introduction chapter.
- b) Chapter 2: Begins with a literature review of structural elements which are explored through the current study. Detailing mathematical optimization techniques, such as truss and topology optimization, how they may be applied to the design processes in the aerospace industry, and what benefit may be obtained through their routine application. Background information is also provided concerning the field of aerospace design and additive manufacture.
- c) Chapter 3: With two major approaches to optimization considered, a comparison is made between topology and truss optimization to judge how efficient each process is in the optimization itself, and subsequent utilisation of the results in preparation for AM. Two case studies are assessed based on aerospace components to determine which optimizer is of the greatest benefit to reduce the weight of the components, reducing fuel burn and emission of CO<sub>2</sub> into the atmosphere, in a computationally efficient manner.

- d) Chapter 4: Defines the problem of component resonance as a result of excitation frequencies, and a novel solution to optimize away from these frequencies is proposed using a member adding algorithm and a semi-definite programming solver adding an additional constraint to the traditional layout optimization problem. The process is outlined and numerical examples provided to show the effectiveness of the optimizer in both 2D and 3D.
- e) Chapter 5: Building on the previous chapter, a proposal is made to further develop the optimization techniques for application to frame structures, which will act in a more similar way to continuum bodies than pin-jointed structures. An algorithm is proposed to perform layout optimization with semidefinite frequency constraints on problems utilising fully-connected ground-structures. The capability of the algorithm is explored to understand convergence characteristics and the size of problem that can be solved. The results of the algorithm are demonstrated via 2D numerical examples.
- f) Chapter 6: Implications of the findings of the previous chapters are discussed and additional information not entirely within the scope of the proposed papers has been included. Points that must be considered in the application of the proposed techniques are also explored. This chapter considers how the suggested methods may be applied to real-world scenarios.
- g) Chapter 7: The achievements, contributions and conclusions of this work are summarised.
- h) Chapter 8: Proposals are made concerning the recommended direction of future work in this field.

## Chapter 2

# Literature review and background to study

This study considers the application of numerical optimization techniques and their applicability to the design of aerospace components, and so needs to begin with an introduction to existing optimization techniques and the complexities of engineering practice in aerospace. This chapter provides such an introduction to design optimization (Section 2.1) in order to provide a framework for the text to follow. Background on the types of structural elements will then be presented (Section 2.2) followed by an overview of the mathematical techniques used in optimization (Sections 2.3 to 2.5). How those techniques are applied in practice (Sections 2.1 and 2.8) are then considered, and an introduction to additive manufacturing is given (Section 2.12). How all this relates to the design process in the aerospace industry (Section 2.13) is then assessed, including the importance of determining a structure’s natural frequencies (Section 2.13.2). Finally, remaining challenges are identified, and proposals made for how these may be addressed.

### 2.1 Design optimization

Dieter (2000) states that *“generally there is more than one solution to a design problem, and the first solution is not necessarily the best”*. This is true of almost every attempt to design any product. Different designers with varying backgrounds will invariably approach a problem from slightly different perspectives, generating multiple design solutions. It may even be true of a single designer who may have many ways of solving a particular problem when faced with a highly variable design space with hundreds, or sometimes thousands, of different solutions. In order to avoid this time consuming and

sometimes misleading process, Dieter argues that *“the need for design optimization is inherent in the design process”*.

It is paramount that the customer be involved in all aspects of the optimization but most critically at the beginning when the focus is on identifying the requirements that will ultimately influence the product’s design. In most cases, a product is optimized to suit the requirements of the customer; however it may not be clear how the design of the product directly affects these without further analysis. The ultimate goal of any optimization attempt is to achieve the correct balance between the requirements given, for example a component will have a healthy balance between weight, durability, cost and producibility; this is known as a ‘robust design’.

Robustness in a component or system design context is defined as the lack of sensitivity to external influences or noises and not, as the word generally implies, a bigger, heavier, or stronger component. A robust design can only be achieved when the designer fully understands all of the potential variations in the design space. At this point there will be a clear line where a design will become infeasible, i.e. it is not suited to the requirements and any design point falling the wrong side of that line may be disregarded. Ideally, the chosen final design would be at the global optimum point of the design space (Section 2.3.1); however this is often close to, or exactly located on the feasible/infeasible line, meaning that there would be some occasions where the component may have variation that takes it outside of the feasible zone. Robust design seeks to ensure that a chosen design point will remain within the feasible region under all sources of variation (Figure 2.1).

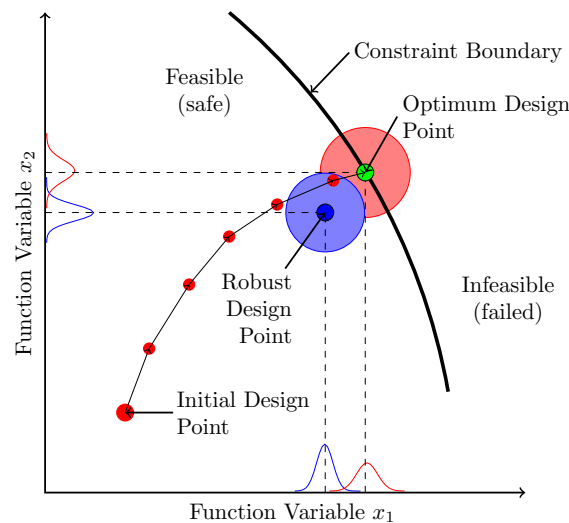


FIGURE 2.1: Concept of robust optimization to ensure that any sources of variation do not take the design beyond the feasible limit.

One of the major obstacles with optimization is that it is often tempting to try to over-optimize; i.e. to have too many goals using too many parameters. This is highly inefficient because the optimum solution cannot be guaranteed because the optimizer may have focused on the wrong target or parameters. In order to remedy this, it is generally necessary to focus the optimization only on certain features of the component. This can be done purely on common sense or experience of the engineer; however it is much more productive to begin as if the component were completely novel and start right from the beginning with a structured approach.

## 2.2 Structural elements

This thesis focuses primarily on the optimization of truss structures, both as simplistic pin-jointed arrangements, and with rigid joints to create frames. Truss structures have been chosen for their elegant efficiency in material utilisation and optimization. It is therefore necessary to introduce these elements to ensure a good understanding of their makeup and how each individual element contributes to a structure as a whole. An individual truss is shown in Figure 2.2(a) with a worked example to demonstrate how it contributes to the overall mass and stiffness matrices required for vibrational analysis later in this chapter. Subsequently, with the addition of a few terms in the matrices, we can adapt these trusses into more rigid frames, suitable for manufacturing via additive methods.

### 2.2.1 Trusses

Trusses are widely used in structural engineering solutions due to their elegant simplicity; a truss structure is comprised of one or more straight bars designed to react an axial force along its length, such that deformation is only observed in the axial direction. Due to this simplistic nature, the actual cross-sectional shape of the truss is of little importance but in general the cross-sectional area will be much smaller than the length. When referring to a system of trusses, each individual truss is referred to as an element. Trusses may be categorised as either planar (2D), where the nodal coordinates are described by  $x$  and  $y$  dimensions only, and space trusses where there is also a  $z$  component, creating a 3D structure. Typically a truss structure will be pin jointed, therefore limiting transmission between elements to forces and not moments.

When applied to layout optimization, the solution is considered optimal when the elements within a truss structure are fully stressed in the reaction of the applied forces. This is known as being in equilibrium. However, for the determination of the structure's

natural frequency of vibration it is necessary to derive the stiffness and mass matrices for the individual elements and the system as a whole. Figure 2.2(a) shows an individual truss of length  $l_i$  with a uniform cross-section  $a$ , and is bounded by two nodes  $j$  and  $k$ ; Figure 2.2(b) shows a simple three element truss structure to illustrate the method for deriving the global mass and stiffness matrices; Table 2.1 gives the length and cross-section for each element as well as directional cosines,  $c, s$ , and mechanical properties for Young's Modulus,  $E$ , and density  $\rho$ . In the interests of brevity this is restricted to a planar truss system; a space truss will have additional degrees of freedom to account for the  $z$  direction.

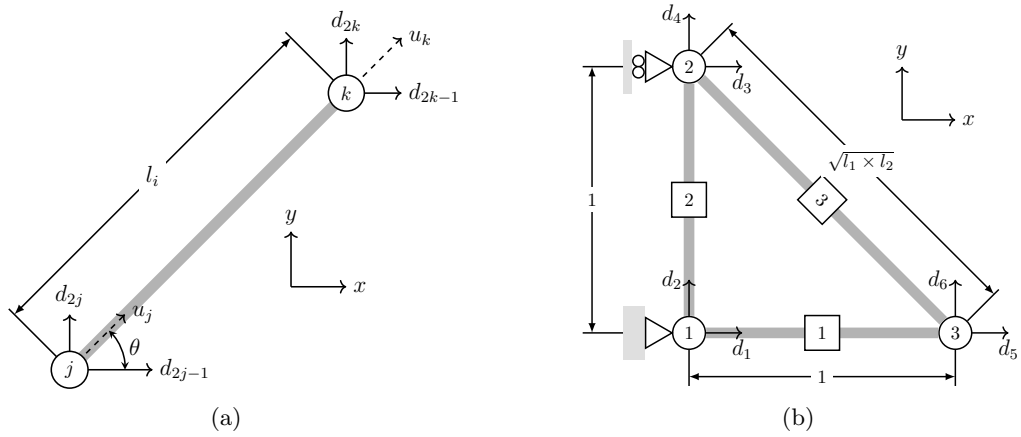


FIGURE 2.2: (a) A typical truss element arrangement with nodes and degrees of freedom, and (b) an example structure used in the assemblage of the global mass and stiffness matrices. Unless otherwise stated all dimensions are in metres.

TABLE 2.1: Geometric properties of the example truss structure defined in Figure 2.2(b).

Element $i$	$l$ (m)	$a$ (m <sup>2</sup> )	$c$	$s$	$E$ (GPa)	$\rho$ kg m <sup>-3</sup>
1	1		1	0		
2	1	0.1	0	1	110	2710
3	$\sqrt{2}$		$-1/\sqrt{2}$	$1/\sqrt{2}$		

When considering the structure shown in Figure 2.2(b) the first operation is to determine the stiffness and mass matrices in local coordinates. This is achieved using Eq. (2.3a) for stiffness ( $\mathbf{k}_i$ ) and Eq. (2.3b) for mass ( $\mathbf{m}_i$ ). To mathematically model the mass and stiffness of the overall structure, these must be transposed into global coordinates using Eq. (2.1) for stiffness and Eq. (2.2) for mass, where  $\mathbf{T}$  is the transposition matrix for a truss Eq. (2.3c);  $c = \cos \theta$ ; and  $s = \sin \theta$ . The resulting mass matrix  $\mathbf{M}_i$  is symmetric positive definite, and the stiffness matrix  $\mathbf{K}_i$  is symmetric and either positive or positive semi-definite.

$$\mathbf{K}_i = \mathbf{T}^T \mathbf{k}_i \mathbf{T} \quad (2.1)$$

$$\mathbf{M}_i = \mathbf{T}^T \mathbf{m}_i \mathbf{T} \quad (2.2)$$

$$\mathbf{k}_i = \frac{a_i E}{l_i} \begin{bmatrix} & u_j & & u_k \\ 1 & & -1 & \\ -1 & & 1 & \end{bmatrix} \begin{matrix} u_j \\ u_k \end{matrix} \quad (2.3a)$$

$$\mathbf{m}_i = \frac{\rho a_i l_i}{6} \begin{bmatrix} & u_j & & u_k \\ 1 & & 0 & \\ 0 & & 1 & \end{bmatrix} \begin{matrix} u_j \\ u_k \end{matrix} \quad (2.3b)$$

$$\mathbf{T} = \begin{bmatrix} c_{jk} & s_{jk} & 0 & 0 \\ 0 & 0 & c_{jk} & s_{jk} \end{bmatrix} \quad (2.3c)$$

For a simple planar truss system, the stiffness and mass matrices may be simplified to single equations (2.4a) and (2.4b) by pre-multiplying the standard form and the transposed form of the matrix  $\mathbf{T}$ . Each entry into both the local and global element matrices represents a single degree of freedom of that element: 2 nodes with 2 degrees of freedom each.

$$\mathbf{K}_i = \mathbf{T}^T \mathbf{k}_i \mathbf{T} = \frac{a_i E}{l_i} \begin{bmatrix} & d_{2j-1} & d_{2j} & d_{2k-1} & d_{2k} \\ c_{jk}^2 & cs_{jk} & -c_{jk}^2 & -cs_{jk} \\ cs_{jk} & s_{jk}^2 & -cs_{jk} & -s_{jk}^2 \\ -c_{jk}^2 & -cs_{jk} & c_{jk}^2 & cs_{jk} \\ -cs_{jk} & -s_{jk}^2 & cs_{jk} & s_{jk}^2 \end{bmatrix} \begin{matrix} d_{2j-1} \\ d_{2j} \\ d_{2k-1} \\ d_{2k} \end{matrix} \quad (2.4a)$$

$$\mathbf{M}_i = \mathbf{T}^T \mathbf{m}_i \mathbf{T} = \frac{\rho a_i l_i}{6} \begin{bmatrix} & d_{2j-1} & d_{2j} & d_{2k-1} & d_{2k} \\ 2c_{jk}^2 & 2cs_{jk} & c_{jk}^2 & cs_{jk} \\ 2cs_{jk} & 2s_{jk}^2 & cs_{jk} & s_{jk}^2 \\ c_{jk}^2 & cs_{jk} & 2c_{jk}^2 & 2cs_{jk} \\ cs_{jk} & s_{jk}^2 & 2cs_{jk} & 2s_{jk}^2 \end{bmatrix} \begin{matrix} d_{2j-1} \\ d_{2j} \\ d_{2k-1} \\ d_{2k} \end{matrix} \quad (2.4b)$$

Once the individual element matrices have been determined in global coordinates, they are assembled into  $2n \times 2n$  matrices, where  $n$  is the total number of nodes in the structure,



for stiffness  $\mathbf{K}$  and mass  $\mathbf{M}$  by populating the appropriate degrees of freedom from the local matrices. To illustrate this process the element stiffness matrices Eqs. (2.5a), (2.5b), and (2.5c) are determined and assembled into the structural stiffness matrix Eq. (2.6) with each contribution highlighted for clarity: red for element [1] Eq. (2.5a), blue for element [2] Eq. (2.5b) and teal for element [3] Eq. (2.5c).

$$\mathbf{K}_1 = \mathbf{T}^T \mathbf{k}_1 \mathbf{T} = \frac{a_i E}{l_i} \begin{bmatrix} d_1 & d_2 & d_5 & d_6 \\ 1 & 0 & -1 & 0 \\ 0 & 0 & 0 & 0 \\ -1 & 0 & 1 & 0 \\ 0 & 0 & 0 & 0 \end{bmatrix} \begin{matrix} d_1 \\ d_2 \\ d_5 \\ d_6 \end{matrix} \quad (2.5a)$$

$$\mathbf{K}_2 = \mathbf{T}^T \mathbf{k}_2 \mathbf{T} = \frac{a_i E}{l_i} \begin{bmatrix} d_1 & d_2 & d_3 & d_4 \\ 0 & 0 & 0 & 0 \\ 0 & 1 & 0 & -1 \\ 0 & 0 & 0 & 0 \\ 0 & -1 & 0 & 1 \end{bmatrix} \begin{matrix} d_1 \\ d_2 \\ d_3 \\ d_4 \end{matrix} \quad (2.5b)$$

$$\mathbf{K}_3 = \mathbf{T}^T \mathbf{k}_3 \mathbf{T} = \frac{a_i E}{l_i} \begin{bmatrix} d_3 & d_4 & d_5 & d_6 \\ 0.5 & -0.5 & -0.5 & 0.5 \\ -0.5 & 0.5 & 0.5 & -0.5 \\ -0.5 & 0.5 & 0.5 & -0.5 \\ 0.5 & -0.5 & -0.5 & 0.5 \end{bmatrix} \begin{matrix} d_3 \\ d_4 \\ d_5 \\ d_6 \end{matrix} \quad (2.5c)$$

$$\mathbf{K} = \sum_{i=1}^m \mathbf{K}_i = \begin{bmatrix} d_1 & d_2 & d_3 & d_4 & d_5 & d_6 \\ \begin{matrix} 11.0 & 0 \\ 0 & 11.0 \end{matrix} & \begin{matrix} 0 & 0 \\ 0 & -11.0 \end{matrix} & \begin{matrix} 0 & 0 \\ 3.89 & -3.89 \end{matrix} & \begin{matrix} -11.0 & 0 \\ 0 & 14.9 \end{matrix} & \begin{matrix} -11.0 & 0 \\ 3.89 & -3.89 \end{matrix} & \begin{matrix} 0 & 0 \\ 3.89 & -3.89 \end{matrix} \\ \begin{matrix} 0 & 0 \\ -11.0 & 0 \end{matrix} & \begin{matrix} 0 & 0 \\ 0 & 0 \end{matrix} & \begin{matrix} 3.89 & -3.89 \\ -3.89 & 3.89 \end{matrix} & \begin{matrix} -3.89 & 3.89 \\ 14.9 & -3.89 \end{matrix} & \begin{matrix} -3.89 & 3.89 \\ 3.89 & -3.89 \end{matrix} & \begin{matrix} 3.89 & -3.89 \\ -3.89 & 3.89 \end{matrix} \\ \begin{matrix} -11.0 & 0 \\ 0 & 0 \end{matrix} & \begin{matrix} 0 & 0 \\ 0 & 0 \end{matrix} & \begin{matrix} -3.89 & 3.89 \\ 3.89 & -3.89 \end{matrix} & \begin{matrix} 14.9 & -3.89 \\ -3.89 & 3.89 \end{matrix} & \begin{matrix} 3.89 & -3.89 \\ -3.89 & 3.89 \end{matrix} & \begin{matrix} -3.89 & 3.89 \\ 3.89 & -3.89 \end{matrix} \end{bmatrix} \begin{matrix} d_1 \\ d_2 \\ d_3 \\ d_4 \\ d_5 \\ d_6 \end{matrix} \times 10^9 \quad (2.6)$$

Once assembled, the supported degrees of freedom ( $d_1$ ,  $d_2$  &  $d_3$ ) are removed from the matrix as they have no effect on its solving.

$$\mathbf{K} = \begin{bmatrix} & d_4 & d_5 & d_6 \\ 14.9 & 3.89 & -3.89 \\ 3.89 & 14.9 & -3.89 \\ -3.89 & -3.89 & 3.89 \end{bmatrix} \begin{matrix} d_4 \\ d_5 \\ d_6 \end{matrix} \quad (2.7)$$

The structural mass matrix is assembled following the same procedure.

### 2.2.2 Beams

A beam element, Figure 2.3(a), is similar to a truss element in that it is a straight bar with a uniform cross-section; however it deforms only in a direction perpendicular to its axis, and therefore the load carried by the beam is said to be transverse and not axial. Typically beams will be welded together instead of pinned or hinged, and therefore moments are transmitted from one beam to another via what is known as a rigid joint. All beam elements considered here are based upon the Euler-Bernoulli beam theory, applicable to thin beams. The element stiffness and mass matrices are presented in (2.8a) and (2.8b) respectively. Transposition of the local matrices into the global matrices is theoretically possible with beam elements; however where two beams are connected with different orientations the structure is more commonly referred to as a frame and is therefore analysed as such.

$$\mathbf{k}_i = \begin{bmatrix} & d_1 & d_2 & d_3 & d_4 \\ \frac{12EI}{l^3} & \frac{6EI}{l^2} & -\frac{12EI}{l^3} & \frac{6EI}{l^2} \\ \frac{6EI}{l^2} & \frac{4EI}{l} & -\frac{6EI}{l^2} & \frac{2EI}{l} \\ -\frac{12EI}{l^3} & -\frac{6EI}{l^2} & \frac{12EI}{l^3} & -\frac{6EI}{l^2} \\ \frac{6EI}{l^2} & \frac{2EI}{l} & -\frac{6EI}{l^2} & \frac{4EI}{l} \end{bmatrix} \begin{matrix} d_1 \\ d_2 \\ d_3 \\ d_4 \end{matrix} \quad (2.8a)$$

$$\mathbf{m}_i = \frac{\rho al}{420} \begin{bmatrix} & d_1 & d_2 & d_3 & d_4 \\ 156 & 22l & 54 & -13l \\ 22l & 4l^2 & 13l & -3l^2 \\ 54 & 13l & 156 & -22l \\ -13l & -3l^2 & -22l & 4l^2 \end{bmatrix} \begin{matrix} d_1 \\ d_2 \\ d_3 \\ d_4 \end{matrix} \quad (2.8b)$$

### 2.2.3 Frames

Frame elements in Figure 2.3(b) are considered as a combination of both truss and beam elements as they can deform in directions both in line with, and perpendicular to, the

central axis and carry axial and transverse forces and moments. Frame structures are very common outside of theoretical analysis as real-world loading would be a combination of axial and transverse forces. Similar to trusses, frame structures can be either planar or space frames; however all of the joints will be rigidly fixed, enabling both forces and moments to be transferred between elements.

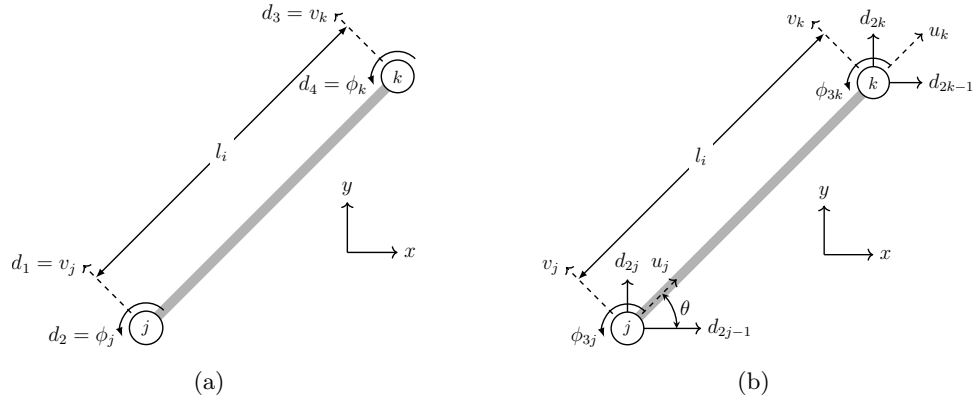


FIGURE 2.3: (a) A single beam element arrangement with nodes and degrees of freedom and (b) a frame element. Note that the frame element is a combination of the truss in Figure 2.2(a) beam in Figure 2.3(a).

The stiffness and mass matrices are similarly treated as a combination of those for trusses and beams. In this latter case, each consists of six degrees of freedom (three at each node) for  $u_{j,k}$ ,  $v_{j,k}$  and rotation  $\phi_{j,k}$ . The element matrices for trusses and beams are expanded to 6 degrees of freedom, Eqs. (2.9a) and (2.9b) respectively and then combined into a single frame stiffness matrix  $\mathbf{k}_i^{frame}$  Eq. (2.9c).

$$\mathbf{k}_i^{truss} = \begin{bmatrix} d_{3j-2} & d_{3j-1} & d_{3j} & d_{3k-2} & d_{3k-1} & d_{3k} \\ \frac{aE}{l} & 0 & 0 & -\frac{aE}{l} & 0 & 0 \\ 0 & 0 & 0 & 0 & 0 & 0 \\ 0 & 0 & 0 & 0 & 0 & 0 \\ -\frac{aE}{l} & 0 & 0 & \frac{aE}{l} & 0 & 0 \\ 0 & 0 & 0 & 0 & 0 & 0 \\ 0 & 0 & 0 & 0 & 0 & 0 \end{bmatrix} \begin{matrix} d_{3j-2} \\ d_{3j-1} \\ d_{3j} \\ d_{3k-2} \\ d_{3k-1} \\ d_{3k} \end{matrix} \quad (2.9a)$$

$$\mathbf{k}_i^{beam} = \begin{bmatrix} d_{3j-2} & d_{3j-1} & \phi_{3j} & d_{3k-2} & d_{3k-1} & \phi_{3k} \\ 0 & 0 & 0 & 0 & 0 & 0 \\ 0 & \frac{12EI}{l^3} & \frac{6EI}{l^2} & 0 & -\frac{12EI}{l^3} & \frac{6EI}{l^2} \\ 0 & \frac{6EI}{l^2} & \frac{4EI}{l} & 0 & -\frac{6EI}{l^2} & \frac{2EI}{l} \\ 0 & 0 & 0 & 0 & 0 & 0 \\ 0 & -\frac{12EI}{l^3} & -\frac{6EI}{l^2} & 0 & \frac{12EI}{l^3} & -\frac{6EI}{l^2} \\ 0 & \frac{6EI}{l^2} & \frac{2EI}{l} & 0 & -\frac{6EI}{l^2} & \frac{4EI}{l} \end{bmatrix} \begin{matrix} d_{3j-2} \\ \phi_{3j-1} \\ d_{3j} \\ d_{3k-2} \\ d_{3k-1} \\ \phi_{3k} \end{matrix} \quad (2.9b)$$

$$\mathbf{k}_i^{frame} = \begin{bmatrix} d_{3j-2} & d_{3j-1} & \phi_{3j} & d_{3k-2} & d_{3k-1} & \phi_{3k} \\ \frac{aE}{l} & 0 & 0 & -\frac{aE}{l} & 0 & 0 \\ 0 & \frac{12EI}{l^3} & \frac{6EI}{l^2} & 0 & -\frac{12EI}{l^3} & \frac{6EI}{l^2} \\ 0 & \frac{6EI}{l^2} & \frac{4EI}{l} & 0 & -\frac{6EI}{l^2} & \frac{2EI}{l} \\ -\frac{aE}{l} & 0 & 0 & \frac{aE}{l} & 0 & 0 \\ 0 & -\frac{12EI}{l^3} & -\frac{6EI}{l^2} & 0 & \frac{12EI}{l^3} & -\frac{6EI}{l^2} \\ 0 & \frac{6EI}{l^2} & \frac{2EI}{l} & 0 & -\frac{6EI}{l^2} & \frac{4EI}{l} \end{bmatrix} \begin{matrix} d_{3j-2} \\ \phi_{3j-1} \\ d_{3j} \\ d_{3k-2} \\ d_{3k-1} \\ \phi_{3k} \end{matrix} \quad (2.9c)$$

the element mass matrix for a frame is thus:

$$\mathbf{m}_i = \frac{\rho al}{420} \begin{bmatrix} d_{3j-2} & d_{3j-1} & \phi_{3j} & d_{3k-2} & d_{3k-1} & \phi_{3k} \\ 140 & 0 & 0 & 70 & 0 & 0 \\ 0 & 156 & 22l & 0 & 54 & -13l \\ 0 & 22l & 4l^2 & 0 & 13l & -3l^2 \\ 70 & 0 & 0 & 140 & 0 & 0 \\ 0 & 54 & 13l & 0 & 156 & -22l \\ 0 & -13l & -3l^2 & 0 & -22l & 4l^2 \end{bmatrix} \begin{matrix} d_{3j-2} \\ d_{3j-1} \\ \phi_{3j} \\ d_{3k-2} \\ d_{3k-1} \\ \phi_{3k} \end{matrix} \quad (2.9d)$$

## 2.2.4 Eigenvalue analysis

The definition of eigenvalues and eigenvectors in mathematical terms can be expressed geometrically from the symmetrical stiffness matrices shown in the previous section. The

stiffness matrices relate displacements,  $\mathbf{d}$ , to forces,  $\mathbf{p}$ , at the same coordinates of the structure

$$\mathbf{K}\mathbf{d} = \mathbf{p} \quad (2.10)$$

where  $\mathbf{p}$  is a vector of applied forces and  $\mathbf{d}$  a vector of resulting displacements. If the geometric vectors  $\{x\}$  and  $\mathbf{K}\{x\}$  point in the same direction, then the vector  $\{x\}$  is referred to as an eigenvector of  $\mathbf{K}$ . Associated with this is the ratio between vector  $\mathbf{K}\{x\}$  and vector  $\{x\}$  and is called the eigenvalue,  $\lambda$ , of  $\mathbf{K}$ , paired with eigenvector  $\{x\}$ . The standard eigenvalue problem is thus:

$$\mathbf{K}\{x\} = \lambda\{x\} \quad (2.11)$$

Frequency optimization falls within the realm of eigenvalue optimization, a field extensively studied by the mathematical programming community. Researchers have explored various approaches to tackle the underlying semidefinite programming (SDP) problem. For instance, [Fox and Kapoor \(1970\)](#) adopted a feasibility-based approach, [Grandhi and Venkayya \(1988\)](#) and [Khot \(1985\)](#) utilized the optimality criteria method. And [Kaveh and Ghazaan \(2016\)](#) employed non-smooth optimization techniques to size existing truss structures, ensuring they meet specific frequency requirements, [Achtziger and Kočvara \(2007\)](#) also leveraged semidefinite programming to address similar problems. [Aroztegui et al. \(2011\)](#) developed a feasible direction SDP algorithm specifically aimed at maximizing fundamental frequencies in simple fully-connected ground-structure problems.

Consider a structure consisting of  $m$  elements, connecting a pre-determined set of  $n$  nodes. A large external force  $P$  is applied to a specific node, with internal forces transmitted through the structure, resulting in small displacements at each node. This may be considered to be a static problem. To take account of the vibration characteristics of the structure, it is necessary to consider the following dynamic problem derived from the equation for motion:

$$\mathbf{K}\{\mathbf{u}\} + \mathbf{M}\{\ddot{\mathbf{u}}\} = 0, \quad (2.12)$$

where  $\mathbf{K}$  and  $\mathbf{M}$  represent the global stiffness and mass matrices respectively. The mass and stiffness matrices are represented as symmetric  $2n \times 2n$  matrices when modelling a two-dimensional truss structure and  $3n \times 3n$  matrices for a three-dimensional truss structure. The size of these global matrices will be reduced by the number of supported degrees of freedom, since there are no displacements at these locations. Given that the

displacement vector is harmonic, Eq. (2.12) may be restructured into the generalized eigenvalue problem:

$$\mathbf{K}\phi_j = \lambda_j(\mathbf{M} + \mathbf{M}_0)\phi_j, \quad (2.13)$$

where  $\mathbf{M}$  refers to the global mass matrix for the structure's elements;  $\mathbf{M}_0$  refers to the additional mass of the nodes connecting each element; and  $\lambda_j$  represents the eigenvalue for a given mode of vibration  $\phi_j$ , ( $j = 1, 2, 3, \dots$ ). The free vibrations of a structure are equal to the square root of the eigenvalues  $\omega_j^2 = \lambda_j$  in  $\text{rad s}^{-1}$ , and thus the natural frequencies and normal modes of vibration for the structure may be determined.

## 2.3 Mathematical optimization

Mathematical programming is the study of optimization problems where the minimisation or maximisation is sought of a real function of real or integer variables, subject to constraints on the variables. If the basic descriptions involved take the form of linear algebraic equations, the technique is described as 'linear programming'. If more complex forms are required, the term 'nonlinear programming' is applied. [Boyd and Vandenberghe \(2004\)](#) presents this in its basic form as:

$$\text{minimize } f_0(\mathbf{x}) \quad (2.14a)$$

$$\text{subject to } f_i(\mathbf{x}) \leq b_i, \quad i = 1, \dots, m \quad (2.14b)$$

where  $\mathbf{x} = (\mathbf{x}_1, \dots, \mathbf{x}_n)$  is a vector of unknown variables;  $f_0 : \mathbb{R}^n \rightarrow \mathbb{R}$  is the objective function and here, as in much of this work the objective is to minimize the values of  $\mathbf{x}$ ;  $f_i : \mathbb{R}^n \rightarrow \mathbb{R}$ ,  $i = 1, \dots, m$  are the constraint functions which must not be violated in the minimisation of  $\mathbf{x}$ , in this case an inequality constraint and  $b_i$  is the limit to the constraint. A value of  $\mathbf{x}$  may be considered optimal if  $f_i(\mathbf{x}) \leq b_i$  for all constraints  $i$ ; if no optimal point is found then the problem is considered infeasible.

### 2.3.1 Convexity and local/global optima

Different types of mathematical programming problems can result in different kinds of optimal solutions. In general these are referred to as local and global optima: a local optimum is a point that has a lower value of the objective function than all feasible

neighbouring points, whereas a global optimum will represent the minimum value for the function over the whole of the domain. Thus a global optimum point will also be a local optimum; however it is not necessarily the case that a local optimum will be the global solution. This is an important consideration in mathematical optimization to ensure that there is no better solution available at another point in the solution space.

Figure 2.4 shows the definition and results of convex and non-convex (concave) optimization and highlights the potential differences between local and global optimal solution points. Figures 2.4(a) and 2.4(b) show examples of convex and non-convex constraints respectively; it is clear that in convex optimization any local optimum will also be the global optimum. To aid in the definition of a convex set, as in Figure 2.4(c), if all the points on the line segment  $A - B$  are within a set  $S$  then  $S$  is a convex set; however  $S$  can be said to be a non-convex set when there are points on the line segment  $A - B$  which are outside of  $S$ , Figure 2.4(d). For this reason convex problems are generally preferred in optimization as they are significantly easier to solve; also, if the problem can be formulated as a linear program, then the computational costs in solving the problem are relatively small.

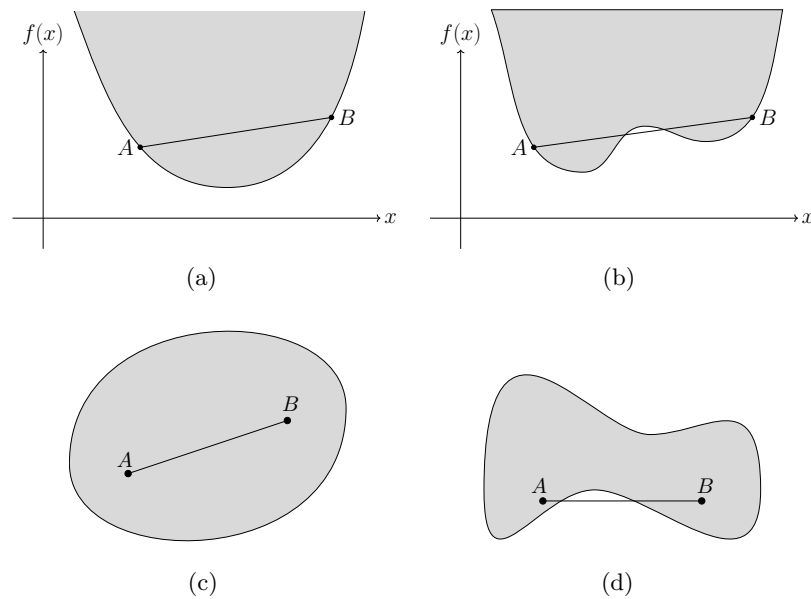


FIGURE 2.4: Examples of convex and non-convex problems: (a) a convex problem demonstrating a local optimum to also be the global optimum, and (b) a non-convex problem highlighting a local optimum where a better solution exists elsewhere. Also (c) a well defined convex problem where all points reside within the solution space as opposed to a non-convex problem (d) with the potential for isolated local optima.

## 2.4 Linear programming

The problem defined by (2.14) is considered linear if all the functions  $f$  are linear in the optimization variables; every linear programming problem is convex and therefore the solution will always be the global optimum. Owing to the more simplistic form, linear programs will solve more quickly than nonlinear problems (Section 2.5). Linear programming formulations have been presented in a number of forms over time, one such example is given by Vanderbei (2001):

$$\text{minimize } \mathbf{c}^T \mathbf{x} \quad (2.15a)$$

$$\text{subject to } \mathbf{A}\mathbf{x} \leq \mathbf{b} \quad (2.15b)$$

$$\mathbf{x} \geq \mathbf{0} \quad (2.15c)$$

where  $\mathbf{x}$  is a vector containing the optimization variable;  $\mathbf{c}$  contains the objective coefficients,  $\mathbf{A}$  the coefficients for the constraints, and  $\mathbf{b} = [b_1, b_2, \dots, b_m]^T$  are the constant parts of the constraint. This formulation is also referred to as the primal-form of a linear program.

There currently exist three widely used approaches for solving linear programming problems:

**Graphical** methods of linear programming solve problems by finding the highest or lowest point of intersection between the objective function line and the solution space on a graph (Figure 2.5). The solution space (shaded) is formed by lines representing the constraints on the problem, and additional lines representing the objective function are superimposed on top. This method is generally limited to two variables to reduce the complexity of the solution space.

**Simplex** method introduced by Dantzig (1949) solves linear programming problems by reviewing a series of solutions and iteratively improving upon the previous results, with each new iteration improving the objective function. It is determined that when no further iterations are possible then the optimal solution has been identified.

**Interior Point** method is considered superior to the simplex method due to its ability to solve large scale problems in a short time. Originally proposed by Karmarkar (1984) it is different to the simplex method where the problem is solved in steps along the boundary as the interior point method moves through the interior of the solution space. An interior point algorithm will generally combine different optimal points in a convex fashion equally to find the ultimate global optimum.



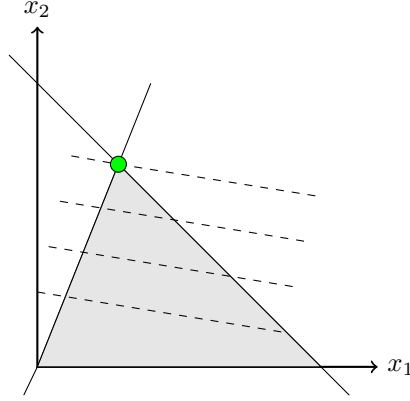


FIGURE 2.5: Example graphical approach to solve a linear program Eq. (2.15). The grey area is the search region, solid lines represent the constraints, dashed lines represent the contour lines of the objective function, and the green circle the optimum value for a maximisation objective.

### 2.4.1 Duality theory

Duality theory (Nocedal and Wright, 2006; Vanderbei, 2001) states that every linear programming problem has its dual-form, Eq. (2.16), formulation which is generally solved alongside the primal-form, Eq. (2.15). A bound on the objective function of each form can be gained from a feasible, but not necessarily optimal, solution of one or the other. The dual-form may be presented as:

$$\text{minimize } \mathbf{b}^T \mathbf{y} \quad (2.16a)$$

$$\text{subject to } \mathbf{A}^T \mathbf{y} \geq \mathbf{c} \quad (2.16b)$$

$$\mathbf{y} \geq \mathbf{0} \quad (2.16c)$$

where  $\mathbf{b}$ ,  $\mathbf{A}$  and  $\mathbf{c}$  are as given for the primal problem in Eq. (2.15), and  $\mathbf{y}$  is the vector containing the dual optimization variables. The duality theorem states that the optimal solutions of the primal problem and dual problem are equal. For linear problems, this holds in all cases where an optimal solution exists (Vanderbei, 2001).

## 2.5 Nonlinear programming

A non-linear programming (NLP) problem arises in mathematical programming models when the objective function, Eq. (2.14), incorporates non-linear functions and/or the feasible region is defined by constraints involving non-linear equalities or inequalities. In contrast to linear programming, where the objective function and constraints are linear,

NLP deals with more complex functions that can be convex, concave, or have multiple local optima. Broadly, non-linear optimization may be categorized into gradient-based methods and direct search methods.

Gradient-based methods iteratively adjust design variables based on the gradient of the objective function. Minimisation is achieved by seeking the area on a curve with the steepest descent, this may be referred to as a first derivative approach. A second derivatives approach augments the gradient method with Hessian matrices to guide the optimization process. This approach will often converge more quickly than those employing gradient alone but require additional computational burden, examples are: the sequential quadratic programming (SQP) method (Wilson, 1963), the augmented Lagrangian method (Hestenes, 1969) and the non-linear interior point method (Fiacco, 1969). Whilst the interior point method may be used to solve these types of problems it is likely that a local optimum will be identified if the problem is non-convex. These local optima lie within the feasible region and have no better feasible solutions in their immediate neighbourhood. However, they cannot be improved by considering nearby configurations. NLP solvers converge to a local optimal point, but additional local optima may exist beyond the immediate neighbourhood. These distant optima could have better objective values than the local optimum determined by the NLP solver. Achieving a globally optimal solution to a non-linear program is generally computationally expensive (Horst and Tuy, 1995), which is why for many practical applications mathematically based methods have been replaced with meta-heuristic methods, these techniques aim to find a local optimal solution or a good approximation to the global optimal solution.

Conversely, direct search methods do not use derivative information and as a result generally converge more slowly. Examples of solvers developed to treat non-linear programs include: Genetic Algorithms (Holland, 1992), which uses the theory of genetic evolution, a generational approach combining the strongest of the previous generation to produce a population of potential solutions; or Particle Swarm Optimization (Kennedy and Eberhart, 1995) techniques, which are generally based in the natural movement of many creatures including bees, ants or fireflies. Regardless, the premise is based upon the position of agents within a solution space, moving at a velocity towards their individual, and, if possible, best positions.

As stated in Section 2.3.1, a convex optimization problem will generally avoid the issue of local optimum points being identified, and usually a globally optimum solution is found. Often formulations can be shown to be convex, including some in conic optimization (MOSEK ApS, 2017). Boyd and Vandenberghe (2004) state that formulating a problem as convex essentially solves the problem.

### 2.5.1 Semidefinite programming

Semidefinite programming (SDP) is a subfield within mathematical optimization with this aim of optimizing a linear objective function subject to linear equality constraints, also, an additional constraint that a specific matrix formed by the decision variables is positive semidefinite is included. Positive semidefiniteness is a generalization of positive definiteness for symmetric matrices, meaning that all its eigenvalues are non-negative. The distinctive feature of SDP is the requirement that a specific matrix (often denoted as  $X$ ) formed by the decision variables is positive semidefinite. Mathematically the symmetric matrix  $X$  is positive semidefinite if  $x^T X \geq 0$  for all vectors of  $x$ . This constraint adds significant complexity to the optimization problem.

Previously, SDP has found application in optimizing truss structures, notably: Ben-Tal and Nemirovski (1997) and later Kanno (2018) employed SDP to design robust structures resilient to uncertainties in loading, while Giniünaité (2015) utilized SDP for identifying minimum mass structures. Various solvers, both commercial and open-source, capable of handling semidefinite problems of different complexities are available, such as `fminsd` (Thore, 2018); MOSEK (v8+) (MOSEK ApS, 2017); PENLAB (Fiala et al., 2013) and CVX (Grant and Boyd, 2014). Similar to linear programming, SDP also has a dual problem associated with it, referred to as the duality gap. The difference between the optimal values of the primal and dual problems is measured, and when the difference is zero the primal problem is feasible and bound.

To optimize for the natural frequencies of a structure, a novel constraint equation derived from the generalized eigenvalue problem Eq. (2.13) is used. After determining the coefficient matrices for stiffness and mass, a precautionary measure is taken to prevent the optimization from yielding a structure prone to low-frequency vibrations. This is achieved by setting a threshold, ensuring that the smallest eigenvalue from Eq. (2.13) is greater than or equal to a predefined minimum value. Thus Eq. (2.13) may be transformed into the following constraint:

$$\mathbf{K}(\mathbf{a}) - \lambda(\mathbf{M}(\mathbf{a}) + \mathbf{M}_0) \succcurlyeq 0, \quad (2.17)$$

where  $\mathbf{K}(\mathbf{a}) = \sum_{i=1}^m a_i \mathbf{K}_i$  and  $\mathbf{M}(\mathbf{a}) = \sum_{i=1}^m a_i \mathbf{M}_i$  are the global stiffness and mass matrices respectively;  $a_i$  refers to the cross-sectional area of member  $i$ ;  $\lambda$  is the eigenvalue derived from the minimum specified natural frequency ( $\omega_1$ ) for the specified mode of vibration  $\phi_j$ ; and  $\succcurlyeq$  indicates that the matrix to its left is symmetric and positive semidefinite. For the purposes of this contribution, the connecting nodes are not considered and therefore the mass associated with joints  $\mathbf{M}_0 = 0$ .



## 2.6 Elastic & plastic design

Building on these mathematical programming techniques, some sound engineering design fundamentals are now included in structural optimization. The most critical of these concerns fundamental to a number of studies is how a material will behave when put under load; more specifically the relationship that the material has between strain and stress. With reference to the example stress-strain curve shown in Figure 2.7(a) it can be seen that as a load is applied, the material will go through two main phases of deformation: elastic and plastic. In the elastic phase stress and strain have a linear relationship, the slope of the line being the Young's Modulus  $E$  of the material. It is in this phase that the material may return to its original state when the load is removed. In the plastic deformation stage, where deformation in the material becomes permanent, the relationship between stress and strain is no longer linear up to the point where the material will fail.

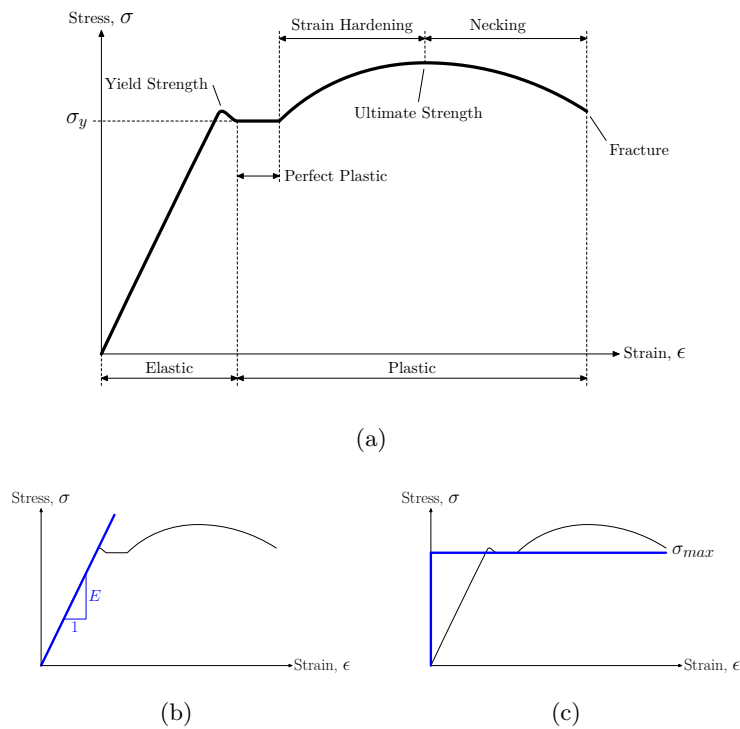


FIGURE 2.7: Stress-strain relationship: (a) the stress-strain curve for a typical material showing the different stages involved; (b) the elastic stress-strain relationship; (c) and the rigid-plastic relationship.

The plastic deformation stage is then sub-divided into two further stages: strain hardening and necking. Strain hardening begins, in certain materials, with the perfect plastic stage where stress is maintained at the same level as strain increases, resulting in the formation of Lüders bands, before proceeding on to a region where the stress increases as the material elongates. Once the Ultimate Tensile Strength (UTS) of the material

is reached, the necking stage begins where stress decreases as the strain increases. In a typical tensile test bar, the material will locally reduce in cross-section up to the point of rupture. Thus a typical stress-strain curve is non-linear and non-convex, leading to significant computational difficulty when subjected to analysis.

An engineering design will generally strive to ensure that any deformation in the part occurs only in the elastic region thus, not accounting for fatigue, the part returns to its original state. As long as no part of the entire structure reaches the yielding stress, then the loading capacity of this structure is considered to be achieved. However, the elastic phase of the stress-strain curve shown in Figure 2.7(a) is relatively short, which can lead to a considerable waste of material. Alternatively, a rigid-plastic model is used which assumes that the stress-strain relationship is always perfect plastic, ensuring that the material's plastic capacity is also employed. In reality, a material which exhibits a rigid-plastic stress-strain relationship doesn't exist, but for ductile materials with a plastic deformation phase much larger than the elastic phase this model applies (Nielsen and Hoang, 2011) and simplifies an optimization calculation by removing the non-linearity.

## 2.7 Continuum & discrete representations

Two main approaches to the representation of geometry exist in optimization tools:

Discrete representations, such as those used in layout optimization (Section 2.10), begin with a predefined arrangement of members, commonly forming trusses, in a set configuration. Layout optimization was performed as a size optimization on all potential connections present in the ground-structure until Pearson (1958) observed that some of the connections would disappear completely. To remedy this Dorn et al. (1964) proposed the ground-structure method, connecting every node in the domain to every other node with potential connections, with these potential connections providing every possible load path required to react an applied force. The most optimal load path was then identified through optimization to yield the most efficient layout and material utilisation; i.e. the least amount of material required.

Continuum representations are now highly popular and are used extensively in topology optimization (Section 2.11). Such representations may assign material to the entirety of a design domain and through an iterative optimization process reduce the density of the material in specific areas where the strain energy is lower (Bendsøe, 1989), thus indicating where material is not required in the final design. Originally the results of topology optimization using continuum based representations were difficult to realize in real-world applications, with the highly complex results being challenging, if not

impossible, to produce through traditional manufacturing methods. However, more recently additive manufacturing techniques have enabled these forms to be produced. A disadvantage of continuum representations is their inefficiency at low volume fractions (the volume of the material in the optimized component relative to the original volume of the design domain). [Bendsøe and Haber \(1993\)](#) demonstrated that when applied to the perforated plate problem, a continuum approach would result in a form very similar to one of Michell's least-weight trusses ([Michell, 1904](#)).

## 2.8 Programming applied to structural optimization

The purpose of structural topology optimization, as per the publication of the seminal paper by Australian engineer Anthony George Maldon [Michell \(1904\)](#), is to ensure that for a given design domain the material contained within is distributed in the most optimal manner for a given set of functional requirements. Today, the optimal distribution is often achieved through a combination of a defined initial domain, a set of boundary conditions (loads and supports), and a Finite Element Analysis (FEA). Key to successful structural optimization is a clear objective to which the distribution of the material will be driven. Commonly this is defined as minimising the mass of a structure or maximising its stiffness, subject to one or more associated constraints. Sadly, perhaps due to its highly mathematical nature, this field of study went largely ignored for fifty years until the advent of computers capable of fully exploring the potential of the theories that Michell had presented.

Structural optimization either falls into one of three distinct categories, or be a combination of two or more of these: size, geometry/shape and topology/layout optimization. [Figure 2.8](#) shows the differences between these three categories. The terms 'geometry' and 'layout' are commonly used where discrete representations are concerned, and 'shape' and 'topology' are commonly used for continuum structures.

In accordance with Moore's Law ([Moore, 1965](#)), computing power has been increasing rapidly over recent decades, such that an engineer has a computer on their desk that contains an ever increasing number of transistors on a chip of the same size. This increase in computing power has opened up the potential to create ever more elaborate models in CAD and larger FEA files. Such complexity increases the effort required for loops of re-design activity in the early phases of product development. To counter this, a number of methods have been developed to automate the process of multi-disciplinary optimization, allowing the engineer to be away from the machine, performing other tasks (or even sleeping!) whilst the computer generates, analyses, and ranks many thousands of different design iterations.

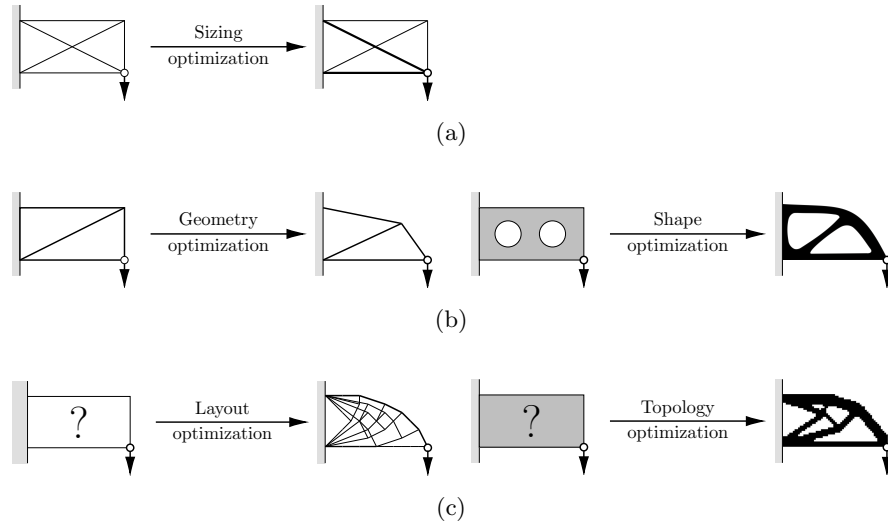


FIGURE 2.8: Types of optimization with examples: (a) size optimization where existing geometry is modified in size until the objective is reached, all elements will remain part of the final solution; (b) Geometry and shape optimization, where the size and position of elements/material is changes to suit the objective; and (c) Layout and topology optimization where material inside the domain is free to change in size, shape and geometry in order to meet the objective.

A summary of the most notable optimization methods (categorized as geometry, topology, and layout) is presented below, followed by an example of their usage applied to the well known Michell cantilever problem (with the exception of geometry optimization). The problem definition for the cantilever is shown in Figure 2.9. Where applicable the following parameters will be used: The prescribed volume fraction  $V_{frac} = 0.5$ , penalisation  $p = 3$  and the filter radius  $r_{min} = 1.2$ .

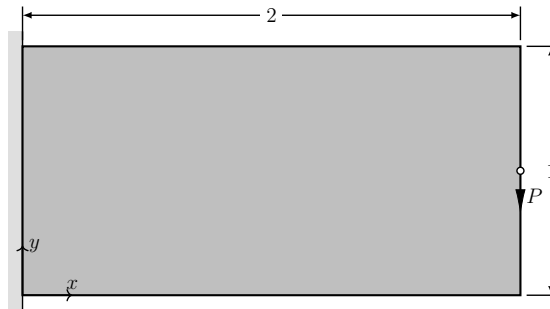


FIGURE 2.9: Problem definition for Michell cantilever from Wu and Tseng (2010). Load ( $P$ ) = 1, Young's Modulus ( $E$ ) = 1, Poisson's ratio ( $\nu$ ) = 0.3 and thickness = 1.

## 2.9 Geometry optimization

The original and simplest structural optimization technique is that of size and/or shape optimization. Shape optimization is generally performed on continuous structures by



modifying pre-defined variables that describe the boundaries of the design domain. Shape and size optimization routines can be used separately or together to achieve the same goal because shape optimization may be defined as the search for the optimal design by modifying size vectors such as the cross-sectional areas of trusses or the thickness of plates. Unless a simple 2D structure is defined, most shape optimization will contain variables for the third dimension, thereby producing a combined result. Originally this process occurred manually, with an engineer iterating by hand or producing prototypes, and then changing the design to address failures, a time consuming and costly process.

The advent of desktop computers has made this process much quicker, automating hand calculations used in analysis and the use of CAD to generate new geometries. It is now possible to review several thousands of design iterations every minute, where it may have taken hours or days for a single one using manual approaches. The ability to use greater numbers of processing cores, more memory and storage means that the complexity of analysis models is now so far advanced that a component may be broken down into elements of less than 1mm per side and optimized.

## 2.10 Layout optimization

Following on from the original theories of [Maxwell \(1864\)](#), [Michell \(1904\)](#) determined criteria concerning the optimal topology of trusses. More specifically Michell sought the optimal layout which would react a given single load case whilst exhibiting the minimum possible volume, or mass. This optimality criterion was proposed thusly:

*“A frame therefore attains the limit of economy of material possible in any frame-structure under the same applied forces, if the space occupied by it can be subjected to an appropriate small deformation, such that the strains in all the bars of the frame are increased by equal fractions of their length, not less than the fractional change of length of any element of the space.”*

Michell then went on to demonstrate this premise on a number of cases, many of which are now benchmark problems in layout optimization. For example, the cantilever problem shown in [Figure 2.9](#) may have the solution shown in [Figure 2.10](#). One of the guiding principles from Michell’s studies is that for near-optimality the members in tension and compression should cross each other at close to 90°, something that features heavily in other Michell structures that meet the optimality criterion.

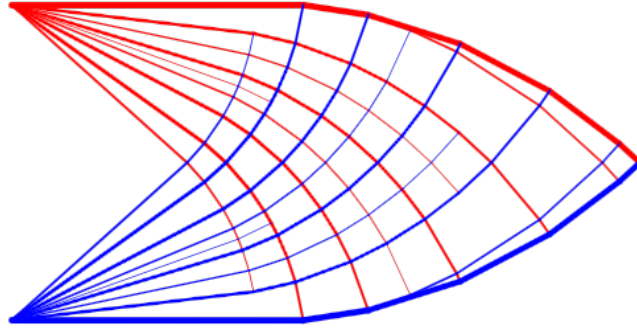


FIGURE 2.10: Layout optimization solution to the Michell cantilever beam problem shown in Figure 2.9.

### 2.10.1 Ground-structure method

Numerical layout optimization stands out as a highly efficient method for precisely determining the minimum volume for truss geometry under specific boundary conditions. The foundational approach, known as the 'ground-structure' procedure, was first introduced by Dorn et al. (1964). It was initially applied to single load case problems with an assumption of a plastic material model, however over time this method has evolved and been augmented. The fundamental formulation for a plastic layout optimization problem involving  $n$  nodes and  $m$  members is expressed in Eq. (2.18) and can be effectively addressed using a Linear Programming (LP) solver.

$$\text{minimize } V = \mathbf{l}^T \mathbf{a} \quad (2.18a)$$

$$\text{subject to } \mathbf{B}\mathbf{q} = \mathbf{p} \quad (2.18b)$$

$$-\sigma^- a_i \leq q_i \leq \sigma^+ a_i, \quad \forall i \quad (2.18c)$$

$$a_i \geq 0, \quad \forall i \quad (2.18d)$$

where  $V$  is the total volume of the structure;  $\mathbf{l}$  is a vector of individual element lengths  $\{l_1, l_2, \dots, l_m\}$ ;  $\mathbf{a}$  is a vector containing element cross-sectional areas  $\{a_1, a_2, \dots, a_m\}$ ;  $\mathbf{B}$  is a suitable  $(2n \times m \text{ or } 3n \times m)$  equilibrium matrix containing direction cosines (for 2D or 3D problems);  $\mathbf{q}$  is a vector of element axial forces,  $\mathbf{q} = \{q_1, q_2, \dots, q_m\}$ , where  $q_i$  is the force in element  $i$ ;  $\mathbf{p}$  is a vector of applied loads and  $\mathbf{p} = \{p_1^x, p_1^y, p_1^z, p_2^x, p_2^y, p_2^z, \dots, p_n^z\}$  where  $p_j^x, p_j^y, p_j^z$  are the  $x$ ,  $y$  and  $z$  direction components of the load applied to node  $j$  ( $j = 1, \dots, n$ ). Finally  $\sigma^+$  and  $\sigma^-$  are, respectively, the limiting tensile and compressive stresses that can be sustained by the material. Problems of this nature may be solved using linear programming.

The variables in Eq. (2.18) are area  $a$ , and axial force  $q$ , and the goal is to react the axial forces with the minimum possible amount of material. This will lead to elements being reduced in size until some are very close to an area of zero, thus an optimal subset of elements can be determined to be the optimum.

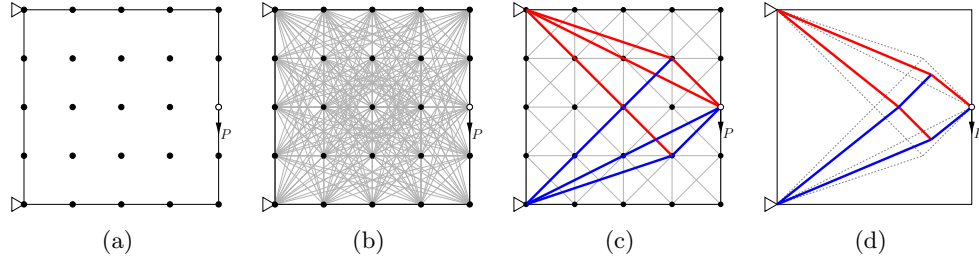


FIGURE 2.11: Steps in layout optimization: (a) the domain is created and populated with equally spaced nodes; (b) each node is connected to every other node in the domain to form a fully-connected ground-structure, alternatively (c) each node is connected only to neighbouring nodes to form a minimally-connected ground-structure and member-adding employed, the resulting optimized layout is the same either way; and (d) the rationalized structure following geometry optimization. Note that red and blue bars indicate those in tension and compression respectively.

In order to begin a design study using layout optimization it is essential to understand the domain in which the potential structure will reside; positions of supports are required as well as the location and magnitude of any applied loads, Figure 2.11(a). The compressive and tensile strength capability of the material will be used in the optimization to balance member areas with axial forces. Once the domain is defined, the ground-structure may be generated. The size and detail of the ground-structure is dependent upon the level of granularity required in the analysis; if a more accurate result is required then more nodes should be added to the domain. The designer must be cautious as this increase in nodes will lead to a rapid increase in computational time, as exemplified in Table 2.3. These example results were obtained from multiple runs of the cantilever beam shown in Figure 2.9 using MATLAB 2022b on a desktop PC with an Intel Core i5 processor.

### 2.10.2 Hemp's theory

The work of both Michell and Dorn was then combined by Hemp (1973), who applied duality to the ground-structure approach yielding the following formulation:

TABLE 2.3: Computational times for increasing numbers of potential connections in a full ground-structure. Note the steep increase in CPU cost once 1000000 connections is reached.

The graph illustrates the exponential growth of computational time as the number of elements increases. The x-axis, labeled 'No. of Elements', uses a logarithmic scale ranging from  $10^3$  to  $10^8$ . The y-axis, labeled 'Time (s)', ranges from 0 to 600. The curve remains near zero for  $10^3$  to  $10^5$  elements, then begins to rise, reaching approximately 600 seconds at  $10^7$  elements.

No. of Elements	Time (s)
$10^3$	0.311
$10^4$	1.113
$10^5$	9.822
$10^6$	47.271
$10^7$	145.813
$10^8$	337.751

No. of Nodes	No. of Elements	CPU Cost (s)
91	4095	0.311
435	94395	1.113
1035	535095	9.822
1891	1786995	47.271
3003	4507503	145.813
4371	9550635	337.751
5151	13263825	594.182

$$\text{maximize } W = \sum_{j=1}^n P_j u_j / \sigma \epsilon \quad (2.19a)$$

$$\text{subject to } \sigma^+ |\epsilon| / \sigma + \sigma^- |\epsilon_i| / \sigma \leq \epsilon \quad (2.19b)$$

where  $W$  is the total virtual work;  $P_j$ ,  $u_j$  are the external forces and displacements respectively at node  $j$ ;  $\epsilon_i$  is the strain of member  $i$ ; and  $\sigma$  and  $\epsilon$  are constants of a Lagrangian multiplier.

Referring back to duality theory, Section 2.4.1, when volume,  $V$ , in Eq. (2.18) is at a minimum then virtual work,  $W$ , in Eq. (2.19a) must be at a maximum, with the strain in each member satisfying Eq. (2.19b). When considering Michell's optimality criterion, Hemp suggests that all members meeting constraint (2.20) will be active in the structure and those which satisfy constraint (2.21) will not be active members.

$$\sigma^+ |\epsilon| / \sigma + \sigma^- |\epsilon_i| / \sigma = \epsilon \quad (2.20)$$

$$\sigma^+ |\epsilon| / \sigma + \sigma^- |\epsilon_i| / \sigma < \epsilon \quad (2.21)$$

The following optimality criteria were proposed by Hemp:

1. Any generated structure should be capable of successfully carrying its alternative system of forces.

2. Each member should be fully stressed to either its tensile limit  $\sigma_+$  or its compressive limit  $\sigma_-$ .
3. A virtual displacement is allowed at the structures nodes, producing non-negative strains in members loaded to stress  $\sigma_+$ , non-positive strains in members loaded to a stress  $\sigma_-$ , and zero strains in members not stressed to these limits.
4. Strains of members that exist in the optimal topology must satisfy constraint (2.20).
5. Strains in all members (including those not present in the optimum structure), corresponding to the virtual displacement of criteria 3, must satisfy constraint (2.19b).

It should be noted that criteria 4 and 5 above can be used to govern whether or not there is an advantage in including a prescribed member in the optimal truss, connecting Michell's optimality criterion and Dorn's ground-structure approach.

### 2.10.3 Efficiency improvement

The full ground-structure as used by Dorn et al. (1964) spreads the nodes equally throughout the domain and then joins each one with a potential connection, Figure 2.11(b), so that if necessary every node could be connected to every other node in the domain. This method will lead to a total of  $n(n-1)/2$  potential connections for a 2D or 3D domain, where  $n$  is the total number of nodes in the domain. Though thorough, this level of detail cannot be sustained for larger problems as the number of potential connections can quickly exceed 100,000,000. The majority of these connections will have an area equal or close to zero following the optimization and so do not contribute to the final structure.

Despite advances in computer technology and increasingly efficient algorithms there are still limitations on the size of problem that can be solved with a full ground-structure, a problem that is even more pronounced when attempting to optimize in 3D. To address the limitations of the original methodology, a new technique was proposed by Gilbert and Tyas (2003) to make the algorithm more efficient with the incorporation of a customized column generation based 'member-adding' process as part of the overall solving mechanism. With this method, nodes in the initial ground-structure are only connected to their immediate neighbours, Figure 2.11(c), instead of to every other node in the domain, Figure 2.11(b). An iterative process is then used, with elements added to the current ground-structure from the list of potential connections. Newly-added elements

are introduced into the solution using the Michell-Hemp criterion Eq. (2.22) developed from Eq. (2.19b), which specifies limits on the virtual strain ( $\epsilon_i$ ) experienced by each potential element ( $i$ ), given a prescribed limiting stress ( $\sigma$ ):

$$-\frac{1}{\sigma^-} \leq \epsilon_i \leq \frac{1}{\sigma^+}, \quad i = 1, \dots, m. \quad (2.22)$$

Gilbert and Tyas (2003) not only proved that improvements in efficiency were possible using the ‘member-adding’ method, reducing total CPU time to just 8% of the time taken with a full-connected ground structure, they also demonstrated how different arrangement for initial connectivity may influence the time taken and numbers of iterations required. It was proven that for a problem containing 353,330 potential members the ‘member-adding’ algorithm obtained results which were identical in volume and structure using 5 different initial connectivity states as well as a full-connected ground structure. The most efficient being an initial connectivity state where each node was connected only to its adjacent neighbour.

#### 2.10.4 Geometry rationalisation

When applied to layout optimization, the addition of member-adding has been proven to provide an improvement in computational efficiency for solving large problems. However, as the size of the problem increases the complexity of the result also increases, often containing a large number of crossing members. These crossing members can make the resulting structure impossible to manufacture; thus He and Gilbert (2015) proposed an additional step to reduce the complexity of the structure through a post-optimization geometry rationalisation step. To achieve this, the nodes connecting the resulting members are reviewed and those adjacent to one another within a certain radius are combined, additionally combining the members into fewer bars; further optimization allows the positions of the nodes to be shifted.

A non-linear, non-convex algorithm is employed to achieve this and, as this stage of the processes is applied to a sub-set of the original ground-structure, the computational burden is minimal. This form of geometry optimization has been shown to improve upon the original results for the layout optimization (He and Gilbert, 2015; He et al., 2019a). Therefore it is proven possible to define a structure using layout optimization and geometry rationalisation, with minimal additional computational cost, which may then be suitable for manufacture.

## 2.11 Topology optimization

Two main topology optimization methodologies have emerged over the years, though there are others: Evolutionary Structural Optimization (ESO), and Solid Isotropic Material with Penalisation (SIMP). Both are iterative processes that operate on the principle that any material within the structure which carries only a small load can be deemed to be inefficient and may therefore be removed.

### 2.11.1 Evolutionary structural optimization

The ESO method (Xie and Steven, 1993) is an iterative type of optimization based upon the FE analysis conducted within a design space. At the beginning of the analysis the entire design space is filled with a pre-determined number of elements, connecting the load to the supports. Standard FEA is then carried out to determine the level of Von Mises stress in each element. Those with the lowest stress are removed prior to the next iteration in order to achieve a reasonably uniform stress distribution across the design space. Chu et al. (1996) went on to modify the pre-existing techniques by introducing a means of maximising the stiffness of the structure whilst maintaining a defined volume constraint. More impactful was the introduction of the BESO (Bi-Directional ESO) (Querín et al., 1998), whereby elements can be both added and removed from the design space in a single iteration. The primary advantage of this method is the time-saving offered due to the structure growing from a small initial state rather than reducing it from a much larger design space.

In general two varieties of BESO algorithms are in use: The ‘soft-kill’ method assigns a very low Young’s Modulus to each element to be removed from the design domain, thereby making their effect on the structure negligible, and the ‘hard-kill’ method which removes the elements entirely. Due to its relative simplicity and efficiency, BESO has been implemented in a number of commercial packages which claim to offer the ability to produce the optimum design to solve a given problem. It has also been subject to a number of improvements and alterations in the near twenty years since its inception. Figure 2.12 demonstrates the form achieved by a BESO algorithm for the Michell cantilever benchmark<sup>1</sup>.

One such improvement was an initial attempt to make the optimization routine ‘process aware’ (Brackett et al., 2011) with additive manufacturing being the focus. Some success was had with examples that had been optimized in 2D. After each iteration the

---

<sup>1</sup>Produced using the soft-kill BESO program introduced in Huang and Xie (2010) and available from <http://www.rmit.edu.au>



FIGURE 2.12: Michell cantilever beam optimized using BESO with  $100 \times 50$  elements resulting in a compliance of 64.26

downward facing edges were identified and their angle in relation to the  $x$  axis measured. Using a penalty function, those faces that violated the self supporting requirements were highlighted for the consideration of the analyst during post-processing. This interesting modification to the BESO algorithm can be considered a building block towards a fully process-aware automated optimization.

One of the key failings of the BESO method lies in the fact that it is not necessarily a tool that will provide the analyst with the ‘global optimum’. In any optimization problem, the global optimum is the point at which the analysis has produced a design that is closer to the required compliance than any other point in the design domain. Without additional knowledge and input from the analyst, there is a danger that a ‘local optimum’ will be produced, which is only optimum when compared with its direct neighbours. This is illustrated in Figure 2.4 and discussed in greater detail in [Rozvany \(2009\)](#) and [Aremu et al. \(2010\)](#).

A secondary concern of the BESO method is its propensity to generate structures that contain either ‘stair-casing’ or ‘checker-boarding’. A great deal of work has been conducted to address these failings, resulting in smoothing mechanisms which assess the structure in the current iteration and filter out the numerical instabilities which lead to checker-boarding ([Fujii and Kikuchi, 2000](#); [Sigmund and Petersson, 1998](#)).

### 2.11.2 Solid isotropic material with penalisation

The SIMP method, as originally discussed by [Bendsøe \(1989\)](#), is perceived to have advantages over BESO algorithms due to a key difference between the two methods: Though both use FEA to determine the ideal material distribution for a given problem, SIMP uses a ‘relative density’ that is characterised by an integer from 0 to 1, whereas BESO simply applies values of 0 or 1 to each element to denote its density. The term



used to govern the relative density in the SIMP method is ‘penalization’. The Young’s Modulus of the material is interpolated using the penalisation value arrived at using Eq. (2.23). Figure 2.13 illustrates this concept: the BESO method, Figure 2.13(b), identifies which elements in the design space are active or inactive by assigning a 1 or 0 respectively, the SIMP method, Figure 2.13(c), gives the elements an integer between 1 and 0 based upon the penalized Young’s Modulus. The analyst is free to define the cut-off where elements will be removed from the domain, typically this is 0.5.

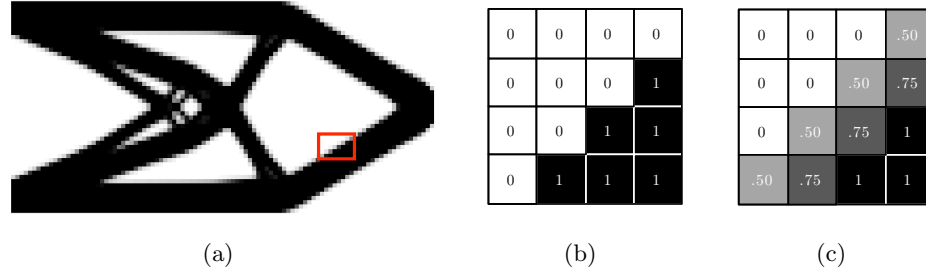


FIGURE 2.13: Comparison of how different approaches apply density to elements in a small area of a typical topology optimization: (a) a typical resulting structure; (b) the BESO method identifies which elements in the design space are active or inactive by assigning a 0 or 1 respectively, and (c) the SIMP method assigns the elements a value between 0 and 1 based upon the penalized Young’s Modulus.

$$E = E_0 \rho^p \quad p > 1 \quad (2.23)$$

Where  $E$  is the new interpolated Young’s Modulus of the material,  $E_0$  is the original Young’s Modulus of the material,  $\rho$  is the material density (0 to 1) and  $p$  is the penalisation factor.

There currently exist a number of additional mechanisms which can be applied to SIMP problems. By far the most commonly used is the Optimality Criteria (OC) method (Zhou and Rozvany, 1991), which utilizes the strain energy of each element to determine whether that element’s density should be increased or decreased at the next iteration. Using the objective function and the applied constraints, a Lagrangian function is formed which is then solved to find the appropriate multiplier for the updated density value. As is common with the BESO algorithm, a filter is applied to the results to prevent numerical instabilities (Sigmund and Petersson, 1998) by averaging the elemental sensitivities within a user defined radius (usually defined  $r_{min}$ ).

More recently this method has been applied to 3D problems, for example by Liu and Tovar (2014), who have successfully created a MATLAB program to optimize 3D topologies in just 169 lines of code. This code has the option to add a number of different filters to the algorithm to produce a concept that would be closer to a working design.

The code can make use of an iterative solver to analyse problems of a larger scale on relatively low-powered PCs or laptops, and also output a Standard Triangle Language (STL) file of the resulting structure. This output, however, consists purely of cuboid elements and does not constitute a final design.

Figure 2.14 shows the benchmark problem solved using a SIMP algorithm<sup>2</sup>. It is clear that the elements on the very edges of the structure exhibit a wider density distribution than the simple binary as evidenced by the BESO method (Figure 2.12). The shading of the elements from white to black begins from a density threshold of 0.5.

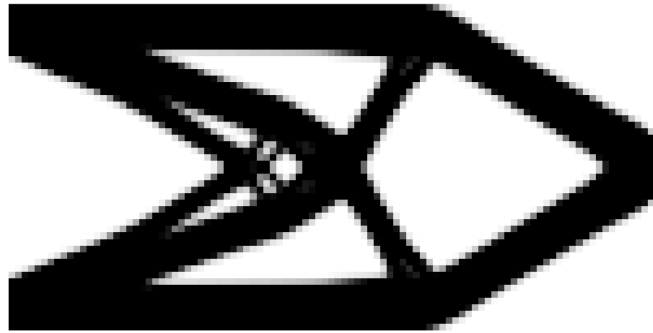


FIGURE 2.14: Michell cantilever beam optimized using SIMP with  $100 \times 50$  elements resulting in a compliance of 63.897

Rozvany (2009) and Huang and Xie (2010) draw comparisons and highlight the relative advantages and disadvantages between of the BESO and SIMP methodologies; the conclusion that can be drawn is that over the time since their inception each method has been adapted and updated, and today the two have similarities. As previously discussed, the fundamental difference remains in the way each method deals with the density of the elements in the problem. The SIMP approach is arguably likely to produce results which are closer to the mathematical optimum than the rather blunt on/off methodology of BESO. With this in mind, it is critical to remember that neither method will guarantee the global-optimum and that both methods are capable of providing very similar results in a similar number of iterations, as shown in Figures 2.12 and 2.14.

### 2.11.3 Applications of topology optimization

There have been several instances of topology optimization being applied to aerospace structures in academic literature, unfortunately these have yet to be employed in passenger carrying applications, a few notable studies are provided below for context.

<sup>2</sup>Produced using the 99 line topology optimization program as detailed by Sigmund (2001) and available from <http://www.topopt.dtu.dk>

[Zhu et al. \(2016\)](#) explored the application of density-based topology optimization to multiple examples of aerospace components, where light-weighting was the primary objective whilst maintaining structural load capacity. This study included: a single component which was optimized to generate a materially efficient design for casting; a complex structural pylon which a very high load capacity; and multiple examples where several component are arranged efficiently to form a larger assembly. The conclusion was drawn that while topology optimization proves itself to be a powerful tool, there are still limitations observed when addressing more demanding applications and suggests that more innovative algorithms should be created. [Satya Hanush and Manjaiah \(2022\)](#) provided a study of an engineering bracket which has been optimized using topological methods, the motivation being the reduction in material used at the manufacturing stage and hence cites the use of additive manufacturing as a production method. The analysis of the part identified that a 45% weight reduction could be achieved whilst still maintaining a suitable safety factor. No comment is given as to the process by which the analysis results were converted back to a CAD model suitable for manufacture, however conclusions have been drawn to understand the best orientation to ‘print’ the part. Finally [Karabiyik et al. \(2022\)](#) presented a topology optimization methodology that accounts for the natural frequency constraint in a compliance minimization process to address the challenge of optimizing for both strength and avoidance of excitation. This is successfully demonstrated on two aerospace examples, the ‘GE Bracket’ which has become synonymous with topology optimization problems as well as a satellite bracket. This study does provides details concerning the translation of the geometry from analysis to CAD, and highlights that current capability for NURBs based tools are limited to overlaying new geometry onto the optimization results following the designers ‘instinctive decisions’. However, no details concerning the time taken on this step are provided.

## 2.12 Additive manufacturing

For over 30 years additive manufacturing (or ‘3D printing’) has been used for the rapid prototyping of components as part of the design process, whether this is to demonstrate components fitting into an assembly, or for non-destructive or destructive testing. There are many forms of manufacture under the umbrella of AM: StereoLithography (SLA), Fused Deposition Modelling (FDM), and Selective Laser Sintering (SLS) are among the most widely used. All AM methods follow a similar process: a multi-axis machine head follows a pre-defined route whilst simultaneously melting and fusing material in order to form a three dimensional structure; however the melting technique and material deposition method varies. In a Direct Laser Deposition (DLD) or Electron Beam Melting (EBM) process the energy is directed towards a bed of powder material and follows the

pre-defined path. It simultaneously melts and fuses the powder to the build plate or the preceding layers to generate the three dimensional form. Once the build is completed the un-sintered powder is removed to reveal the finished component. In an FDM process, the material is passed directly to the head, where it is melted, and then pushed out of a nozzle following the pre-defined pattern devised by the engineer or software. Once completed it is a simple case of detaching the part from the build plate and removing any support material. Regardless of the method used to build the part, the form of the component originates in a 3D CAD model.

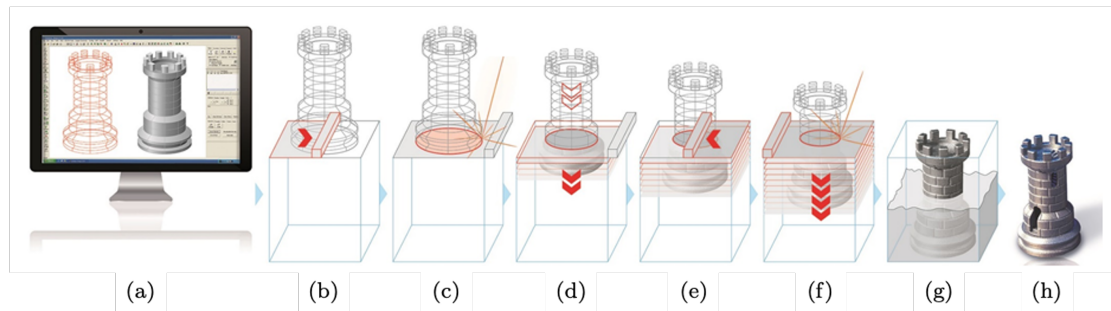


FIGURE 2.15: Typical workflow for a laser powder bed AM process: (a) generation of CAD data and slice file; (b) first layer of powder is laid into the build chamber; (c) the laser scans the outer profile of the part followed by the infill; (d) the platform lowers and the next layer of powder is added (e); (f) stages (c) - (e) are repeated until the full height of the part is reached; (g) the excess powder is removed from the built part to be recycled; and (h) the completed as-built part ready for post-processing. Image adapted from similar by EOS GmbH.

Due to the fact that AM is a layer-by-layer process, parts may be designed with significantly greater complexity than those that could be produced by traditional subtractive methods (turning, milling, drilling etc.) without having a significant impact upon the overall cost of manufacture (Brackett et al., 2011). This inherent complexity that comes seemingly for free allows the engineer a greater freedom when designing the part, and may allow parts to be physically realized closer to the optimum design than ever before. AM is not without its limitations. Application of the technology is fairly new and so its process parameters are not yet fully understood, meaning that there may be unforeseen problems with the manufacture of parts, sometimes leading to defects that cannot be seen with the naked eye. It is therefore critical that the designer be provided with the correct tools to identify where the optimum point in the design space is whilst also being robust enough to accommodate variables in the manufacturing process.

Additive manufacturing is an umbrella term which covers many technologies, summarised below:

**Material Extrusion:** Undoubtedly the widest known AM technology, material extrusion has the capability to produce components on a wide variety of scales, from

micro-electronics to large-scale construction. The primary material of an extrusion process is a thermoplastic that is laid down from a nozzle in beads ranging from 0.1-4.0mm in thickness depending on the machine and the application. The mechanical properties of the part are governed by the fundamentals of the process, ensuring that the next layer is successfully bonded to the previous one, however due to this directionality the final parts are generally anisotropic without further processing. As this is a wholly net process, i.e. there is no powder bed, supports must be provided for all features that overhang the previous layer to avoid unnecessary distortion. In more modern machines, the support process is improved by the use of multi-material feeds enabling supports that easily snap off or can be dissolved away in a solution subsequent to the build. Some materials may be further processed after the build to improve the surface finish, such as mechanical or vapour polishing. These technologies are useful for prototype work but the inherent anisotropy of the built component significantly limits their performance, something which should be considered in the orientation of the part.

**Powder Bed:** Powder bed fusion processes come under many different names, however they all follow the same basic principal of operation. Each can build parts of highly complex geometry in a wide range of materials, though typically limited to those materials that are suited to casting. Components produced by powder bed process often achieve theoretically 100% density of material with a layer resolution down to around 0.02mm. However, the processing that occurs in the build chamber induces significant temperature gradients which can result in residual stresses in the part, thus it is necessary to consider part orientation as well as the proposed scan pattern to ensure that these stresses are limited. It is usual that the component will have a post-build heat treatment applied before it is separated from the build plate. Though a powder bed process can provide some level of support, overhanging features usually still require supports which will need to be initiated from the build plate or an adjacent surface of the component. It is possible to build overhanging features of a few millimetres in length, enabling the construction of lattice structures. A notable exception to this is Selective Laser Sintering (SLS) of polymers, where support structures are not required at all. One limitation, due to the inherent nature of the powder bed, is that the supports must be of the same material as the component itself, necessitating their removal by mechanical means following build and post-build heat treatment. It is also often necessary to improve the surface finish of the component due to stress/life requirements or the need to interface with other components in the assembly. This may be accomplished by a number of methods, machining being the most common.

**Vat Photopolymerisation:** More commonly known as StereoLithography (SLA), this process involves exposing a layer of photo-curable liquid to a scanning laser, UV light source, or a high resolution projected image. Exposure of the liquid initiates a chemical

reaction which transforms it into a cross-linked solid. Machines are available capable of producing parts in the millimetre and meter scales therefore photopolymerisation is suitable for the production of prototype components, models for presentation purposes, short-run tooling as well as some medical devices. It has been successfully used to produce a number of parts for development programmes where the cost of mould tooling for polymer parts would be prohibitive. Parts produced via photopolymerisation usually require a post-build curing to ensure that the part has the required mechanical properties; this then gives the part isotropic qualities. As with many AM processes photopolymerisation requires supports as part of the build for overhanging features, adding to the cost of the material utilisation as well as the post-processing time. In its favour the surface finish of this process can be much better quality than other AM processes, requiring a minimal amount of polishing. A wide range of materials are available depending upon the chemical make-up. In addition to polymers which may be elastic or rigid, it is possible to infuse the resin with metal or ceramic compounds which may be consolidated by post-build sintering.

### 2.12.1 Additive manufacturing benefits

**Rapid Prototyping/Manufacture:** The adoption of AM technologies has been prevalent in the conceptual design phase; the ability to define a CAD model of a part and produce a physical model can be invaluable in iterative problem solving. This ability has evolved more recently to incorporate the use of AM in the production of tooling for low volume components (prevalent in the aerospace sector). The parts themselves may also be produced from AM technologies negating the need for tooling completely. Such advances encourage continuous improvement in designs, improving performance and lowering cost and weight (Singamneni et al., 2019).

**Part Complexity:** An oft-quoted maxim for AM is ‘*complexity for free*’ (Kirchheim et al., 2018) and when compared with traditional machining methods it is true: AM has the ability to produce functional part designs which are no longer constrained by traversing a cutting tool through limiting cartesian coordinates. Advantages may be taken from this complexity: multiple parts in an assembly may be consolidated together removing the requirement for welding or fabrication processes, pipework may be routed in a manner which reduces the losses in the system or advanced cooling passages may be incorporated into parts, Figure 2.16. Significant weight reductions may be achieved through the use of optimization techniques, most prominently topology optimization. Further light-weighting may be achieved through the use of lattice or honeycomb structures in places which would traditionally have been solid metal; such structures can be multi-functional and used for heat dissipation as well as structural purposes. When

combined with the rapidity of AM, these complex designs can be produced, built, and tested in very short timescales improving the overall design process.

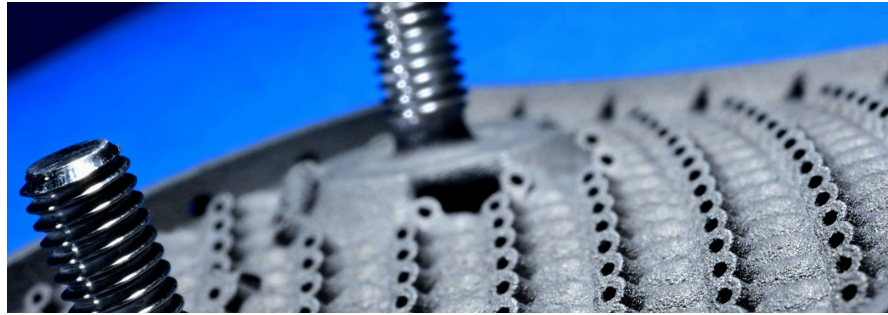


FIGURE 2.16: AM has unlocked the ability to produce complex cooling passages in engine environment hotter than the melting point of the material used. Image courtesy of Rolls-Royce Plc.

**Sustainability:** When compared with traditional methods of manufacture, where a component may be machined from a much larger bar or forging, AM is a near net solution, the final component being machined from a much smaller starting point. In aerospace this is referred to as the ‘buy-to-fly’ ratio, commonly in the region of 15-20 for conventional machining (15-20 times the final component mass is required at the initial blank stage) whereas AM can have a buy-to-fly ratio as little as 1. This has multiple benefits: less machining needs to be carried out, reducing both tool wear and processing time; less material is wasted compared with conventional machining; and reduced overall costs through processing and shipping of smaller components. Specific to a powder bed process, any un-melted powder can be collected and reused repeatedly in subsequent builds leading to an estimated 90% reduction in material wastage and this has a direct impact upon the cost of the component. Aerospace materials are very expensive, with the market reportedly worth US\$21b in 2020 projected to rise to US\$32b by 2027 ([Global Aerospace Materials Industry, 2022](#)). Additive manufacturing can also be used in cases where product tooling may no longer be available or the cost to reproduce it is prohibitively expensive. Instead the component may be produced to drawing directly, or with minimal post-processing machining.

### 2.12.2 Additive manufacturing challenges

Whilst there are many benefits to additive manufacturing, there are also several challenges which remain and should be addressed to build confidence in the technology for demanding environments or industries with stringent safety regulations:

**Design for AM:** Though there have been a great number of contributions in the field of design for additive manufacture (DfAM) ([Tomlin and Meyer \(2011\)](#), [Reddy K et al.](#)



(2016) and Shi et al. (2020) e.g.), there are still a number of challenges. AM offers a level of complexity in part production which can be difficult for the tool generally in use in traditional manufacturing methods. Geometry creation tools require the ability to accurately and efficiently model highly complex components, often containing thousands of features, whilst also having in-built knowledge of the limitations of the AM process such as orientation and surface overhangs; build simulation also offers the ability to predict residual stresses, minimising thermally induced distortion, with the goal of reducing the number of supports required during the build. Such complex design and simulation requires highly skilled engineers, computational power, and well defined material databases to be effective. Lack of maturity at the conceptual stages of the design can lead to non-optimal load paths or designs which are ‘over engineered’ and have unnecessarily high safety margins. Such components will often be overweight, having an impact upon fuel efficiency. The challenge in design is to catch up with the ever evolving technology at the forefront of AM production.

**Certification:** The components used for aerospace applications are subject to stringent regulations from the certifying authorities (EASA, FAA e.g.) before they can be proven suitable for flight. This process requires that every aspect of the component, from its design and analysis, to the manufacturing process, be scrutinised and shown to be consistent and repeatable to the certification authorities. Development of a product to meet the safety rules requires that the Original Equipment Manufacturer (OEM) gains the knowledge and proves that every process involved in the production of a component has a level of risk that is ‘As Low As Reasonably Practicable’ (ALARP). Limitations associated with dimensional non-conformance, process limitations, poor surface finish, lack of part-to-part repeatability are some of the challenges in the certification of AM parts. Certification standards are developing all the time, especially in fast moving fields such as AM. The report by the AIA Additive Manufacturing Group (2020) details some of the current industry best practices covering: development of materials and processes; destructive and non-destructive verification techniques; part and system qualification; and different means of compliance to applicable regulations. This report concludes that the part qualification and its certification can successfully be achieved using the proven established methodologies as a baseline, supplemented with additional focus on issues which are specific to AM.

**Structural Integrity:** Traditionally manufactured aerospace components are routinely subjected to a number of dynamic loading types, such as Low Cycle Fatigue (LCF), High Cycle Fatigue (HCF), thermal cycling, and loads associated with acceleration and deceleration. These are well understood, and the components designed to react such loading within their predicted life. Once the life limit has been reached, it is possible for the component to fail. Additively manufactured parts, however, do not have the



decades of knowledge and materials data behind them to predict lives for LCF and HCF as easily. This lack of knowledge is compounded by inherent defects which may occur in the part through the manufacturing process such as porosity, residual stresses, and poor surface finish. Recent work by [Gupta et al. \(2022\)](#) has endeavoured to fill this gap by producing sample components and test bars to generate HCF lifing data for Ti-6Al-4V, however it will take time before this data is in regular use in industry.

## 2.13 Aerospace design

Aerospace engineering covers all aspects of the aerospace sector including but not exclusive to: civil aircraft (large airliners and business jets), military aircraft, space launch systems, satellites, and missile systems. It has been a traditionally lucrative sector, however a decline in aircraft flying hours have been seen as a result of the SARs COVID-19 pandemic, and growing awareness of the impact of flight on climate change. Despite this, however, the sector is predicted to grow to a revenue of US\$430b by 2025 ([Blakey-Milner et al., 2021](#)) driven by committed long-term orders for large aircraft, global military expenditure, and adoption of sustainable aviation fuels.

Design of products in the aerospace sector is subject to stringent regulations from the FAA/EASA ([Hiemenz, 2020](#)) however with the requirements for weight and fuel burn becoming ever more challenging the products are becoming more complex and there is a greater drive towards lightweight components. To facilitate this desire for lightweight parts, the aerospace sector has been a rapid adopter of additive manufacturing for not only end use parts but also tooling, testing equipment, and design aids. AM is enabling the aerospace sector to become more agile in reducing costs and lead-times for products with tight timescales ([Hiemenz, 2020](#); [Singamneni et al., 2019](#)); as a result there has been significant research and investment in AM over the last 10 years ([Blakey-Milner et al., 2021](#); [Singamneni et al., 2019](#)). There are currently more than 20,000 medium-large commercial aircraft in operation worldwide, and a further 15,000 small business jets. With fleet sizes expected to double over the next 20 years there is a strong case for the greater exploitation of AM technologies in the improvement of aerospace products. Due to the very high level of complexity of aerospace design, specifically in the design of turbo-machinery, there are very few manufacturers who are certified for the production and maintenance of aircraft. Typically the design of any component would be subject to the following requirements:

**Safety:** The number one design aspect considered is always safety. Aerospace components operate in a harsh environment with temperatures ranging from  $-65^{\circ}\text{C}$  outside

the aircraft to 1800 °C in the combustion chamber of the engine, G-force loading, vibration, and a mixture of fuel and oils, all of which must be considered in the design of the products to ensure the safety of those on board and also on the ground.

**Fit, Form & Function:** Aircraft production is a highly complex and highly skilled process and therefore it is essential that all parts brought to the build-line are designed to be as accurate as possible. Careful attention must be paid to the interfaces of the parts to ensure that they can be assembled correctly. The form of the component should be robust enough to be tolerant to small amounts of damage that may occur during its operational life, whilst not being overly large or heavy. And the function of the product must be met, often through the build up of several smaller parts in to highly complex assemblies.

**Certification:** As noted above, all components that go into an aircraft system are subject to the requirements laid down by the governing aerospace bodies, the FAA and EASA. There are different levels of criticality that the parts will need to meet based upon their function. The regulators need to ensure that the products introduced into service are well designed and may be repeatably produced to the same high level of accuracy to ensure safety over the operational life.

**Cost and Lead-time:** Two factors that are important, but are sometimes at odds with the other requirements. Whilst it may be a requirement to design a highly complex part, it would not be acceptable for that part to consume 90% of the budget! Careful management of the cost of the part is maintained through the design process. The time it takes to manufacture the part must be considered: with timescales for introducing new products to the market becoming ever tighter, it is essential that unnecessary delays or lengthy processes are reduced to a minimum.

**Sustainability:** Fuel burn is a critical criterion in aerospace and most, if not all, designs will be evaluated against it in some way, be it a direct impact on aircraft drag or simply the weight of a component. Traditionally, this was evaluated based on the cost of the fuel burned, however more recently this has changed to the quantity of fuel burned and the associated emissions. Light-weighting has always been a mainstay of aerospace design with all unnecessary mass reduced from a part (to a defined factor of safety). The buy-to-fly ratio is a key consideration, the difference between the mass of the finished part vs. the block of material it is produced from, and a good deal of work is performed to ensure that the minimum amount of material should be wasted during production. This results in a part that not only requires less fuel to lift it into the air, but also less energy expended during its production, and all material ‘swarfed off’ in production will be recycled. It is estimated that every kilogram of weight reduced from an aircraft will

save around US\$3000 worth of fuel and the associated emissions per aircraft per year (Singamneni et al., 2019).

There is a high degree of both harmony and conflict between these requirements which often leads to a compromise in one requirement to ensure that another is satisfied. These decisions are usually taken using a knowledge-driven approach to justify the choices made. This is not only sound engineering process, but a requirement for certification of the design. Ultimately the final part will be the optimal compromise between all of the laid out requirements.

### 2.13.1 Design for weight and CO<sub>2</sub> reduction

The convergence of Design for Additive Manufacturing (DfAM) and sustainability underscores the demand for lightweight components. A significant advantage of this approach is the potential to curtail fuel consumption in aircraft, contributing to environmental benefits. Currently, burning of 1 kg of aviation fuel (JET-A) results in the emission of 3.2 kg of CO<sub>2</sub> into the atmosphere. In 2019, the aviation industry consumed approximately 250 million metric tonnes of JET-A, leading to over 800 million metric tonnes of CO<sub>2</sub> emissions annually (RAeS, (2022)). Therefore, any reduction in material weight from a component translates into a substantial decrease in CO<sub>2</sub> emissions throughout the product's lifespan, typically 20-30 years.

To diminish the specific fuel consumption and, consequently, CO<sub>2</sub> emissions of a typical wide-body aircraft by 1%, a weight reduction of approximately 907 kg is required. For instance, a Boeing 787-8 Dreamliner powered by Rolls-Royce Trent 1000, covering the distance between London Heathrow and São Paulo<sup>3</sup> (5155 nm), consumes 19 010 kg of fuel, emitting 60 832 kg of CO<sub>2</sub>. Reducing the aircraft weight by 907 kg results in a 1% fuel consumption reduction, saving 608 kg of CO<sub>2</sub> on each flight. The relationship between a decrease in component mass and a corresponding reduction in CO<sub>2</sub> emissions can be expressed by the following formula:

$$\Delta_{CO_2} = 3.2(\beta \cdot \Delta_w) \quad (2.24)$$

where  $\beta = 0.01F_t/907$ ,  $F_t$  is the total fuel consumed for the flight prior to re-design and  $\Delta_w$  is the weight reduction achieved from the re-design activity. It should be noted that this formula assumes that the component(s) modified have no effect upon the aerodynamic performance of the aircraft. Additionally, this formula determines the reduction in CO<sub>2</sub> *per flight* where in practice a large civil airliner may make in

<sup>3</sup>Aircraft Commerce, Issue 121, Dec 2018/Jan 2019

excess of 50,000 flights in its lifetime. In addition to the highly important reduction in CO<sub>2</sub>, reduced fuel burn also has an economic impact. Revisiting the flight from London Heathrow and São Paulo and with the average price for JET-A1 predicted to be \$0.85/kg over 2023<sup>4</sup> if a 1% reduction in fuel burn can be achieved through weight reduction this equates to a saving of \$162 per flight for the operator; a seemingly small amount per flight but equates to \$8.1m over the life of the aircraft, not accounting for fluctuations in fuel price.

### 2.13.2 Frequency analysis for damage prevention

In the design of modern engineering components many considerations need to be taken into account including safety, cost, weight, and manufacturability. The most prominent of these is safety, taking account of the regime of applied stresses to be sustained over the life of the component. Safety is influenced by the properties of the material employed, which may change as the design evolves. When considering structures that include slender elements in compression, it is necessary to check for buckling instability to ensure safety is maintained. Another key parameter in the aerospace sector is the harmonic frequency of a structure, which should lie outside of the frequency bands of surrounding components. Should a fundamental frequency of one component (e.g. a bracket) overlap with those of its attached neighbours, then resonance in the component may occur, also referred to as forced vibration. Forced vibration and resonance can then lead to HCF in the component, affecting its serviceable life and reducing its time to failure. It should be noted that a component may exhibit multiple resonant frequencies, each corresponding to a mode of vibration, and repeated exposure to these frequencies may reduce the life of the component.

In turbo-machinery the primary source of vibration arises from the interaction of air flowing between static and rotating stages of blades and vanes. This interaction is referred to as Engine Order (EO). Analyses are conducted to fully understand the numbers and frequencies of each EO for the machine, and the resulting values are plotted on a Campbell Diagram, Figure 2.17. The diagram plots frequencies against engine speed. The engine orders emanate from the origin of the diagram in a series of spokes, shown dashed, and each one corresponds with a potential source of resonance excitation. Interpolated frequencies for various modes of vibration for the component being analysed are superimposed on this diagram, shown blue-solid, and anywhere that there is an interaction with an engine order is highlighted, ○. In cases where these circled interactions occur at a dwell speed for the machine, such as max take-off or cruise for an aero engine, then a re-design will be necessary to ensure that no HCF related hazards can occur.

---

<sup>4</sup>Data from: <https://jet-a1-fuel.com/forecast>

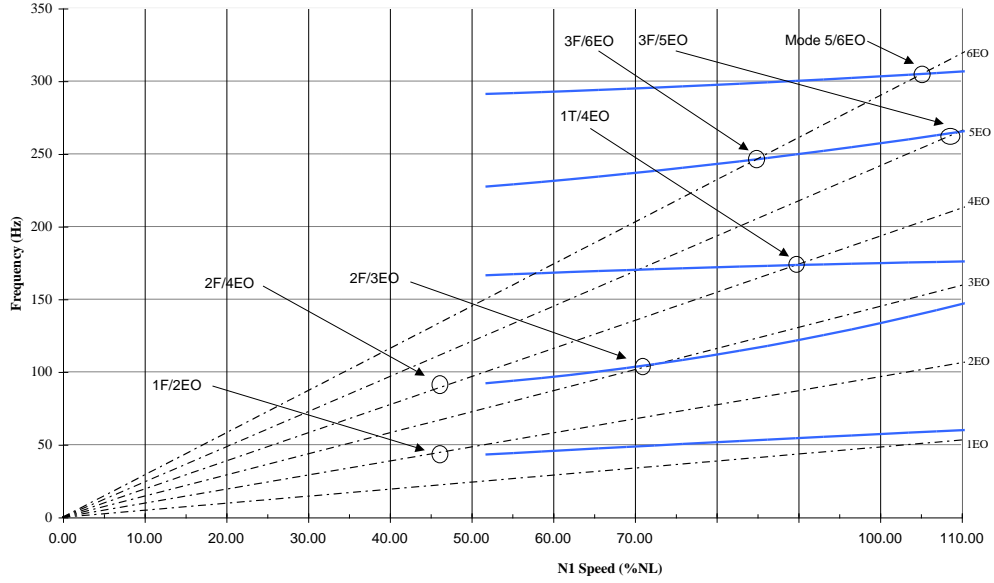


FIGURE 2.17: An example Campbell Diagram showing engine orders, dashed, as sources of resonance. Interpolated natural frequencies are laid on top of the engine order lines to determine where resonance may occur.

There have been numerous recorded HCF-related incidents. A notable example led to the loss of British Midland flight #92 in 1989 (Cooper, 1989). This was initiated by the failure of a fan blade on one of the two CFM International S.A. CFM56-3 turbofan engines. A single blade failed due to a coupling of torsional-flexural transient and non-synchronous oscillation, leading to rapid reduction of the HCF life of the blade. The blade was subsequently released, causing high levels of vibration in the engine and aircraft, contributing to the loss of the aircraft upon attempting an emergency landing at East Midlands Airport in the UK.

## 2.14 Conclusions

The review of available literature has discussed a number of topics and existing research relevant to this thesis and the following conclusions have been drawn; identified shortcomings will be addressed in the following chapters:

- a) There have been numerous studies into the application of topology optimization to aerospace engineering problems (section 2.11.3); however in many cases there has been little demonstration of the remodelling work that is required to move from the numerical results to a fully formed CAD geometry. Furthermore, there are few real-world examples of truss layout optimization being applied to complex engineering problems as a competing technology to topology optimization, and therefore the

salient advantages and disadvantages are not widely known. Previous studies relating to either optimization technique have not fully considered the impact that available weight reduction may have on climate change.

- b) Whilst a number of studies have endeavoured to use automated optimization to control the natural frequency of a truss structure, many have employed heuristic approaches to pre-defined structural forms, for example size optimization of an existing component. Where techniques similar to layout optimization have been used the results have often taken a long time to solve, little evidence has been shown that any have taken advantage of the efficiency improvements available through use of the ‘member-adding’ algorithm.
- c) The influence of the initial form of the layout optimization ground-structure has been studied by [Gilbert and Tyas \(2003\)](#) in terms of computational efficiency for problems solvable via linear programming; however no such study exists for more complex problems requiring semi-definite programming methods, the use of which would make solving problems such as those involving eigenvalues, much more efficient.
- d) Whilst there have been several examples of both layout and topology optimization being applied to truss structures with both compliance and frequency constraints there have been no studies conducted concerning the automated optimization by semidefinite programming of frames using a ground-structure based layout optimization. Frames provide a more appropriate representation of continuum structures indicative of components that may be produced by AM methods and their viability should be assessed.

## Chapter 3

# A comparison of truss and topology optimization as effective tools for reducing mass and CO<sub>2</sub> emissions of aerospace components for production by AM<sup>1</sup>

The climate crisis is driving sectors such as aerospace to take steps to reduce their CO<sub>2</sub> emissions. As well as opportunities to replace kerosene with a more Sustainable Aviation Fuel (SAF) or hydrogen, there is an immediately achievable approach: weight reduction of the component parts of an aeroplane, as this directly correlates with a decrease in CO<sub>2</sub> emissions. Additive manufacturing (AM) is a key technology that can potentially be used to unlock large weight reductions; therefore choosing an appropriate AM component design tool is critical. Topology optimization has long been considered as *the* tool to identify the lowest weight additive designs; however there remain challenges in transitioning from raw optimization results to usable CAD models for manufacture. Where design freedom is significant, truss layout optimization provides an alternative means of optimizing parts, allowing a final geometry to be generated as part of a simple workflow, reducing the time required to remodel raw numerical solutions by approx.

---

<sup>1</sup>The content of this chapter has been prepared for a journal paper: S. J. Salt, M. Gilbert. A comparison of truss and topology optimization as effective tools for reducing mass and CO<sub>2</sub> emissions of aerospace components for production by AM. *Additive Manufacturing*, in review.

70%. This contribution compares the use of topology optimization and truss optimization for two aerospace component case studies, highlighting the benefits and challenges associated with each. It is demonstrated that although each approach can be used to reduce weight, and hence CO<sub>2</sub> emissions, there are differences in the computational costs and remodelling times involved.

### 3.1 Introduction

An aerospace component has the required level of structural integrity when the part is sound and unimpaired such that it can provide the desired level of structural safety, performance, durability and supportability (MIL-STD-1530D, 2016). Robust structural optimization tools provide a designer with the ability to generate lightweight designs that still meet structural performance requirements. The most common technique employed to date is continuum topology optimization, perhaps most notably the solid isotropic material with penalisation (SIMP) approach (Bendsøe, 1989), which has been incorporated into a number of commercial FEA packages (e.g. Altair OptiStruct and Siemens NX). Consequently various examples of successful usage of this optimization approach are described in the literature, e.g. Tomlin and Meyer (2011), Shi et al. (2020), and Reddy K et al. (2016). For example, in the case of the RUAG satellite antenna bracket (Figure 3.1), the use of optimization is reported to have reduced component weight by 40% (EOS GmbH).



FIGURE 3.1: Example aerospace component: RUAG antenna bracket for the Sentinel satellite system. A weight reduction of 40% was reportedly achieved through use of topology optimization whilst maintaining strength and launch vibration requirements.

Image courtesy of EOS GmbH.

However, while topology optimization can be an effective tool, there are a number of issues that have limited the extent to which it has been embraced by designers in industry. These include the need to specify in advance the desired volume fraction (the proportion of the original design domain that will be occupied by material), which will generally



require a number of iterations to establish. Also there can be difficulties associated with moving from the mesh solution obtained to a usable CAD geometry.

Continuum topology optimization begins with a fully occupied design space, i.e. a solid block of material, which is then progressively reduced in size in line with the specified optimization criteria until a solution is found. In many cases this solution will exhibit similarities with an open truss structure, particularly if the degree of design freedom is high (i.e. if the target volume fraction is low). Thus in some cases it may be more efficient to instead use a method that seeks to identify truss structures directly from the outset. Hence, building on the early work of [Michell \(1904\)](#), [Dorn et al. \(1964\)](#) proposed a numerical layout optimization procedure for truss structures. With modern computers this procedure can now be used to produce highly accurate solutions in a short amount of time. This technique is very useful to identify both the optimal means of transmitting forces through a structure, and the associated volume of material required. However, the approach unfortunately often generates extremely complex structures that would be prohibitively costly to produce, or which simply cannot be manufactured via traditional manufacturing methods.

Fortunately, the latter limitation is greatly alleviated by using Additive Manufacturing (AM) techniques. The primary appeal of AM in the aerospace sector is the ability to produce lightweight geometry that, although potentially highly complex in form, possess the high levels of structural integrity required. AM parts can be categorised by the degree to which they deviate in form from a traditional non-AM part, and the concomitant risk:

- a) **Substitution:** A part is made via AM to the same shape and specification as the original and is therefore interchangeable.
- b) **Enhanced Substitution:** Additional performance is gained from the use of AM, e.g. lightweighting, cost reduction, yet the part still remains interchangeable with the original.
- c) **Exclusive Choice:** The extent of the changes made through the introduction of AM render the original component obsolete, or there are sufficient changes to the surrounding component interfaces that it is no longer interchangeable.

It is partially due to the level of risk, and the level of scrutiny that aerospace products receive, that many parts designed for AM to date have similar forms to those designed to be produced via conventional casting or machining techniques. However, using AM potentially allows us to realize the considerable advantages of truss layout optimization: the ability to produce structures where the optimum solution may only consume a small

fraction of the initial design domain, whereas in contrast topology optimization methods may require use of a minimum volume fraction of approx. 10% in order to generate reasonable outcomes (Aage et al., 2013). A number of studies (e.g. Allaire and Bogosel 2018; Leary et al. 2014; Weber et al. 2021) have been made into the design of additively manufactured components that can be produced with minimal or zero supports in the build. Though desirable, this additional constraint is not considered in this contribution as it's introduction constraining the minimum angle of structural members, has the potential to limit design freedom and move us away from truly minimum volume solutions. For aerospace applications, where volume or mass reduction is usually the main goal, it may therefore often be more appropriate to spend additional time in production removing supports with the knowledge that the lightest possible component has been produced.

This contribution is designed to compare the effectiveness of two optimization techniques that can be used to reduce material usage and hence CO<sub>2</sub> emissions by applying them to two example aerospace gas turbine components. The contribution is organized as follows: Section 3.2 provides greater detail pertaining to the optimization methods to be applied to the case studies; Section 3.3 discusses the various methods and challenges involved in translating the results of optimizations into CAD data; and Section 3.4 applies these optimization methods and remodelling activities to two aerospace component case studies, the results of which are discussed in Section 3.5.

## 3.2 Optimization techniques

This contribution focuses on application of optimization methods that can be employed to reduce the volume and hence weight of a component. This has a significant knock on effect on CO<sub>2</sub> emissions; see Section 3.6 for further details. Such optimized forms can potentially be produced via the use of AM techniques, though for the purposes of the present study manufacturing considerations are not considered in the optimization for the reasons outlined in the previous section.

### 3.2.1 Layout optimization

The objective of ground-structure-based truss layout optimization is to arrive at a minimum volume, and hence weight, structure whilst maintaining structural integrity. It begins by defining a design domain, which is the volume in which the optimized structure can reside. Boundary conditions and material properties are also defined to fully describe the problem; see Figure 3.2(a). Using a Cartesian grid, the design domain is

populated with a predefined number of nodes ( $n$ ) in the  $x$  and  $y$  directions (also in the  $z$  direction for 3D problems). It is then joined with potential connections ( $m$ ), or elements, such that each node is connected to every other node in the domain to form a fully-connected ‘ground-structure’, Figure 3.2(b). The fully-connected ground-structure is assumed to contain all possible constituent elements of the optimal solution. Constraints are introduced to ensure equilibrium is enforced at nodes, and to ensure that the cross-sectional area of each element is both a positive number and is sufficiently large to carry the internal forces, given the limiting stress of the material. The plastic single load case formulation can be written as follows (after Dorn et al. 1964):

$$\begin{aligned} & \text{minimize } V = \mathbf{l}^T \mathbf{a} \\ & \text{subject to } \begin{cases} \mathbf{B}\mathbf{q} = \mathbf{p}, \\ -\sigma^- a_i \leq q_i \leq \sigma^+ a_i, & \forall i \\ a_i \geq 0, & \forall i, \end{cases} \end{aligned} \quad (3.1)$$

where  $V$  is the total volume of the structure;  $\mathbf{l}$  is a vector of individual element lengths  $\{l_1, l_2, \dots, l_m\}$ ;  $\mathbf{a}$  is a vector containing element cross-sectional areas  $\{a_1, a_2, \dots, a_m\}$ ;  $\mathbf{B}$  is a suitable  $(2n \times m)$  equilibrium matrix containing direction cosines (for 2D problems);  $\mathbf{q}$  is a vector of element axial forces,  $\mathbf{q} = \{q_1, q_2, \dots, q_m\}$ , where  $q_i$  is the force in element  $i$ ;  $\mathbf{p}$  is a vector of applied loads and  $\mathbf{p} = \{p_1^x, p_1^y, p_1^z, p_2^x, p_2^y, p_2^z, \dots, p_m^x, p_m^y, p_m^z\}$  where  $p_j^x, p_j^y, p_j^z$  are the  $x$ ,  $y$  and  $z$  direction components of the load applied to node  $j$  ( $j = 1, \dots, n$ ). Finally  $\sigma^+$  and  $\sigma^-$  are, respectively, the limiting tensile and compressive stresses that can be sustained by the material. Problems of this nature can be solved using linear programming (LP).

When a fully-connected ground-structure is used problems become computationally expensive to solve when a large number of nodes are involved, since the problem comprises  $n(n-1)/2$  potential connections, where  $n$  is the total number of nodes. Once the optimization is complete, the majority of these connections will have an area equal or close to zero, and therefore do not contribute strongly to the final structure. To address this, an adaptive ‘member adding’ method was proposed by Gilbert and Tyas (2003), which is a customized column generation technique and can be shown to reduce the computational burden significantly in the case of large problems. In this approach, the initial nodes of the ground structure establish connections solely with their immediate neighbours, as depicted in Figure 3.2(c). This contrasts with the scenario in Figure 3.2(b), where every node is connected to all other nodes within the domain. Subsequently, elements are incrementally introduced into the existing ground structure from a list of potential connections. The decision to admit newly added elements to the solution aligns with

the Michell-Hemp criteria. Eq. (3.2), which specifies limits on the virtual strain ( $\epsilon_i$ ) experienced by each potential element ( $i$ ), given a prescribed limiting stress ( $\sigma$ ):

$$-\frac{1}{\sigma^-} \leq \epsilon_i \leq \frac{1}{\sigma^+}, \quad i = 1, \dots, m. \quad (3.2)$$

When utilizing column generation methods (Gondzio and Sarkissian (1996), Desrosiers and Lübbecke (2005), and Gondzio et al. (2013)), new ‘columns’ (problem variables) are added to the LP constraint matrix  $\mathbf{B}$  in (3.1). Once an iteration in the optimization has completed potential connections are ranked, and those most violating the criteria added for use in the next iteration. When no potential connections violating the criteria remain, the algorithm terminates. The solution obtained shown in Figure 3.2(c) is provably optimal, with the computed volume the same as that obtainable using a fully-connected ground-structure from the outset. An extra step, introduced by He and Gilbert (2015), may be performed to rationalize the optimized geometry further, to aid downstream processing and component production; see Figure 3.2(d).

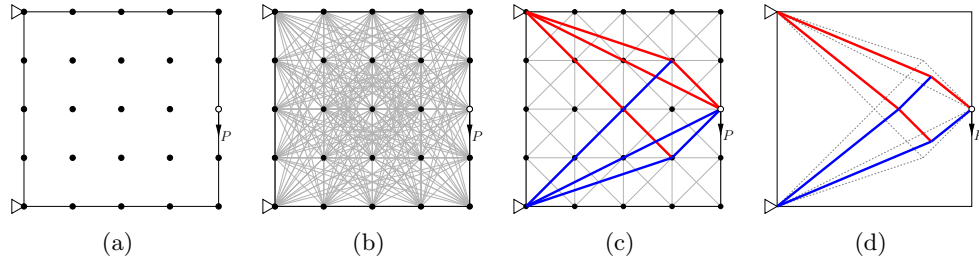


FIGURE 3.2: Steps in truss layout optimization: (a) design domain populated with equally spaced nodes; (b) each node connected to every other node in the domain to form a fully-connected ground-structure; (c) alternatively, each node is connected only to neighbouring nodes to form a minimally-connected ground-structure, with member adding employed to identify the optimized layout; (d) rationalized structure following geometry optimization step. Note that red and blue bars indicate those in tension and compression respectively.

Truss layout optimization may be used to generate 3D forms by introducing additional nodes in the  $z$  direction. However, as this increases the number of potential connections in the problem the use of member adding becomes essential to keep the computational burden manageable.

To undertake the 3D truss optimization studies described herein the software [Limit-State:FORM version 3.5.0, \(2019\)](#) is used. Using the truss layout optimization techniques described above, the software automatically identifies the most efficient arrangement of structural members for a specified objective. The adopted discrete representation of the problem differs from the continuum representation used in the more widely adopted topology optimization approach. After the initial layout optimization step is completed,

a secondary geometry optimization may be performed to further improve the solution by adjusting the positions of nodes leading to a cleaner layout, and also a small reduction in overall volume. Following these two optimization steps, the resulting structure can be converted into a monolithic body and then exported to other platforms for further refinement and/or manufacturing constraints. Due to the ease with which the geometry can be united and exported, this approach is particularly well suited to AM as it becomes possible to take full advantage of the ability of AM to fabricate complex parts.

### 3.2.2 Topology optimization

In contrast to truss layout optimization, where members are added to the structure as needed, topology optimization generally begins with a solid domain lying between loads and supports and then iteratively removes material where it is not needed. The umbrella term, topology optimization, today covers many different iterative techniques including:

- a) Evolutionary structural optimization (ESO) introduced by [Xie and Steven \(1993\)](#) is a design method that gradually removes inefficient material from a structure during the design process; the goal is to gradually evolve the structure toward the optimum shape. Initially the design domain is divided into finite elements, standard finite element analysis (FEA) is then used to calculate the Von Mises stress in each element. Elements with the lowest stress are systematically removed in each iteration. The overall aim of the process is to achieve a uniform stress distribution across the entire design space. The method was modified by [Chu et al. \(1996\)](#) who introduced a means of maximising the stiffness of the structure whilst maintaining a defined volume constraint.
- b) Bi-directional ESO (BESO) introduced by [\(Querin et al., 1998\)](#) allows for both element removal *and* addition within the design space during a single iteration. The key advantage lies in the time saving that is gained: the structure can evolve from a compact initial state rather than being reduced from a much larger design space. Due to its simplicity and efficiency, BESO has been incorporated into several commercial software packages, promising optimal design solutions for various problems.
- c) The Solid Isotropic Material with Penalisation (SIMP) method ([Bendsøe, 1989](#)) differs from ESO/BESO algorithms due to a key differentiator. Though both use FEA to determine the ideal material distribution for a given problem, SIMP assigns a relative value that is characterized by an integer from 0 to 1, whereas BESO simply applies values of 0 or 1 to each element to denote its density. Figure 3.3 illustrates this concept: in the case of SIMP, Figure (c), the designer is free

to define the cut-off where elements will be removed from the domain. The term ‘penalization’ is used to govern the relative density in the SIMP method. The Young’s Modulus of the material is interpolated using the following penalization relation:

$$E = E_0 \rho^p \quad p > 1 \quad (3.3)$$

where  $E$  is the new interpolated Young’s Modulus of the material,  $E_0$  is the original Young’s Modulus of the material,  $\rho$  is the material density (0 to 1) and  $p$  is the penalisation factor.

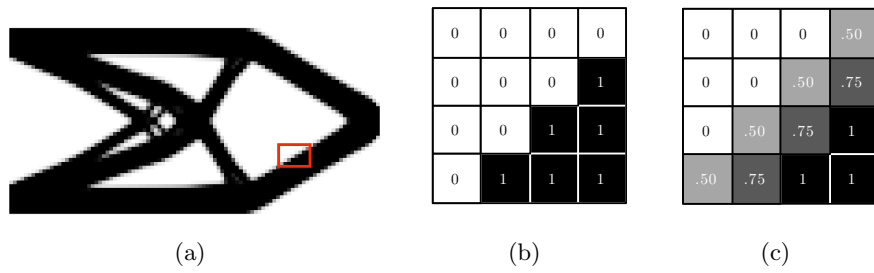


FIGURE 3.3: Comparison of how different topology optimization approaches apply density to elements: (a) typical topology optimization result; (b) the BESO method identifies which elements in the design space are active or inactive by assigning a 0 or 1 respectively; (c) the SIMP method assigns the elements a value between 0 and 1 based upon the penalized Young’s Modulus.

### 3.3 Remodelling of optimization results and workflow

Optimization is just one part of the overall workflow that must be undertaken to generate a component design from the domain stage to being ready for fabrication via additive manufacture. A certain amount of remodelling is usually required in order to achieve a final design, the amount depending upon the optimization method employed. Below is a description of what is involved in moving to a final form. A breakdown of the process for both truss and topology optimization methods highlights the steps required and draws comparisons. This basic workflow is followed in Section 3.4.

#### 3.3.1 Remodelling truss layout optimization results

The raw output from truss layout optimization is a collection of 1D elements that must be converted into a 3D continuum prior to manufacture via AM. For demonstration purposes it shall be assumed that these are converted into cylindrical members, though

more complex forms could be used. The process used in the LimitState:FORM application has been previously documented in detail (Smith et al., 2016), but to provide a comparison with Section 3.3.2 a brief overview is provided here. Once the optimum solution is identified, and the designer is satisfied that it represents an efficient structure following geometry optimization, the process begins. The first stage in translation to CAD is to create a cylindrical surface along the length of each element, the diameter of which directly corresponds to the area identified at the layout optimization stage, Figure 3.4(a). At this stage, it is convenient to generate a sphere at each node that is sized to accommodate the largest member intersecting that node, Figure 3.4(b). An additional lofting operation is then completed that further smooths the transition between each member at the joint, reducing the risk of high joint stresses, Figure 3.4(c). From this point, the body may be converted to a solid allowing further boolean operations to be completed, and the part may be freely exported as a NURBS file for use in further FEA validation processes, or preparation for an AM build. This process is highly automated and therefore takes little time and effort for the designer. Furthermore, since the resulting geometry represents very accurately the values obtained in the optimization routine, minimal errors are generated.

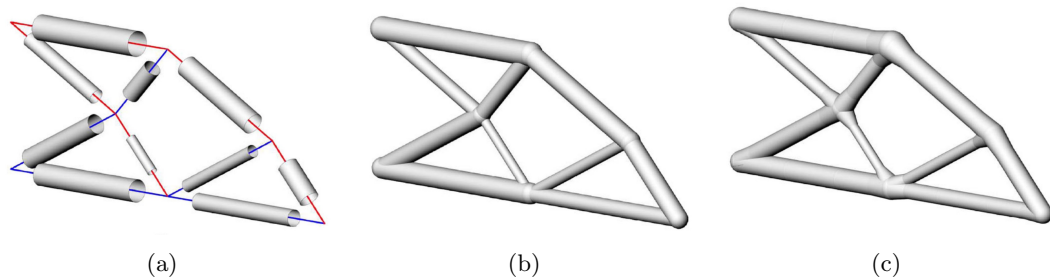


FIGURE 3.4: Translation of layout optimization results to CAD, after Smith et al. (2016): (a) surfaces are wrapped around each line element, representing the optimized cross-sectional area; (b) nodes are created at each end based upon the size of the largest intersecting member; (c) nodes are expanded and smooth transitions added, giving rise to a that may be exported e.g. via STL/STEP/IGES files to other software or directly to an AM machine.

### 3.3.2 Remodelling topology optimization results

As outlined previously, the outcome from a topology optimization study is generally mesh-based. Therefore additional operations must be completed to transform this mesh into a manufacturable geometry. This is complicated by the propensity for topology optimized structures to have a very organic appearance, comprising ligaments that may be curved and/or vary in area non-linearly along their length. This can make the structures very challenging to accurately represent, and challenging to inspect following manufacture. To remedy this a number of commercial packages have made available

processes which aim to convert mesh geometries into solids, ranging from simple sketch and boolean operations, conformal surfaces that seek to drape themselves over the mesh, to implicit modelling methods that generate models using a system of mathematical formulae. For the purposes of this contribution a method of forming surfaces over the mesh will be used.

PolyNURBS is a tool that has been created to partially satisfy the need to convert geometry resulting from a topology optimization into a fully united continuum that is ready for FEA and/or AM build preparation. In practice, it allows the engineer to wrap a surface around the mesh geometry using a series of algorithms to accurately construct the new surface over an undulating mesh. The action of smoothing out the elements means that some will lie within any new outer surface and others outside; therefore care must be taken to ensure that the structure remains intact and rational. The tool used as part of this contribution allows for NURBS surfaces to be stretched over a continuous length of a ligament; however it is not possible to automatically form joints at the intersections, something that remains a manual process for the designer to complete. Though the automatic creation of some of the surfaces goes a long way to reduce the burden of remodelling the optimized mesh, there is still considerable work to be done before a manifold solid can be produced ready for downstream processes. Unfortunately, once all the surfaces have been applied and united to create a solid, the ability to further edit the PolyNURBS is lost; thus if any changes are required the process must begin again from the mesh stage. This is not an issue when using the truss layout optimization workflow.

### 3.3.3 Workflow comparison

The major operations required when using a truss layout optimization workflow will now be compared with those required when using a topology optimization workflow (after [Cervantes Herrera 2015](#)); see also Figure 3.5.

Firstly, there are some operations that are common to both workflows, such as preparation of the models for optimization. Once the design domain, boundary conditions and material properties are defined, the optimization may be set up in the respective software packages. At this stage differences in the workflows become evident, with topology optimization generally requiring a number of initial runs to be performed in order to ascertain a suitable volume fraction to be employed; this step is not required when using truss layout optimization.

With both workflows a number of runs may then be undertaken, with the operator making changes e.g. to the design domain or material properties to gain an understanding



of the parameters influencing the outcome. At the end of this stage, in the truss layout optimization workflow the designer will be presented with a solution that satisfies the loading criteria and possesses the minimum possible volume, which will typically be near-globally optimal for the problem considered.

Once the initial optimization is completed, the design can then be refined to clean up the proposed geometry. At this stage, it may be necessary to change the design domain used in the topology optimization to ensure that material does not impede access to tooling or fastener access locations. This can be achieved directly in CAD by simply removing those ligaments, or by removing areas where material is not desired from the design domain entirely. In truss optimization a geometry optimization step is completed directly following the initial layout optimization step and has the effect of simplifying the structure, reducing the numbers of members and joints. Additionally, a level of manual intervention can be performed to select crossing members and create new joints, or delete any members crossing tooling/fastener access areas. The optimal layout for the members is then automatically recalculated following the user's edits. Remodelling of the geometry is carried out as detailed in Section 3.3, and the resulting bodies may be used in stress verification to assess elastic stress/strain and also prepare the components for an AM build.

It may be concluded that there are a greater number of steps to be taken when performing topology optimization when compared with truss optimization, but may also be noted that a number of operations in the latter are performed automatically.

### 3.4 Aerospace optimization case studies

In order to better illustrate the two optimization workflows discussed previously, two case studies have been chosen, each case has the entire design process, from initial concept to AM ready part, presented. For each case the components are designed with minimal manipulation following optimization, with fixed features and/or bolt holes added to the automatically generated design. Both case studies are optimized using the same toolset: topology optimization carried out using OptiStruct (included in [Altair HyperWorks version 2022, \(2022\)](#)); and 3D truss optimization carried out using [LimitState:FORM version 3.5.0, \(2019\)](#). Modelling of the design space and remodelling of the optimized results is conducted in [Siemens NX version 1973, \(2020\)](#). The optimizations were carried out on a 64bit Windows 11 desktop PC equipped with an Intel i5 3.7GHz processor and 32Gb RAM.

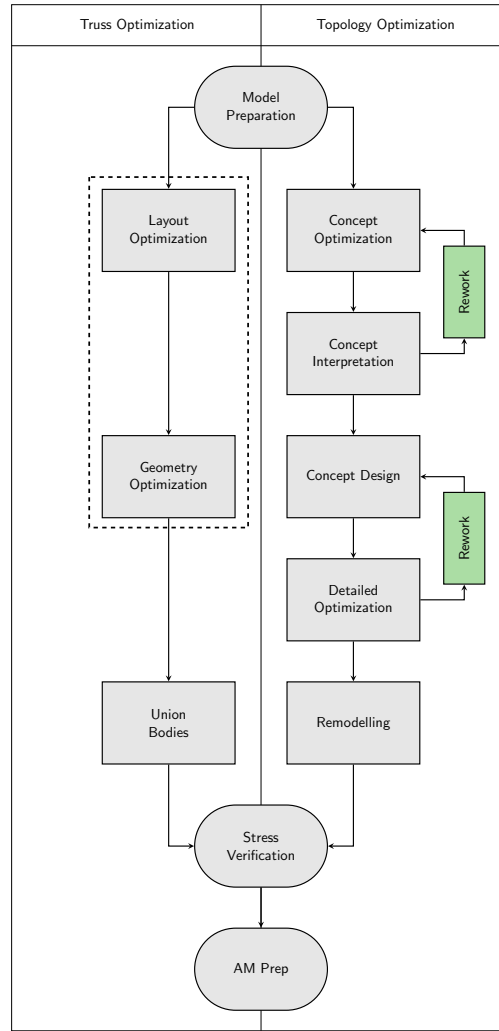


FIGURE 3.5: Flowchart of major operations conducted as part of workflows for topology and truss optimization. Note that the operations in the dashed box are fully automated in truss optimization.

Aerospace applications have been selected specifically as there are significant benefits in employing optimization techniques in order to ‘lightweight’ components, which may be realized physically via additive manufacturing. In the studies undertaken a minimum radius of 1.6 mm (cross-sectional area of 8 mm<sup>2</sup>) has been assumed in each optimization.

The objective of each optimization is to identify a distribution of material which yields a minimum mass solution whilst providing restraint against the applied load(s). For topology optimization this means that a result with minimum compliance is sought using a specified volume fraction, calculated on the designated percentage of weight reduction, to bound the objective. Truss optimization will seek a minimum volume solution with stress limits placed upon the procedure to ensure that each resulting element in the structure is maximally stressed.

TABLE 3.1: Material properties used in the two case studies for all optimization studies. Case study 1 (CS1) materials data at room temperature for LPBF Ti-6Al-4V from [Gupta et al. \(2022\)](#) and case study 2 (CS2) material properties for LPBF Inco718 at 400 °C.

	CS1 Gear Box Bracket	CS2 Inlet Mount
Tensile Strength ( $\sigma$ , MPa)	1020	943
Yield Strength ( $\sigma_Y$ , MPa)	971	639
Young's Modulus ( $E$ , GPa)	110	170
Poisson's Ratio ( $\nu$ )	0.31	0.28
Shear Modulus ( $G$ , GPa)	41.9	66.4
Density ( $\rho$ , kg/m <sup>3</sup> )	4429	8080

### 3.4.1 Case Study 1 - Gear Box Bracket

The first case study supports a gear box attached to a small business jet engine. It is an interesting case as due to the available mounting location, the load acts on a position forwards of the mountings at a 45 degree angle, Figure 3.6(b). The bracket is attached to a flange at the forward support, and to the outer skin of the casing at the rearwards end. Due to the direction of the applied load, both of the mounting positions are required. The single load of 110 kN is applied via a tie rod terminating in a clevis at the forward end of the bracket. For the purposes of both optimization methods, the clevis is treated as rigid and therefore is outside of the design domain, shown shaded in Figure 3.6(b). The tie rod and clevis arrangement allows for movement in the tangential,  $Z$ , direction, and rotation on the  $Z$  axis accounts for movement of the gear box in the axial  $X$  direction; therefore the loading applied to the components comes in the radial,  $Y$ , direction as shown.

The existing component is produced from a forged billet of Ti64 which is extensively machined to produce the final form. This is a costly and wasteful process, which can be improved upon via AM ([Allen, 2006](#)). In addition, the existing part does not satisfy its mass target, being overweight by 30% (0.21 kg). A new part has been proposed to be produced from LPBF (Laser Powder Bed Fusion) Ti64 following optimization to define a part that has the required structural capability whilst reducing both mass and cost; material properties for the laser powder bed fusion (LPBF) Ti64 material used are detailed in Table 3.1.

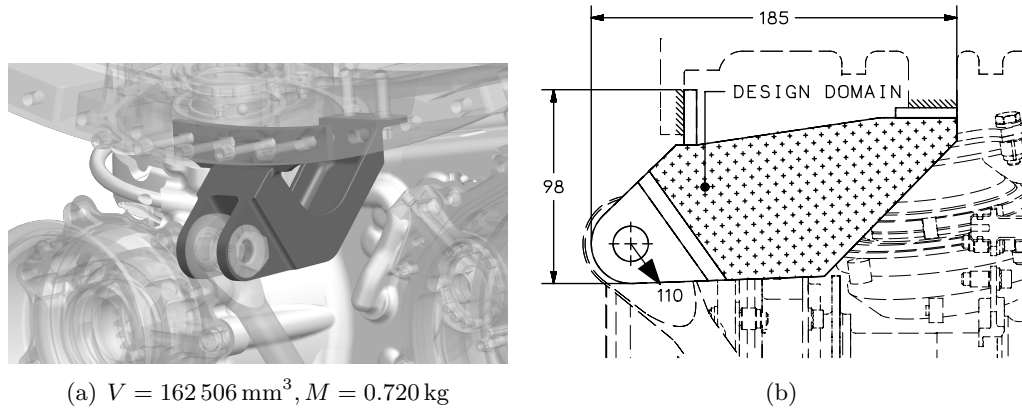


FIGURE 3.6: Gear box bracket case study: (a) original part to be redesigned via optimization to reduce its weight; (b) problem definition, showing the overall size of the part and boundary conditions; the hatched area highlights the design domain, which is subject to optimization. Unless otherwise stated all dimensions are in mm and loads in kN.

### 3.4.1.1 Topology optimization workflow

Detailed descriptions of the steps to be followed when setting up a topology optimization in OptiStruct are available elsewhere<sup>2</sup> so the process will not be documented in detail herein; however specific steps relevant to this particular study will be outlined. Firstly, in common with all traditional topology optimization studies, the target volume fraction first has to be specified in advance. The aim in this case study is to reduce mass by approx. 30%; however the clevis and the support regions will not be changed as a result of the re-design, and thus the reduction must come entirely from within the design space. The current part has a total volume  $V_i = 162\,506\text{ mm}^3$  and the static features have a combined volume  $V_s = 74\,369\text{ mm}^3$ ; therefore the target volume for the optimization was  $V_t = 0.7(V_i - V_s) = 61\,695\text{ mm}^3$ . The target for the optimization is expressed as a percentage of the design space that has volume  $V_{ds} = 424\,819\text{ mm}^3$ ; dividing  $V_t$  by  $V_{ds}$  yields a volume fraction target  $V_{frac} = 14.5\%$ . An element size of 1 mm was applied to both design and non-design domains, supports were added to the mating faces of the part, and the load was divided between the two sides of the clevis; see Figure 3.7(a).

The OptiStruct solver completed in 25 minutes and consumed 1.5Gb of memory. The result of the optimization is shown in Figure 3.7(c) and consists of the raw mesh elements that remain once all excess material has been removed. It would not be possible or appropriate to manufacture the part in this state, nor is it convenient to analyse this further until the solution has been translated into NURB (Non-Uniform Rationalized B-spline) surfaces in CAD. In the case of this example, remodelling was carried out by sketching and extruding the structure using the topology optimized results as a guide,

<sup>2</sup>Altair OptiStruct 2022 manual available at [www.help.altair.com](http://www.help.altair.com).

taking the engineer undertaking the work 5.5 hours to complete. The final form shown in Figure 3.7(e) has a volume of  $124\,369\text{ mm}^3$ , including the non-design features and a mass of 0.551 kg, equating to a total weight reduction of 23.4%. Although this is a significant reduction, it is below the original 30% target.

### 3.4.1.2 Truss layout optimization workflow

In order to maintain commonality between the truss and topology optimization workflows, the same design space geometry was reused; however the way in which the design/non-design domains are handled differs slightly. The version of LimitState:FORM used models non-design domain features as rigid bodies, such that any loading applied to these will move them without deformation, and with limits on stresses not considered. In addition, in this workflow it is possible to take advantage of symmetry to reduce computational effort, by adding a mirror plane along the central axis to split the domain in half. The load was applied at the centre of a bar through the holes in the clevis, spreading it to both sides equally, and the supports were added to the same faces as in the topology optimization. The model setup used in the truss layout optimization workflow is shown in Figure 3.7(b).

As previously discussed, truss layout optimization does not require a target volume fraction to be specified in advance, and the form and extent of the generated structure depends on the specified allowable stress limits for the material. In this case the solution obtained will possess the minimum possible mass when the constituent elements are stressed to the maximum allowable stress limit. To ensure longevity of the component, a factor of safety of 2 is applied during the optimization, ensuring that each element only reaches half the maximum allowable stress, prolonging its life and ensuring the safety of the aircraft. Although not specified in the optimization as a constraint, the volume fraction can be calculated after undertaking an initial optimization; thus the volume of the optimized component was found to be  $V_t = 113\,754\text{ mm}^3$ , which is 27% of the original design space and 70% of the volume of the existing part.

A layout optimization was then undertaken using a fine nodal density, followed by a geometry optimization rationalization step, generating the structure shown in Figure 3.7(d), shown with members unioned together to form a continuum. As a solid body has at this point been created, it is a straightforward operation to also connect the design to the flange plates in CAD, as shown in Figure 3.7(f); this step consumed just 1 hour of engineering time. The final volume of the part comes to  $104\,734\text{ mm}^3$ , and a mass of 0.464 kg, which represents a reduction in weight of 35.5%. The optimization took 10 minutes when using a fine nodal density and consumed a maximum of 807Mb

of memory. In comparison with the topology optimization result, the truss problem was solved in 40% of the time and consumed 46% less memory, yet achieved a greater weight reduction.

### 3.4.2 Case Study 2 - Inlet Mounting

The second example is a unit mount for the gas turbine engine of a large civil aviation aeroplane. The mount is located on the exterior of a hot casing and supports an inlet for a cooling system. The current design consists of four individual brackets formed from sheet metal and joined together using mechanical fasteners upon engine assembly. The existing parts are produced from pre-formed sheets of Inconel 625. As this grade is not available in powder form, Inconel 718 shall be used for the LPBF process. Mechanical properties at the environment's temperature of 400 °C are listed in Table 3.1.

The objectives of this design and optimization exercise are four-fold:

1. To consolidate all four of the existing parts into a single component in order to reduce build and assembly time. The design space will therefore be defined as a large block instead of four smaller ones;
2. To include multiple load paths, to ensure safety in the event of failure of a single path;
3. To maintain existing mounting points, though not all points need to be used if the design/optimization shows that the required level of performance can be achieved using fewer points;
4. To support the mass of the payload  $F_1 = 75 \text{ N}$  and also retain the inlet during any off-design event, such as a core blade-off event. For this latter case a shock load of 20G is to be assumed, resulting in a load on the part of  $F_2 = 197 \text{ N}$  for each load case. Refer to Table 3.2 for a full list of load cases.

#### 3.4.2.1 Topology optimization workflow

As with case study 1, the inlet mounting was optimized using OptiStruct. Initially, the design space was defined to fully enclose just the original parts; however it was noted that this left a large amount of unoccupied space surrounding the domain. The design space was therefore enlarged to provide greater design freedom for the optimization. The topology optimization workflow used in the previous case study was adopted, though given

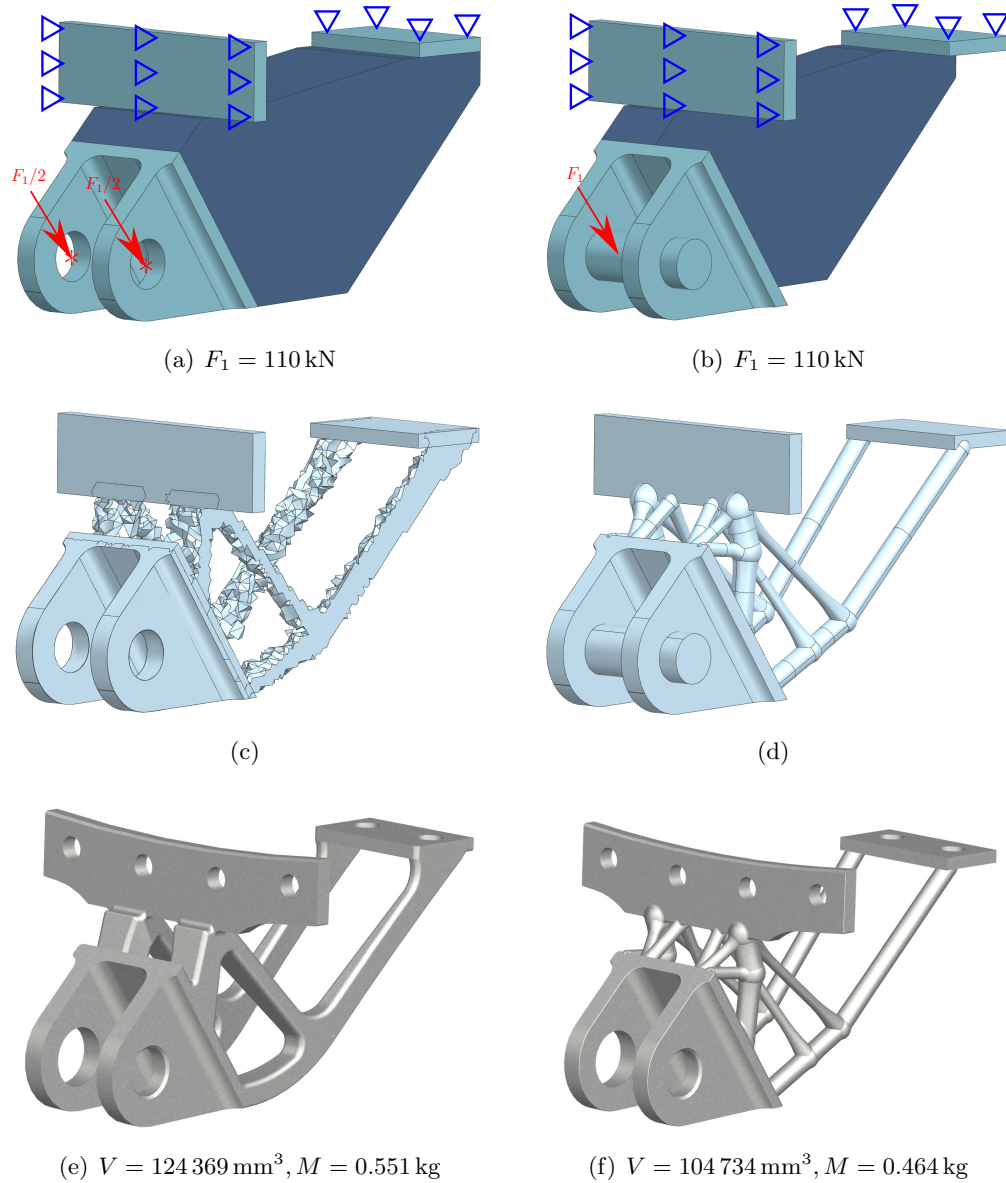


FIGURE 3.7: Gear box bracket case study - stages and results for topology optimization (left) and truss layout optimization (right) workflows: (a) topology optimization model setup within Altair HyperWorks, showing support conditions and loading spread evenly to 1D rigid nodes at the centres of clevis holes; (c) raw topology optimization results; (e) final form of the component following CAD remodelling, with the flanges and bolting arrangement from the original part merged in; (b) truss layout optimization model setup in LimitState:FORM, showing support conditions and loading applied to the centre of a bar through the clevis holes; (d) result of layout optimization and geometry optimization rationalization, with members unioned together to form a continuum; (f) final form of the component, with the original flanges added in CAD in preparation for manufacture. Note that in (a) and (b) the dark area indicates the design domain and the lighter areas rigid, non-design, regions.

TABLE 3.2: Inlet mounting case study: Load cases applied to optimization procedures, to be read in conjunction with the boundary condition diagram, Figure 3.8(b). Note that the payload,  $F_1$ , will always be applied at the  $180^\circ$  direction as viewed, however the shock load,  $F_2$ , will be applied at the directions indicated;  $0^\circ$  at top dead centre and progressing clockwise.

Load Case	Load(s)	$F_2$ Direction
LC1	$F_1$	—
LC2	$F_1 + F_2$	$0^\circ$
LC3	$F_1 + F_2$	$45^\circ$
LC4	$F_1 + F_2$	$90^\circ$
LC5	$F_1 + F_2$	$135^\circ$
LC6	$F_1 + F_2$	$180^\circ$
LC7	$F_1 + F_2$	$225^\circ$
LC8	$F_1 + F_2$	$270^\circ$
LC9	$F_1 + F_2$	$315^\circ$

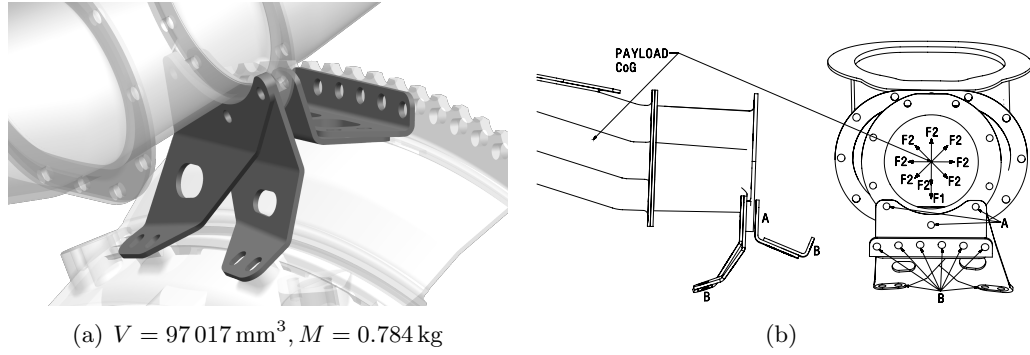


FIGURE 3.8: Inlet mounting case study: (a) the original part to be redesigned via optimization to reduce its weight and (b) the design space including boundary conditions. Note that in (b) loads  $F_1$  and  $F_2$  originate at the payloads centre of gravity and are translated to holes **A** via bodies assumed to be rigid, the part is supported in all direction at holes **B**. Off-design events may occur in any direction, therefore shock load  $F_2$  applies in multiple directions whereas mass load  $F_1$  applied radially towards the engine centreline.

the larger volume of design space, the mesh element size was set to a maximum of 3mm to ensure the optimization could be run on a desktop PC. Once again a target volume fraction was defined by reducing the volume of the current components ( $97\,017\text{ mm}^3$ ) by 30%, hence targeting a 30% reduction in overall mass ( $V_t = 66\,735\text{ mm}^3$ ,  $M_t = 0.539\text{ kg}$ ). To translate this into the optimization routine this target volume was expressed as a percentage of the total design space volume as a constraint  $V_{frac} = 5\%$ . Material properties (Table 3.1) and boundary conditions were applied and the optimization was solved in 30 iterations, taking 68 minutes and consuming 5.2 Gb of memory. The outcome of the optimization is shown in Figure 3.9(c). Similar to the result at this stage for case



study 1, the geometry is element based and though it is generally a continuum structure there are areas where the ligaments thin down to almost nothing; the part also has a very rough surface due to the faceted nature of the tetrahedral mesh employed. Thus CAD remodelling was at this point required.

As this is a much more complex shape than the raw structure obtained in the previous case study, in this case PolyNURBS were used. Despite this approach being quicker than sketching around the mesh and then creating multiple solids to form a body, application of PolyNURBS and blending the structure still took around 20 hours to complete to the point where it was considered suitable for the next stages (i.e. analysis and then manufacture). In its final form the component has a volume of  $67\,450\text{ mm}^3$  and a mass of  $M_t = 0.545\text{ kg}$ .

### 3.4.2.2 Truss layout optimization workflow

As with the previous case study, in the interests of comparability the truss layout optimization workflow employed the same design space as the topology optimization workflow, with the problem divided in two and a mirror plane added. The load was applied to the clevises within the design domain and the values applied accordingly for each load case. Again, it was not necessary to specify a target volume in advance of the optimization, though it is intended that a volume of  $V_t = 66\,735\text{ mm}^3$ , 70% of the combined volume of the existing parts could be achieved. A factor of safety of 2 was also specified in the optimization setup.

The same nodal density was used as per case study 1, and the resulting structure is shown in Figure 3.9(d). Once relatively trivial CAD operations were completed, the final part, Figure 3.9(f), was ready for build preparation. The final volume of this part is  $60\,117\text{ mm}^3$ , and its mass is  $0.486\text{ kg}$ , which represents a weight reduction of 28.9%. The layout optimization solution was identified in 19 iterations, after which a geometry optimization rationalization step was completed. The total elapsed time was 60 minutes, with a maximum of 3 Gb of memory consumed.

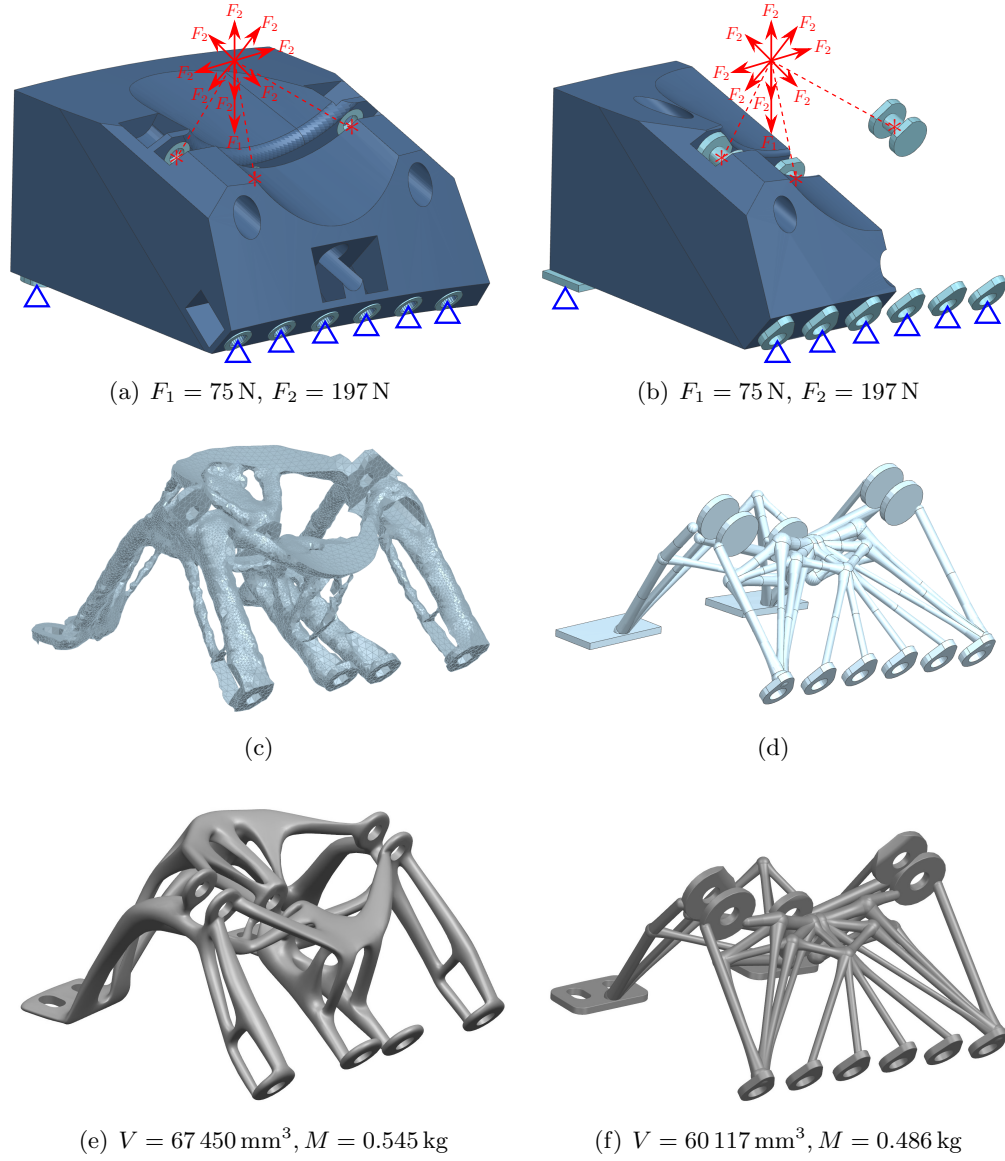


FIGURE 3.9: Inlet mounting case study - stages and results for topology optimization (left) and truss layout optimization (right) workflows: (a) topology optimization model setup within Altair HyperWorks, showing support conditions and loading; (c) raw topology optimization result; (e) remodelled component in CAD, with flanges connected with the optimized model; (b) truss layout optimization model setup in LimitState:FORM, showing support and loading conditions; (d) result of layout optimization and geometry optimization rationalization, with members unioned to form a continuum; (f) final form of the component, with geometry refined in CAD to make the part ready for manufacture. Note that in (a) and (b) the dark area indicates the design domain and the lighter areas the rigid, non-design, regions.

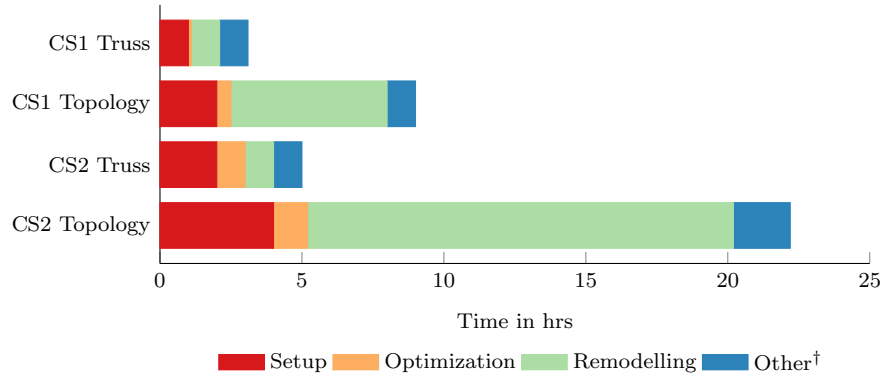


FIGURE 3.10: Case study results: comparison of the time taken to complete model setup, optimization and remodelling of the gear box bracket (CS1) and inlet mount (CS2). <sup>†</sup> Refers to operations that do not fit into the preceding categories, such as model import/export, loading/saving of files etc.

### 3.5 Comparison of topology optimization and truss layout optimization workflows

#### 3.5.1 Required engineering time

It is clear from the results shown in Figures 3.7 & 3.9 and Table 3.3, that both topology and truss layout optimization workflows can be used to provide significant reductions in volume, and hence mass, to an aerospace component, although for case study 1 the topology optimization result fell a little short of the target set. Given this, it is of interest to compare the two approaches in terms of the time taken to generate the end result. Thus Figure 3.10 shows that the truss layout optimization workflow offers a substantial reduction in the engineering time required to generate a solution. This can be largely attributed to the much shorter time required to transform the result of the optimization into a continuum structure in CAD.

TABLE 3.3: Case study results: numerical results for mass and CO<sub>2</sub> reductions achieved for topology and truss layout optimization workflows for the gear box bracket (CS1) and the inlet mount (CS2). Unless stated otherwise all values are in kg.

Mass (kg)	Topology		Truss	
	CS1	CS2	CS1	CS2
Initial	0.720	0.770	0.720	0.770
Final	0.551	0.545	0.464	0.486
Delta	0.169	0.225	0.256	0.284
Delta (%)	23.43	28.88	35.55	36.94
CO <sub>2</sub> (Flight $\Delta$ )	0.443	0.584	0.671	0.747
CO <sub>2</sub> (Life $\Delta$ ) <sup>†</sup>	22,125	29,183	33,567	37,333

<sup>†</sup>assumes 50,000 flights service life.

### 3.5.2 Quality of results obtained

It is also of significant interest to check the quality of the results obtained when using the two workflows. This is here validated via FEA using [Siemens NX version 1973, \(2020\)](#) simulation. To verify the results, a static analysis has been conducted on each structure using the same load cases and boundary conditions as used in the optimization runs. The goal is to ensure that the maximum Von Mises stress for the critical case (where the peak stress is the greatest) is below the yield strength of the material (Table [3.1](#)), with a reserve factor (RF) greater than 1; contour plots from the analysis results for all cases are shown in Figure [3.11](#).

It is clear that all results from the case studies are below the yield strength of the material, giving reserve factors ranging from 1.1 to 4.5. The components would therefore be deemed suitable to be considered for entry into service. The results indicate that the highest stresses are at the interfaces between the optimized geometry and the rigid/non-design bodies; further work in these locations may be necessary to ensure smoother transitions, and thereby reduced stresses.

The results for the gear box bracket, Figures [3.11\(a\)](#) & [3.11\(b\)](#), have reserve factors of 1.2 and 1.1 respectively, indicating that the material is being used efficiently and there is little room for improvement in overall mass. The results for LC9 of the inlet mounting, Figures [3.11\(c\)](#) & [3.11\(d\)](#), show much larger reserve factors of 3.6 and 4.5 respectively. For the truss optimized version this is a result of the minimum area constraint being applied, which has resulted in some members being larger than the true optimal solution would require; the topology optimized version still has some members much larger than the 8 mm<sup>2</sup> minimum. However, the aim of this study was to follow the topology optimization result as closely as possible; therefore there may still be some improvements that could be made if a secondary optimization is conducted. There is potential for buckling of elements to occur during off-design events, this has not been considered in this study but could be factored in as a post-processing step in future optimizations.

### 3.5.3 Assessment of optimized load path

It has been demonstrated that both topology and truss optimization are capable of achieving suitable results for a given specific load case and can successfully be transferred back into a CAD environment for further analysis. However, further examination of the topologically optimized structure for case study 1 (Section [3.4.1.1](#)) shows that the material forming the lower load path is curved; see Figure [3.12\(a\)](#). However, when the load is applied through a curved member, bending moments will be induced, suggesting

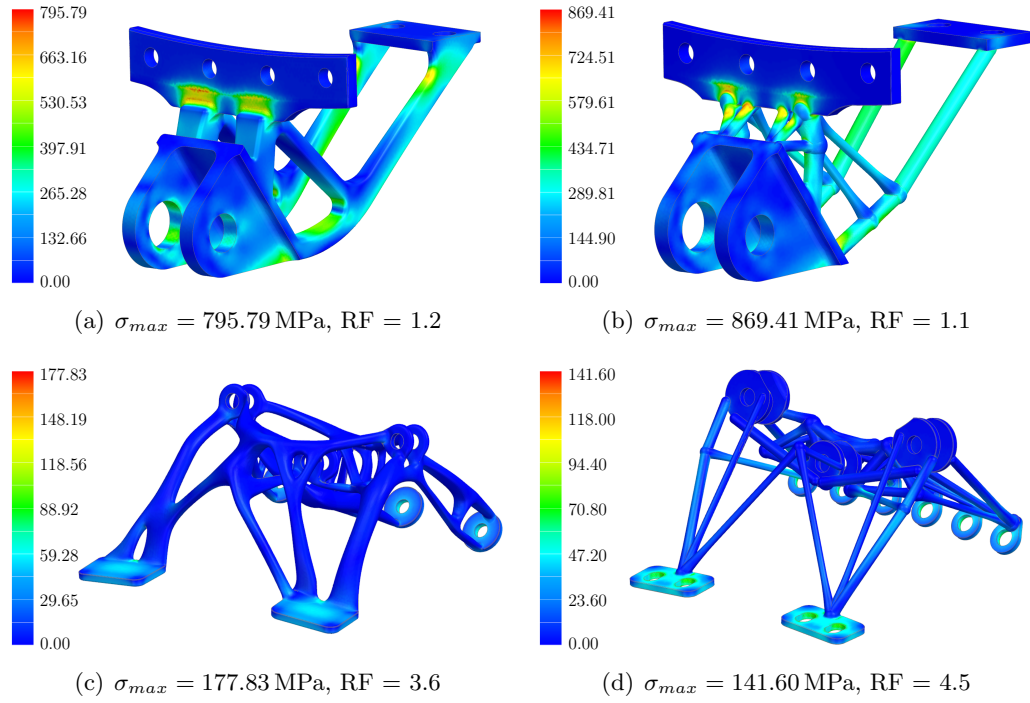


FIGURE 3.11: FEA results for case studies: (a) topology optimized gear box bracket model; (b) optimized truss gear box bracket model; (c) topology optimized inlet mounting model; (d) optimized truss inlet mounting model. Reserve factors (RF) indicated; colour fringes indicate Von Mises stress in MPa.

that the form is suboptimal, Figure 3.12(b). A more efficient solution is to use a series of straight elements that carry the load directly along their axes, Figure 3.12(c). This holds true whether the elements are in tension or compression.

This more efficient way to transmit the load is likely one of the reasons why, for this case study, the structure optimized using truss layout optimization was found to be lighter than its topologically optimized counterpart, where additional mass is required in the elements to carry induced bending moments.

### 3.6 Impact on CO<sub>2</sub> emissions

A prime benefit to aerospace of ‘strong yet light’ components is the associated reduction in fuel burn. Currently for every 1 kg of aviation fuel (JET-A) that is burned, 3.2 kg of CO<sub>2</sub> is emitted into the atmosphere; in 2019 some 250m metric tonnes of JET-A was consumed in aviation, equating to just over 800m metric tonnes of CO<sub>2</sub> per annum (RAeS, (2022)). Thus for every kg of material that can be removed from a component there is a substantial reduction in CO<sub>2</sub> emissions over the life of the product (typically 20-30 years).

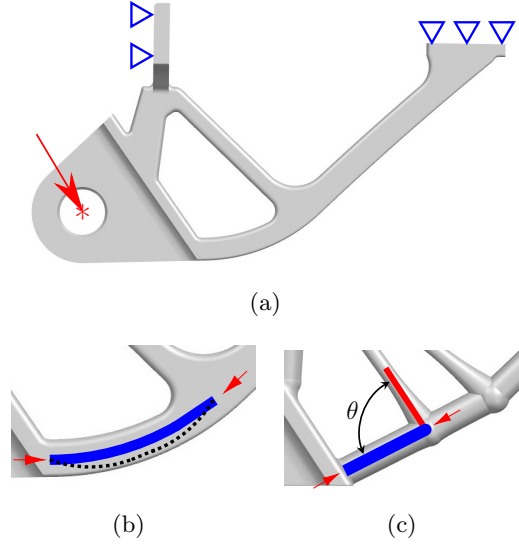


FIGURE 3.12: Assessment of optimized load path: (a) topology optimized result for case study 1 with the boundary conditions superimposed; (b) load applied directly to a curved member; (c) the same location defined using truss elements that carry the load axially to minimize bending.

In order to reduce the specific fuel consumption, and therefore CO<sub>2</sub> emissions, of a typical wide-body aircraft by 1%, a weight reduction of around 907 kg must be achieved. For example, a Rolls-Royce Trent 1000 powered Boeing 787-8 Dreamliner will consume 19 010 kg of fuel over the 5155 nm distance between London Heathrow and São Paulo<sup>3</sup>, releasing 60 832 kg of CO<sub>2</sub> into the atmosphere. Reducing the aircraft weight by 907 kg reduces fuel consumption by 1% and will therefore save 608 kg of CO<sub>2</sub> on each flight. A formula equating reduction in component mass to a reduction in CO<sub>2</sub> emissions is thus:

$$\Delta_{CO_2} = 3.2(\beta \cdot \Delta_w) \quad (3.4)$$

where  $\beta = 0.01F_t/907$ ,  $F_t$  is the total fuel consumed for the flight prior to a re-design and  $\Delta_w$  is the weight reduction achieved from the re-design activity. It should be noted that this formula assumes that the component(s) modified have no effect upon the aerodynamic performance of the aircraft. Additionally, this formula determines the reduction in CO<sub>2</sub> *per flight* where in practice a large civil airliner may make in excess of 50,000 flights in its lifetime. In addition to the highly important reduction in CO<sub>2</sub>, reduced fuel burn also has an economic impact. Revisiting the flight from London Heathrow and São Paulo and with the average price for JET-A1 predicted to be \$0.85/kg over 2023<sup>4</sup> if a 1% reduction in fuel burn can be achieved through weight reduction this equates to a saving of \$162 per flight for the operator; although a seemingly small amount

<sup>3</sup>Aircraft Commerce, Issue 121, Dec 2018/Jan 2019

<sup>4</sup>Data from: <https://jet-a1-fuel.com/forecast>

per flight, this equates to \$8.1m over the lifetime of the aircraft, neglecting fluctuations in fuel price.

### 3.7 Conclusions

There is a significant and demonstrable need for the aerospace industry to take advantage of additive manufacturing (AM) to reduce the weight of components, benefiting both manufacturers and the planet. However, design of these components can be challenging. Topology and truss layout optimization workflows have been considered in this contribution, with both proving valuable when seeking to design lightweight components. The main conclusions are as follows:

- a) The two case studies examined illustrate the benefits that can be achieved in terms of weight reductions, with reductions of up to 37% leading to fuel burn reductions and hence reductions of tens of thousands of kg of CO<sub>2</sub> emissions over their service lifetime. This clearly demonstrates the importance of these technologies to aerospace in the light of the climate crisis, strongly suggesting that they should be exploited more widely. Furthermore, FEA verification of each component designed has demonstrated that the optimization methods are appropriate for finding solutions to engineering problems of this nature, with acceptable reserve factors.
- b) The truss layout optimization workflow was found to lead to greater weight reduction levels than the topology optimization workflow; in the case of the inlet mounting case study a near 37% weight reduction was achieved in the former case, equating to lifetime reductions in CO<sub>2</sub> over 37 000 kg and \$9800 in fuel costs. This is clearly significant, especially given that the weight reduction was just 284g.
- c) Translation of structures generated via topology optimization into CAD was found to be time consuming, and for this method to be more widely employed in industry there needs to be further work to ensure that parts can be remodelled in a more time efficient manner. In contrast it was found that structures generated via truss layout optimization could be rapidly translated into usable CAD models, being ready for production in around one fifth of the time. This increase in efficiency also gives designers greater freedom to explore the design problem, and, for example, to identify opportunities for part consolidation.

Future investigations of this nature should consider the extent to which truss optimization techniques can be more widely used in industry when designing aerospace components; the rapid transition from line model to usable CAD geometry is a significant

advantage of this approach. In addition to considering member stresses, the truss layout optimization workflow should be extended to consider the effect of stresses at interfaces with rigid bodies, to further reduce remodelling time. A further development could be the ability to export a parametric model suitable for subsequent manipulation, instead of a conventional CAD geometry. Recent releases of topology optimization software used in industry have the capability to include constraints on natural frequencies as part of the optimization parameters. This is of considerable importance in aerospace design and is therefore something that should be considered in future releases of truss layout optimization software, to ensure the technology is more fully exploited.



## Chapter 4

# Layout optimization of pin-jointed truss structures with minimum frequency constraints<sup>1</sup>

Controlling the frequency response of an engineering component or structure is important in the aerospace and automotive sectors and is a key consideration when seeking a new, more efficient, design for a given component. In this contribution, the standard truss layout optimization procedure is modified to incorporate semidefinite constraints to limit the minimum value of the first natural frequency. Since this increases the computational expense, and reduces the scale of problem that can be solved, a bespoke algorithm incorporating an adaptive ‘member-adding’ procedure is proposed and applied to a number of benchmark example problems. It is demonstrated that this allows problems to be solved with relatively fine numerical discretisation, allowing modified structures with an acceptable minimum first natural frequency response to be successfully identified.

### 4.1 Introduction

In the design of modern engineering components many considerations need to be taken into account, including safety, cost, weight, and manufacturability. The most prominent of these is safety, taking account of the regime of applied stresses to be sustained over the life of the component. Safety is influenced by the properties of the material employed, which may change as the design evolves. Additionally, when considering structures that

---

<sup>1</sup>The content of this chapter has been previously published in the journal paper: S. J. Salt, A. G. Weldeyesus, M. Gilbert, and J. Gondzio. Layout optimization of pin-jointed truss structures with minimum frequency constraints. *Engineering Optimization*, 2022. A copy of the in-print version is included in Appendix [D](#).

include slender elements in compression, it is necessary to check for buckling instability to ensure safety is maintained. Another key parameter in the aerospace sector is the harmonic frequency of a structure; this should lie outside of the frequency bands of surrounding components. Should a fundamental frequency of one component (e.g. a bracket) overlap with those of its attached neighbours, then resonance in the component may occur, also referred to as forced vibration. Forced vibration and resonance can then lead to High Cycle Fatigue (HCF) in the component, affecting its serviceable life and reducing its time to failure. It should be noted that a component may exhibit multiple resonant frequencies, each corresponding to a mode of vibration; repeated exposure to any one of these frequencies may reduce the life of the component. However, this phenomenon is beyond the scope of the current contribution. Considering component manufacture, it is important to note that traditional manufacturing methods may limit the design freedom available; however in the present contribution it is assumed that Additive Manufacturing (AM) methods are available. The use of AM means that complex truss forms can potentially be fabricated, beyond the scope of traditional subtractive manufacturing methods.

There have been numerous recorded HCF related incidents. A notable example led to the loss of British Midland flight #92 in 1989 ([Cooper, 1989](#)). This was initiated by the failure of a fan blade on one of the two CFM International S.A. CFM56-3 turbofan engines. A single blade failed due to a coupling of torsional-flexural transient and non-synchronous oscillation, leading to rapid reduction of the HCF life of the blade. The blade was subsequently released, causing high levels of vibration in the engine and aircraft, contributing to the loss of the aircraft upon attempting an emergency landing at East Midlands Airport in the UK.

Given the potentially catastrophic consequences of failure, the design optimization of components with stress and frequency constraints has been of interest for many years. Forced vibration problems can be avoided by (a) redesign of the component being analysed; (b) redesign of the stimuli to change its frequency characteristics; and/or (c) introduction of a damping mechanism into the system. The most straightforward of these options is often (a) redesigning a component to move its fundamental frequencies away from those where resonance may occur. This may be achieved, for example, by adding stiffening ribs to the part, or strategically increasing the volume of material.

Computer aided methods have been employed to treat such problems, largely focused upon the use of topology optimization in works such as [Bendsøe and Sigmund \(2003\)](#) where links can be formed between discrete and continuum structures ([Achtziger, 1999](#)). Additionally [Du and Olhoff \(2007\)](#) formulated simple and multiple eigenfrequency optimization techniques for linear elastic structures without damping. This contribution will

focus upon the design of truss structures, which are attractive when there is significant available design freedom. In practice it is rare that the available design freedom is fully exploited, usually due to limitations associated with the manufacturing method involved. However, AM allows the available design freedom to be exploited to a much greater extent than when traditional subtractive manufacturing methods are employed. Since the ground-structure method was first introduced by [Dorn et al. \(1964\)](#) to solve plastic truss design problems, layout optimization has provided an effective means of identifying the most efficient arrangement of elements (also referred to herein as ‘members’ or ‘bars’) to form a truss structure. This methodology has been well used to identify minimum volume truss structures ([Dorn et al. \(1964\)](#), [Hemp \(1973\)](#), [Gilbert and Tyas \(2003\)](#), [Smith et al. \(2016\)](#)), using linear programming (LP) and member-adding (column generation) to solve single load case problems efficiently. These methods have been further extended by [Pritchard et al. \(2005\)](#) and [Sokoł \(2014\)](#) to include application to multiple load cases. To keep the underlying layout optimization problem formulation reasonably simple, this contribution will focus on single load case problems with a single specified minimum frequency, usually chosen so as to lie away from the frequencies of any sources of excitation. However, frequency analysis is a non-linear problem and so semidefinite programming (SDP) must be used to treat the constraints.

SDP is a subset of convex optimization and aims to minimize a linear function subject to the constraint that an affine combination of symmetric matrices is positive semidefinite. SDP has previously been applied to the optimization of truss structures: [Ben-Tal and Nemirovski \(1997\)](#) and later [Kanno \(2018\)](#) used SDP to produce structures which were robust against uncertainty in the loading, and [Giniūnaitė \(2015\)](#) applied SDP to identify minimum mass structures. A number of solvers are available which are capable of treating semidefinite problems of varying complexity: `fminsdp` ([Thore, 2018](#)); MOSEK (v8+) ([MOSEK ApS, 2017](#)); PENLAB ([Fiala et al., 2013](#)) and CVX ([Grant and Boyd, 2014](#)) are a few examples. However, a bespoke approach is required when combining generative truss design with optimization for frequency constraints.

Frequency optimization belongs to the field of eigenvalue optimization in mathematics, which has been studied extensively by the mathematical programming community: [Fox and Kapoor \(1970\)](#) adopted a feasibility approach to solve the underlying semidefinite programming problem, [Grandhi and Venkayya \(1988\)](#) and [Khot \(1985\)](#) used the optimality criteria method and [Kaveh and Ghazaan \(2016\)](#) used non-smooth optimization to perform size optimization of existing truss structures to meet certain frequency requirements. Additionally, [Achtziger and Kočvara \(2007\)](#) used semidefinite programming to solve similar problems, and [Aroztegui et al. \(2011\)](#) developed a feasible direction algorithm for semidefinite programming in order to maximize the fundamental frequencies based upon simple fully-connected ground-structures. Considering optimization of

frequency in isolation, [Azad et al. \(2018\)](#) assessed the simultaneous size and geometry optimization of steel structures under excitation using the ‘big bang - big crunch’ algorithm, with mixed results when considering the optimum solutions, whilst [Taheri and Jalili \(2016\)](#) and [Tejani et al. \(2018\)](#) used other meta-heuristic methods to impose frequency constraints in truss optimization problems.

In many of these studies, the design variable was treated as continuous, but the number and arrangement of the variables were assumed to be finite and arrived at by utilising the most efficient members from a pre-defined ground-structure. In contrast, here an alternative methodology is proposed in which standard equilibrium constraints are supplemented by semidefinite constraints to enable problems involving both frequency and strength considerations to be tackled. The ground-structure method is employed to provide a large search space, with an adaptive member-adding algorithm used to significantly reduce the associated computational burden. In the interests of simplicity, buckling instability and other issues are not explicitly considered in this contribution, though members susceptible to buckling would need to be checked for prior to e.g., usage in a qualified aerospace application.

This contribution is organized as follows: Section [4.2](#) describes the basic formulations relevant to the frequency problem at hand, with examples used to illustrate limitations; Section [4.3](#) then proposes a new formulation that is significantly more computationally efficient; the new formulation is then applied to various example problems in Section [4.4](#); and conclusions are drawn in Section [4.5](#).

## 4.2 Basic formulations

### 4.2.1 Truss layout optimization formulation

Ground-structure-based layout optimization begins with the definition of a design domain, the volume of space in which the optimized structure can reside, with materials, loads and supports then also prescribed to fully describe the problem, see Figure [4.1\(a\)](#). The objective is to arrive at a structure of minimum volume, and hence mass, whilst maintaining structural integrity. With a Cartesian grid, the design domain is populated with a predefined  $n$  number of nodes in the  $x$  and  $y$  directions (also in the  $z$  direction for 3D problems). It is then joined with  $m$  potential connections, or elements, such that each node is connected to every other node in the domain to form a ground-structure, as in Figures [4.1\(b\)](#) and [4.1\(c\)](#). Herein, each example will employ a number of nodes expressed in terms of number of nodal divisions, e.g. referring to Figure [4.1\(b\)](#), the domain has  $4 \times 2$  nodal divisions, with 4 divisions and 5 nodes in the  $x$  direction and 2 divisions

and 3 nodes in the  $y$  direction, giving 15 nodes in total. Constraints are introduced to ensure equilibrium is enforced at nodes, and to ensure that the cross-sectional area of each element is both a positive number and is sufficiently large to carry the internal forces, given the limiting stress of the material. The plastic single load case formulation can be written (after [Dorn et al. 1964](#)):

$$\begin{aligned} \min_{\mathbf{a}, \mathbf{q}} \quad & V = \mathbf{l}^T \mathbf{a} \\ \text{s.t.} \quad & \begin{cases} \mathbf{B}\mathbf{q} = \mathbf{p}, \\ -\sigma^- a_i \leq q_i \leq \sigma^+ a_i, \quad \forall i \\ a_i \geq 0, \quad \forall i, \end{cases} \end{aligned} \quad (4.1)$$

where  $V$  is the total volume of the structure;  $\mathbf{l}$  is a vector of individual element lengths  $\{l_1, l_2, \dots, l_m\}$ ;  $\mathbf{a}$  is a vector containing element cross-sectional areas  $\{a_1, a_2, \dots, a_m\}$ ;  $\mathbf{B}$  is a suitable  $(2n \times m \text{ or } 3n \times m)$  equilibrium matrix containing direction cosines (for 2D or 3D problems);  $\mathbf{q}$  is a vector of element axial forces,  $\mathbf{q} = \{q_1, q_2, \dots, q_m\}$ , where  $q_i$  is the force in element  $i$ ;  $\mathbf{p}$  is a vector of applied loads and  $\mathbf{p} = \{p_1^x, p_1^y, p_1^z, p_2^x, p_2^y, p_2^z, \dots, p_n^z\}$  where  $p_j^x, p_j^y, p_j^z$  are the  $x$ ,  $y$  and  $z$  direction components of the load applied to node  $j$  ( $j = 1, \dots, n$ ). Finally  $\sigma^+$  and  $\sigma^-$  are, respectively, the limiting tensile and compressive stresses that can be sustained by the material. Problems of this nature may be solved using linear programming.

Employing a fully-connected ground-structure of this type is computationally expensive, with the problem comprising  $n(n-1)/2$  potential connections for a domain, where  $n$  is the total number of nodes. The majority of the connections will have an area equal or close to zero following the optimization and so do not contribute to the final structure. This issue may be alleviated by applying the adaptive ‘member-adding’ method proposed by [Gilbert and Tyas \(2003\)](#) which is a customized column generation technique. With this method, nodes in the initial ground-structure are only connected to their immediate neighbours, Figure 4.1(d), instead of to every other node in the domain, Figure 4.1(c). An iterative process is then used, with elements added to the current ground-structure from the list of potential connections. Newly added elements are introduced into the solution using the Michell-Hemp criterion Eq. (4.2), which specifies limits on the virtual strain ( $\epsilon_i$ ) experienced by each potential element ( $i$ ), given a prescribed limiting stress ( $\sigma$ ):

$$-\frac{1}{\sigma^-} \leq \epsilon_i \leq \frac{1}{\sigma^+}, \quad i = 1, \dots, m. \quad (4.2)$$

In the parlance of column generation method ([Gondzio and Sarkissian \(1996\)](#), [Desrosiers and Lübbcke \(2005\)](#), [Gondzio et al. \(2013\)](#)), new columns are added to the LP constraint

matrix  $\mathbf{B}$  in Eq. (4.1). At the end of each iteration, potential connections are ranked, with those most violating the criteria then added for use in the next iteration. Once there are no potential connections violating the criteria remaining, the algorithm terminates. The solution obtained shown in Figure 4.1(e) is provably optimal, with the computed volume the same as that obtained using a fully-connected ground-structure.

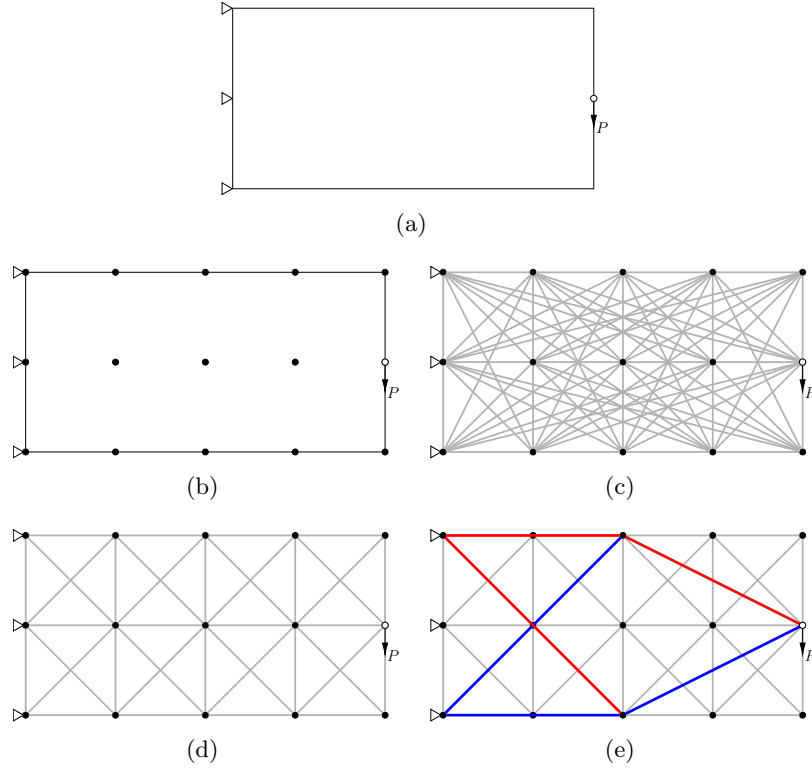


FIGURE 4.1: Steps in layout optimization: (a) definition of the problem domain and boundary conditions; (b) domain populated with equally spaced nodes; (c) each node is connected to every other node in the domain to form a fully-connected ground-structure, or (d) each node is connected only to neighbouring nodes to form a minimally-connected ground-structure; and (e) the resulting optimized layout using a member-adding algorithm (red and blue bars indicate those in tension and compression respectively).

#### 4.2.2 General eigenvalue equation

Consider a truss structure consisting of  $m$  elements, connecting a pre-determined set of  $n$  nodes. A large external force  $P$  is applied to a specific node, with internal forces transmitted through the structure, resulting in small displacements at each node; this may be considered to be a static problem. To take account of the vibration characteristics of the structure, it is necessary to consider the following dynamic problem derived from the equation for motion:

$$\mathbf{K}\{\mathbf{u}\} + \mathbf{M}\{\ddot{\mathbf{u}}\} = 0, \quad (4.3)$$

where  $\mathbf{K}$  and  $\mathbf{M}$  represent the global stiffness and mass matrices respectively. The mass and stiffness matrices are represented as symmetric  $2n \times 2n$  matrices when modelling a two-dimensional truss structure and  $3n \times 3n$  matrices for a three-dimensional truss structure. The size of these global matrices will be reduced by the number of supported degrees of freedom, since there are no displacements at these locations. Given that the displacement vector is harmonic, Eq. (4.3) may be restructured into the generalized eigenvalue problem:

$$\mathbf{K}\phi_j = \lambda_j(\mathbf{M} + \mathbf{M}_0)\Phi_j, \quad (4.4)$$

where:  $\mathbf{M}$  refers to the global mass matrix for the structures bar elements;  $\mathbf{M}_0$  refers to the additional mass of the nodes connecting each element; and  $\lambda_j$  represents the eigenvalue for a given mode of vibration  $\Phi_j$ , ( $j = 1, 2, 3 \dots$ ). The free vibrations of a structure are equal to the square root of the eigenvalues  $\omega_j^2 = \lambda_j$  in *rad/s*, and thus the natural frequencies and normal modes of vibration for the structure may be determined.

### 4.2.3 Frequency formulation

#### 4.2.3.1 Determine the reference frequencies

To determine conformance with the original design problem, it is necessary to calculate the natural frequencies of the structure. If a candidate design has been obtained via layout optimization then this can be performed using the connectivity and member cross-sectional areas generated in the optimization. The areas for each element are multiplied by the corresponding mass and stiffness coefficients before being assembled into the global matrices ( $\mathbf{K}$  and  $\mathbf{M}$ ) at the row/column index corresponding with the degrees of freedom associated with the member end nodes, with rows and columns related to the supported degrees of freedom omitted. The eigenvalues can be extracted e.g. using the built-in MATLAB `eigs` functionality. Previous studies (e.g. [Du and Olhoff \(2007\)](#)) have considered multiple eigenfrequencies, however this contribution will concentrate on just the first natural frequency in Hz for the structure to ensure it will not resonate when exposed to a source of excitation.

#### 4.2.3.2 Semidefinite constraint

In order to perform an optimization targeting the natural frequencies of the structure, a new constraint equation must be derived from the generalized eigenvalue problem Eq. (4.4). Once the coefficient matrices for stiffness and mass are determined, in order

to avoid the optimization generating a structure prone to low frequency vibration, a threshold can be set such that the smallest eigenvalue from Eq. (4.4) is greater than or equal to a defined minimum value. Thus Eq. (4.4) may be transformed into the following constraint:

$$\mathbf{K}(\mathbf{a}) - \lambda(\mathbf{M}(\mathbf{a}) + \mathbf{M}_0) \succcurlyeq 0, \quad (4.5)$$

where  $\mathbf{K}(\mathbf{a}) = \sum_{i=1}^m a_i \mathbf{K}_i$  and  $\mathbf{M}(\mathbf{a}) = \sum_{i=1}^m a_i \mathbf{M}_i$  are the global stiffness and mass matrices respectively;  $a_i$  refers to the cross-sectional area of member  $i$ ;  $\lambda$  is the eigenvalue derived from the minimum specified natural frequency ( $\omega_1$ ) for the specified mode of vibration  $\Phi_j$  and  $\succcurlyeq$  indicates that the matrix to its left is symmetric and positive semidefinite. For the purposes of this contribution, the connecting nodes are not considered, and therefore the mass associated with joints  $\mathbf{M}_0 = 0$ .

Thus when incorporated into the layout optimization formulation, Eq. (4.1) the problem may be written as:

$$\begin{aligned} \min_{\mathbf{a}, \mathbf{q}} \quad & V = \mathbf{l}^T \mathbf{a} \\ \text{s.t.} \quad & \begin{cases} \mathbf{B}\mathbf{q} = \mathbf{p}, \\ \mathbf{K}(\mathbf{a}) - \lambda_0 \mathbf{M}(\mathbf{a}) \succcurlyeq 0 \\ -\sigma^- a_i \leq q_i \leq \sigma^+ a_i, \quad \forall i \\ a_i \geq 0, \quad \forall i, \end{cases} \end{aligned} \quad (4.6)$$

Fixing the smallest eigenvalue ( $\lambda_0$ ) to be greater than or equal to the minimum specified frequency ensures that the areas of the elements are adjusted as part of the optimization until the inequality constraint is achieved. Incorporation of the semidefinite constraint means that a semidefinite programming solver is now required to solve the problem. Note that SDP problems are convex, enabling a globally optimal solution to be obtained, but are considerably more computationally demanding to solve than their LP counterparts.

#### 4.2.4 Short cantilever example

Two means of optimizing a short cantilever structure based on a prescribed minimum first natural frequency will now be outlined, using the example problem defined in Figure 4.2 to illustrate salient points. For this problem  $P = 1 \times 10^3 \text{N}$ ;  $E = 210 \times 10^9 \text{N m}^{-2}$ ;  $\rho = 8050 \text{kg m}^{-3}$  and the limiting tensile and compressive stresses  $\sigma = 350 \times 10^6 \text{Pa}$ . The prescribed constraint on the fundamental natural frequency is  $f_1 \geq 425 \text{Hz}$ . All numerical



examples in this contribution were run on a 64bit Windows 10 desktop PC equipped with an Intel i5 3.7GHz processor and 32Gb RAM, using a script programmed using MATLAB 2020b. A number of semidefinite solvers are available and are compared by Tyburec and Zeman (2017). This contribution will initially employ the MOSEK ApS (2017) v8.1 solver using the Java Fusion MATLAB interface. It should be noted that unless otherwise specified all layouts presented in the figures are filtered to only include elements with areas greater than  $1 \times 10^{-6} m^2$ . This may occasionally result in elements which appear to be disconnected from the overall structure. Additionally, to facilitate comparison with other published works, non-dimensional volumes  $V$  are presented throughout the paper, with scaled volumes  $V(P/\sigma)$  in  $m^3$  also included in accompanying tables for completeness.

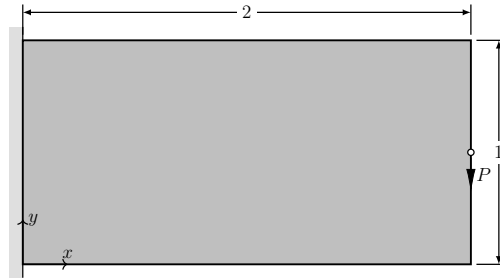


FIGURE 4.2: Short cantilever example: design domain, loading and support details. All dimensions in metres.

#### 4.2.4.1 Two phase optimization approach

Since SDP problems are computationally expensive to solve, initially the efficacy of a two phase optimization approach is evaluated. With this approach a traditional layout optimization is first undertaken, without considering frequency constraints; if prescribed frequency requirements are not met by the generated design then a size optimization is subsequently performed to ensure that these are met, modifying only the subset of elements present in the optimal structure; i.e. in this second phase the areas of each element  $a_i$  are adjusted to ensure the semidefinite constraint Eq. (4.5) is met. In the interests of computational efficiency only those elements that have an area greater than a predetermined minimum (taken as  $1 \times 10^{-6} m^2$ ) are included in the optimization; these elements will henceforth be referred to as members.

Considering first the example problem defined in Figure 4.2, an initial layout optimization is carried out to provide reference values for the volume and first natural frequency of the structure; see Table 4.1 and Figure 4.3(a). The structure shown is similar to that obtained by He et al. (2019b).

However the reference structure contains many members so, for the first phase of the proposed two phase procedure, a domain with fewer nodes is used to enable a more practical layout to be generated, containing fewer ‘fibrous’ elements. This is achieved by both reducing the number of nodes and introducing a joint penalty, after [Parkes \(1975\)](#). This results in the structure shown in [Figure 4.3\(b\)](#), which has fewer joints and elements than the benchmark, but which has a similar volume.

In the second phase, the structure from the first phase is re-optimized using the modified formulation that includes frequency constraints [Eq. \(4.6\)](#) to revise member sizes ensuring the frequency is not less than 425Hz. In the re-optimization, it is found that the areas of diagonal members radiating from the support line, along with some members interconnecting these, need to be modified (resized members are highlighted in green in [Figure 4.3\(c\)](#) in the online version of the paper).

It is evident that the solver has been successful in achieving the desired minimum natural frequency, at minimal CPU cost; however this has, in this case, come at a relatively high cost in terms of increase in volume (8.7%). This suggests that changing the size of the elements alone may not lead to the most efficient solution, and a better one may be available if a wider solution space was made available.

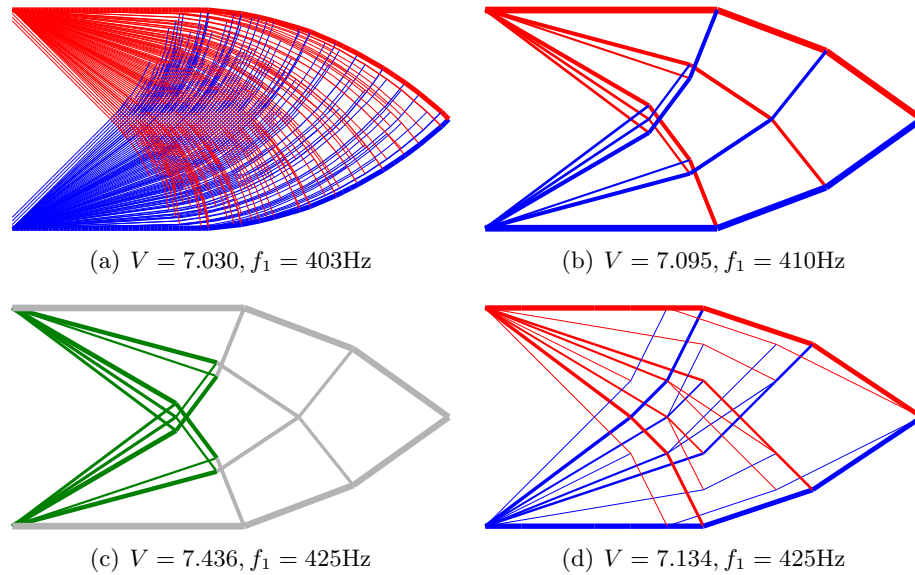


FIGURE 4.3: Short cantilever example: (a) reference LP solution achieved using layout optimization using  $120 \times 60$  nodal divisions; (b) more practical LP layout, achieved by reducing the nodal divisions to  $40 \times 20$  and penalising joints; (c) outcome of the SDP frequency optimization performed on the practical layout from (b); (d) layout generated using SDP optimization of the full ground-structure, incl. frequency constraint using  $12 \times 6$  nodal divisions. (Key: red = tension; blue = compression; green = members in (c) whose areas have been modified compared with (b); grey = members whose areas are as per the layout in (b)).

Next consider the classical half-wheel problem shown in Figure 4.4, as originally studied by [Michell \(1904\)](#). The problem involves a central point load  $P = 1 \times 10^3 \text{N}$  applied at midspan between statically determinate supports, limiting tensile and compressive stresses  $\sigma = 350 \times 10^6 \text{Pa}$ , and in common with the other presented examples  $E = 210 \times 10^9 \text{N m}^{-2}$  and  $\rho = 8050 \text{kg m}^{-3}$ . The optimal solution obtained when using  $16 \times 8$  nodal divisions is shown in Figure 4.4(b) and has a non-dimensional volume  $V = 3.191$ . This includes a short vertical member above each of the supports, leading to a structure that is in unstable equilibrium with the applied loading. This arises because only equilibrium (and strength) constraints are enforced in phase one. A byproduct of this is that subsequently adjusting the sizes of structural members alone in the second phase, with a view to achieving a natural frequency of, for example,  $f_1 = 200 \text{Hz}$  will fail due to the inherent instability in the problem. This highlights a further limitation of the two phase optimization approach.

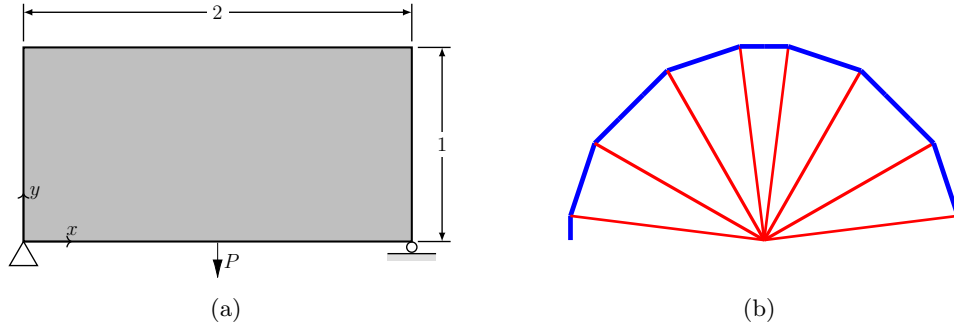


FIGURE 4.4: Half wheel example: (a) problem definition; (b) optimal structure obtained after phase one of the two phase method (i.e. not considering frequency constraints). All dimensions in metres

#### 4.2.4.2 Holistic optimization

Although the two phase approach described in the preceding section is computationally efficient for problems where it can obtain viable solutions, if the increase in volume in the second phase is large, then the question arises as to whether a more materially efficient design exists.

This can be checked by applying the formulation, including an SDP frequency constraint, to the full ground-structure. The associated computational expense means that only a coarse nodal grid ( $12 \times 6$ ) can be used in this case. For the short cantilever example, the solution obtained using the finest nodal density achievable with the available memory is shown in Figure 4.3(d). When compared with a reference structure consisting of the same size it demonstrates that a modified design enables the target frequency to be met with little impact on the overall volume of the structure. The optimum point where the

equilibrium and frequency constraints are satisfied requires a different layout to that of the structural optimization alone. However, it must be noted that the largest problem that could be solved with a fully-connected ground-structure is much smaller than the one that could be solved using the two phase approach.

TABLE 4.1: Short cantilever example: linear programming (LP) and semidefinite programming (SDP) results (target frequency for SDP problem = 425Hz).

Fig.	Model	Nodal Divisions	$V$	$V(P/\sigma)$ ( $10^{-5}m^3$ )	$f_1$ (Hz)	Time (s)
4.3(a)	LP (fine ref.)	$120 \times 60$	7.030	2.009	403	146
4.3(b)	LP	$40 \times 20$	7.095	2.027	410	26
4.3(c)	SDP (size only)	...	7.436	2.125	425	3
...	LP (coarse ref.)	$12 \times 6$	7.116	2.033	407	9
4.3(d)	SDP (full)	$12 \times 6$	7.134	2.038	425	1472

### 4.3 Semidefinite programming formulation with member-adding

To solve complex problems of this nature with a large initial ground-structure efficiently, a special-purpose solver based on the Mehrota-type primal-dual interior point method (Fujisawa et al. 2000) was developed. The approach and its implementation follows Weldeyesus et al. (2019), which describes the optimization of truss structures with constraints on global stability modelled via semidefinite programming. In Weldeyesus et al. (2019), the proposed method is capable of obtaining solutions to relatively large problems that could not otherwise have been solved. Due to similarities in the mathematical properties of the optimization problem considered in this paper, and the problem discussed in Weldeyesus et al. (2019), only the member-adding method is explained here in detail. Issues such as exploiting sparsity and low rank property of the element stiffness matrices  $\mathbf{K}_i$  and mass matrices  $\mathbf{M}_i$  when forming the linear systems arising in the interior point algorithm for SDP are not repeated here, but play a crucial role in the overall efficiency of the approach. As outlined in Section 4.2.1, the adaptive member-adding approach (which is based on column generation technique, see Gondzio and Sarkissian (1996), Desrosiers and Lübbecke (2005), Gondzio et al. (2013)) is an iterative process originally proposed in Gilbert and Tyas (2003), and also applied to other problems by e.g. Sokół and Rozvany (2013), Weldeyesus. and Gondzio (2018), who employed linear programming to obtain solutions. The method was extended to treat semidefinite programming problems by Weldeyesus et al. (2019). The procedure starts by solving a minimum connectivity ground-structure problem (Figure 4.1(d)), and proceeds by

adding elements from a potential connection list until a solution that satisfies the original fully-connected ground-structure problem is obtained. This approach enables the method to obtain the solution using a small fraction of the large number of potential connections: see [Gilbert and Tyas \(2003\)](#) and [Weldeyesus et al. \(2019\)](#) for supporting numerical results.

### 4.3.1 Details of the SDP member-adding algorithm

Here, a mathematical description of the member-adding procedure akin to that described in Section 4 of [Weldeyesus et al. \(2019\)](#) is presented. The primal problem Eq. (4.6) has an associated dual problem Eq. (4.7) where  $\mathbf{u} \in \mathbb{R}^n$  and  $\mathbf{X} \in \mathbb{S}_+^n$  (i.e.  $\mathbf{X}$  is symmetric and positive semidefinite) are the Lagrange multipliers for the equilibrium equation and the matrix inequality constraints in Eq. (4.6), respectively. Note that in some literature, for example [Wolkowicz et al. \(2000\)](#), the primal formulation Eq. (4.6) is stated as dual and the dual problem formulation Eq. (4.7) as primal.

$$\begin{aligned}
 & \underset{\mathbf{u}, \mathbf{X}}{\text{maximize}} && \mathbf{p}^T \mathbf{u} \\
 & \text{subject to} && -\frac{1}{\sigma^-} (l_i - (\mathbf{K}_i - \lambda \mathbf{M}_i) \bullet \mathbf{X}) \leq (\mathbf{B}^T \mathbf{u})_i, \\
 & && \forall i \\
 & && (\mathbf{B}^T \mathbf{u})_i \leq \frac{1}{\sigma^+} (l_i - (\mathbf{K}_i - \lambda \mathbf{M}_i) \bullet \mathbf{X}), \\
 & && \forall i \\
 & && \mathbf{X} \succeq 0.
 \end{aligned} \tag{4.7}$$

After solving, the dual violations can be obtained using only the variables  $\mathbf{u}$  and  $\mathbf{X}$  in Eq. (4.7). The process is as follows:

For any variable corresponding to member  $i$  to be dual feasible, formulation Eq. (4.7) implies that the relation

$$-\frac{1}{\sigma^-} \leq \frac{1}{l_i - (\mathbf{K}_i - \lambda \mathbf{M}_i) \bullet \mathbf{X}} (\mathbf{B}^T \mathbf{u})_i \leq \frac{1}{\sigma^+} \tag{4.8}$$

is satisfied. Now suppose that  $I_0 \subset \{1, \dots, m\}$  is a set of indices of members for which the primal problem Eq. (4.6) and its dual Eq. (4.7) are currently solved. After solving problem Eq. (4.6), and obtaining dual values corresponding to Eq. (4.7), for all members with indices in  $I_0$ , condition Eq. (4.8) can be used for all  $i \in \{1, \dots, m\} \setminus I_0$  to generate a set  $I$  of member indices to be added, given by

$$I = \left\{ i \in \{1, \dots, m_0\} \setminus I_0 \mid \frac{1}{l_i - (\mathbf{K}_i - \lambda \mathbf{M}_i) \bullet \mathbf{X}^*} (\sigma^- \varepsilon_i^- + \sigma^+ \varepsilon_i^+) \geq 1 + \beta \right\}, \quad (4.9)$$

where virtual strains are  $\varepsilon_i^+ = \max\{(\mathbf{B}^T \mathbf{u}^*)_i, 0\}$  and  $\varepsilon_i^- = \max\{-(\mathbf{B}^T \mathbf{u}^*)_i, 0\}$  with  $\mathbf{u}^*$  and  $\mathbf{X}^*$  being optimal points of the preceding subprogram, and  $\beta > 0$  is an allowed tolerance decided by the user. If  $I = \emptyset$  the member-adding procedure terminates; otherwise, members with indices in  $I$  are added to the subsequent problem, filtering these using the heuristic techniques described in [Weldeyesus. and Gondzio \(2018\)](#) if necessary to avoid problem size growing too rapidly.

### 4.3.2 Revisiting the short cantilever and half-wheel examples

In order to establish the gains in efficiency from utilising the new member-adding-based SDP algorithm, the problem given in Figure 4.2 will be revisited, initially replicating the problem in Figure 4.3(d) to demonstrate the efficiency gains of using the member-adding algorithm.

TABLE 4.2: Short cantilever example: fully-connected ground-structure and member-adding approaches (target frequency = 425Hz).

Fig.	Model	Nodal Divisions	$V$	$V(P/\sigma)$ ( $10^{-5}m^3$ )	Time (s)	Speed Up	Memory (Mb)
<a href="#">4.3(d)</a>	SDP (full)	$12 \times 6$	7.134	2.038	1472	...	16,081
<a href="#">4.5(a)</a>	SDP (mem. add.)	$12 \times 6$	7.134	2.038	8	$\times 183$	5

Results for coarse nodal grids are presented in Table 4.2 and in Figure 4.5(a). It is evident that the optimal volumes are identical irrespective of whether a fully-connected ground-structure or member-adding is employed, and the optimal truss solutions shown in Figure 4.3(d) and 4.5(a) are also virtually identical. Most significantly, it is also evident that the proposed member-adding algorithm can obtain a solution over two orders of magnitude quicker than when a fully-connected ground-structure is used, with the memory requirements reduced by three orders of magnitude. These efficiency improvements mean that problems involving relatively fine nodal grids can now be tackled, which was not possible before. Thus revisiting the problem shown in Figure 4.3(a), a new solution obtained via member-adding is presented in Figure 4.5(b), with additional solutions presented for higher minimum target frequencies in Figures 4.5(c-d). Corresponding computational details are shown in Table 4.3. This shows that relatively fine grid problems can be tackled, and that the geometry of the optimal structure changes when higher target frequencies are specified, with the overall volume also increasing.

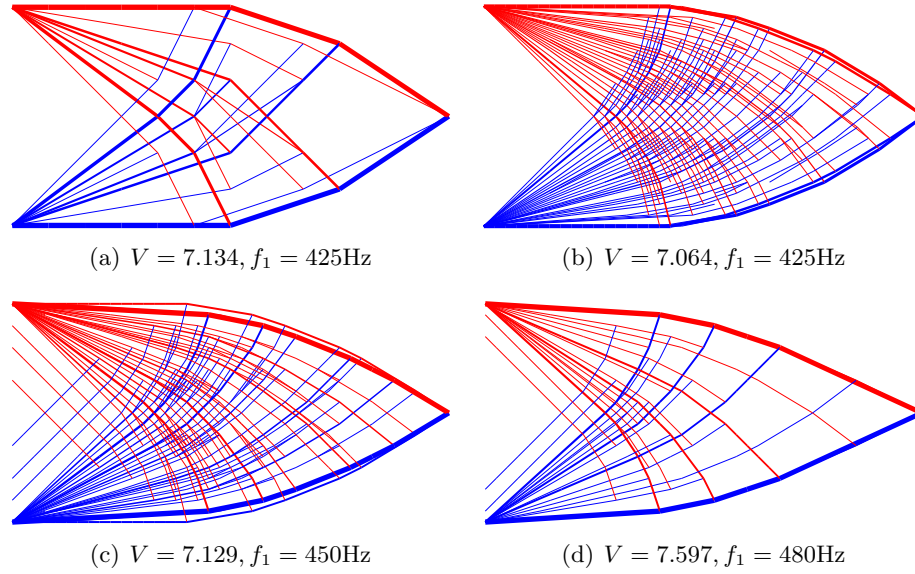


FIGURE 4.5: Short cantilever example: results obtained using the SDP member-adding method for a range of minimum frequencies. A total of  $12 \times 6$  nodal divisions are used in case (a) and  $40 \times 20$  in cases (b)-(d).

TABLE 4.3: Short cantilever example: results from SDP member-adding algorithm.

Fig.	Nodal Divisions	$V$	$\Delta V^\dagger$ (%)	$V(P/\sigma)$ ( $10^{-5}m^3$ )	$f_1$ (Hz)	Time (s)
4.5(b)	$40 \times 20$	7.064	+0.5	2.018	425	4915
4.5(c)	$40 \times 20$	7.129	+1.4	2.037	450	11655
4.5(d)	$40 \times 20$	7.597	+8.0	2.171	480	17671

<sup>†</sup>Percentage change compared with the volume of the reference structure shown in Figure 4.3(a).

Now revisiting the half wheel example: by applying the procedure proposed in this contribution, a structure that satisfies both equilibrium and frequency constraints can be generated. For a target frequency of 200Hz the generated solution is negligibly higher in non-dimensional volume (now  $V = 3.193$ , just 0.05% greater than before); see Figure 4.6. Significantly, to satisfy the frequency constraint, it is evident that additional stabilizing members have been added - although in this case some of these are very thin, with some radial members below the filter cut-off (in this case area =  $6 \times 10^{-8}m^2$ ) omitted.

### 4.3.3 Influence of initial member arrangement on computation

It has been demonstrated that the inclusion of a member-adding step in the optimization reduces the memory burden and enables problems of significant size to be tackled. To further understand the performance of the member-adding method, the examples originally considered by Gilbert and Tyas (2003) are used to investigate the influence

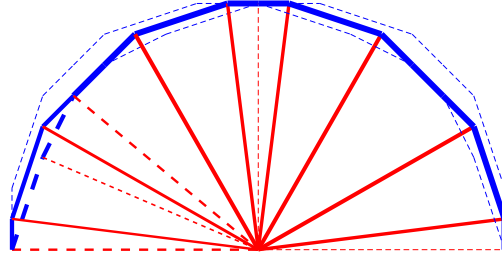


FIGURE 4.6: Half wheel example: structure obtained using combined equilibrium and frequency constraints for a target frequency of 200Hz (dashed lines indicate members added to satisfy the frequency constraint, also helping to stabilize the structure).

of the chosen initial nodal connectivity on the solution, the computational time, and the required memory footprint. A  $28 \times 28$  nodal division square domain is used; in this contribution overlapping connections are omitted as they can lead to instability in the frequency calculations due to multiple members coexisting in the same space. Due to the significant memory requirements of the fully-connected ground-structure example (circa 400Gb), an additional set of results is obtained using a domain comprising a reduced number of  $14 \times 14$  nodal divisions.

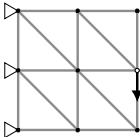
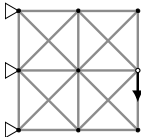
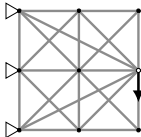
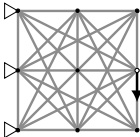
Applying the same physical parameters as the example shown in Figure 4.2, the original optimal truss structure from Gilbert and Tyas (2003) was assessed and found to have a first natural frequency of  $f_1 = 945\text{Hz}$ ; therefore an initial frequency target of  $f_1 = 950\text{Hz}$  was considered appropriate for the starting problem as it is close to the original yet includes an active frequency constraint. The target frequency was then increased by 10% to help verify the extent to which the influence of the initial member connectivity is common across a range of target frequencies.

Table 4.4 shows the four initial ground-structures considered, (a) - (d), together with results for the two target frequencies for each of the two nodal division discretisations; note that to maintain a basis for comparison, all presented volumes are non-dimensional. The resulting volumes for all the cases are within 1% of those provided in the original paper, demonstrating that in this case the frequency constraint does not come at a high cost in terms of structural efficiency, however CPU times are markedly increased. In contrast to the findings in the original paper by Gilbert and Tyas (2003), here it is also clear that the most efficient initial ground-structure in terms of CPU time comprises a ground-structure with the supports directly connected to the load (case (c)); this leads to a lower number of peak LP variables, indicating a reduced memory burden. Figure 4.7 shows the outcome of the initial iteration for each of the three initial ground-structures investigated when using the member-adding scheme for the  $14 \times 14$  nodal division case. It is evident that although the supports are in each case connected to the load, in the case of (c) this is predominantly achieved through the use of just two diagonal elements that directly connect the load with the supports.



TABLE 4.4: Influence of initial member connectivity on efficiency of member-adding scheme:

- (a) adjacent nodes connected (right to left upward diagonals in all cells);  
 (b) minimally-connected ground-structure, comprising nearest neighbour connectivity;  
 (c) minimally-connected ground-structure plus connections between boundary and loaded nodes;  
 (d) traditional fully-connected ground-structure (without overlapping bars).

		(a)	(b)	(c)	(d)	
						
$28 \times 28$	$f_1 = 950\text{Hz}$	Volume, V	2.432	2.432	2.432	-
		No. of iterations	9	6	7	-
		Initial No. of bars	2408	3192	3221	-
		Peak No. of bars	36151	8000	5881	-
		Time to $1.001 \times V$ (s)	63875.1	2209.9	804	-
		CPU Time (s)	182738.9	3811.6	2102.8	-
	$f_1 = 1045\text{Hz}$	Volume, V	2.441	2.441	2.441	-
		No. of iterations	12	7	8	-
		Initial No. of bars	2408	3192	3221	-
		Peak No. of bars	33964	10710	7005	-
		Time to $1.001 \times V$ (s)	192161.2	4054.9	992	-
		CPU Time (s)	289679.8	8555.2	2852.6	-
$14 \times 14$	$f_1 = 950\text{Hz}$	Volume, V	2.435	2.435	2.435	2.437
		No. of iterations	9	6	6	-
		Initial No. of bars	616	812	827	15556
		Peak No. of bars	4239	1982	1197	15556
		Time to $1.001 \times V$ (s)	660.2	69.9	29.1	-
		CPU Time (s)	1379.1	116.7	51.2	5501.3
	$f_1 = 1045\text{Hz}$	Volume, V	2.443	2.443	2.443	2.448
		No. of iterations	9	6	5	-
		Initial No. of bars	616	812	827	15556
		Peak No. of bars	3365	1936	1265	15556
		Time to $1.001 \times V$ (s)	346	67.4	33.8	-
		CPU Time (s)	748.1	134.8	45.5	5089.7

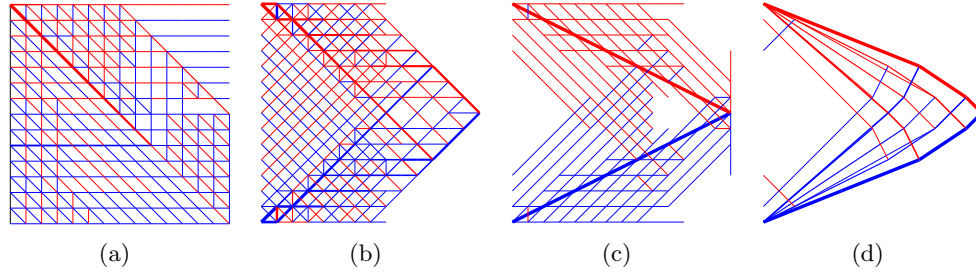


FIGURE 4.7: Influence of initial connectivity in member-adding scheme: (a) adjacent nodes connected (right to left upward diagonals in all units), iteration 1; (b) minimally-connected ground-structure with nearest neighbour nodes connected, iteration 1; (c) minimally-connected ground-structure plus boundary/loaded nodes connected, iteration 1; (d) final optimized structural form common to all starting points.

It should be noted that when member-adding is used, ground-structure (a) has the longest associated CPU time, and also the greatest number of LP variables at the end of the optimization process. Ground-structure (c) has the shortest associated CPU time, the fewest LP variables, and hence also the lowest memory consumption. For the sake of simplicity, initial ground-structure (b) will be used for all subsequent examples in this contribution. Finally, it should also be noted that although the optimized volume obtained when using a fully-connected ground-structure from the outset, (d), is marginally higher than obtained in the other three cases, this is likely due to the contribution to the volume of a large number of elements with areas very close to zero.

## 4.4 Numerical examples

A wider range of examples are now considered to further investigate the efficacy of the presented SDP member-adding algorithm when used to optimize a component, considering simultaneously equilibrium, strength, and first natural frequency constraints. Classical Hemp cantilever and MBB beam examples are first considered. A 3D cantilever designed to carry a point load is then considered, with different minimum specified natural frequencies used to show the resulting variation in form and associated volume. Each example begins with a minimum connectivity ground-structure.

### 4.4.1 Hemp cantilever example

The initial example considered was first studied by [Hemp \(1973\)](#) and consists of a square domain with single point load located at mid-height between two supports, as shown in Figure 4.8(a). Hemp determined the non-dimensional analytical volume to be approximately 4.34; later [He and Gilbert \(2015\)](#) applied more precise methods and geometry

rationalisation further reducing the optimum volume to 4.3228. Here a nodal grid comprising  $72 \times 72$  nodal divisions and the following material properties  $P = 1 \times 10^3 \text{N}$ ;  $E = 210 \times 10^9 \text{N m}^{-2}$ ;  $\rho = 8050 \text{kg m}^{-3}$  and the limiting tensile and compressive stresses  $\sigma = 350 \times 10^6 \text{Pa}$  were used to obtain a reference LP solution with a volume  $V = 4.332$ , within 0.5% of the improved optimum figure. The associated structure is shown in Figure 4.8(b). The first natural frequency of this reference structure was computed to be  $f_1 = 616 \text{Hz}$ .

In order to generate solutions in a reasonable timescale for the SDP analyses the nodal density was reduced to  $48 \times 48$ . An additional LP reference was obtained at this density which has negligible impact on volume but changes the first frequency to 686Hz. SDP analyses were conducted with target first natural frequencies of  $f_1 = 700 \text{Hz}$  and  $1000 \text{Hz}$  to identify changes in the generated structure. Results of the associated optimization runs are presented in Table 4.5 and Figures 4.8(c) and 4.8(d) respectively.

In the first case, the impact on the resulting generated structure and associated volume is small, with the increase in volume being less than 1% and little difference in overall layout. In the second case, increasing the minimum frequency to  $f_1 = 1000 \text{Hz}$  can be observed to have a much more significant impact, with the overall structural depth and complexity of the result both reduced.

TABLE 4.5: Hemp cantilever example: results obtained from equilibrium optimization and with inclusion of the frequency constraints.

Fig.	Model	Nodal Divisions	$V$	$\Delta V$ (%)	$V(P/\sigma)$ ( $10^{-5} \text{m}^3$ )	$f_1$ (Hz)	Time (s)
4.8(b)	REF	$72 \times 72$	4.332	...	1.238	616	194
...	LP	$48 \times 48$	4.339	+0.01%	1.240	623	17
4.8(c)	SDP	$48 \times 48$	4.340	+0.01%	1.240	700	42676
4.8(d)	SDP	$48 \times 48$	4.794	+10.6%	1.370	1000	75004

#### 4.4.2 MBB beam example

The Messerschmidt-Bölkow-Blohm (MBB) beam is attributed to the German aircraft company of the same name, and can still be found in an Airbus passenger aircraft. Though the real-world problem includes a number of design constraints, in the literature a simpler problem is normally considered, involving simple loading and boundary conditions, and usually targeting minimum volume or compliance. The exact analytical layout for the MBB structure with stress constraints was derived by Rozvany (1998), with the optimal non-dimensional volume  $V = 13.597$  for a beam length of 3. As the beam is symmetrical only the right half is shown in Figure 4.9(a). An optimization was

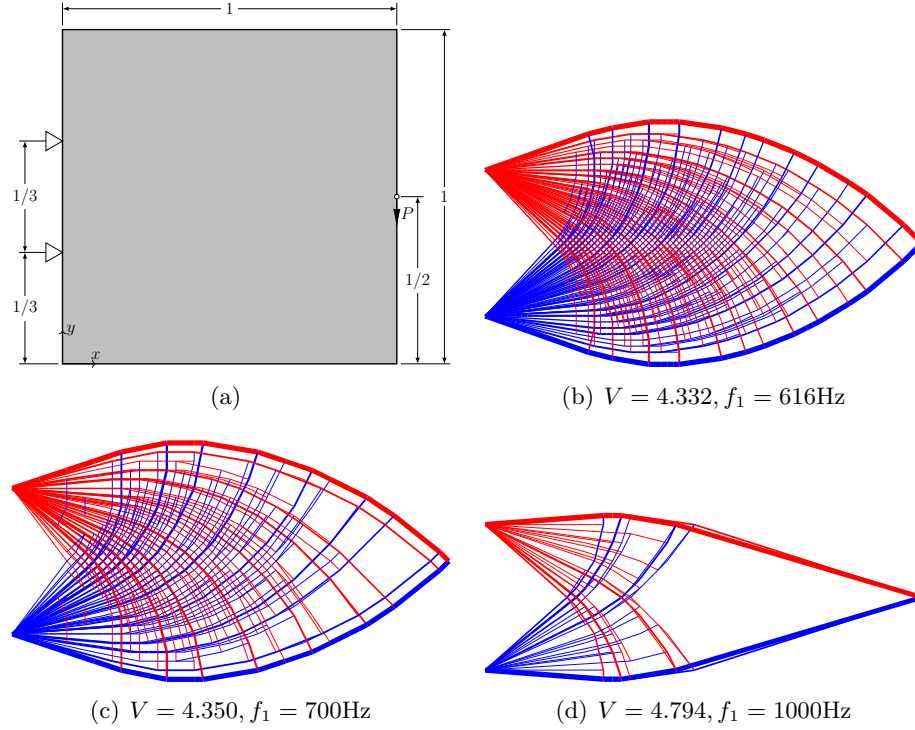


FIGURE 4.8: Hemp cantilever example: (a) problem definition with dimensions in metres; (b) reference LP solution, obtained with  $72 \times 72$  nodal divisions; (c) SDP member-adding solution obtained for a target frequency of 700Hz; (d) SDP member-adding solution obtained for a target frequency of 1000Hz. Note that both (c) and (d) have  $48 \times 48$  nodal divisions.

carried out with nodes directly along the symmetry plane free to move vertically whilst the bottom right corner was fixed in the vertical direction and free to move horizontally. The example assumes aerospace grade aluminium is used with  $P = 1 \times 10^3\text{N}$ ,  $\sigma = 90 \times 10^6\text{Pa}$ ,  $E = 68.9 \times 10^9\text{N m}^{-2}$  and  $\rho = 2770\text{kg m}^{-3}$ .

An initial LP optimization was carried out to obtain a reference volume and frequency for the structure, using  $60 \times 20$  nodal divisions to provide a balance between accuracy and computational efficiency (Figure 4.9(b)). SDP solutions were then sought for two minimum target frequencies; the solutions obtained (Table 4.6 and Figures 4.9(c) and 4.9(d)) demonstrate that the introduction of a frequency constraint has enabled minimum volume structures satisfying a given minimum frequency to be obtained, with very little impact on overall volume. However, it is evident that the time required to complete a frequency optimization is clearly considerably longer than that required for a basic LP optimization.

TABLE 4.6: MBB beam example: SDP member-adding algorithm results.

Fig.	Model	Nodal Divisions	$V$	$\Delta V$ (%)	$V(P/\sigma)$ ( $10^{-4}m^3$ )	$f_1$ (Hz)	Time (s)
4.9(b)	LP	$60 \times 20$	14.136	...	1.571	374	8
4.9(c)	SDP	$60 \times 20$	14.238	+0.72%	1.582	400	31781
4.9(d)	SDP	$60 \times 20$	14.631	+3.5%	1.626	425	46317

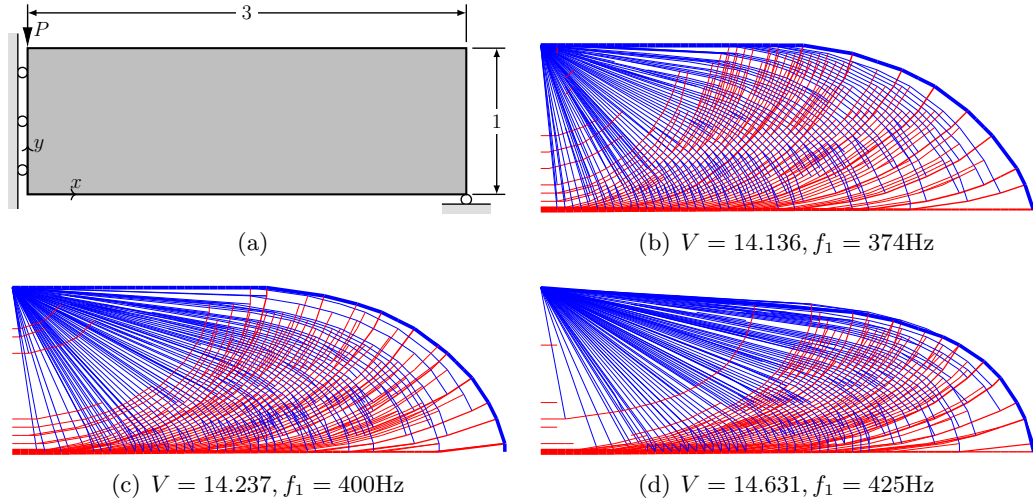


FIGURE 4.9: MBB beam example: (a) problem definition with dimensions in metres; (b) reference solution obtained for this example with the determined first natural frequency; (c) SDP member-adding solution obtained for a target frequency of 400Hz; (d) a target of 425Hz.

#### 4.4.3 3D cantilever example

The third example is a simple 3D cantilever beam, as shown in Figure 4.10(a). To improve the clarity of the results, and to minimize the additional computational burden associated with solving 3D problems, the number of nodal divisions has been reduced to  $6 \times 2 \times 2$  to ensure solutions are obtained in a manageable time-frame. The properties for this example are as follows:  $P = 1 \times 10^3 \text{N}$ ;  $E = 210 \times 10^9 \text{N m}^{-2}$ ;  $\rho = 8050 \text{kg m}^{-3}$  and maximum tensile and compressive stresses  $\sigma = 350 \times 10^6 \text{Pa}$ . Various target first natural frequencies are used to demonstrate the change in structural form that results from including a frequency constraint.

Full results for this example are shown in Table 4.7. Figure 4.10(b) shows the layout of the optimal structure based solely upon equilibrium and strength considerations, with the natural frequency of the resulting structure being found to be 57Hz. When a frequency constraint  $f_1 = 100 \text{Hz}$  is introduced (Figure 4.10(c)), the structure begins to change, with new members added to the structure. Similar to the 2D examples, these additional elements brace the structure, adding stiffness and therefore increasing the

frequency; however the use of member-adding has allowed this to happen in a short amount of time and with limited impact on the overall volume of the structure. As the target frequency is increased further to 150Hz and 200Hz as shown in Figures 4.10(d) and 4.10(e) respectively, a more dramatic change begins to take place, with the members that are primarily taking the load and providing structural stiffness becoming longer and growing in cross-section.

TABLE 4.7: 3D cantilever example: SDP member-adding algorithm results.

Fig.	Model	Cons	$V$	$\Delta V$ (%)	$V(P/\sigma)$ ( $10^{-5}m^3$ )	$f_1$ (Hz)	Time (s)
4.10(b)	LP	474	30.676	...	8.765	57	5.8
4.10(c)	SDP	566	30.883	+0.6	8.824	100	9.9
4.10(d)	SDP	633	33.233	+8.3	9.495	150	12.6
4.10(e)	SDP	582	38.111	+24.2	10.889	200	13.3

## 4.5 Conclusions

Numerical layout optimization provides an efficient means of generating optimal truss structures for a given set of design requirements. However, traditional linear programming-based formulations are limited, and cannot, for example, accommodate frequency constraints. In this contribution, extended semi-definite programming-based formulations are considered that allow the minimum first natural frequency of a structure to be specified. The main conclusions are as follows:

- a) The use of a two phase approach, in which the traditional LP layout optimization formulation is used in the first phase and an SDP size optimization is used in the second phase, provides a computationally efficient means of generating solutions satisfying a specified frequency constraint. However, the solutions obtained are likely to be sub-optimal, with the resulting structures having higher than necessary volume.
- b) Alternatively, a constraint on frequency can be introduced in the optimization directly, furnishing layouts that satisfy both structural performance and first natural frequency requirements. However, when using a fully-connected ground-structure and a standard SDP solver, the computational cost and memory requirements have been found to be high, severely limiting the scale of problem that can be tackled.
- c) The use of a bespoke solver and an adaptive member-adding solution strategy, which involves starting with a sparsely connected ground-structure and only adding

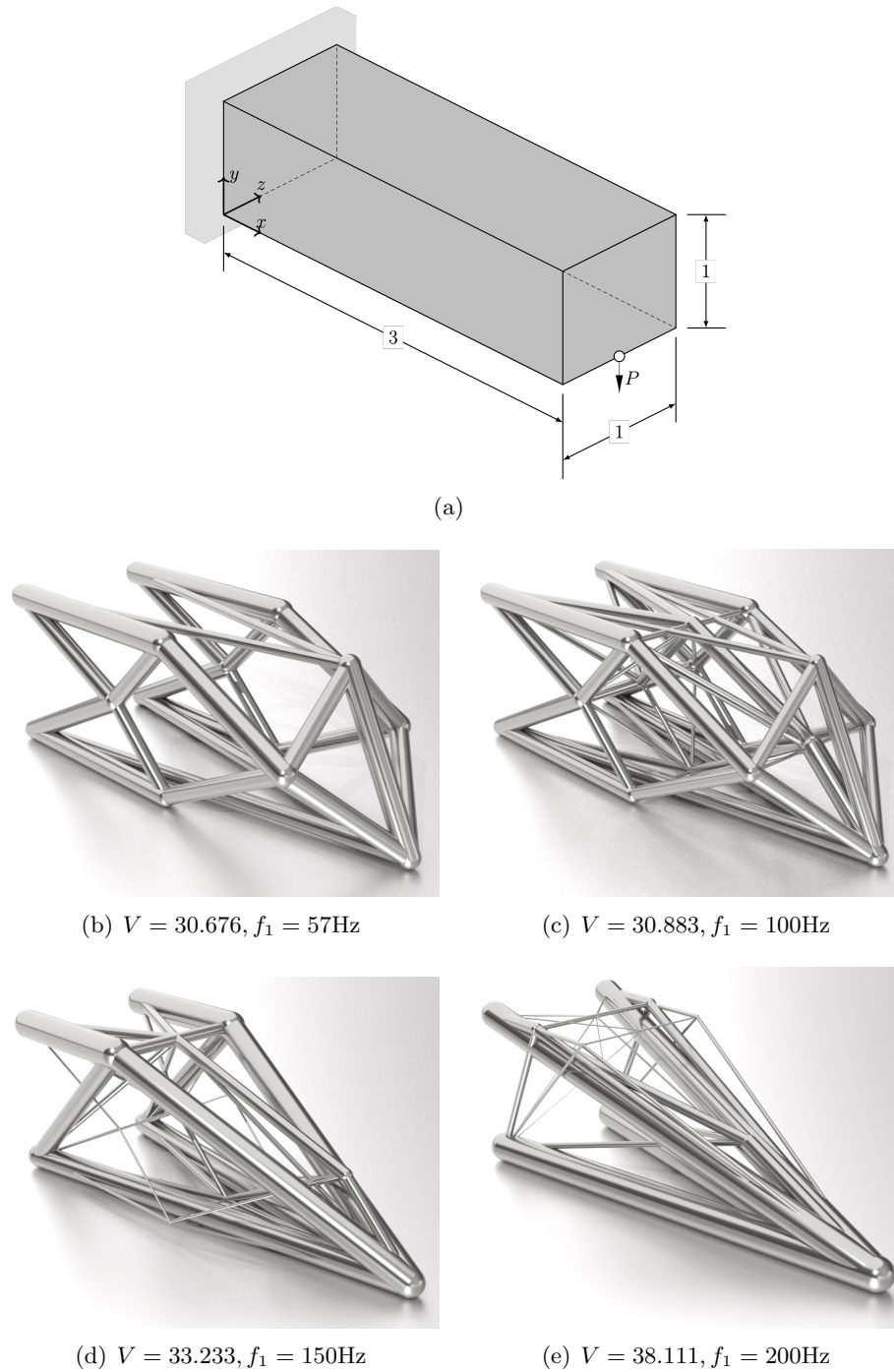


FIGURE 4.10: 3D cantilever example: (a) problem definition with dimensions in metres; (b) LP solution (no frequency constraint); (c) SDP member-adding solution for a target frequency of 100Hz; (d) a target of 150Hz; (e) a target of 200Hz. All cases employ  $6 \times 2 \times 2$  nodal divisions.

members as required until the optimal solution is found, allows solutions to be obtained in a much shorter time-frame (183 times quicker in the case of one of the examples considered), and with much lower memory consumption. This approach has been successfully applied to a range of 2D and 3D problems in this paper.

In future studies, the influence of joints on vibration characteristics will be considered in more detail with, for example, differences in optimal layout and volume being evaluated when rigid-joints as opposed to pin-joints are assumed. In addition, consideration will be given to limiting the number and arrangement of members within a final design, to ensure the resulting component is readily manufacturable.



## Chapter 5

# Layout optimization of rigid frame structures with semidefinite frequency constraints

The ability to target the frequency response of an engineering component or structure is critical in the aerospace and automotive sectors, and is therefore a key consideration when seeking any new, more efficient, design. This contribution demonstrates that structurally efficient frame structures can be identified using layout optimization, targeting constraints on both limiting stresses and first natural frequency, using an iterative solution procedure involving successive application of semidefinite programming (SDP). The proposed optimization algorithm uses a fully-connected ground-structure, which provides significant design freedom, to arrive at the arrangement of structural members minimizing structural volume. In each step of the iterative procedure described, the second moment of area is assumed to vary linearly with the area of each member. The efficacy of the method is demonstrated via application to a number of benchmark problems, showing that acceptable minimum first natural frequency responses can successfully be identified. Details of a parameter study focusing on assessing the influence of nodal resolution on the solutions obtained and computational time are also presented.

### 5.1 Introduction

Structural topology and layout optimization methods have received considerable attention over the years, with both heuristic (e.g. [Xie and Steven \(1993\)](#); [Querin et al. \(1998\)](#)), and gradient-based (e.g. [Bendsøe and Sigmund \(2003\)](#); [Rozvany and Lewiński \(2014\)](#)) approaches proposed. Although heuristic optimization methods are versatile in terms

of the number and variety of different problems that can be solved, they are usually inefficient due to the lack of an underpinning mathematical framework. On the other hand, gradient-based methodologies are generally much more computationally efficient, though require some mathematically-derived information to be available before a solution can be found. For the problem considered here, this information is readily available and thus the present contribution focuses on the application of gradient-based methods to component design problems involving strength and minimum natural frequency constraints.

The ground-structure method, initially introduced by [Dorn et al. \(1964\)](#), has been instrumental in solving plastic truss design problems. Layout optimization, based on this methodology, aims to identify the most efficient arrangement of elements within a truss structure. Researchers have widely used this approach to find minimum volume truss structures. Notable studies by [Hemp \(1973\)](#), [Gilbert and Tyas \(2003\)](#), [Smith et al. \(2016\)](#), have explored this topic, initially using linear programming (LP) and later incorporating an adaptive ‘member-adding’ (column generation) technique for efficient solutions in single load case problems. Extensions by [Pritchard et al. \(2005\)](#) and [Sokół \(2014\)](#) allow for solving multiple load case problems. In terms of computational efficiency, the focus remains on single load case scenarios, where a specified minimum frequency is chosen to avoid interference with other excitation frequencies. Frequency analysis involves matrix constraints, necessitating the use of semidefinite programming (SDP) rather than LP. SDP has previously been applied to truss structure optimization by [Ben-Tal and Nemirovski \(1997\)](#) and later [Giniūnaitė \(2015\)](#) where the goal was to achieve minimum mass structures. Soon after [Kanno \(2018\)](#) proposed an algorithm to address cases where lack of certainty in the applied loading required the derivation of structures which were robust against variation. SDP has been developed into a number open source and commercially available solver packages: `fminsdp` ([Thore, 2018](#)); MOSEK (v8+) ([MOSEK ApS, 2017](#)); PENLAB ([Fiala et al., 2013](#)) and CVX ([Grant and Boyd, 2014](#)) are a few examples.

The optimization of a component or systems natural frequency is part of eigenvalue analysis, a distinct field of mathematics, and has been extensively studied by the mathematical programming community. An initial approach by [Fox and Kapoor \(1970\)](#) addressed the underlying SDP problem by adopting a feasibility approach. This was then further augmented using the optimality criterion method by [Grandhi and Venkayya \(1988\)](#) and [Khot \(1985\)](#). Later, [Kaveh and Ghazaan \(2016\)](#) performed size optimization on existing truss structures through the employment of non-smooth optimization, to drive them to meet specific frequency requirements; similar problems were also addressed using SDP by [Achtziger and Kočvara \(2007\)](#). [Aroztegui et al. \(2011\)](#) then developed a feasible direction SDP algorithm capable of maximizing fundamental frequencies when applied to

relatively simple full-connected ground-structure problems. When considering frequency optimization in isolation, [Azad et al. \(2018\)](#) assessed simultaneous size and geometry optimization for steel structures subjected to external excitation using the ‘big bang - big crunch’ algorithm. However, their results were mixed when compared to known optimal solutions. Meanwhile, [Taheri and Jalili \(2016\)](#) and [Tejani et al. \(2018\)](#) explored alternative meta-heuristic methods to impose frequency constraints in truss optimization problems. Recently, [Salt et al. \(2022\)](#) proposed a customized SDP-based truss layout optimization procedure. Their approach capitalizes on an adaptive ‘member-adding’ strategy, effectively addressing optimization problems related to eigenvalue frequency constraints.

Although [Salt et al. \(2022\)](#) were able to successfully optimize pin-jointed truss structures with constraints on natural frequency, there are a limited number of practical application areas for such structures. This is because such structures or components will, more commonly, possess fully rigid joints. This rigidity is usually the result of the chosen manufacturing method which may include fabrication by welding or riveting, machining from solid or by AM techniques. This contribution will focus on identifying frame structures incorporating rigid joints with constraints on natural frequency produced by AM. Targeting AM as a production method increases the available design freedom, which can therefore be exploited to a much greater extent than when traditional subtractive manufacturing methods are employed, opening up greater opportunities to realize least-weight structures. Specifically, use of AM allows the considerable benefits of layout optimization to be realized in practice, i.e. the ability of the optimization procedure to identify structures where the optimal solution may consume only a small fraction of the specified design domain. In contrast, other optimization methods such as continuum topology optimization based methods, may typically require the use of a volume fraction of at least 10% of the design domain ([Aage et al., 2013](#)) in order to be manufacturable. SDP calculations for frame layout optimization with frequency constraints were put forward by [Kanno and Ohsaki \(2007\)](#), and demonstrated to work for problems with minimally-connected ground-structures comprising a small number of nodes ( $7 \times 7$  nodes). [Ye et al. \(2017\)](#) also focused on the design of frame structures via layout optimization, integrating the proposed approach in the Rhino-Grasshopper parametric modelling software and citing a 30% reduction in material usage for the demonstrated case study. [Larsen et al. \(2018\)](#) proposed a novel method to obtain near-optimal frame structures generated from homogenization-based topology optimization results, focusing on bending stiffness and solving problems in relatively short time-frames. Finally, [Zakian \(2021\)](#) applied the heuristic ‘adaptive charged system search’ algorithm to the optimal design of steel frame structures in the presence of frequency constraints.

Here the focus is on the development and application of an iterative SDP-based layout optimization procedure to identify minimum volume frames in the presence of frequency constraints. Specifically, in this contribution the constituent material is assumed to operate in the elastic phase for the imposed frequency constraints, with maximum stress constraints also present to ensure a suitable margin of safety exists against overloading. All frequencies quoted are undamped natural frequencies. The contribution is organized as follows: Section 5.2 describes the basic formulations relevant to the frequency problem at hand; Section 5.3 then proposes a new analysis tool for the layout optimization of frame structures with frequency constraints; the new tool is then applied to various example problems in Section 5.4; Section 5.5 provides a study on the impact of using a fully-connected ground-structure on computational efficiency, compared with a ‘member-adding’ alternative; finally conclusions are drawn in Section 5.6.

## 5.2 Truss layout optimization

### 5.2.1 Minimum volume with stress constraints formulation

The solving of any truss optimization based on the ground-structure method begins with the definition of the design domain, it is within this space that the final resulting structure will be generated once key parameters governing material, loads and supports has been applied to fully describe the problem, see Figure 5.1(a). In general layout optimization will seek to obtain the lowest volume/mass/weight solution whilst maintaining the overall integrity of the structure, i.e. remaining below the stress threshold of the material. The design domain is discretised with a predefined number of nodes ( $n$ ) in the  $x$  and  $y$  directions, Figure 5.1(b), and are then linked with potential connections ( $m$ ), connecting each node to every other node in the domain, Figure 5.1(c), this is referred to as a fully-connected ground-structure. Alternatively, each node may be connected only to its closest adjacent neighbour only to form a minimally-connected ground-structure, Figure 5.1(d) which has been proven to be more computationally efficient when compared with full-connected ground-structures (Gilbert and Tyas, 2003). Herein, each example will employ a number of nodes expressed in terms of number of nodal divisions, e.g. referring to Figure 5.1(b), the domain has  $4 \times 2$  nodal divisions, with 4 divisions (and 5 nodes) in the  $x$  direction and 2 divisions (and 3 nodes) in the  $y$  direction (giving 15 nodes in total).

The basic truss layout optimization formulation, Eq. (5.1), provides a highly efficient means of identifying a minimum volume truss geometry for any given set of boundary and loading conditions. Constraints are introduced to ensure equilibrium is enforced

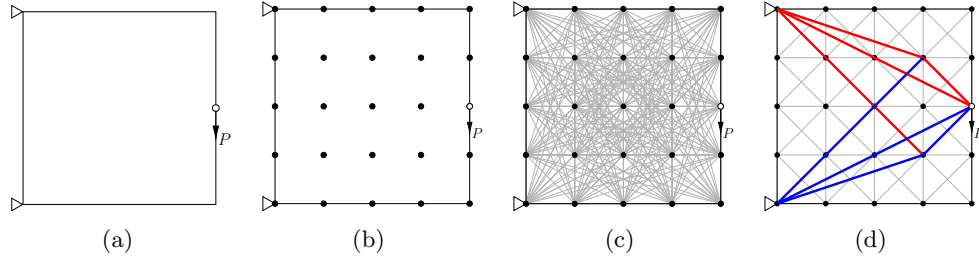


FIGURE 5.1: Steps in the truss layout optimization procedure: (a) design domain, load and support conditions; (b) design domain populated with nodes; (c) each node connected to every other node to form a fully-connected ground-structure; (d) alternatively each node connected only to neighbouring nodes to form a minimally-connected ground-structure, with additional connections added as necessary via ‘member-adding’ algorithm to obtain the optimal structure (comprising members shown in red and blue, indicating respectively elements in tension and compression).

at nodes, and to ensure that the cross-sectional area of each element is both a positive number and is sufficiently large to carry the internal forces, given the limiting stress that can be sustained by the material employed. The formulation for a single load case plastic truss layout optimization problem comprising  $n$  nodes and  $m$  members may be solved using a Linear Programming (LP) solver:

$$\begin{aligned} & \text{minimize } V = \mathbf{l}^T \mathbf{a} \\ & \text{subject to } \begin{cases} \mathbf{B}\mathbf{q} = \mathbf{p}, \\ -\sigma^- a_i \leq q_i \leq \sigma^+ a_i, & \forall i \\ a_i \geq 0, & \forall i, \end{cases} \end{aligned} \quad (5.1)$$

where  $V$  is the total volume of the structure;  $\mathbf{l}$  is a vector of individual element lengths  $\{l_1, l_2, \dots, l_m\}$ ;  $\mathbf{a}$  is a vector containing element cross-sectional areas  $\{a_1, a_2, \dots, a_m\}$ ;  $\mathbf{B}$  is a suitable  $(2n \times m)$  equilibrium matrix containing direction cosines (for 2D problems);  $\mathbf{q}$  is a vector of element axial forces,  $\mathbf{q} = \{q_1, q_2, \dots, q_m\}$ , where  $q_i$  is the force in element  $i$ ;  $\mathbf{p}$  is a vector of applied loads and  $\mathbf{p} = \{p_1^x, p_1^y, p_1^z, p_2^x, p_2^y, p_2^z, \dots, p_m^z\}$ , where  $p_j^x, p_j^y, p_j^z$  are the  $x, y$  and  $z$  direction components of the load applied to node  $j$  ( $j = 1, \dots, n$ ). Finally  $\sigma^+$  and  $\sigma^-$  are, respectively, the limiting tensile and compressive stresses that can be sustained by the material.

### 5.2.2 Semidefinite frequency constraint

Salt et al. (2022) revised formulation Eq. (5.1) to allow inclusion of frequency constraints; the resulting formulation Eq. (5.2) allows layout optimization of truss structures with constraints on both limiting stress and frequency:

$$\begin{aligned}
& \min_{\mathbf{a}, \mathbf{q}} \quad V = \mathbf{l}^T \mathbf{a} \\
& \text{s.t.} \quad \begin{cases} \mathbf{B}\mathbf{q} = \mathbf{p}, \\ \mathbf{K}(\mathbf{a}) - \lambda_0 \mathbf{M}(\mathbf{a}) \succcurlyeq 0 \\ -\sigma^- a_i \leq q_i \leq \sigma^+ a_i, \quad \forall i \\ a_i \geq 0, \quad \forall i, \end{cases} \quad (5.2)
\end{aligned}$$

where  $\mathbf{K}(\mathbf{a}) = \sum_{i=1}^m \mathbf{K}_i a_i$  and  $\mathbf{M}(\mathbf{a}) = \sum_{i=1}^m \mathbf{M}_i a_i$  are the global stiffness and mass matrices respectively;  $a_i$  refers to the cross-sectional area of member  $i$ ;  $\lambda$  is the eigenvalue derived from the minimum specified natural frequency ( $\omega_1$ ) for the specified mode of vibration  $\phi_j$ ; and  $\succcurlyeq$  denotes the matrix to its left is symmetric and positive semidefinite. All remaining terms are as per formulation Eq. (5.1). For the purposes of this contribution, the connecting nodes are not considered and therefore the mass associated with the joint  $\mathbf{M}_0 = 0$ .

Note that Eq. (5.2) includes semidefinite constraints and was solved by Salt et al. (2022) using a bespoke solver based on the Mehrota primal-dual interior point method (Fujisawa et al. 2000). The basic approach and its implementation followed that proposed by Weldeyesus et al. (2019), where the focus was on treating truss layout optimization problems involving constraints on global stability, solved via semidefinite programming. Also, to reduce the computational burden associated with problems containing a large number of potential connections, an adaptive ‘member-adding’ routine was employed. This is based on the column generation technique (see Gondzio and Sarkissian (1996), Desrosiers and Lübbecke (2005), Gondzio et al. (2013)) and was originally proposed for basic truss optimization problems by Gilbert and Tyas (2003), and later also employed by workers such as Sokół and Rozvany (2013), Weldeyesus. and Gondzio (2018).

### 5.3 Frame layout optimization

A typical truss structure will be pin-jointed, therefore limiting transmission between elements to axial forces and not moments or shear forces. Whereas a beam element, though similar to a truss in that it is usually a straight element of uniform cross-section, deforms only in a direction perpendicular to its axis, such that the load carried by the beam is transverse and not axial. A frame element can be considered as a combination of both a truss and a beam element, as they can deform in directions both in line with, and perpendicular to, the central axis and carry axial and transverse forces and moments. Frame structures are common in practice as real-world loading typically imparts a combination of axial and transverse forces. As with trusses, a frame structure

can be either planar or be a space frame; however all joints may be rigidly fixed to enable axial and shear forces, and also moments to be transferred between elements.

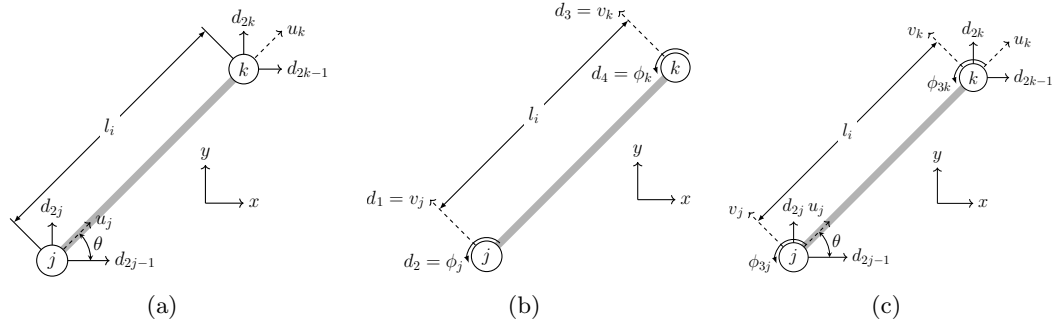


FIGURE 5.2: Comparison of the degrees of freedom in local coordinates  $u$ ,  $v$  &  $\phi$  and global coordinates  $d_i$  for the following element types: (a) truss; (b) beam; and (c) frame.

### 5.3.1 Stiffness and mass matrices for frames

In the study conducted by Salt et al. (2022), the stiffness and mass matrices for each individual truss element were constructed with the variable for area,  $a$ , outside of the matrix and constants for  $E$ ,  $\rho$ , and  $l$  contained within; these were termed coefficient matrices,  $\bar{\mathbf{K}}_i$  and  $\bar{\mathbf{M}}_i$ . This enabled the matrix for each element to be multiplied by the design variable, area  $a_i$ , at each iteration in the optimization, until the solution was found. However, as noted above, in a frame both axial forces and shear forces / bending moments contribute to the overall structural performance; the stiffness matrix Eq. (5.3a) for a frame element combines these effects:

$$\mathbf{k}_i = \begin{bmatrix} d_{3j-2} & d_{3j-1} & \phi_{3j} & d_{3k-2} & d_{3k-1} & \phi_{3k} \\ \frac{aE}{l} & 0 & 0 & -\frac{aE}{l} & 0 & 0 \\ 0 & \frac{12EI}{l^3} & \frac{6EI}{l^2} & 0 & -\frac{12EI}{l^3} & \frac{6EI}{l^2} \\ 0 & \frac{6EI}{l^2} & \frac{4EI}{l} & 0 & -\frac{6EI}{l^2} & \frac{2EI}{l} \\ -\frac{aE}{l} & 0 & 0 & \frac{aE}{l} & 0 & 0 \\ 0 & -\frac{12EI}{l^3} & -\frac{6EI}{l^2} & 0 & \frac{12EI}{l^3} & -\frac{6EI}{l^2} \\ 0 & \frac{6EI}{l^2} & \frac{2EI}{l} & 0 & -\frac{6EI}{l^2} & \frac{4EI}{l} \end{bmatrix} \begin{matrix} d_{3j-2} \\ d_{3j-1} \\ d_{3j} \\ d_{3k-2} \\ d_{3k-1} \\ d_{3k} \end{matrix} \quad (5.3a)$$

where  $E$  is the Young's modulus of the material and  $I$  is the second moment of area of element  $i$ . Note that the terms in the matrix that refer to axial force effects are taken from the stiffness matrix of a truss, whilst the remaining terms are taken from the stiffness matrix of a beam. Similarly the mass matrix for a frame element Eq. (5.3b) combines terms from trusses and beams as follows:

$$\mathbf{m}_i = \frac{\rho al}{420} \begin{bmatrix} & d_{3j-2} & d_{3j-1} & \phi_{3j} & d_{3k-2} & d_{3k-1} & \phi_{3k} \\ 140 & 0 & 0 & 70 & 0 & 0 & \\ 0 & 156 & 22l & 0 & 54 & -13l & \\ 0 & 22l & 4l^2 & 0 & 13l & -3l^2 & \\ 70 & 0 & 0 & 140 & 0 & 0 & \\ 0 & 54 & 13l & 0 & 156 & -22l & \\ 0 & -13l & -3l^2 & 0 & -22l & 4l^2 & \end{bmatrix} \begin{matrix} d_{3j-2} \\ d_{3j-1} \\ \phi_{3j} \\ d_{3k-2} \\ d_{3k-1} \\ \phi_{3k} \end{matrix} \quad (5.3b)$$

where  $\rho$  is the density of material.

It must be noted that in the case of a frame structure, the stiffness matrix now includes terms for the second moment of area,  $I_i$ , which is not directly proportional to the cross-sectional area  $a_i$  meaning the matrix in its current form cannot be multiplied by area,  $a$ ; the consequences of this are considered further in the next section.

### 5.3.2 Relationship between cross-sectional area & second moment of area





The relationship between the area  $a_i$  and second moment of area  $I_i$  of a cross-section depends on the type of cross-section used, and the way in which it is allowed to vary - see Table A.1 in the Appendix, which provides the formulae used to calculate  $I$  for a range of cross-section geometries.

Although not usually directly proportional, in the case of some cross-section geometries the relationship between  $a_i$ , and  $I_i$  is near-linear. Table 5.1 shows values for cross-sectional areas  $a_i$ , and second moments of area  $I_i$ , calculated using the formulae in Table A.1; these values are also plotted in Figure 5.3. The plot shows that there is a linear relationship between area and second moment of area for the I-section beam when only the widths of the web and flanges are changed ( $B$  in Table A.1); this is also observed when the height  $h$  of the rectangular cross-section is kept constant and only the width  $b$  is modified to change the area. Conversely, there is a near-linear relationship between area and second moment of area for the rhombus and circular cross-sections. Thus, by linearizing the relationship between  $I_i$  and  $a_i$  it is still possible for  $a_i$  to remain as the



main design variable, and to use this as a multiplier of the stiffness and mass coefficient matrices,  $\bar{\mathbf{K}}_i$  and  $\bar{\mathbf{M}}_i$ .

TABLE 5.1: Second moment of area calculated for a selection of element cross-sections (also plotted in Figure 5.3). Images indicate how each cross-section is assumed to vary with change in area; dark shading indicates original form, light shading indicates growth.

Area $a$ (mm <sup>2</sup> )	Second moment of area $I_{xx}$ (mm <sup>4</sup> )			
	I-Section	Rhombus	Circle	Rectangle
				
1.873	7.841	0.292	0.279	4.214
2.05	8.672	0.35	0.334	4.613
2.346	10.061	0.459	0.438	5.279
2.961	12.943	0.731	0.698	6.662
5.004	22.518	2.087	1.993	11.259
5.782	26.164	2.786	2.66	13.009
7.077	32.234	4.173	3.985	15.922
7.772	35.492	5.033	4.806	17.486
8.176	37.389	5.571	5.32	18.397
8.386	38.372	5.86	5.596	18.868
11.05	50.858	10.175	9.716	24.862
11.724	54.020	11.455	10.939	26.380
12.779	58.963	13.608	12.995	28.752

### 5.3.2.1 Solid rectangular cross-section of fixed height

Through rearrangement of expression (A.7) (see Appendix A),  $I$  can be made a constant in the stiffness matrix  $\mathbf{K}_i$  and dependent upon the design variable  $a$ :

$$I_{xx} = \frac{BH^3}{12} = a_i \frac{H^2}{12} \quad (5.4)$$

where  $B = a_i/H$ , whilst  $H$  is fixed. The terms for  $I$  in Eq. (5.3a) can be replaced with  $H^2/12$ . The entirety of  $\mathbf{K}_i$  can then be multiplied by  $a_i$  in the optimization iterations, and therefore  $I$  is treated correctly. It should be noted that for sake of simplicity herein,  $H$  has been assumed to be constant for every element in the structure, though this could easily be changed in future studies.

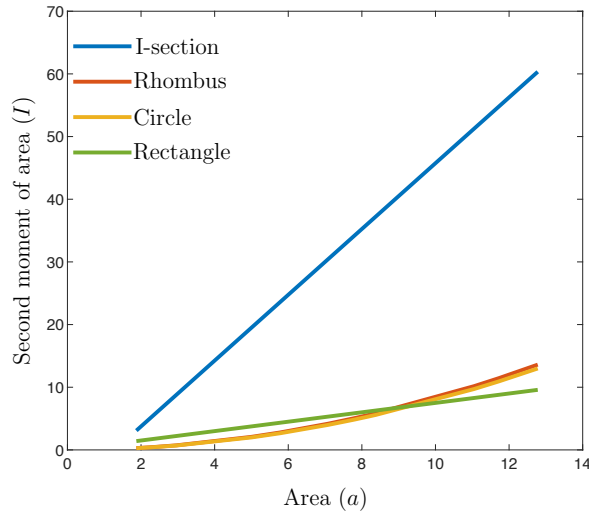


FIGURE 5.3: Second moment of area for the four cross-sections considered plotted against cross-sectional area (data from Table 5.1). Note that both the I-section and rectangular forms have a linear relationship when the geometry is controlled; also the curves for the rhombus and circular cross-sections are near-linear, and could potentially be accurately approximated using a series of linear segments.

### 5.3.2.2 I-section beam with fixed height

For the I-section beam shown in Figure 5.4, where the heights  $H$  and  $h$  are fixed, Eq. (A.8) in Appendix A can be rearranged in terms of area ( $a_i$ ), assuming that only the widths of the flanges and web can vary. The following values pertaining to the geometric form of the beam must be set: 1) a ratio between the cross-sectional area of the beam  $a_i$  and the total occupied area  $a_T$ , Eq. (5.5a); and 2) a further ratio to control the breadth of the flanges and the web thickness, Eq. (5.5b), which is also proportional to  $a_i$ . Thus the total area that the beam occupies,  $a_T = BH$ , and the empty void area between the flanges, lightly shaded in Figure 5.4,  $a_E = 2bh$ , each may be expressed as a ratio to one another, and  $a_i$ ;  $a_E$  will always be smaller than  $a_T$

$$k_1 = \frac{a_{T0}}{a_0} \quad (5.5a)$$

$$k_2 = \frac{a_{T0}}{a_{E0}} \quad (5.5b)$$

where  $a_{E0} = a_{T0} - a_0$ . The resulting equation for  $I_{xx}$  is therefore:

$$I_{xx} = \frac{BH^3 - 2bh^3}{12} = \left[ \left( \frac{a_{T,i}H^2}{12} \right) - \left( \frac{a_{E,i}h^2}{12} \right) \right] = a_i \left[ \left( \frac{k_1H^2}{12} \right) - \left( \frac{k_2h^2}{12} \right) \right] \quad (5.6)$$

where  $a_{T,i} = a_i k_1$ , and  $a_{E,i} = a_{T,i} - a_i$ . Applying the terms within square brackets in Eq. (5.6), which are now constant, to the element stiffness matrix  $\mathbf{K}_i$  enables the matrix to be multiplied by  $a_i$ , and the correct values for  $I_{xx}$  used in the optimization.

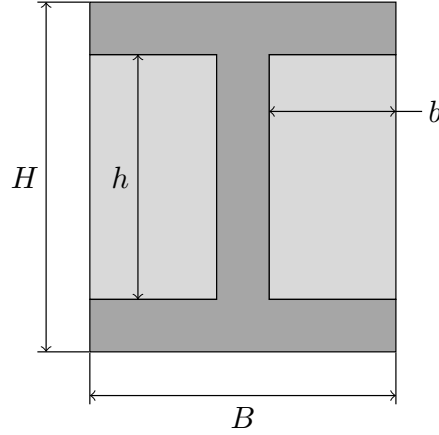


FIGURE 5.4: Example I-section beam with fixed height: dark grey shading indicates the cross-sectional area of the beam,  $a_i$ ; light grey shading indicates the empty void area between the flanges,  $a_E$ ; the sum of the two shaded areas is the total enclosed area of the beam cross-section,  $a_T = a_i + a_E$ .

### 5.3.3 Iterative solution procedure for frame layout optimization with frequency constraints

#### 5.3.3.1 Overview

Here the goal is to develop a tool that is capable of finding optimal, minimum volume, frame layouts with constraints on natural frequency. Using the proposed tool, three steps are carried out: (i) layout optimization; (ii) frequency solver; and (iii) solution refinement; each step is discussed and then demonstrated via the simple numerical example described below.

Thus a 10-bar cantilever structure is shown in Figure 5.5(a). It has pinned supports at the top and bottom of the left edge and carries a single point load at the top right. For this example  $l = 100\text{mm}$ ;  $P = 1 \times 10^3\text{N}$ ;  $E = 64 \times 10^9\text{N m}^{-2}$ ;  $\rho = 2711\text{kg m}^{-3}$ ; and the limiting tensile and compressive stresses  $\sigma = 275\text{MPa}$ . Note that for sake of simplicity in this worked example, only the elements specified in Figure 5.5(a) are assumed to exist; i.e. no additional connections can be added.

#### 5.3.3.2 Frame layout optimization

The first step of the proposed procedure is frame layout optimization, comprising the operations shown in Figure 5.6. This is where the size and shape of the domain is set,

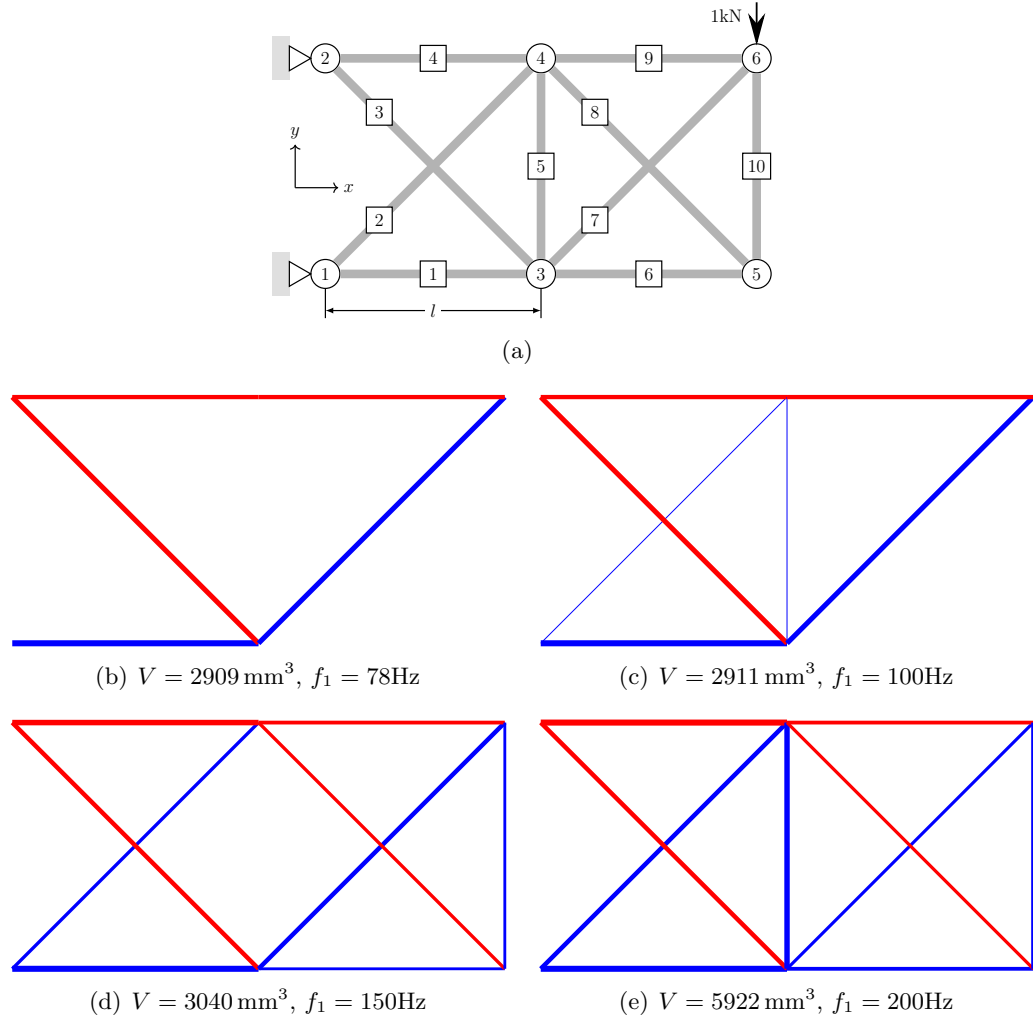


FIGURE 5.5: 10 bar frame example: (a) problem domain, ground-structure and boundary conditions; (b) results from an LP optimization (ignoring frequency constraints); (c) results from SDP optimization targeting 100Hz; (d) 150Hz; (e) 200Hz. (Key: red = tension; blue = compression; line thicknesses are shown in proportion to element areas).

the mechanical properties of the chosen material are input, the cross-sectional shape used to form the elements is chosen, and any predefined geometric constants for the cross-section are selected. The nodal density of the domain is also chosen, dictating how many potential connections will be present in the fully-connected ground-structure. The number of nodes specified will also dictate the quantity of memory consumed in any subsequent SDP optimization. The coefficient matrices for stiffness  $\bar{\mathbf{K}}_i$  and mass  $\bar{\mathbf{M}}_i$  are then generated using Eq. (5.4) or (5.6). For this numerical example, an I-section beam with overall height  $H = 5\text{mm}$ , and distance between the flanges  $h = 3\text{mm}$  has been chosen. The fully-connected ground-structure is shown in Figure 5.5(a).

An initial layout optimization using formulation Eq. (5.1) is then carried out, assuming at this stage that the optimal structure will take the form of a pin-jointed truss, as

shown in Figure 5.5(b). This step is computationally efficient to perform and provides an ideal layout for the minimum material condition. Using the coefficient matrices, the frequency is then calculated assuming rigid frame conditions ( $f_1$ ). At this point, a decision may be made concerning the frame frequency. If the value is acceptable for the given design problem, the optimization procedure can be ended at this point; however, if the frequency is below the minimum required for a frame structure, the optimization procedure can be progressed to the next step, involving the use of a frequency solver.

For the 10-bar frame currently under consideration, it is assumed that the designer is looking to identify a structure with an increased minimum frequency, and therefore progresses to the next step. It should be noted that some of the elements fall below the threshold cross-sectional area ( $1 \times 10^{-6} \text{mm}^2$ ) and are excluded from the visualisations. However, their contribution to the frequency, although small, is still included in the calculations.

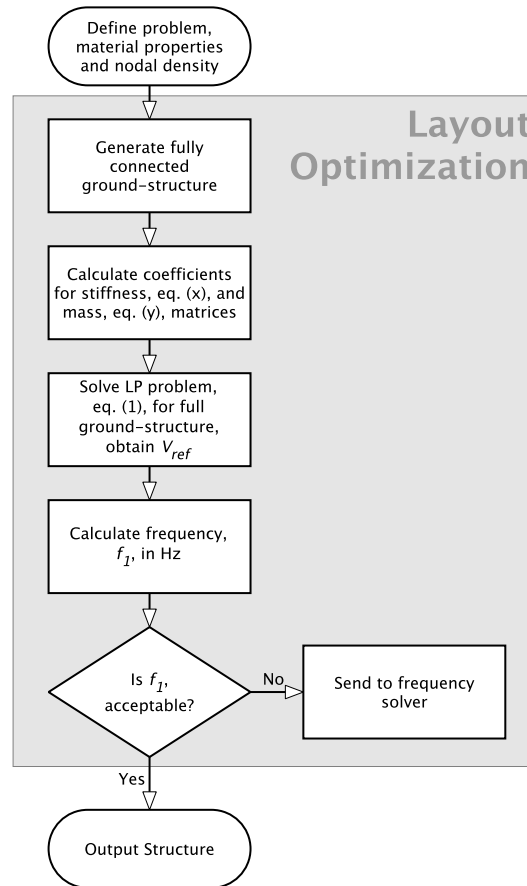


FIGURE 5.6: Layout optimization step of the iterative solution procedure.

### 5.3.3.3 Frequency solver

The second step of the proposed procedure is application of the frequency solver, comprising the operations shown in Figure 5.7. Here a minimum volume solution satisfying stress and frequency constraints is sought. The problem variables are the cross-sectional areas of each element in the ground-structure, which are used as multipliers on the element stiffness  $\bar{\mathbf{K}}_i$  and mass  $\bar{\mathbf{M}}_i$  coefficient matrices, that in turn contribute to the global  $\mathbf{K}$  and  $\mathbf{M}$  matrices respectively. The domain, ground-structure, and coefficient information used in the layout optimization step are reused. A value of the minimum acceptable frequency,  $f_{min}$ , is also input at this point. In the case of the 10-bar structure considered here, the desired minimum frequencies have been set as: 100Hz, 150Hz, and 200Hz.

The SDP problem is solved using formulation Eq. (5.2), though now using global matrices  $\mathbf{K}$  and  $\mathbf{M}$  that include frame rather than truss terms. Once completed, the calculated areas are used to verify the frequency, ensuring that it meets the criteria  $f_1 \geq f_{min}$ . A decision can then be made on the volume of the structure compared with the reference volume obtained from the initial layout optimization step,  $V_{ref}$ , and the quality of the structural form, e.g. that shown in Figure 5.10(d). If there is a large difference between the optimized and reference volume values, then the predefined value selected for the height of the cross-section ( $H$ ) may not be appropriate, or there may exist another cross-section shape that would yield a lower volume.

Tables 5.2 and 5.3 show cross-sectional area values,  $a$ , and second moments of area,  $i$ , respectively for the members present in this example. It is evident that the areas of the elements change as the frequency target is increased. As a result of the areas changing, some elements that previously had areas below the threshold ( $1 \times 10^{-6} \text{mm}^2$ ) have now increased so as to influence the frequency of the structure. The SDP optimizations targeting 100Hz and 150Hz have achieved the objective with a modest increase in volume; however when targeting 200Hz, the volume more than doubles, indicating there may be an alternative solution available through further refinement.

### 5.3.3.4 Solution refinement

The third and final step of the proposed procedure is solution refinement, comprising the operations shown in Figure 5.8. In this step, an assessment is undertaken of how the height,  $H$ , of the elements affects the resulting volume. New heights can be input into the solver, either as a single value or as a range of heights to run iteratively. The coefficient matrices for stiffness  $\bar{\mathbf{K}}_i$  and mass  $\bar{\mathbf{M}}_i$  are recalculated with the new values

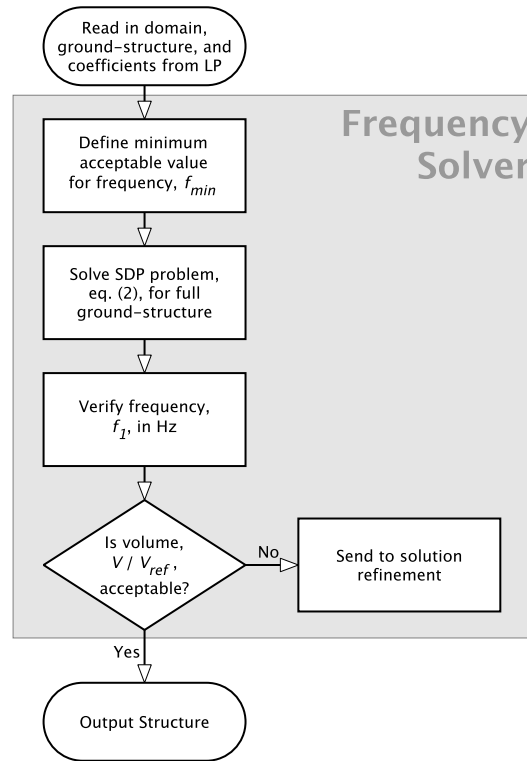


FIGURE 5.7: Frequency solver step of the iterative solution procedure.

TABLE 5.2: 10 bar frame example: LP and frequency optimization results, targeting frequencies of 100Hz, 150Hz, and 200Hz (see also Figure 5.5). An additional result is included for the 200Hz case following refinement of the solution. The resulting volumes are quoted in  $\text{mm}^3$  and the area of each bar quoted in  $\text{mm}^2$ ; the ‘—’ entry is used where the element area is less than  $1 \times 10^{-6} \text{mm}^2$ .

$f_1$	V	$a_1$	$a_2$	$a_3$	$a_4$	$a_5$	$a_6$	$a_7$	$a_8$	$a_9$	$a_{10}$
LP	2909	7.273	—	5.143	3.636	—	—	5.143	—	3.636	—
100Hz	2911	7.252	0.029	5.114	3.657	0.020	—	5.143	—	3.636	—
150Hz	3040	5.963	1.852	3.291	4.946	—	1.309	3.291	1.852	2.327	1.309
200Hz	5922	9.075	5.196	5.194	9.176	7.341	3.611	2.516	2.627	3.588	4.462
Following refinement:											
200Hz	3097	5.440	2.591	2.551	5.469	—	1.832	2.551	2.591	1.804	1.882

TABLE 5.3: 10 bar frame example: Corresponding second moment of area values for the results presented in Table 5.2. Values are quoted in  $\text{mm}^4$ .

$f_1$	$I_1$	$I_2$	$I_3$	$I_4$	$I_5$	$I_6$	$I_7$	$I_8$	$I_9$	$I_{10}$
LP	27.272	-	19.284	13.636	-	-	19.284	-	19.284	-
100Hz	27.196	0.1083	19.176	13.712	0.0765	-	19.284	-	13.636	-
150Hz	22.362	6.9435	12.341	18.546	-	4.9097	12.341	6.9435	8.7265	4.9097
200Hz	34.032	19.485	19.476	34.411	27.527	13.539	9.435	9.8497	13.454	16.731
Following refinement:										
200Hz	49.258	23.464	23.098	49.516	-	16.591	23.098	23.464	16.333	17.044

for element height prior to the SDP problem being re-submitted to the frequency solver. The results will be a range of optimized structures with varying volumes, which can be expressed as a ratio of  $V_{ref}$ . The designer is then free to choose which structure and volume is suitable.

It should be noted that if multiple element heights are specified, since an SDP solver run is required for each one, the time required to complete all runs can be considerable, particularly if a nodally-dense domain is being used. In the iterative case of the structure shown in Figure 5.5(e) to determine if a lower volume was available, increasing the height in 0.1mm increments identified that increasing the beam height to 7.3mm was sufficient to bring the volume of the structure down to  $V = 3097 \text{ mm}^3$ , an increase of 6.4% from  $V_{ref}$ , whilst maintaining the target of 200Hz. The resulting structure resembles that shown in Figure 5.5(d); modified areas are shown in Table 5.2.

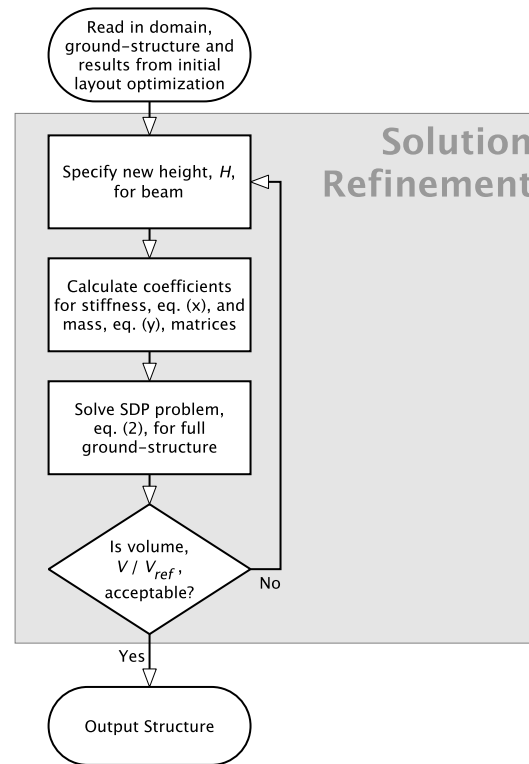


FIGURE 5.8: Solution refinement step of the iterative solution procedure.

## 5.4 Numerical examples

Now that details of the proposed iterative solution procedure for frame layout optimization have been outlined, it will now be applied to a series of more demanding numerical examples. All numerical examples were run on a 64bit Windows 11 desktop PC equipped with an Intel i5 3.7GHz processor and 32Gb RAM, using scripts programmed



in MATLAB 2022a and solved using the [MOSEK ApS \(2022\)](#) v10 solver. Unless otherwise stated, all examples use 6061-T6 Aluminium with the following assumed material properties:  $E = 64 \times 10^9 \text{ N m}^{-2}$ ;  $\rho = 2711 \text{ kg m}^{-3}$ ; and limiting tensile and compressive stresses  $\sigma = 275 \text{ MPa}$ .

#### 5.4.1 Simply-supported cantilever

Figure 5.9(a) shows details of the problem definition for a classical simply-supported cantilever with a single point load,  $P = 1 \times 10^3 \text{ N}$ . An initial design for the structure is performed using the basic truss layout optimization formulation, Eq. (5.1), providing reference values of the volume,  $V$ , and truss and frame structure frequencies,  $f_T$  and  $f_F$  respectively, see Figure 5.9(b). In this case, a rectangular cross-section has been selected for elements, adopting a fixed height,  $H$ , for every element in the domain; here  $H = 3 \text{ mm}$  has been selected. This problem has been defined with a relatively sparse nodal density comprising 15 nodes and 74 potential connections. Note that in the interests of simplicity, the stress limits computed in the frequency optimization are calculated assuming purely axial transmission of forces through elements, corresponding to the plastic design case.

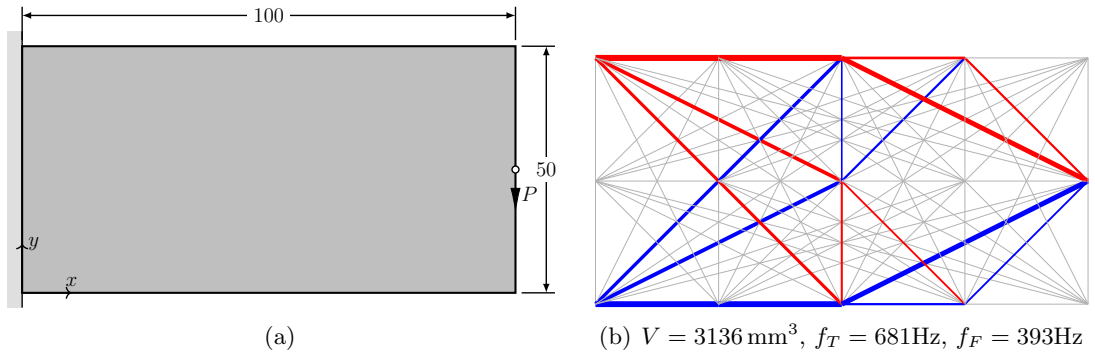


FIGURE 5.9: Simply supported cantilever: (a) problem definition - design domain, loading, and support details; (b) solution from reference LP optimization. All dimensions are in mm.

##### 5.4.1.1 Optimize frame frequency whilst maintaining section depth

The problem is now optimized with the semidefinite constraint on frequency Eq. (5.2) to obtain new member areas, satisfying the need for a frame structure to have a defined minimum frequency.

Figure 5.10 shows the resulting structures obtained when running the SDP solver with targets of 400Hz, 450Hz, 500Hz, and 600Hz; each was solved in less than 1 second of CPU time. Whilst the overall layout of the majority of the member elements has not changed,

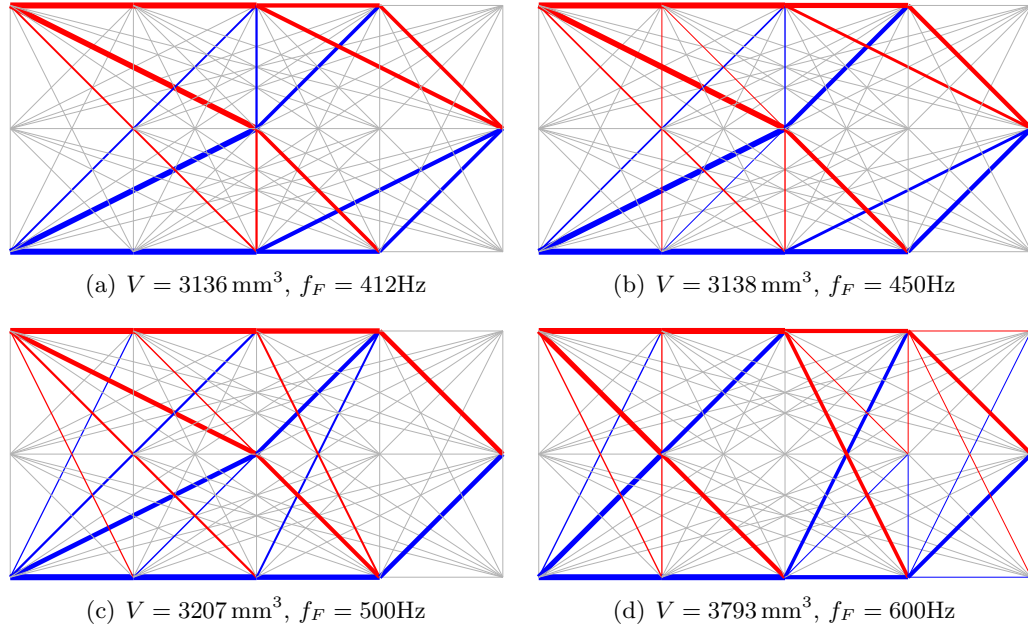


FIGURE 5.10: Simply supported cantilever - results obtained for target first natural frequencies of: (a) 400Hz; (b) 450Hz, (c) 500Hz; and (d) 600Hz. Note that the number and layout of members with an area greater than the filter has changed with the frequency target.

there are some members which have been increased in area to meet the frequency targets and which now form part of the final structure. Whilst there is no volume increase to meet the frequency target of 400Hz in Figure 5.10(a), when the target frequency is further increased, so does the resulting structural volume. The increase in volume is relatively small for the 450Hz and 500Hz cases, being  $\leq 1\%$  and  $2.2\%$  respectively, but when targeting 600Hz the volume increases by 21% and, as may be seen from Figure 5.10(d), the quality of the overall structure appears to deteriorate.

This sharp increase in volume and apparent deterioration in form may be attributed to the selected height of the beam no longer being sufficient to provide a structure that has the correct frequency capability. In this instance, an improved result may be obtained using a beam with a modified value of  $h$ .

#### 5.4.1.2 Refinement by modifying section depth

A further iterative optimization of the structure targeting 600Hz is now conducted, with the height of the beams modified at each iteration; in this case the problem is solved with the same optimization algorithm as employed in the previous step. The results shown in Figure 5.11 indicate that by increasing the height of the beams, the overall volume of the structure reduces, though this improvement is bounded by a minimum feasible beam width. Additional points have been plotted on Figure 5.11 to show the total volume

of material required if the beam width is prevented from dropping below the feasible minimum width; in such cases the beam widths are increased to the minimum width as a post-processing step. In a number of cases this penalization increases the volume considerably; however it can be seen that there are three instances where the points closely align with the original curve, at beam heights of 4.2mm, 7.5mm, and 9.3mm; the lowest volume of  $3355 \text{ mm}^3$  corresponds to a beam height of 9.3mm. Whether this increase in height can be accommodated in practice will depend on the specific application involved.

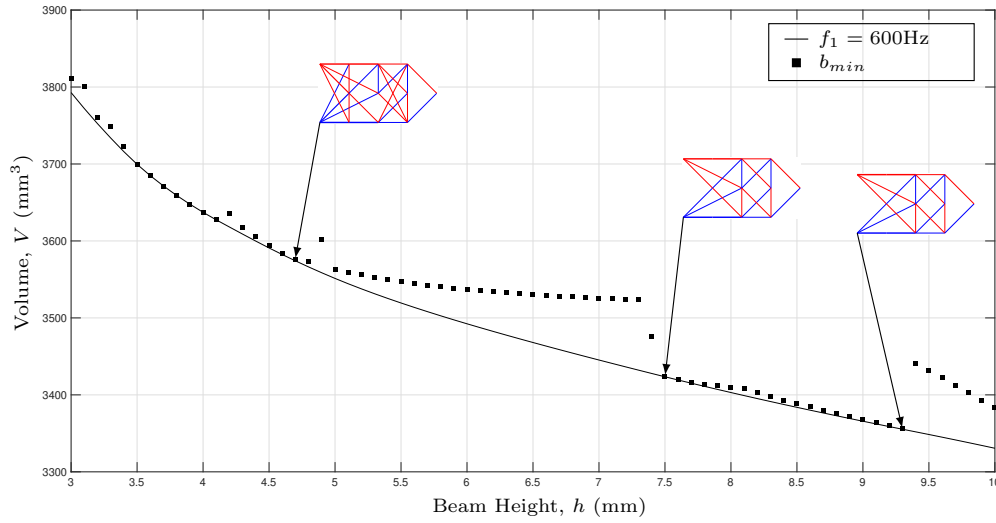


FIGURE 5.11: Simply supported cantilever example: solid line shows the effect of increasing beam height  $h$  has on the volume of the optimized structure. The volumes of structures where the widths of all elements have been increased to  $b_{min} = 0.8\text{mm}$  as a post-processing step are also shown as discrete points. (Target frequency = 600Hz.)

It may also be the case that the initial ground-structure does not contain enough potential connections to solve the frequency problem with a lower volume; addition of more potential connections in a computationally-efficient manner would therefore be advantageous.

#### 5.4.1.3 Increasing nodal density

Considering a target frequency target of 500Hz, the number of nodes in the domain is now increased to assess the influence of this on the results obtained, see Figure 5.12. Each of the results has the same constraint on the height of the rectangular cross-section employed, and all structures successfully attain the target frequency.

It is clear as the nodal density is increased, reasonably significant reductions in overall structural volume can be obtained. This, however, comes at the cost of computational

time; the structure shown in Figure 5.12(c) has a 7% lower volume than the structure shown in Figure 5.12(a), but took 54 times as long to solve.

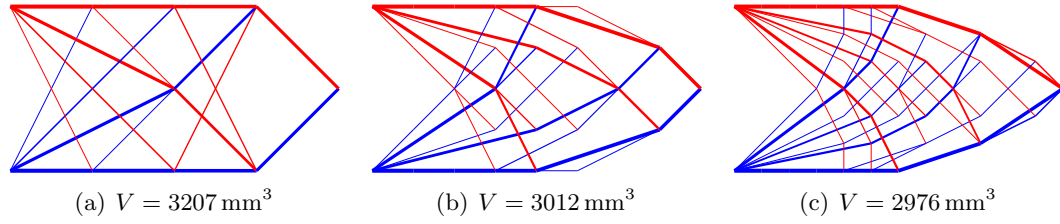


FIGURE 5.12: Simply supported cantilever - effects of increasing nodal density: (a) 15 nodes and 74 potential connections, solved in 0.3 seconds; (b) 45 nodes and 632 potential connections, solved in 85 seconds; and (c) 91 nodes and 2542 potential connections, solved in 4634 seconds. A further example with 153 nodes and 7180 potential connections exceeded the 32Gb of available memory on the PC. (Target frequency = 500Hz.)

#### 5.4.2 L-shaped bracket

Figure 5.13(a) shows details of the problem definition for an L-shaped bracket with a single point load,  $P = 1 \times 10^3 \text{ N}$ . This problem is discretized using 27 nodes and 188 potential connections. Once again, an initial design for the structure is performed using the basic truss layout optimization formulation, Eq. (5.1), providing reference values of the volume,  $V$ , and truss and frame structure frequencies,  $f_T$  and  $f_F$  respectively, see Figure 5.13(b). A rectangular cross-section has been selected with a fixed height  $h = 2.5 \text{ mm}$  for every element in the domain.

Figures 5.13(c) - 5.13(f) show the resulting structures obtained when running the SDP solver with targets of 50Hz, 70Hz, 90Hz and 100Hz; each was solved in less than 6 seconds of CPU time. Again, the figure shows that there is little change to members that are providing the bulk of the strength, whilst additional connections have been included to augment the structure to satisfy changes in frequency requirements. The change in volume is much reduced for this example, the largest being an increase of  $\leq 1\%$  from the baseline value. This may be attributed to the greater design freedom available in this domain compared with the previous example. Because of this, and because there is no appreciable deterioration in the quality of the solutions, there is no need to perform a further optimization with variable cross-section heights.

Optimal designs of this nature may be taken forwards into manufacture, with the methods that can be utilized varying depending upon the complexity of the result. Figure 5.14 shows what the optimal result for the L-shaped bracket targeting a minimum frequency 50Hz might look like if it was cut from a sheet of metal. The height of each beam may be cut to the set height uniformly, and the width of each member milled to the

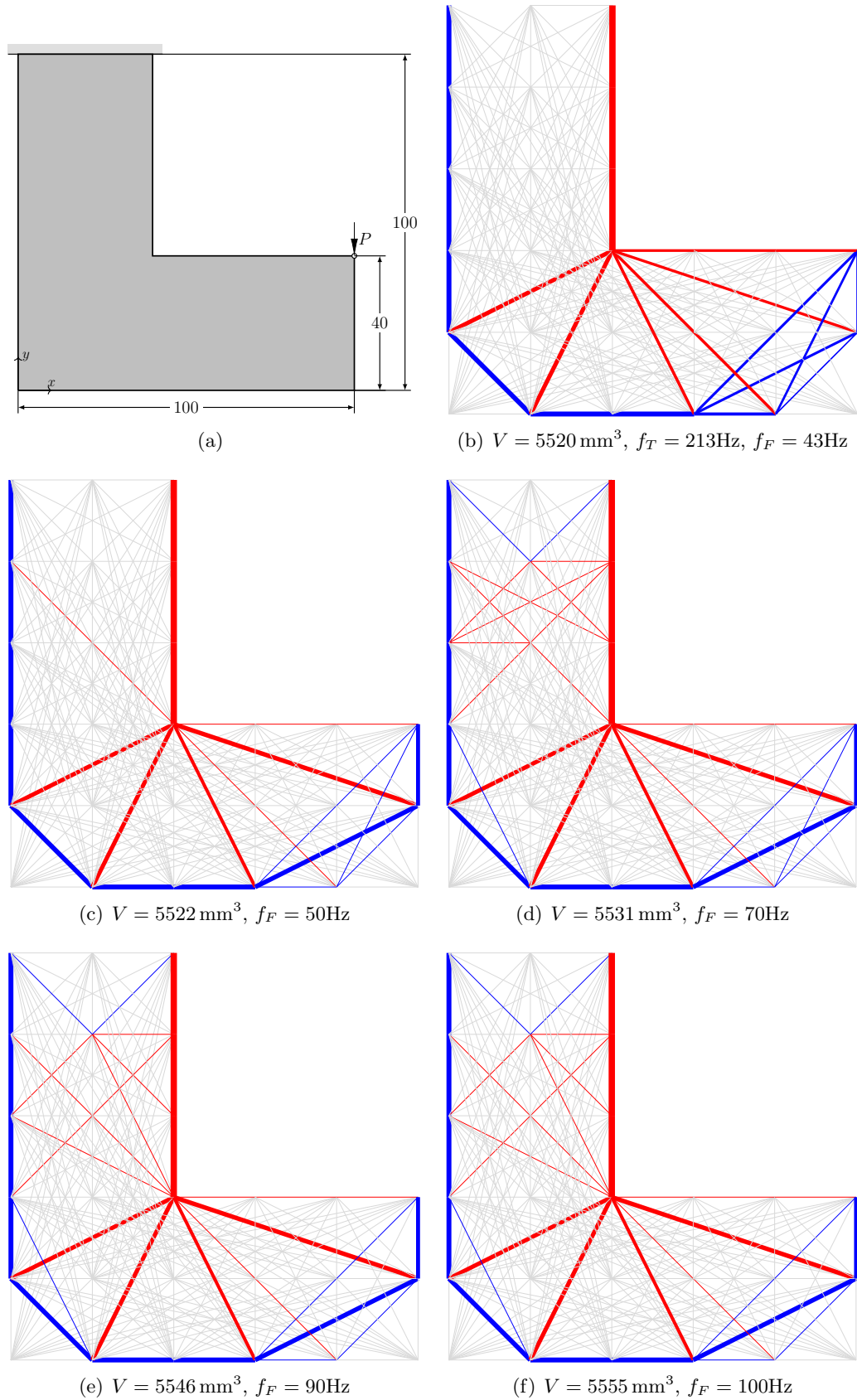


FIGURE 5.13: L-shaped bracket: (a) problem definition - design domain, loading, and support details; (b) LP reference solution; (c) 50Hz solution; (d) 70Hz solution; (e) 90Hz solution; (f) 100Hz solution. All dimensions are in mm.

necessary dimension on each side. Material at the nodes has been expanded to ensure that the elements meet each other completely, and radii have been added to smooth out tight corners and to accurately represent the capability of the cutters.

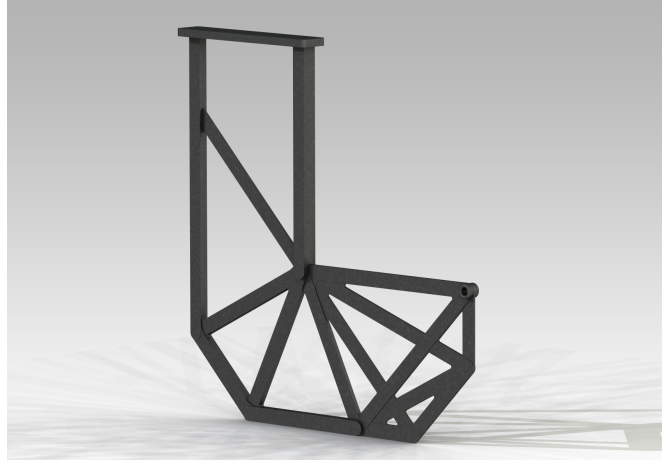


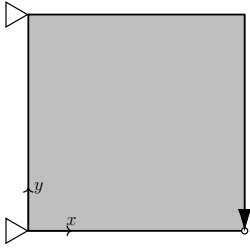
FIGURE 5.14: L-shaped bracket: representation of manufactured optimal design targeting 50Hz minimum frequency. Bracket produced from sheet metal following the beam widths derived from optimal element areas. Note, elements with an area below  $1 \times 10^{-6} \text{ mm}^2$  are omitted. (Only in-plane vibrations are considered in the analysis of this representation).

## 5.5 Discussion

The examples presented to date have primarily involved relatively sparse nodal densities. To better highlight the computational cost associated with the SDP computations, a further study has been conducted on truss domains of increasing nodal densities, containing between 36 and 7260 nodal connections. For this example, a more powerful machine was employed; this was a Windows 10 workstation PC equipped with an Intel i9 5GHz processor and 64Gb RAM using scripts programmed in MATLAB 2022a and solved using the [MOSEK ApS \(2022\)](#) v10 solver. In all instances the target frequency for the SDP solver was set to 450Hz. The results obtained, shown in Figure 5.15 and Table 5.4, confirm that reduced volume structures can be identified if the nodal density is increased, but that this comes at significant cost in terms of CPU time; memory consumption was also observed to increase rapidly. The volume reductions achievable diminish as nodal density is increased, indicating that there is a point at which in practice it no longer makes sense to keep adding more nodes. Figure 5.15(j) shows a plot of CPU time against the number of potential connections when using both a full ground-structure, and when using an adaptive ‘member-adding’ truss algorithm; in both cases SDP frequency constraints are present. Clearly there is a significant advantage in utilising ‘member-adding’ to treat cases where a problem must be solved with an SDP constraint.

Further rationalisation of the geometry obtained from the solver would offer the ability to reduce complexity, and address issues with intersecting members. For planar truss optimization, members that intersect away from a node are likely to have little effect on the overall strength of the structure. However when frequency constraints are involved, intersections change the allocation of mass and stiffness contributions in the corresponding matrices, so that performing a post-processing step that adds in new nodes prior to performing a new optimization should be considered.

TABLE 5.4: Nodal refinement study: problem definition (left) and results (right) for SDP optimization based on fully-connected ground-structures with increasing numbers of potential connections. CPU costs expressed in seconds. Tabulated results to be read in conjunction with Figure 5.15.

	Figure	No. of Nodes	Potential Cons.	V (mm <sup>3</sup> )	CPU Cost (s)
	5.15(a)	9	36	1265	0.020
	5.15(b)	16	120	1185	0.139
	5.15(c)	25	300	1151	0.727
	5.15(d)	36	630	1145	5.618
	5.15(e)	49	1176	1143	27.66
	5.15(f)	64	2016	1143	115
	5.15(g)	81	3240	1142	543
	5.15(h)	100	4950	1139	1896
	5.15(i)	121	7260	1139	71236

## 5.6 Conclusions

An iterative solution procedure designed to tackle frame layout optimization problems involving constraints on stress and minimum natural frequency has been developed and demonstrated. The three-step procedure uses semidefinite programming (SDP) to impose frequency constraints when seeking minimum volume frame structures. The results obtained have been found to be repeatable and applicable to a range of frequency targets, for a range of nodal densities. Key conclusions are as follows:

- Examples have been used to demonstrate that a minimum volume frame structure with a specified minimum frequency constraint can be obtained using the ground-structure based layout optimization approach employed, using a modern SDP solver to obtain solutions.
- In the proposed procedure, the second moment of areas  $I$  of the beam elements employed are linearized with respect to cross-sectional area by fixing the heights ( $H, h$ ) of these elements, with the element widths ( $B, b$ ) allowed to vary.

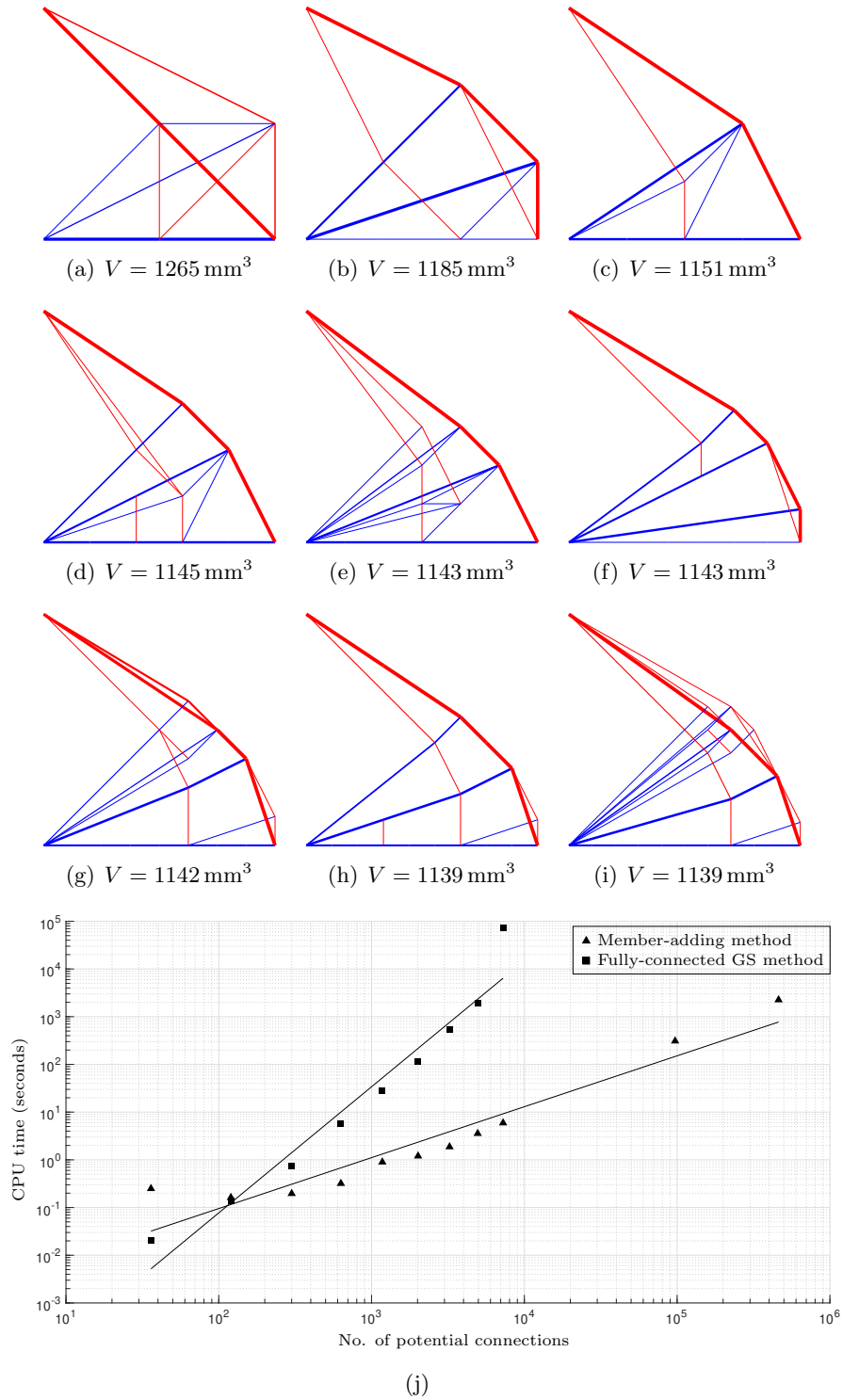


FIGURE 5.15: Nodal refinement study: (a)-(i) optimal structural layouts for domains containing increasing numbers of nodes and potential connections, as detailed in Table 5.4; (j) CPU cost for each domain, for optimizations conducted using fully-connected ground-structure (squares), and adaptive ‘member-adding’ methods (triangles).



- c) To obtain improved solutions, the values of  $H, h$  can then be modified, with the problem then solved again using the SDP solver, as part of an iterative solution procedure. For the example described in Section 5.4.1 of this contribution, the overall volume of the structure was reduced from 20% to 9% above the reference value using this method, in this case employing a single value of  $H, h$  for all elements. However, the computations involved as part of this iterative procedure will be time-consuming for problems containing large numbers of nodes and potential connections, and therefore may not be practicable in all scenarios.

In future it would be significant to implement the adaptive ‘member-adding’ algorithm to reduce computational time and memory footprint. This is likely to be especially important should the proposed procedure be applied to 3D frames, which generally contain considerably more ground-structure connections than their 2D counterparts. Similarly, when the iterative solution procedure is adopted, the use of the ‘member-adding’ algorithm becomes particularly attractive due to the computational expense involved. The iterative solution procedure can also be enhanced by using a different  $H$  value for each element.

## Chapter 6

# Discussion and potential applications

The research objective of this thesis has been to determine whether automated optimization techniques such as layout optimization and topology optimization are suitable for use on representative aerospace case study components. Furthermore, it endeavoured to discover if layout optimization can be augmented to include constraints on natural frequency in order to generate optimized components for aerospace applications in efficient timescales. This scope included applying the frequency constraints to both truss and frame structures to faithfully model real-world production of the optimized geometry.

Following a review of current research in the field to date (Chapters 1 and 2), Chapter 3 compared the use of layout optimization and topology optimization for the generation of designs for aerospace components. It was successfully proven that while both offer the ability to reduce the mass of components, and consequently the CO<sub>2</sub> emissions arising from fuel burn, layout optimization has the capability to provide greater weight reduction opportunities. Layout optimization of truss and frame structures has proven to be a powerful tool for identifying the most efficient use of material leading to minimum weight structures. Chapter 4 extended the use of layout optimization to target design problems with specific constraints on natural frequencies, creating and testing the use of a bespoke tool for computationally efficient analysis. This innovative tool was applied to a number of design problems that were solved in an efficient manner due to the use of a member-adding algorithm in the iterative process. This chapter went on to investigate the implementation of the member-adding algorithm into the frequency SDP solver, and compared the results with those achieved by Gilbert and Tyas (2003), with correlation in terms of volume achieved to within 1%. Chapter 5 took this work further and applied the SDP constraint on frequency to frames, a continuum structure more akin

to products made by AM. A second new tool which is capable of optimizing a frame structure with a frequency constraint based on a fully-connected ground-structure was successfully developed and demonstrated on a number of examples. Along with these successes, a number of challenges were also encountered through this research and are discussed further in this chapter to aid future work in this field.

## 6.1 Application of generative design in aerospace

Both the topology and layout optimization techniques discussed in this thesis fall into the category of generative design. Generative design may be considered to be any computer-aided semi-autonomous design exploration process that generates a set of component design solutions that meet a given set of constraints and parameters (such as materials, size, weight, strength, manufacturing methods and cost). This is in contrast to traditional design, which may begin with a model based on a previous component or an engineer's knowledge. Conventional parametric design and optimization provides a valuable approach to explore a problem, but the potential solutions are constrained by the topology, which is in turn defined by the parametrisation. Significant design decision-making, engineering judgment, and modelling effort are required by the designer to build the parametric model. Generative design eliminates parametric restrictions and enables the topological freedom that can generate more radical design solutions that the designer may not have considered.

Chapter 3 looked at two example aerospace components optimized using generative design tools and concluded that both offered advantages when it came to optimizing a component for a specific set of objectives and constraints. However, it was shown that truss layout optimization holds an advantage over topology optimization in translation of the part from the analysis tool to traditional CAD for post-processing and manufacture.

### 6.1.1 Topology optimization

Topology optimization is recommended as a key enabler for high-performing, multi-functional and lightweight components; the technology is capable of novel design solutions that a designer may not be able to configure manually. These algorithms can generate complex and/or freeform design solutions that unleash the potential of additive manufacturing. Whilst it remains true that topology optimization has been used in aerospace on a few select examples, it has not yet been fully exploited as the efficient concept design tool it claims to be and is therefore not in regular use. Similarly, AM has not yet achieved its full potential, and where it has been used, in aerospace, more

traditional design techniques have been employed. For topology optimization and AM to reach their full potential they must be developed and paired to fully unlock the advantages that each can offer. Through the research conducted during in preparation of this thesis several factors were identified which may account for the delay in exploitation.

It was observed in Chapter 3 that there are some difficulties when it comes to translating the optimized design into a manufacturable CAD model. The effort to translate the mesh, which is often the result of generative design, into a continuum structure can be quite time consuming, see Figure 3.10, and is open to interpretation if not governed by a fixed set of rules and procedures. For application to aerospace this time would need to be significantly reduced to enable rapid iterations to be produced at each stage of the design spiral, Figure 1.2, whilst new topology optimization algorithms and software are addressing this shortfall, there is significant effort required to prove confidence in the results for certified components. Additionally, the material added to the optimized mesh for smoothing or to satisfy manufacturing constraints may add further weight to the final part (Gu, 2013) driving the need for further iterations to meet the component requirements.

One additional aspect which was out of scope for Chapter 3 concerns the processes which follow on from the AM build of the optimized component. When a more organic or freeform geometry is produced, it becomes far more complex to inspect to a point where traditional CMM inspection is impossible through the sheer complexity in geometry or as-built areas having poorer surface finish. This directs the manufacturer towards more expensive 3D scanning technologies to validate their production, as a consequence there are limits on the supply chain blocking the routine production of topology optimized AM components.

Finally, it should be noted that design, analysis, and manufacturing are traditionally separate engineering functions, with their own specialisms and associated expertise. A generative design approach requires the analyst to be conversant in all of these disciplines for the best outcomes. Whilst growing, there is limited availability of these multi-skilled engineers. It is hoped that this study, along with associated further work, will help to grow this field and its interdisciplinary engineering knowledge base.

### 6.1.2 Opportunities for layout optimization

Beyond optimization of truss structures, layout optimization has further potential applications in aerospace that may be enabled by AM or traditional machining techniques. Consider the structure shown in Figure 6.1(a): an isogrid is a partially hollowed-out structure usually formed from a single metal sheet that is machined to reveal pockets

and stiffening ribs; typically an isogrid will comprise a repeating pattern of triangles or other forms. They provide structural stiffness for a component, allowing the remainder of the plate to be relatively thin compared to the stiffening ribs. The use of layout optimization techniques offers the ability to define bespoke patterns of stiffeners onto the skin of the component in order to react load(s) or pressures put upon the structure. Such a structure could be machined from a thick metal plate, applied additively to the surface of the skin by blown powder or wire deposition AM, or could be produced in a single piece through casting or hot isostatic pressure powder forming.

There is a concern that least-weight truss or frame structures in an aerospace application may get damaged through handling or in service Foreign Object Damage (FOD) events. Damage tolerance is a critical factor in the design of parts for aerospace applications, and often goes hand in hand with the theories of robust design. By their very definition, an optimized truss/frame structure offers the least-weight solution to the specified design problem, therefore there is typically limited capability in the individual elements to offer a reserve factor to account for damage without increasing their size. An alternative would be to utilize layout optimization to define frame structures which could be used on the inside of components, hollowing out the bulk of the material and offering strength and support, Figure 6.1(b). A similar approach is used in a number of AM design packages, using the complexity that the manufacturing process affords to replace solid material with lattices, reducing the mass of components. A number of lattices are applied in design packages as unit cells, reducing the density of material in specific regions to offer a weight reduction whilst maintaining an element of virtual strain (similar to topology optimization). Layout optimization has the advantage that solutions can be generated efficiently, in short timescales and can be tailored to suit constraints on frequency as discussed in Chapters 4 and 5, or buckling as described by [Weldeyesus et al. \(2020\)](#).

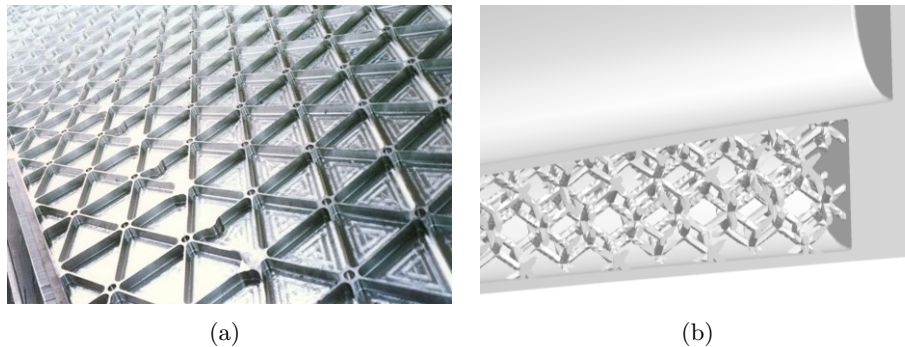


FIGURE 6.1: Opportunities for layout optimization in aerospace: (a) a traditionally designed geometric isogrid with each pocket defined identically; and (b) typical hollowing of an AM part using standard lattice forms. Each could be optimized further with layout optimization.

## 6.2 Methods for geometry rationalisation of truss and frame structures

A number of results have been obtained through layout optimization formulations for a variety of truss and frame structures, and these have been proven to be acceptable outcomes based upon the defined input parameters. It was found there are some instances where these structures require further refinement prior to being suitable for further analysis, e.g. frequency analysis, verification by FEA, or for manufacturing preparation.

In the studies described in Chapters 4 and 5, a number of issues associated with ill-conditioned stiffness matrices were experienced. The stiffness matrix in global coordinates,  $\mathbf{K}$ , is assembled from the stiffness matrix of each element in local coordinates,  $\mathbf{k}_i$ , multiplied by the transformation matrix,  $T$ :

$$\mathbf{K} = \sum_{i=1}^m \mathbf{K}_i \quad (6.1)$$

where  $\mathbf{K}_i = \mathbf{T}_i^T \mathbf{k}_i \mathbf{T}_i$ . Considering an element with non-zero stiffness connecting Degree of Freedom (DoF)  $i$  with DoF  $j$  (for a 1 DoF system), then  $k_{ii}$ ,  $k_{jj}$ , and  $k_{ij} = k_{ji}$  are all non-zero, consequently  $\mathbf{K}$  is a symmetric matrix with few non-zero entries per row. The stiffness matrix  $\mathbf{K}$  can, however, become ill-conditioned when its columns are nearly linearly dependent for the following reasons:

1. The structure has one or more pairs or tuples of DoFs that do not have sufficient connectivity with the rest of the structure, or
2. Certain DoFs have stiffnesses disproportionate with the rest of the structure.

It is possible for reason 1 to occur when elements do not have sufficient connectivity, e.g. where there is no restraint on rotation at a node, creating a mechanism and leading to a singular matrix. Reason 2 may occur due to a badly scaled matrix resulting from collinear members being split in one or more locations along their length. In order to avoid ill-conditioned matrices it is necessary to treat the structure; rectifying the error can be a case of fixing the unconstrained DoF, for example achieved by rationalising the structure to reduce its complexity.

The following sections discuss the rationalisation that is required in such cases and how this may be achieved.

### 6.2.1 Reducing the number of elements

When applied to layout optimization, the addition of member-adding has been proven to provide an improvement in computational efficiency for solving large problems. However, as the size of the problem increases, the complexity of the result also increases, often leading to a large number of crossing members. These crossing members can make the optimized structure impossible to manufacture, so [He and Gilbert \(2015\)](#) proposed an additional step to reduce the complexity of the structure through a post-optimization geometry rationalisation step. To achieve this, the nodes connecting the resulting members are reviewed and those adjacent to one another within a certain radius are combined, additionally amalgamating the members into fewer bars. Further optimization allows the positions of the nodes to be shifted, [Figure 6.2](#).

A non-linear, non-convex algorithm is employed to achieve this and, as this stage of the processes is applied to a sub-set of the original ground-structure, the computational burden is minimal. This form of geometry optimization has been shown to improve upon the original results for the layout optimization ([He and Gilbert, 2015](#); [He et al., 2019a](#)). It is therefore possible to generate a structure using layout optimization and geometry rationalisation, with minimal additional computational cost, which may then be suitable for manufacture.

Application of this strategy to frames and truss structures, such as those obtained in [Chapters 4 and 5](#), would result in geometric forms with fewer members. This reduction in complexity not only makes translation of the structure to a CAD environment easier, but also paves the way for the components to be manufactured via both traditional or additive manufacturing technologies.

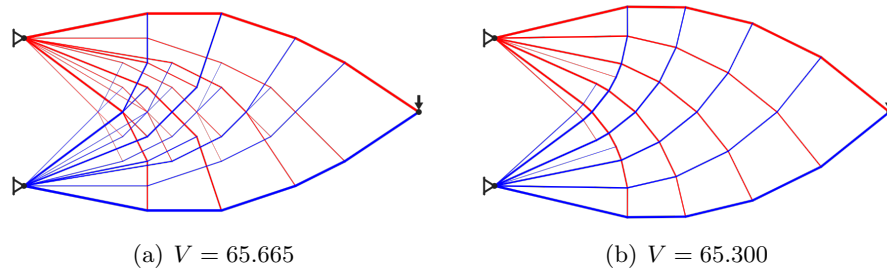


FIGURE 6.2: Geometry rationalisation for truss and frame structures: (a) Hemp cantilever optimized using layout optimization; and (b) the same problem following geometry rationalisation. Note that the volume,  $V$ , of the rationalized version has reduced compared with the original result. Produced using the LayOpt web app available at <http://www.layopt.com> and detailed in [Fairclough et al. \(2021\)](#).

### 6.2.2 Collinear and intersecting elements

Though rigorous, the ground-structure approach to frequency layout optimization has a tendency to lead to complex solutions, potentially containing many thousands of elements.

Collinear elements, those which have the same cross-sectional area but are not connected to any other elements but each other, should be consolidated into a single element. Though they do not directly impact on the result of the structural analysis, they introduce additional degrees of freedom into the mass and stiffness matrices used for frequency assessment. Consolidating collinear elements into single elements removes these additional terms and thus reduces the computational burden and potential for numerical instability.

Once all the collinear elements have been found and combined, any elements that intersect away from a pre-existing node should then be identified. Intersection of elements is acceptable when it occurs at a pre-existing node; however the nature of the ground-structure method, which involves connecting each node to every other node, will invariably lead to intersections that occur away from nodes. For planar truss problems this has very little effect on the resulting strength of the structure, but for frequency analysis it fundamentally changes the allocation of mass and stiffness contributions in the corresponding matrices and may also lead to numerical instabilities.

To address these arising geometric issues in the structure following layout optimization, such as the one shown in Figure 6.3(a), the following procedure could usefully be completed as a post-processing stage:

- a) The elements that are above the threshold for area, the ‘members’ of the solution, should be isolated from the redundant ground-structure. This will reduce the computational burden on the following steps and also begin to provide a structure suitable for manufacture, Figure 6.3(b). If calculation of the frequency of the structure is required, the member nodes and elements should be renumbered consecutively starting from the Cartesian coordinate origin. This ensures that the stiffness and mass matrices are as small as possible, reducing the memory requirements for the problem.
- b) Elements that are collinear and have the same cross-sectional area should be combined as in reality they would be produced as a single element, Figure 6.3(c). Additionally, similar to point 1, this operation reduces the size of the mass and stiffness matrices by removing unnecessary degrees of freedom.



- c) Any elements that intersect away from an existing node should be identified, a new node added at the intersection, and the existing elements split to meet at the new node, Figure 6.3(d). This more accurately represents the form of the structure in the mass and stiffness matrices.
- d) Reducing the number of elements, combining collinear elements, and adding nodes at intersections will impact on the geometric form of the structure and the contributions to the mass and stiffness matrices. This refined structure should then be re-submitted to the solver to ensure that it still meets the objective(s) with the geometrical changes.

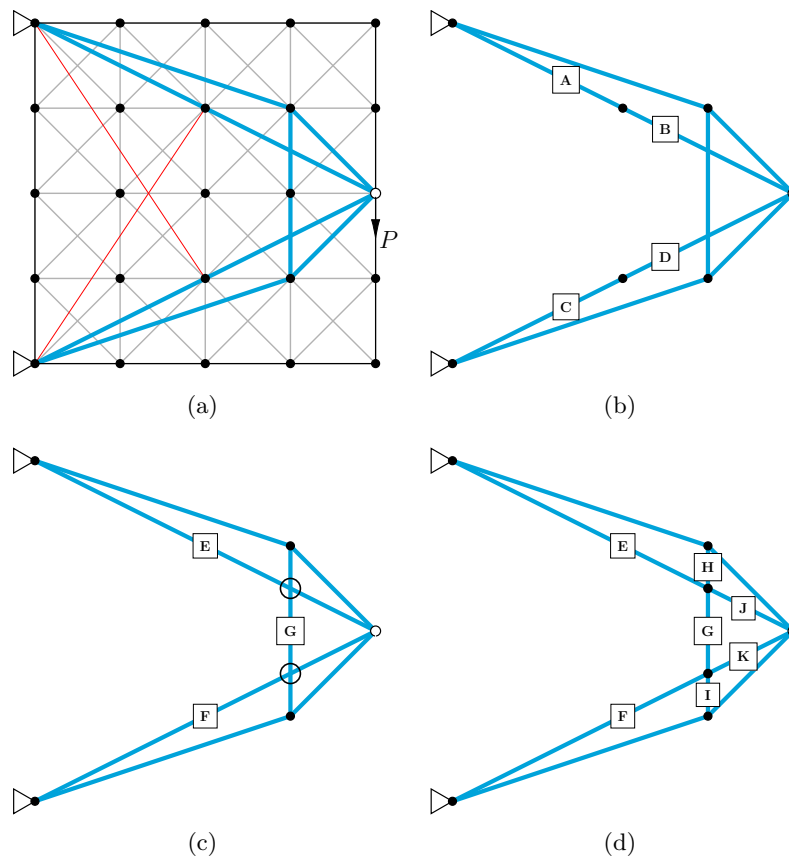


FIGURE 6.3: Rationalisation of a solution generated via layout optimization: (a) the results of the layout optimization, elements in red are below the cross-section area threshold; (b) the members of the structure with areas for rationalisation highlighted, elements A & B, and C & D are collinear, share the same cross-sectional area and may be combined; (c) collinear elements have been combined to form elements E and F, however they intersect element G away from existing nodes; (d) new nodes are added at the intersections of E,G and F,G and the elements are split at these new nodal locations forming 4 new elements, H, I, J & K, elements E, F & G are shortened accordingly.

It should be noted that simply adding the new nodes to the end of the list will lead to the contributions from the connected members being in the wrong locations in the mass and stiffness matrices, causing numerical instabilities. Any new node that is added to

the list should therefore be inserted at the correct degrees of freedom based on its  $x$  and  $y$  coordinates from the origin. When the search is completed, all the nodes should be numbered consecutively from 1 to  $n$ . This ensures that the elemental contributions are applied to the correct locations in the mass and stiffness matrices, avoiding the risk of the stiffness matrix being ill-conditioned.

A bespoke MATLAB code to identify intersecting elements, add a new node at the intersection point, and to split the existing elements is provided in Appendix B.1.

### 6.3 Element transitions for 3D trusses and frames

In Chapter 3 truss optimization in 3D was performed on two aerospace case studies to arrive at a fully united solid body suitable for manufacture. Each of these was further scrutinized by FEA to confirm the suitability of each design and that the maximum stress in the parts was below the yield stress as per the optimization targets. One of the outcomes of this study was that the highest stress regions occurred at locations where key elements met one another, or where they met the non-design rigid bodies in the model, Figure 6.4. High stresses in locations such as those where there is a transition between geometries, Figure 6.4, is considered a potential crack initiation site; a small crack may form due to the stresses and spread rapidly into the surrounding material. It is therefore imperative that stress concentrations such as these are removed to prevent product failure.

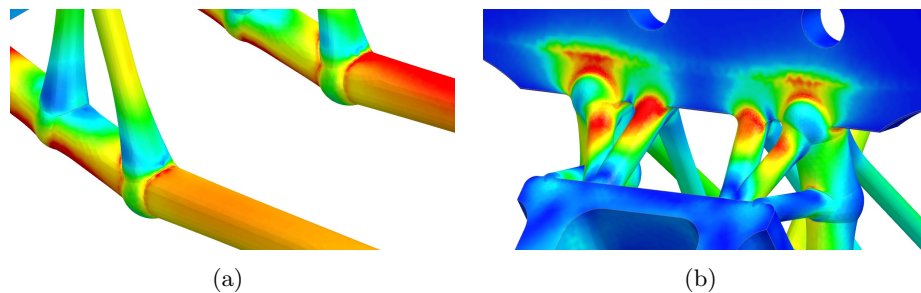


FIGURE 6.4: Transitions between each element and rigid bodies: (a) high stresses observed at nodal locations; and (b) high stresses between the optimized geometry and the rigid (non-design) bodies.

Overcoming these high stresses requires manual intervention in the CAD model to smooth the geometry between the applicable areas. This can be completed in one of the following ways: 1) by the application of fillets; 2) increasing the diameter of the elements along the whole length or; 3) increasing the diameter of the elements local to the concentration, forming a cone. A level of iteration is necessary to increase the size of

the fillets, reapply the mesh to the part, and rerun the FEA until the high stress levels are reduced.

It is recommended that for future development of the truss optimization tool, the focus is on ensuring that the transition between design and non-design geometry is as smooth as possible, potentially performing FEA as part of the process to generate transitions between geometries.

## 6.4 AM build of optimized structures

One of the major challenges for generative design is that the freeform geometries created by such tools are often not suitably designed for manufacture or inspection. Though AM offers considerable design freedom, there are still manufacturing considerations, such as overhang angles, that must be met to ensure parts can be manufactured successfully. Awareness of these considerations at the design stage reduces the risk of issues arising during manufacturing and eases inspection demands. When twinned with AM, ‘process-aware’ generative design can deliver high-performance, low-weight, novel solutions also capable of reducing the manufacturing cost for complex components reducing: part count, assembly costs, tooling costs, and machining operations. It is very important to note, however, that generative design is not limited exclusively to AM applications and the freeform designs can be realized through casting.

To highlight the importance of process awareness, the two case studies conducted in Chapter 3 have subsequently undergone preparation for production via AM. For each case, both the truss and topologically optimized structures have been imported into Materialise Magics to obtain the most appropriate orientation of the part in the build chamber, and supports have been applied to overhanging features. EOSPrint, the software which accompanies the AM hardware, has been used to obtain estimates for build time and cost. The parts in their as-built state are shown in Figure 6.5; material utilisation, costs and build times are presented in Table 6.1.

These results in Table 6.1 are indicative of components that, through the respective optimization routines, are reasonably well suited to the AM build process. There are still opportunities to improve upon the designs by ensuring that more of each component is self-supporting, i.e. no additional material is required to hold the elements in place during the build. This would reduce the buy-to-fly ratio for the components. It is clear that the components produced by truss optimization have lower ratios for buy-to-fly and as a consequence lower costs, demonstrating that truss optimization should be pursued further in aerospace engineering, though with an increased focus on manufacturability.

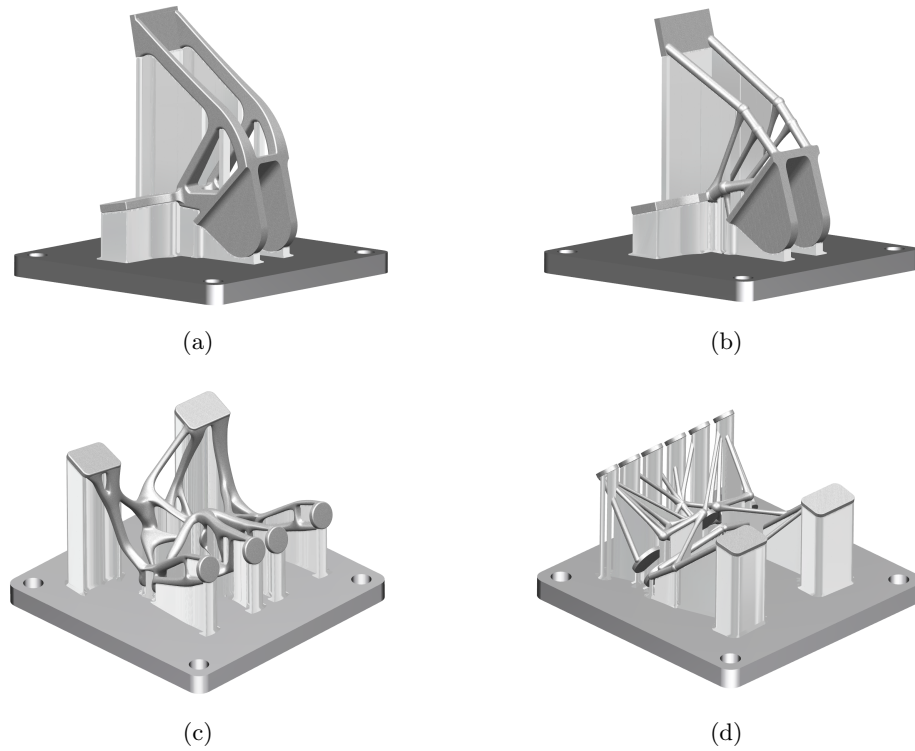


FIGURE 6.5: AM build preparation for aerospace case studies: (a) the topology optimized gear box bracket; (b) the truss optimized gear box bracket; (c) the topology optimized inlet mounting; and (d) the truss optimized inlet mounting. Each has been prepared for AM build with Materialise Magics and EOSPrint for the EOS M290 platform, the gear box bracket is produced from Ti-6Al-4V and the inlet mounting is Inco718.

TABLE 6.1: AM build preparation for aerospace case studies: numerical metrics concerning the efficiency of the case study results for AM build. Note that costs are for the material and build of the part and do not include heat treatments.

	Topology		Truss	
	Gear Box Bracket	Inlet Mounting	Gear Box Bracket	Inlet Mounting
Part Volume (mm <sup>3</sup> )	124369	67450	104734	60117
Support Volume (mm <sup>3</sup> )	6692	5619	3292	2980
Buy-to-Fly Ratio	1.11:1	1.14:1	1.08:1	1.10:1
Build Time (hrs)	50.2	60.5	42.7	38.5
Cost (£)	950	1293	831	947

## 6.5 An outline for a frame structure with frequency toolkit

Whilst the method for optimization presented in Chapter 5 can be used to yield results for a frame with constraints on eigenfrequency, there are still a number of assumptions, such as the linearisation of  $I$ , and some manual intervention required in refining the process to arrive at a satisfactory result. To remedy this, a more numerically-pure method is here proposed based upon a number of existing, but not currently connected, tools.

In order to cope with larger scale problems, solving those with more nodes and potential connections in a computationally efficient manner, it is proposed that the formulae for the treatment of frame structures with semidefinite constraints on eigenvalues be combined with a bespoke SDP solver. This brings together a number of capabilities which can be employed in the optimization of frame structures with constraints on specific natural frequencies, or where other non-linear constraints may be required. A proposed algorithm encompassing this is presented in Figure 6.6.

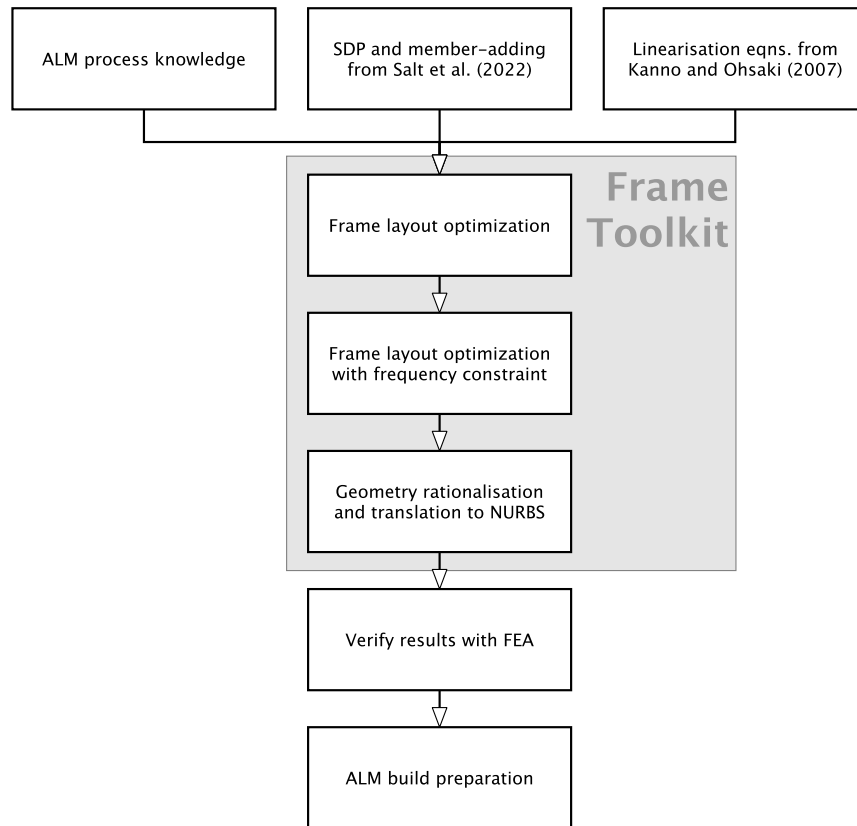


FIGURE 6.6: Proposed algorithm for an SDP frame tool: the ‘building blocks’ of the tool that should be used in its construction are at the top, the major processes the tool should be able to carry out are within the shaded box, and will run sequentially. The outputs from the toolkit are at the bottom and would be performed in existing commercial packages.

### 6.5.1 Further linearisation of $I$ for frame analysis

Kanno and Ohsaki (2007) proposed a methodology to separate the terms of the stiffness matrix, isolating the contributions from truss and beam elements. As per Section 5.3.1, and Euler-Bernoulli beam theory, we express the stiffness matrix contribution to the SDP constraint:

$$\mathbf{K}(\mathbf{a}) - \lambda(\mathbf{M}(\mathbf{a}) + \mathbf{M}_0) \succcurlyeq 0, \quad (6.2)$$

as:

$$\mathbf{K} = \sum_{i=1}^m \mathbf{K}_i^{truss} a_i + \sum_{i=1}^m \mathbf{K}_i^{beam} I_i \quad (6.3)$$

where  $\mathbf{K}_i^{truss}$  and  $\mathbf{K}_i^{beam}$  are constant and positive semidefinite matrices, and  $a_i$  and  $I_i$  are variables dependent on one another. The contribution of the mass matrix remains unchanged and is still directly linear with the design variable  $a$ :

$$\mathbf{M} = \sum_{i=1}^m \mathbf{M}_i a_i \quad (6.4)$$

where  $\mathbf{M}_i (i = 1, 2, \dots, m)$  is constant and a positive semidefinite matrix. Use of Eq. (6.3) in the semidefinite eigenvalue constraint is dependent upon the geometric cross-section of the beams, and the way in which the design variable  $a$  is used in the optimization. When considering applicability to engineering components, two cross-sections that may be produced by additive manufacturing are detailed below:

#### Solid circular beams

For a frame structure consisting of beams with solid circular cross-sections of radius  $r_i$ , both area and second moment of inertia can be expressed as:

$$a_i = \pi r_i^2, \quad I_i = \frac{\pi r_i^4}{4} \quad (6.5)$$

Using Eqs. (6.2) - (6.5), the SDP formulation for bars with a circular cross-section may be defined as:

$$\sum_{i=1}^m (A_i^{(2)} a_i^2 + A_i^{(1)} a_i) - \omega \left( \sum_{i=1}^m B_i^{(1)} a_i + M_0 \right) \succcurlyeq 0 \quad (6.6)$$

where  $A_i^{(2)} = \frac{1}{4\pi} \mathbf{K}_i^{beam}$ ,  $A_i^{(1)} = \mathbf{K}_i^{truss}$ ,  $B_i^{(1)} = \mathbf{M}_i$ .  $M_0$  is the mass matrix for non-structural mass, for the purposes of this thesis it has been considered to be zero, the inclusion of non-structural mass will, however, more accurately model the behaviour of the structure.

### Rhomboid cross-section with equal width and height

A rhomboid cross-section where width ( $b_i$ ) and height ( $h_i$ ) are equal is treated in a similar manner to the circular solid beams with area ( $a_i$ ) and second moment on inertia defined:

$$a_i = \frac{b_i h_i}{2}, \quad I_i = \frac{b_i h_i^3}{48} = \frac{a_i^2}{12} \quad (6.7)$$

and incorporated into Eq. (6.6) in the same manner, keeping all terms the same with the exception of  $A_i^{(2)}$  which is now expressed as  $A_i^{(2)} = \frac{1}{12} \mathbf{K}_i^{beam}$ .

### Rectangular cross-section with fixed width

In contrast to the scenarios presented in Chapter 5, Kanno and Ohsaki (2007) suggest that the width  $b_i$  of the beam should be fixed and the optimization design variable be changed to the height  $h_i$  of the beam instead of the area  $a_i$ . They proposed the following equations contributing to the semidefinite constraint:

$$a_i = b_i h_i, \quad I_i = \frac{b_i h_i^3}{12} \quad (6.8)$$

$$\sum_{i=1}^m (A_i^{(3)} h_i^3 + A_i^{(4)} h_i) - \omega \left( \sum_{i=1}^m B_i^{(2)} h_i + M_0 \right) \succcurlyeq 0 \quad (6.9)$$

where  $A_i^{(3)} = \frac{b_i}{12} \mathbf{K}_i^{beam}$ ,  $A_i^{(4)} = b_i \mathbf{K}_i^{truss}$ ,  $B_i^{(2)} = b_i \mathbf{M}_i$ .

While this method still requires some forethought on the width to use, there is reduced potential for malformed beams as a minimum value can be applied for  $h_i$  in the optimization algorithm. From a practical stance the width may be determined by the

availability of sheet metal, and the minimum height derived according to the capability of the process involved to cut the form of the structure.

### 6.5.2 SDP frame solver

The SDP calculations put forward by [Kanno and Ohsaki \(2007\)](#) have been proven to work on layout-optimized structures with a limited nodal density, comprising  $7 \times 7$  nodes, and with a minimally-connected ground-structure. If these formulations are embedded within the bespoke tool and framework devised by [Salt et al. \(2022\)](#) there is the potential to utilize the member-adding capability to optimize for minimum volume using greater nodal densities, with constraints on equilibrium and natural frequency.

The member-adding procedure begins by solving a minimum connectivity ground-structure problem (such as in [Figure 5.1\(d\)](#)). Once completed, elements are added from a list of potential connections until a solution that satisfies the original fully-connected ground-structure problem is obtained. This approach obtains the solution using only a small fraction of the much greater number of potential connections; see [Gilbert and Tyas \(2003\)](#) and [Weldeyesus et al. \(2019\)](#) for supporting numerical results. The advantage of this approach is that there will be reduced computational burden arising from the quantity of matrix calculations required for a large fully-connected ground-structure. It may also be possible to obtain solutions with a lower overall volume by considering a greater number of potential connections overall.

To improve manufacturability of the resulting components, AM process knowledge should if possible be included as an input to the solver, thereby ensuring that any solution found by the tool can be produced with the minimum of intervention from the engineer. Such knowledge should include the orientation of the resulting component in the build, and consequently the allowable overhang for the members, to ensure that zero or little support material will be required. Such knowledge will assist in the selection of the appropriate form of the members (e.g. rhombus, rectangle, circular etc). A tool that is “additive-aware” should consider the effect that build orientation may have upon material anisotropy (different properties in the  $xy$  and  $z$  direction) in the optimization studies. Anisotropy may result in the material being weaker in the  $z$  direction than in the  $xy$  plane, this can lead to weakness of the final component if not properly accounted for in the analysis.

As discussed in [Section 6.2.2](#), to accurately model the structure and avoid numerical instability, it is important to ensure that a new node is added at locations where members intersect. It is recommended that rationalisation of the geometry be conducted following the initial optimization, and then a further verification or optimization performed on



just those elements with an area above a certain threshold to ensure that all of the initial constraints are still met.

Finally, it is essential to ensure that any optimized output can be realized in a traditional CAD package, and then be processed for AM build preparation or further validation via FEA. A method for translating the results of layout optimization was proposed by [Smith et al. \(2016\)](#) and incorporated into the LimitState:FORM software package. This method is suited to circular members; however further study will be required to understand how this method may apply to more complex forms. Ideally the output from the tool should be a NURBS (Non-Uniform Rational B-Splines) model so that it can be easily manipulated, if necessary, in CAD to modify the element-element transitions and union them with any other geometry as required.

## Chapter 7

# Conclusions

The objective of this thesis has been to investigate design optimization of aerospace components via layout optimization, with specific emphasis on optimization scenarios involving frequency constraints. Elements of the work have gone on to look at how these optimized components may be produced via additive manufacturing. The major achievements from this research are as follows:

- a) The research conducted and reported in this thesis has demonstrated that numerical optimization techniques can be successfully applied to complex aerospace problems with the goal of reducing both mass and CO<sub>2</sub> emissions. Truss optimization was successfully shown to achieve these targets with structural loading in efficient timescales.
- b) Layout optimization can be effectively augmented with frequency constraints to drive the resulting structure to have a natural frequency equal to or greater than a pre-determined minimum. Research conducted in the preparation of this thesis has further developed this theory and combined it with member-adding to solve non-linear frequency problems in efficient timescales.
- c) A method has been proposed to further develop frequency layout optimization and apply it to frame structures which would be fully representative of continuum structures produced via AM. To achieve this a method is proposed where the second moment of area may be made linear to area to reduce the computational burden.

The conclusions already provided in each individual chapter are summarised below:

**Chapter 3:** A review of generative design methods was conducted, focusing on topology and truss layout optimization algorithms on 3D aerospace components, with the goal of

providing weight reductions that are not possible without the use of these automated tools. Two case studies were addressed: a gear box bracket and an inlet mounting. Each were optimized and it was found that truss optimization provided the largest weight reduction (37% for the inlet mounting study, which gives an additional benefit of saving US\$9800 in fuel costs over the service lifetime and reduces CO<sub>2</sub> emissions by over 37 000 kg). This offers a huge potential to aerospace, if truss optimization techniques can be further explored and validated for flight-worth applications. It was also concluded from this chapter that translation of analysis data from a topology optimized solution took significantly longer to achieve than for truss layout optimization, by a factor of almost five times.

**Chapter 4:** An investigation was conducted into the application of truss layout optimization to problems involving constraints on natural frequency. Whilst computationally efficient, a two phase approach to frequency optimization of pin-jointed truss structures was found to produce outcomes that were likely sub-optimal, exhibiting results with greater than expected volumes. With the semidefinite constraint on frequency included directly into the optimization formulation, more optimal results were achievable on fully-connected ground-structures. This, however, could not be applied to larger and more nodally-dense domains due to the additional computational burden of the non-linear frequency constraint. A new bespoke tool was introduced which included a member-adding algorithm, enabling the optimization to begin with a minimally connected ground-structure and with elements added as required. This approach dramatically reduced the computational burden and elapsed time to achieve a result. It was proven to modify the first natural frequency of truss structures for a range of 2D and 3D examples, with limited impact upon the overall volume of the structure.

**Chapter 5:** Further developed the work conducted in Chapter 4 to apply a similar method for frequency optimization with semidefinite constraints to frame structures. It was identified that to apply a similar optimization algorithm, where area,  $a$ , is the design variable, the relationship with the second moment of area,  $I$ , had to be made linear; techniques for linearising this were presented. A tool was devised which can treat problems where frequency constraints are applicable to frame structures and demonstrated initially via a 10 bar ground-structure before applying it to more complex numerical examples. This tool utilized a fully-connected ground-structure for the basis of the optimization, leading to a high computational burden when using nodally dense domains. It was demonstrated that similar size problems can be rapidly treated with member-adding. Chapter 5 concludes by recommending that the tool be developed further to incorporate member-adding and geometry rationalisation techniques to provide the capability to design and optimize a part ready for manufacture.

**Chapter 6:** Discussed a number of opportunities that remain in the field of layout optimization in the presence of frequency constraints. The currently available tools for topology and layout optimization have some, albeit limited, AM process-awareness, which may lead to cases where a support structure needs to be over-engineered in order to reliably produce the components. Having process-awareness included so that build orientation of the component and overhanging angles can be considered as part of the optimization would be of significant benefit to industry, as well as embedding materials data to account for anisotropy and spatial variation in density.

## Chapter 8

# Recommended future work

Areas which may benefit from further work in this field of research are:

- a) The benefits of design optimization methods have been demonstrated and discussed as part of this thesis, looking at both truss and topological methods. One key finding was that moving the numerical solution to a CAD model for further processing was not a streamlined process. It is recommended that further attention be given to methods for transferring a truss or frame structure from the layout optimization environment to a CAD tool in a manner where it may be altered parametrically, instead of being simply exported as a body. This will enhance the workflow by providing geometry that can easily be manipulated, e.g. for FEA activities or AM build preparation. Greater freedom to manipulate the geometry would reduce the potential for stress concentrations to arise.
- b) It has been proven in this thesis with numerical demonstrations that it is possible to optimize truss and frame structures with constraints on frequency. It is recommended that further case study examples are considered, with these then produced physically via AM and subjected to vibrational analysis to better understand the real-world problem. Further work should then refine the numerical model to represent the real-world findings, with a ‘digital-twin’ of the physical component being the objective.
- c) The proposed frame structure optimization with frequency constraints procedure developed has scope for improvement, particularly via inclusion of a member-adding algorithm to reduce the computational burden associated with the number of SDP variables involved in large ground-structures. This would enable domains with a greater number of nodes to be solved in shorter timescales. It would also

allow for a greater number of iterations to be assessed and provide an allowance for changes that often occur in the normal course of the design process.

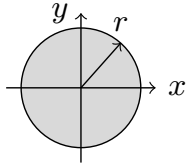
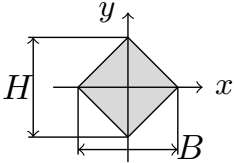
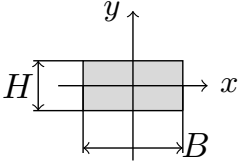
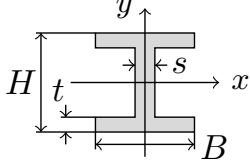
- d) The SDP frame solver outlined in Section 6.5 should be developed to provide a more streamlined workflow for the generation of frame structures with constraints on frequency. Once combined with a member-adding method, AM process awareness, geometry rationalisation, and smooth transition to CAD, a complete toolkit for the automated optimization and design of AM components with frequency constraints may be realized. This will bring significant benefits to industries such as the aerospace industry, where automated and reliable tools for optimization may be employed on components with frequency constraints. Such a tool may not only provide benefit in terms of engineering efficiency but also help to reduce CO<sub>2</sub> emissions and the impact of aviation on climate change, something that is a matter of ever-increasing urgency for our planet.

# Appendix A

## Second Moment of Area

### A.1 Second moment of area formulae for various bar forms

TABLE A.1: Sample of bar forms with method for calculating second moment of area  $I_x$ .

Shape	Figure	$I_x$ Formula
Circle		$I_x = \frac{\pi r^4}{4} \quad (\text{A.5})$
Rhombus		$I_x = \frac{BH^3}{48} \quad (\text{A.6})$
Rectangle		$I_x = \frac{BH^3}{12} \quad (\text{A.7})$
I-section		$I_x = \frac{BH^3 - (B - s)(H - 2t)^3}{12} \quad (\text{A.8})$

## Appendix B

# Bespoke MATLAB codes

### B.1 Identify member intersections and add new nodes

The procedure below can be used to identify the coordinates of a new node required at the intersection of two elements. The node is added and each element is divided in two at the new node. The newly split elements are added to the list of elements so that they can be assessed again in cases of multiple intersections on the same element.

---

```
1 function [nodes,elements,forces] = ...
    intersections(nodes,elements,material,forces)
2
3 %=====
4 % Structural & Frequency Truss Structure Optimization Element Intersection ...
    Detection Script
5 % S.J.Salt - 24 September 2018
6 % (C) Rolls-Royce Plc and University of Sheffield
7 %=====
8
9 %% Identify crossing elements and generate new nodes
10
11 elements(:,5:end) = [];
12
13 n_nodes = size(nodes,1); %Number of nodes at initialisation
14 n_elements = size(elements,1); %Number of elements at initialisation
15
16 sf = 6;
17
18 count = 0;
19 i=1;
20 %for i = 1:n_elements-1
21 while i < n_elements
22     line1 = [nodes(elements(i,2),2:3) ; nodes(elements(i,3),2:3)];
23     for j = i+1:n_elements
24         line2 = [nodes(elements(j,2),2:3) ; nodes(elements(j,3),2:3)];
25
26         slope = @(line) (line(2,2) - line(1,2))/(line(2,1) - line(1,1));
27         m1 = slope(line1);
28         m2 = slope(line2);
29
30         intercept = @(line,m) line(1,2) - m*line(1,1);
31         b1 = intercept(line1,m1);
32         b2 = intercept(line2,m2);
```



---

```

33         xintersect = (b2-b1)/(m1-m2);
34         yintersect = m1*xintersect + b1;
35
36         isPointInside = @(xint,myline) ...
37             (xint ≥ myline(1,1) && xint ≤ myline(2,1)) || ...
38             (xint ≥ myline(2,1) && xint ≤ myline(1,1));
39         inside = isPointInside(xintersect,line1) && ...
40             isPointInside(xintersect,line2);
41
42         if inside == 1
43             if ismember([round(xintersect,sf) ...
44                 round(yintersect,sf)],[round(nodes(elements(:,2),[2 3]),sf); ...
45                 round(nodes(elements(:,3),[2 3]),sf)],'rows') == 0
46                 count = count+1;
47                 ints(count,:) = [elements(i,1) elements(j,1) ...
48                     round(xintersect,sf) round(yintersect,sf) n_nodes+count];
49
50                 elements(end+1,:) = [elements(end,1)+1 elements(i,3) ...
51                     ints(count,5) elements(i,4)];
52                 elements(i,3) = ints(count,5);
53
54                 elements(end+1,:) = [elements(end,1)+1 elements(j,3) ...
55                     ints(count,5) elements(j,4)];
56                 elements(j,3) = ints(count,5);
57
58                 forces(end+1,1) = forces(i,1);
59                 forces(end+1,1) = forces(j,1);
60                 n_elements = n_elements+2;
61
62                 nodes(end+1,1:3) = [n_nodes+count round(xintersect,sf) ...
63                     round(yintersect,sf)];
64             end
65         end
66         i = i+1;
67     end
68
69     % Member lengths for full connectivity list
70     elements(:,5) = sqrt((nodes(elements(:,2),2)-nodes(elements(:,3),2)).^2+...
71         (nodes(elements(:,2),3)-nodes(elements(:,3),3)).^2);
72
73     % Add cosines to element list (cols 6&7)
74     elements(:,[6 7]) = ...
75         [(nodes(elements(:,3),2)-nodes(elements(:,2),2))./elements(:,5)...
76         (nodes(elements(:,3),3)-nodes(elements(:,2),3))./elements(:,5)]];
77
78     % Replace material constant data
79     elements(:,9) = material.E./elements(:,5);
80     elements(:,10) = (material.rho.*elements(:,5))/3;
81 end

```

---

## Appendix C

# Poster presentation of research into frequency constrained truss structures

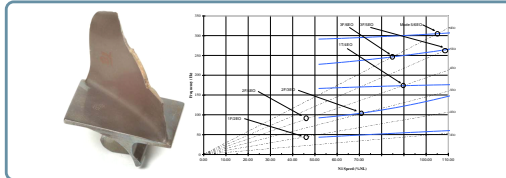
# Frequency Constrained Truss Structures

Steve Salt - [steve.salt@sheffield.ac.uk](mailto:steve.salt@sheffield.ac.uk)



## 1. Introduction

The design of modern engineering components is based upon several key attributes; most prominent are cost, weight, and manufacturability. Each of these attributes are linked through the properties of the component's material and a change in one can have an impact upon another. For many applications, specifically those in the aerospace sector, the harmonic frequencies of a component are a critical design constraint to ensure that they do not lie within an undesirable band. Avoidance of overlapping frequencies is essential as a component with the same natural frequency as an input excitation frequency may resonate with disastrous consequences.

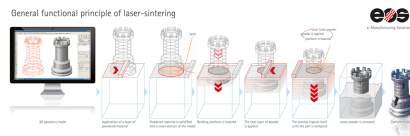


## 2. Research Themes

The purpose of this research is to develop an algorithm with processes that enable the automatic generation of a stress and frequency constrained component with the minimal possible volume, ideally suitable for additive manufacture. Truss structures and additive manufacture have been selected to provide a level of complexity and weight saving not available with conventional manufacturing.

### Aims & Objectives

- Develop a layout optimization programme to generate the domain and store the problem metrics in an efficient manner.
- Calculate the geometry dependent matrices required for generation of the global mass ( $\mathbf{M}$ ) and stiffness ( $\mathbf{K}$ ) matrices.
- Optimize the rationalised structure to ensure that the minimum natural frequency  $\omega_1$  is greater than or equal to a prescribed minimum value.
- Perform rationalisation on the optimized geometry to obtain a practical structure. This simplification should only marginally impinge upon the overall volume.
- Expand into 3D structures and investigate whether the same principles can be applied to rigid-jointed frames.



## 3. Optimization Algorithm

Based upon the objectives, the algorithm for optimization consists of four major operations as per the layout below. At the end of the frequency analysis if the resulting volume is outside the allowable increase the process begins again.



### Layout Optimization:

Use a combination of linear programming with a member adding algorithm to assess structures with a fine nodal density. This is used as a reference point for the overall volume.

### Geometric Coefficients:

Values are calculated which contain all the required information, except for area, to assemble the mass and stiffness matrices. Each matrix is multiplied by area later as this is a variable in the optimization problem.

### Layout & Frequency Optimization:

The design domain and boundary conditions are submitted to a semi-definite programming solver with member adding to perform the optimization considering stress and natural frequency. The target is to minimise the volume of the structure.

### Geometry Rationalisation:

Using the results of the previous step, members with an area above a preset minimum are extracted and assessed. Where members intersect new nodes are added and the frequency of the structure checked again.

## 4. Optimizing the Frequency

A derivation of the equation for motion, termed the generalised eigenvalue problem (1), is used to evaluate the natural frequencies of a body. In this case it is assumed that the body being evaluated has no internal or applied damping.

$$\mathbf{K}\phi_j = \lambda_j(\mathbf{M} + \mathbf{M}_0)\phi_j \quad (1)$$

Expanding on (1) a non-linear constraint may be derived for an optimization routine targeting minimum volume. It is possible to use the relationship between frequency and eigenvalue to impose a minimum frequency upon the structure. The optimization problem is as per (2) below.

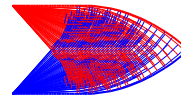
$$\begin{aligned} \text{minimise } \mathbf{V} &= \sum_{i=1}^m l a_i \\ \text{subject to } &\begin{cases} \mathbf{K}(a) - \lambda(\mathbf{M}(a) + \mathbf{M}_0) \succ 0 \\ a \geq 0 \\ \lambda = \omega_1^2 \end{cases} \end{aligned} \quad (2)$$

### The Role of $\lambda$

$\lambda$  in the above equation denotes the eigenvalue of the matrices. Specifying this figure in advance drives the area variable ( $a$ ) to ensure that the frequency constraint equals 0.

## 5. Process Example

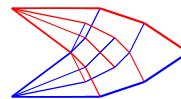
The example Michell cantilever below shows how this process can be used to generate a structure, make it practical for further analysis, and then optimized to ensure that the first natural frequency is greater than or equal to the specified minimum of 400Hz.



### Layout Optimization

The prescribed domain has been optimized for layout targeting minimum volume. However, it can be seen that the structure is impractical with over 169,000 elements.

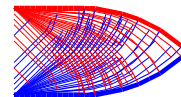
$$V = 7.116, f_1 = 375\text{Hz}, t = 471.9\text{s}, M = 6\text{Gb}$$



### COTS SDP Solver

Using a commercial off the shelf SDP solver the layout of the structure can be optimized with an additional constraint on frequency as described above, however it is very slow to compute and consumes a lot of memory, therefore fewer bars may be included in the problem.

$$V = 7.116, f_1 = 407\text{Hz}, t = 1628\text{s}, M = 21\text{Gb}$$



### Bespoke SDP Solver

Coupling the problem domain and frequency constraint to a bespoke SDP solver has yielded a structure both optimized for layout and for the first natural frequency but with less memory consumed. Practicality to be addressed.

$$V = 7.051, f_1 = 400\text{Hz}, t = 1791\text{s}, M = 1.2\text{Gb}$$

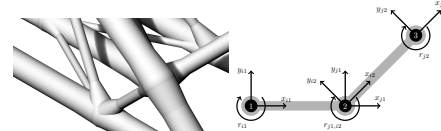
## 6. Conclusions & Future Work

Since its outset this research has explored the role that optimization plays in the design of components for additive manufacture, identified a focus of optimizing for frequencies, and determined a suitable method for application.

### Conclusions

- Layout optimization yields a globally optimum structure of minimum volume/mass without pre-determining the fraction. This value may be treated as a mathematically pure reference volume.
- The natural frequency of the structure can be tailored to suit a minimum constraint by modifying the area and layout of the structural members.
- A semi-definite programming algorithm is required instead of linear programming to assess the non-linear constraints of the mass and stiffness matrices. Use of this solver has proven that truss structures can be optimized for frequency. Use of this algorithm has shown a significant decrease in CPU time and memory consumption.

The next phase of this research will transition from pin-jointed frames to rigid-jointed, more accurately representing an additively manufactured aerospace component. This will utilise beam elements in a frame configuration and require a  $\mathbf{K}$  matrix capable of accommodating reactionary moments.



The author wishes to acknowledge and thank Rolls-Royce Plc. for its support and continued sponsorship of this research.



## Appendix D

# Layout optimization of pin-jointed truss structures with minimum frequency constraints

ENGINEERING OPTIMIZATION  
2023, VOL. 55, NO. 8, 1403–1421  
<https://doi.org/10.1080/0305215X.2022.2086539>



Taylor & Francis  
Taylor & Francis Group

OPEN ACCESS



## Layout optimization of pin-jointed truss structures with minimum frequency constraints

S. J. Salt <sup>a</sup>, A. G. Weldeyesus <sup>b</sup>, M. Gilbert <sup>c</sup> and J. Gondzio <sup>b</sup>

<sup>a</sup>Rolls-Royce plc, Derby, UK; <sup>b</sup>School of Mathematics and Maxwell Institute, The University of Edinburgh, Edinburgh, UK; <sup>c</sup>Department of Civil and Structural Engineering, University of Sheffield, Sheffield, UK

### ABSTRACT

Controlling the frequency response of an engineering component or structure is important in the aerospace and automotive sectors and is a key consideration when seeking a new and more efficient design for a given component. In this contribution, the standard truss layout optimization procedure is modified to incorporate semidefinite constraints to limit the minimum value of the first natural frequency. Since this increases the computational expense and reduces the scale of the problem that can be solved, a bespoke algorithm incorporating an adaptive ‘member adding’ procedure is proposed and applied to a number of benchmark example problems. It is demonstrated that this allows problems to be solved with relatively fine numerical discretization, allowing modified structures with an acceptable minimum first natural frequency response to be successfully identified.

### ARTICLE HISTORY

Received 26 June 2021  
Accepted 25 March 2022

### KEYWORDS

Layout optimization;  
topology optimization; truss  
structures; frequency  
constraints

## 1. Introduction

In the design of modern engineering components, many considerations need to be taken into account including safety, cost, weight and manufacturability. The most prominent of these is safety, taking account of the regime of applied stresses to be sustained over the life of the component. Safety is influenced by the properties of the material employed, which may change as the design evolves. Additionally, when considering structures that include slender elements in compression, it is necessary to check for buckling instability to ensure safety is maintained. Another key parameter in the aerospace sector is the harmonic frequency of a structure. This should lie outside the frequency bands of surrounding components. Should a fundamental frequency of one component (e.g. a bracket) overlap with those of its attached neighbours, then resonance in the component may occur, also referred to as forced vibration. Forced vibration and resonance can then lead to High Cycle Fatigue (HCF) in the component, affecting its serviceable life and reducing its time to failure. It should be noted that a component may exhibit multiple resonant frequencies, each corresponding to a mode of vibration; repeated exposure to these frequencies may reduce the life of the component. However, this phenomenon is beyond the scope of the current contribution. Considering component manufacture, it is important to note that traditional manufacturing methods may limit the design freedom available; however, in the present contribution, it is assumed that Additive Layer Manufacturing (ALM) methods are available. The use of ALM means that complex truss forms can potentially be fabricated, beyond the scope of traditional subtractive manufacturing methods.

**CONTACT** M. Gilbert  [m.gilbert@sheffield.ac.uk](mailto:m.gilbert@sheffield.ac.uk)

© 2022 The Author(s). Published by Informa UK Limited, trading as Taylor & Francis Group

This is an Open Access article distributed under the terms of the Creative Commons Attribution License (<http://creativecommons.org/licenses/by/4.0/>), which permits unrestricted use, distribution, and reproduction in any medium, provided the original work is properly cited.

There have been numerous recorded HCF related incidents. A notable example led to the loss of British Midland flight #92 in 1989 (Cooper 1989). This was initiated by the failure of a fan blade on one of the two CFM International S.A. CFM56-3 turbofan engines. A single blade failed owing to the coupling of a torsional–flexural transient and a non-synchronous oscillation, leading to rapid reduction of the HCF life of the blade. The blade was subsequently released, causing high levels of vibration in the engine and aircraft, contributing to the loss of the aircraft upon attempting an emergency landing at East Midlands Airport in the UK.

Given the potentially catastrophic consequences of failure, the design optimization of components with stress and frequency constraints has been of interest for many years. Forced vibration problems can be avoided by (a) redesigning the component being analysed, (b) redesigning the stimuli to change its frequency characteristics, and/or (c) introducing a damping mechanism into the system. The most straightforward of these options is often (a), redesigning a component to move its fundamental frequencies away from those where resonance may occur. This may be achieved, for example, by adding stiffening ribs to the part or strategically increasing the volume of material.

Computer aided methods have been employed to treat such problems, largely focusing upon the use of topology optimization in works such as Bendsoe and Sigmund (2003), where links can be formed between discrete and continuum structures (Achtziger 1999). Additionally, Du and Olhoff (2007) formulated simple and multiple eigenfrequency optimization techniques for linear elastic structures without damping. The present contribution will focus upon the design of truss structures that are attractive when there is significant available design freedom. In practice, it is rare that the available design freedom is fully exploited, usually due to limitations associated with the manufacturing method involved. However, ALM allows the available design freedom to be exploited to a much greater extent than when traditional subtractive manufacturing methods are employed. Since the ground structure method was first introduced by Dorn, Gomory, and Greenberg (1964) to solve plastic truss design problems, layout optimization has provided an effective means of identifying the most efficient arrangement of elements (also referred to herein as ‘members’ or ‘bars’) to form a truss structure. This methodology has been well used to identify minimum volume truss structures (Dorn, Gomory, and Greenberg 1964; Hemp 1973; Gilbert and Tyas 2003; Smith *et al.* 2016) using Linear Programming (LP) and member adding (column generation) to solve single load case problems efficiently. These methods have been further extended by Pritchard, Gilbert, and Tyas (2005) and Sokół (2014) to include application to multiple load cases; to keep the underlying layout optimization problem formulation reasonably simple, the present contribution will focus on single load case problems with a single specified minimum frequency, usually chosen so as to lie away from the frequencies of any sources of excitation. However, frequency analysis is a nonlinear problem and so semidefinite programming (SDP) must be used to treat the constraints.

SDP is a subset of convex optimization and aims to minimize a linear function subject to the constraint that an affine combination of symmetric matrices is positive semidefinite. SDP has been applied to the optimization of truss structures previously by Ben-Tal and Nemirovski (1997), and later Kanno (2018) used SDP to produce structures that were robust against uncertainty in the loading, and Giniünaitė (2015) applied SDP to identify minimum mass structures. A number of solvers are available that are capable of treating semidefinite problems of varying complexity: *fminsdp* (Thore 2018); *MOSEK* (v8+) (*MOSEK ApS* 2017); *PENLAB* (Fiala, Kočvara, and Stingl 2013) and *CVX* (Grant and Boyd 2014) are a few examples. However, a bespoke approach is required when combining generative truss design with optimization for frequency constraints.

Frequency optimization belongs to the field of eigenvalue optimization in mathematics, which has been studied extensively by the mathematical programming community: Fox and Kapoor (1970) adopted a feasibility approach to solve the underlying semidefinite programming problem, Grandhi and Venkayya (1988) and Khot (1985) used the optimality criteria method and Kaveh and Ghazvaan (2016) used non-smooth optimization to perform size optimization of existing truss structures to meet certain frequency requirements. Additionally, Achtziger and Kočvara (2007) used SDP to solve similar problems, and Aroztegui *et al.* (2011) developed a feasible direction algorithm for SDP

in order to maximize the fundamental frequencies based upon simple fully connected ground structures. Considering optimization of frequency in isolation, Azad *et al.* (2018) assessed the simultaneous size and geometry optimization of steel structures under excitation using the ‘big bang–big crunch’ algorithm, with mixed results when considering the optimum solutions, whilst Taheri and Jalili (2016) and Tejani *et al.* (2018) used other meta-heuristic methods to impose frequency constraints in truss optimization problems.

In many of these studies, the design variable was treated as continuous but the number and arrangement of the variables were assumed to be finite and arrived at by utilizing the most efficient members from a pre-defined ground structure. By contrast, in the present article an alternative methodology is proposed in which standard equilibrium constraints are supplemented by semidefinite constraints to enable problems involving both frequency and strength considerations to be tackled. The ground structure method is employed to provide a large search space, with an adaptive member adding algorithm used to reduce the associated computational burden significantly. In the interests of simplicity, buckling instability and other issues are not considered explicitly in this contribution, though would need to be checked prior to, for example, usage in a qualified aerospace application.

This article is organized as follows: Section 2 describes the basic formulations relevant to the frequency problem at hand, with examples used to illustrate limitations; Section 3 then proposes a new formulation that is significantly more computationally efficient; the new formulation is then applied to various example problems in Section 4; and conclusions are drawn in Section 5.

## 2. Basic formulations


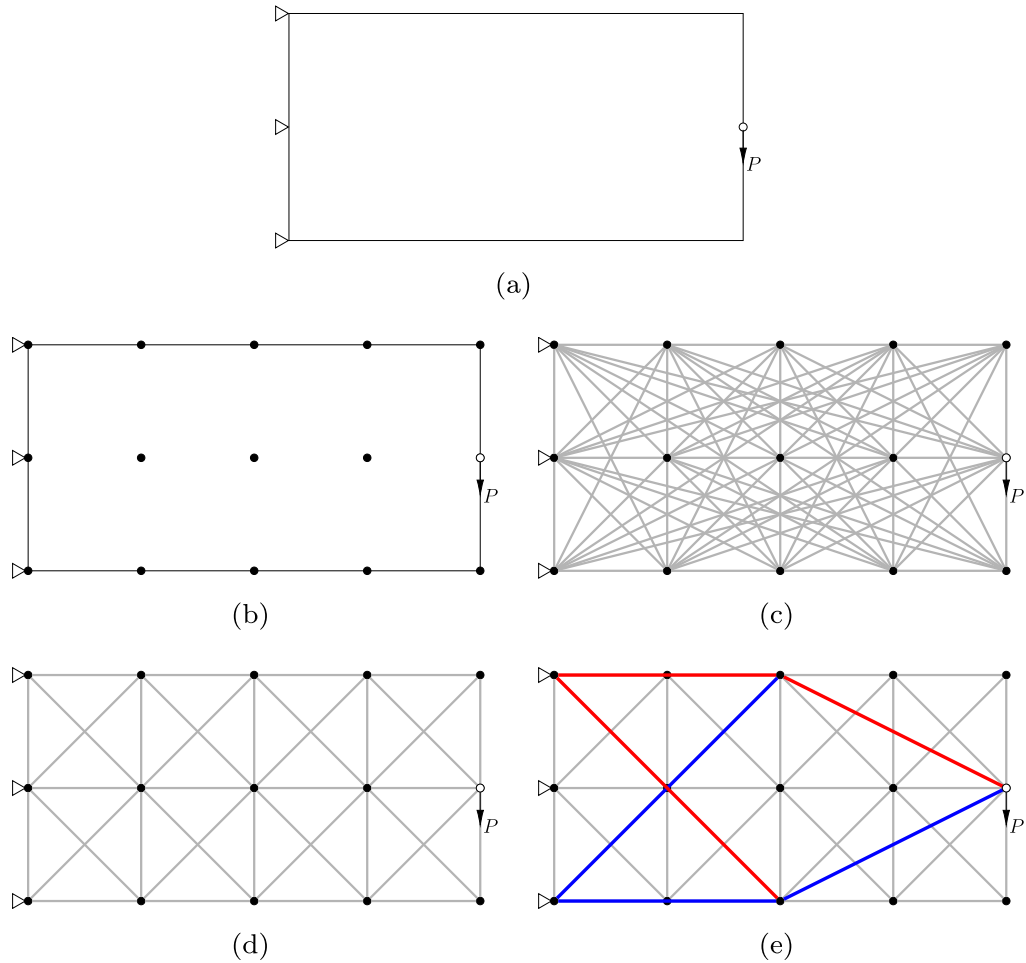
### 2.1. Truss layout optimization formulation

Ground structure-based layout optimization begins with the definition of a design domain, the volume of space in which the optimized structure can reside, with materials, loads and supports then also prescribed to describe the problem fully, see Figure 1(a). The objective is to arrive at a structure of minimum volume, and hence mass, whilst maintaining structural integrity. With a Cartesian grid, the design domain is populated with a predefined number of nodes  $n$  in the  $x$ - and  $y$ -directions (also in the  $z$ -direction for 3D problems). It is then joined with  $m$  potential connections, or elements, such that each node is connected to every other node in the domain to form a ground structure, as in Figures 1(b) and 1(c). Herein, each example will employ a number of nodes expressed in terms of the number of nodal divisions, *e.g.* referring to Figure 1(b), the domain has  $4 \times 2$  nodal divisions, with 4 divisions and 5 nodes in the  $x$ -direction and 2 divisions and 3 nodes in the  $y$ -direction, giving 15 nodes in total. Constraints are introduced to ensure equilibrium is enforced at nodes, and to ensure that the cross-sectional area of each element is both a positive number and is sufficiently large to carry the internal forces, given the limiting stress of the material. The plastic single load case formulation can be written as (after Dorn, Gomory, and Greenberg 1964):

$$\begin{aligned} \min_{\mathbf{a}, \mathbf{q}} \quad & V = \mathbf{l}^T \mathbf{a} \\ \text{s.t.} \quad & \begin{cases} \mathbf{B}\mathbf{q} = \mathbf{p}, \\ -\sigma^- a_i \leq q_i \leq \sigma^+ a_i, & \forall i \\ a_i \geq 0, & \forall i, \end{cases} \end{aligned} \quad (1)$$

where  $V$  is the total volume of the structure;  $\mathbf{l}$  is a vector of individual element lengths  $\{l_1, l_2, \dots, l_m\}$ ;  $\mathbf{a}$  is a vector containing element cross-sectional areas  $\{a_1, a_2, \dots, a_m\}$ ;  $\mathbf{B}$  is a suitable  $(2n \times m$  or  $3n \times m)$  equilibrium matrix containing direction cosines (for 2D or 3D problems);  $\mathbf{q}$  is a vector of element axial forces,  $\mathbf{q} = \{q_1, q_2, \dots, q_m\}$ , where  $q_i$  is the force in element  $i$ ;  $\mathbf{p}$  is a vector of applied loads and  $\mathbf{p} = \{p_1^x, p_1^y, p_1^z, p_2^x, p_2^y, p_2^z, \dots, p_n^z\}$  where  $p_j^x, p_j^y, p_j^z$  are the  $x$ -,  $y$ - and  $z$ -direction components of the load applied to node  $j$  ( $j = 1, \dots, n$ ). Finally  $\sigma^+$  and  $\sigma^-$  are, respectively, the limiting tensile and



1406  S. J. SALT ET AL.

**Figure 1.** Steps in layout optimization: (a) definition of the problem domain and boundary conditions; (b) domain populated with equally spaced nodes; (c) each node is connected to every other node in the domain to form a fully connected ground structure or (d) each node is connected only to neighbouring nodes to form a minimally connected ground structure; and (e) the resulting optimized layout using a member adding algorithm (red and blue bars indicate those in tension and compression, respectively [online only]).

compressive stresses that can be sustained by the material. Problems of this nature may be solved using linear programming.

Employing a fully connected ground structure of this type is computationally expensive, with the problem comprising  $n(n-1)/2$  potential connections for a domain, where  $n$  is the total number of nodes. The majority of the connections will have an area equal or close to zero following the optimization and so do not contribute to the final structure. This issue may be alleviated by applying the adaptive ‘member adding’ method proposed by Gilbert and Tyas (2003), which is a customized column generation technique. With this method, nodes in the initial ground structure are only connected to their immediate neighbours, Figure 1(d), instead of to every other node in the domain, Figure 1(c). An iterative process is then used, with elements added to the current ground structure from the list of potential connections. Newly added elements are introduced into the solution using the Michell–Hemp criterion (2), which specifies limits on the virtual strain ( $\varepsilon_i$ ) experienced by each potential element ( $i$ ), given a prescribed limiting stress ( $\sigma$ ):

$$-\frac{1}{\sigma^-} \leq \varepsilon_i \leq \frac{1}{\sigma^+}, \quad i = 1, \dots, m. \quad (2)$$



In the parlance of the column generation method (Gondzio and Sarkissian 1996; Desrosiers and Lübbecke 2005; Gondzio, González-Brevis, and Munari 2013), new columns are added to the LP constraint matrix  $\mathbf{B}$  in (1). At the end of each iteration, potential connections are ranked, with those most violating the criteria then added for use in the next iteration. Once there are no potential connections violating the criteria remaining, the algorithm terminates. The solution obtained shown in Figure 1(e) is provably optimal, with the computed volume the same as that obtained using a fully connected ground structure.

## 2.2. General eigenvalue equation

Consider a truss structure consisting of  $m$  elements connecting a pre-determined set of  $n$  nodes. A large external force  $P$  is applied to a specific node, with internal forces transmitted through the structure, resulting in small displacements at each node; this may be considered to be a static problem. To take account of the vibration characteristics of the structure, it is necessary to consider the following dynamic problem derived from the equation of motion:

$$\mathbf{K}\{\mathbf{u}\} + \mathbf{M}\{\ddot{\mathbf{u}}\} = 0, \quad (3)$$

where  $\mathbf{K}$  and  $\mathbf{M}$  represent the global stiffness and mass matrices, respectively. The mass and stiffness matrices are represented as symmetric  $2n \times 2n$  matrices when modelling a two-dimensional truss structure and  $3n \times 3n$  matrices for a three-dimensional truss structure. The size of these global matrices will be reduced by the number of supported degrees of freedom, since there are no displacements at these locations. Given that the displacement vector is harmonic, (3) may be restructured into the generalized eigenvalue problem:

$$\mathbf{K}\phi_j = \lambda_j(\mathbf{M} + \mathbf{M}_0)\phi_j, \quad (4)$$

where  $\mathbf{M}$  refers to the global mass matrix for the structure's bar elements,  $\mathbf{M}_0$  refers to the additional mass of the nodes connecting each element and  $\lambda_j$  represents the eigenvalue for a given mode of vibration  $\phi_j$  ( $j = 1, 2, 3, \dots$ ). The free vibrations of a structure are equal to the square root of the eigenvalues  $\omega_j^2 = \lambda_j$  in radians per second, and thus the natural frequencies and normal modes of vibration for the structure may be determined.


## 2.3. Frequency formulation

### 2.3.1. Determine the reference frequencies

To determine conformance with the original design problem, it is necessary to calculate the natural frequencies of the structure. If a candidate design has been obtained via layout optimization, then this can be performed using the connectivity and member cross-sectional areas generated in the optimization. The areas for each element are multiplied by the corresponding mass and stiffness coefficients before being assembled into the global matrices ( $\mathbf{K}$  and  $\mathbf{M}$ ) at the row/column index corresponding to the degrees of freedom associated with the member end nodes, with rows and columns related to the supported degrees of freedom omitted. The eigenvalues can be extracted *e.g.* using the built-in MATLAB® `eigs` functionality. Previous studies, *e.g.* Du and Olhoff (2007), have considered multiple eigenfrequencies; however, this contribution will concentrate on just the first natural frequency in hertz for the structure to ensure it will not resonate when exposed to a source of excitation.

### 2.3.2. Semidefinite constraint

In order to perform an optimization targeting the natural frequencies of the structure, a new constraint equation must be derived from the generalized eigenvalue problem (4). Once the coefficient matrices for stiffness and mass are determined, in order to avoid the optimization generating a structure prone to low frequency vibration, a threshold can be set such that the smallest eigenvalue from (4)

1408  S. J. SALT ET AL.

is greater than or equal to a defined minimum value. Thus (4) may be transformed into the following constraint:

$$\mathbf{K}(\mathbf{a}) - \lambda(\mathbf{M}(\mathbf{a}) + \mathbf{M}_0) \succcurlyeq 0, \quad (5)$$

where  $\mathbf{K}(\mathbf{a}) = \sum_{i=1}^m a_i \mathbf{K}_i$  and  $\mathbf{M}(\mathbf{a}) = \sum_{i=1}^m a_i \mathbf{M}_i$  are the global stiffness and mass matrices, respectively,  $a_i$  refers to the cross-sectional area of member  $i$ ,  $\lambda$  is the eigenvalue derived from the minimum specified natural frequency ( $\omega_1$ ) for the specified mode of vibration  $\phi_j$  and  $\succcurlyeq$  indicates that the matrix to its left is symmetric and positive semidefinite. For the purposes of this contribution, the connecting nodes are not considered and therefore the mass associated with joints  $\mathbf{M}_0 = 0$ .

Thus, when incorporated into the layout optimization formulation (1), the problem may be written as

$$\begin{aligned} \min_{\mathbf{a}, \mathbf{q}} \quad & V = \mathbf{I}^T \mathbf{a} \\ \text{s.t.} \quad & \begin{cases} \mathbf{B}\mathbf{q} = \mathbf{p}, \\ \mathbf{K}(\mathbf{a}) - \lambda_0 \mathbf{M}(\mathbf{a}) \succcurlyeq 0 \\ -\sigma^- a_i \leq q_i \leq \sigma^+ a_i, \quad \forall i \\ a_i \geq 0, \quad \forall i. \end{cases} \end{aligned} \quad (6)$$

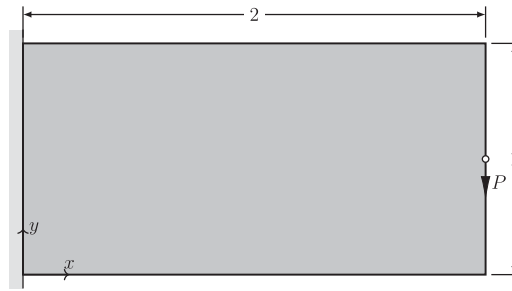
Fixing the smallest eigenvalue ( $\lambda_0$ ) to be greater than or equal to the minimum specified frequency ensures that the areas of the elements are adjusted as part of the optimization until the inequality constraint is achieved. Incorporation of the semidefinite constraint means that an SDP solver is now required to solve the problem. Note that SDP problems are convex, enabling a globally optimal solution to be obtained, but are considerably more computationally demanding to solve than their LP counterparts.

## 2.4. Short cantilever example

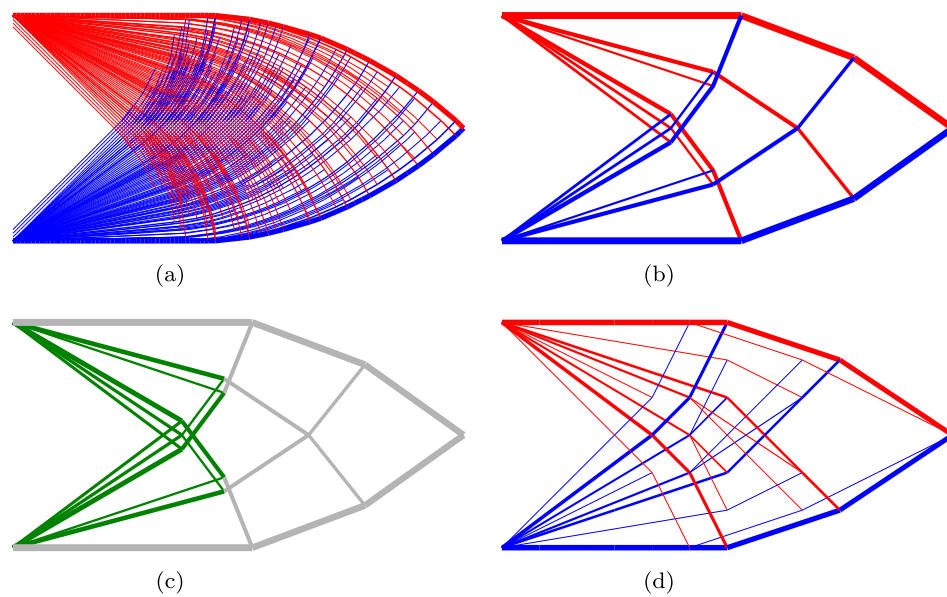
Two means of optimizing a short cantilever structure based on a prescribed minimum first natural frequency will now be outlined, using the example problem defined in Figure 2 to illustrate salient points. For this problem:  $P = 1 \times 10^3$  N;  $E = 210 \times 10^9$  N m<sup>-2</sup>;  $\rho = 8050$  kg m<sup>-3</sup>; and the limiting tensile and compressive stresses  $\sigma = 350 \times 10^6$  Pa. The prescribed constraint on the fundamental natural frequency is  $f_1 \geq 425$  Hz. All numerical examples in this contribution were run on a 64 bit Windows® 10 desktop PC equipped with an Intel® i5 3.7 GHz processor and 32 GB of RAM, using a script programmed using MATLAB 2020b. A number of semidefinite solvers are available and are compared by Tyburec and Zeman (2017). This contribution will initially employ the MOSEK ApS (2017) v8.1 solver using the Java Fusion MATLAB interface. It should be noted that unless otherwise specified all layouts presented in the figures are filtered to include only elements with areas greater than  $1 \times 10^{-6}$  m<sup>2</sup>. This may occasionally result in elements that appear to be disconnected from the overall structure. Additionally, to facilitate comparison with other published work, non-dimensional volumes  $V$  are presented throughout the article, with scaled volumes  $V(P/\sigma)$  in cubic metres also included in accompanying tables for completeness.

### 2.4.1. Two phase optimization approach

Since SDP problems are computationally expensive to solve, initially the efficacy of a two phase optimization approach is evaluated. With this approach, a traditional layout optimization is first undertaken without considering frequency constraints; if prescribed frequency requirements are not met by the generated design, then a size optimization is subsequently performed to ensure that these are met, modifying only the subset of elements present in the optimal structure; *i.e.* in this second phase the areas of each element  $a_i$  are adjusted to ensure the semidefinite constraint (5) is met. In the interests of computational efficiency, only those elements that have an area greater than a pre-determined minimum (taken as  $1 \times 10^{-6}$  m<sup>2</sup>) are included in the optimization; these elements will henceforth be referred to as members.



**Figure 2.** Short cantilever example: design domain, loading and support details. All dimensions are in metres.




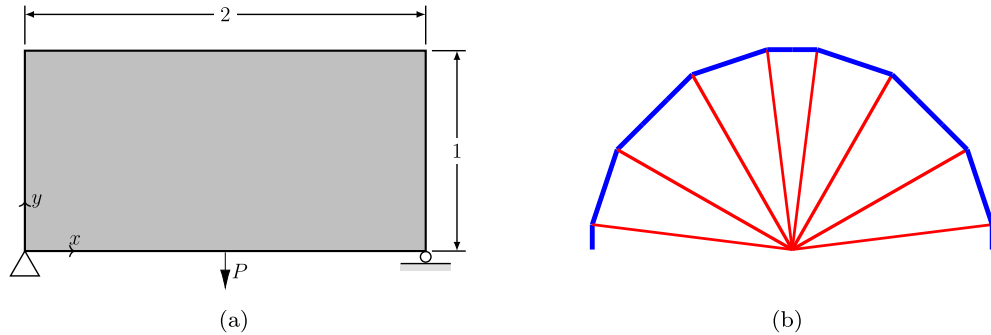
**Figure 3.** Short cantilever example: (a) reference LP solution achieved using layout optimization using  $120 \times 60$  nodal divisions; (b) more practical LP layout, achieved by reducing the nodal divisions to  $40 \times 20$  and penalising joints; (c) outcome of the SDP frequency optimization performed on the practical layout from (b); (d) layout generated using SDP optimization of the full ground structure, including frequency constraint using  $12 \times 6$  nodal divisions. (Key: red = tension; blue = compression; green = members in (c) whose areas have been modified compared with (b); grey = members whose areas are as per the layout in (b) [online only]). (For (a)  $V = 7.030$ ,  $f_1 = 403$  Hz. (b)  $V = 7.095$ ,  $f_1 = 410$  Hz. (c)  $V = 7.436$ ,  $f_1 = 425$  Hz and (d)  $V = 7.134$ ,  $f_1 = 425$  Hz.)

**Table 1.** Short cantilever example: LP and SDP results (target frequency for the SDP problem = 425 Hz).

Figure	Model	Nodal divisions	$V$	$V(P/\sigma)$ ( $\times 10^{-5} \text{m}^3$ )	$f_1$ (Hz)	Time (s)
3(a)	LP (fine ref.)	$120 \times 60$	7.030	2.009	403	146
3(b)	LP	$40 \times 20$	7.095	2.027	410	26
3(c)	SDP (size only)	...	7.436	2.125	425	3
...	LP (coarse ref.)	$12 \times 6$	7.116	2.033	407	9
3(d)	SDP (full)	$12 \times 6$	7.134	2.038	425	1472

Considering first the example problem defined in Figure 2, an initial layout optimization is carried out to provide reference values for the volume and first natural frequency of the structure; see Table 1 and Figure 3(a). The structure shown is similar to that obtained by He, Gilbert, and Song (2019).

However, the reference structure contains many members, so for the first phase of the proposed two phase procedure a domain with fewer nodes is used to enable a more practical layout to be generated, containing fewer ‘fibrous’ elements. This is achieved by both reducing the number of nodes and

1410  S. J. SALT ET AL.

**Figure 4.** Half wheel example: (a) problem definition; (b) optimal structure obtained after phase one of the two phase method (*i.e.* not considering frequency constraints). All dimensions are in metres.

introducing a joint penalty, after Parkes (1975). This results in the structure shown in Figure 3(b), which has fewer joints and elements than the benchmark but which has a similar volume.

In the second phase, the structure from the first phase is re-optimized using the modified formulation that includes frequency constraints (6) to revise member sizes ensuring the frequency is not less than 425 Hz. In the re-optimization it is found that the areas of diagonal members radiating from the support line, along with some members interconnecting these, need to be modified (resized members are highlighted in green in Figure 3(c) in the online version of the paper).

It is evident that the solver has been successful in achieving the desired minimum natural frequency, at minimal CPU cost; however, this has in this case come at a relatively high cost in terms of increased volume (8.7%). This suggests that changing the size of the elements alone may not lead to the most efficient solution, and a better one may be available if a wider solution space were to be made available.

Next consider the classical half-wheel problem shown in Figure 4, as originally studied by Michell (1904). The problem involves a central point load  $P = 1 \times 10^3$  N applied at midspan between statically determinate supports, limiting tensile and compressive stresses  $\sigma = 350 \times 10^6$  Pa and, in common with the other presented examples,  $E = 210 \times 10^9$  N m<sup>-2</sup> and  $\rho = 8050$  kg m<sup>-3</sup>. The optimal solution obtained when using  $16 \times 8$  nodal divisions is shown in Figure 4(b) and has a non-dimensional volume  $V = 3.191$ . This includes a short vertical member above each of the supports, leading to a structure that is in unstable equilibrium with the applied loading. This arises because only equilibrium (and strength) constraints are enforced in phase one. However, a byproduct of this is that subsequently adjusting the sizes of structural members alone in the second phase, with a view to achieving a natural frequency of for example  $f_1 = 200$  Hz, will fail owing to inherent instability in the problem. This highlights a further limitation of the two phase optimization approach.

#### 2.4.2. Holistic optimization

Although the two phase approach described in the preceding section is computationally efficient for problems where it can obtain viable solutions, if the increase in volume in the second phase is large then the question arises as to whether a more materially efficient design exists.

This can be checked by applying the formulation including an SDP frequency constraint to the full ground structure. The associated computational expense means that only a coarse nodal grid ( $12 \times 6$ ) can be used in this case. For the short cantilever example, the solution obtained using the finest nodal density achievable with the available memory is shown in Figure 3(d). When compared with a reference structure consisting of the same size, it demonstrates that a modified design enables the target frequency to be met with little impact on the overall volume of the structure. The optimum point where the equilibrium and frequency constraints are satisfied requires a layout different from that of the structural optimization alone. However, it must be noted that the largest problem that could be solved with a fully connected ground structure is much smaller than the one that could be solved using the two phase approach.

### 3. SDP formulation with member adding

To solve complex problems of this nature with a large initial ground structure efficiently, a special purpose solver based on the Mehrota-type primal–dual interior point method (Fujisawa *et al.* 2000) was developed. The approach and its implementation closely follow Weldeyesus *et al.* (2019), which describes the optimization of truss structures with constraints on global stability modelled via SDP. In Weldeyesus *et al.* (2019), the proposed method is capable of obtaining solutions to relatively large problems that could not otherwise have been solved. Owing to similarities between the mathematical properties of the optimization problem considered in this article and those of the problem discussed in Weldeyesus *et al.* (2019), only the member adding method is explained here in detail. Issues such as exploiting sparsity and the low rank property of the element stiffness matrices  $\mathbf{K}_i$  and mass matrices  $\mathbf{M}_i$  when forming the linear systems arising in the interior point algorithm for SDP are not repeated here, but play a crucial role in the overall efficiency of the approach. As outlined in Section 2.1, the adaptive member adding approach—which is based on the column generation technique, see Gondzio and Sarkissian (1996), Desrosiers and Lübbecke (2005) and Gondzio, González-Brevis, and Munari (2013)—is an iterative process originally proposed in Gilbert and Tyas (2003), and also applied to other problems by *e.g.* Sokół and Rozvany (2013) and Weldeyesus and Gondzio (2018), who also employed linear programming to obtain solutions. The method was extended to treat SDP problems by Weldeyesus *et al.* (2019). The procedure starts by solving a minimum connectivity ground structure problem (Figure 1(d)), and proceeds by adding elements from a potential connection list until a solution that satisfies the original fully connected ground structure problem is obtained. This approach enables the method to obtain a solution using a small fraction of the large number of potential connections: see Gilbert and Tyas (2003) and Weldeyesus *et al.* (2019) for supporting numerical results.

#### 3.1. Details of the SDP member adding algorithm

Here, a mathematical description of the member adding procedure akin to that described in Section 4 of Weldeyesus *et al.* (2019) is presented. The primal problem (6) has an associated dual problem (7), where  $\mathbf{u} \in \mathbb{R}^n$  and  $\mathbf{X} \in \mathbb{S}_+^n$  (*i.e.*  $\mathbf{X}$  is symmetric and positive semidefinite) are the Lagrange multipliers for the equilibrium equation and the matrix inequality constraints in (6), respectively. Note that, in some literature, for example Wolkowicz, Saigal, and Vandenberghe (2000), the primal formulation (6) is stated as dual and the dual problem formulation (7) as primal.

$$\begin{aligned}
 & \underset{\mathbf{u}, \mathbf{X}}{\text{maximize}} && \mathbf{p}^T \mathbf{u} \\
 & \text{subject to} && -\frac{1}{\sigma^-} (l_i - (\mathbf{K}_i - \lambda \mathbf{M}_i) \bullet \mathbf{X}) \leq (\mathbf{B}^T \mathbf{u})_i, \quad \forall i \\
 & && (\mathbf{B}^T \mathbf{u})_i \leq \frac{1}{\sigma^+} (l_i - (\mathbf{K}_i - \lambda \mathbf{M}_i) \bullet \mathbf{X}), \quad \forall i \\
 & && \mathbf{X} \succeq 0.
 \end{aligned} \tag{7}$$

After solving, the dual violations can be obtained using only the variables  $\mathbf{u}$  and  $\mathbf{X}$  in (7). The process is as follows.

For any variable corresponding to member  $i$  to be dual feasible, formulation (7) implies that the relation

$$-\frac{1}{\sigma^-} \leq \frac{1}{l_i - (\mathbf{K}_i - \lambda \mathbf{M}_i) \bullet \mathbf{X}} (\mathbf{B}^T \mathbf{u})_i \leq \frac{1}{\sigma^+} \tag{8}$$

is satisfied. Now suppose that  $I_0 \subset \{1, \dots, m\}$  is a set of indices of members for which the primal problem (6) and its dual (7) are currently solved. After solving problem (6), and obtaining dual


1412  S. J. SALT ET AL.**Table 2.** Short cantilever example: fully connected ground structure and member adding approaches (target frequency = 425 Hz).

Figure	Model	Nodal divisions	$V$	$V(P/\sigma)$ ( $\times 10^{-5} \text{ m}^3$ )	Time (s)	Speed up	Memory (MB)
3(d)	SDP (full)	$12 \times 6$	7.134	2.038	1,472	...	16,081
5(a)	SDP (mem. add.)	$12 \times 6$	7.134	2.038	8	$\times 183$	5

**Table 3.** Short cantilever example: results from the SDP member adding algorithm.

Figure	Nodal divisions	$V$	$\Delta V^a$ (%)	$V(P/\sigma)$ ( $\times 10^{-5} \text{ m}^3$ )	$f_1$ (Hz)	Time (s)
5(b)	$40 \times 20$	7.064	+0.5	2.018	425	4,915
5(c)	$40 \times 20$	7.129	+1.4	2.037	450	11,655
5(d)	$40 \times 20$	7.597	+8.0	2.171	480	17,671

<sup>a</sup>Percentage change compared with the volume of the reference structure shown in Figure 3(a).

values corresponding to (7), for all members with indices in  $I_0$ , condition (8) can be used for all  $i \in \{1, \dots, m_0\} \setminus I_0$  to generate a set  $I$  of member indices to be added, given by

$$I = \left\{ i \in \{1, \dots, m_0\} \setminus I_0 \mid \frac{1}{l_i - (\mathbf{K}_i - \lambda \mathbf{M}_i) \bullet \mathbf{X}^*} (\sigma^- \varepsilon_i^- + \sigma^+ \varepsilon_i^+) \geq 1 + \beta \right\}, \quad (9)$$

where the virtual strains are  $\varepsilon_i^+ = \max\{(\mathbf{B}^T \mathbf{u}^*)_i, 0\}$  and  $\varepsilon_i^- = \max\{-(\mathbf{B}^T \mathbf{u}^*)_i, 0\}$  with  $\mathbf{u}^*$  and  $\mathbf{X}^*$  being optimal points of the preceding subprogram and  $\beta > 0$  is an allowed tolerance decided by the user. If  $I = \emptyset$  the member adding procedure terminates; otherwise, members with indices in  $I$  are added to the subsequent problem, filtering these using the heuristic techniques described in Weldeyesus and Gondzio (2018) if necessary to avoid problem size growing too rapidly.

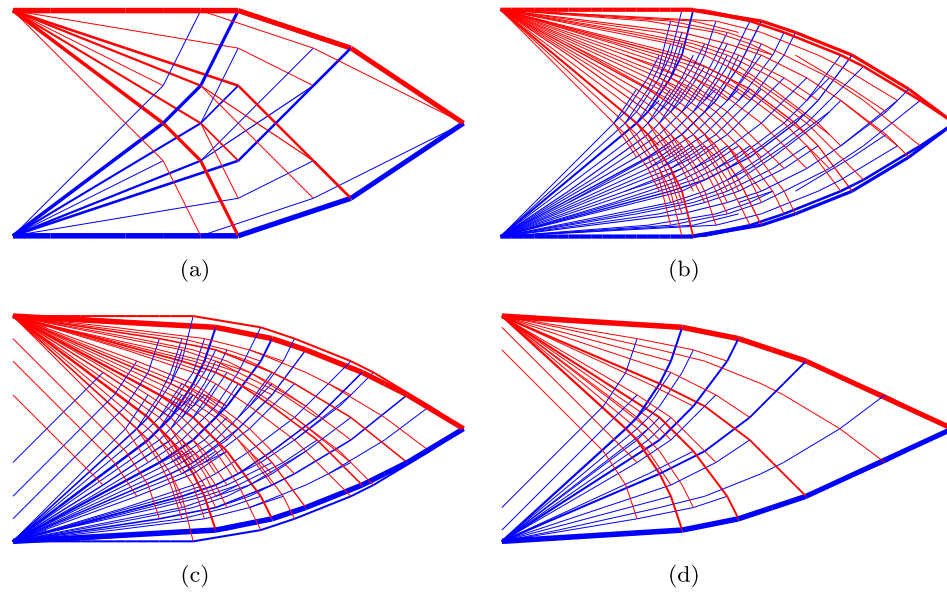
### 3.2. Revisiting the short cantilever and half-wheel examples

In order to establish the gains in efficiency from utilising the new member adding-based SDP algorithm, the problem given in Figure 2 will be revisited, initially replicating the problem in Figure 3(d) to demonstrate the efficiency gains of using the member adding algorithm.

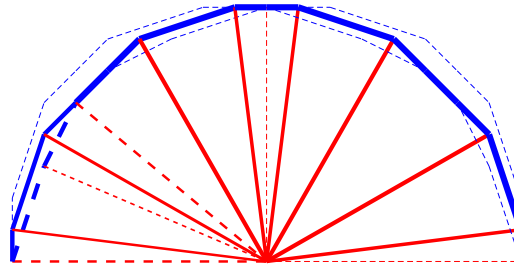
Results for coarse nodal grids are presented in Table 2 and Figure 5(a). It is evident that the optimal volumes are identical irrespective of whether a fully connected ground structure or member adding is employed, and the optimal truss solutions shown in Figures 3(d) and 5(a) are also virtually identical. Most significantly, it is also evident that the proposed member adding algorithm can obtain a solution over two orders of magnitude more quickly than when a fully connected ground structure is used, with the memory requirements reduced by three orders of magnitude. These efficiency improvements mean that problems involving relatively fine nodal grids can now be tackled, which was not possible before. Thus, revisiting the problem shown in Figure 3(a), a new solution obtained via member adding is presented in Figure 5(b), with additional solutions presented for higher minimum target frequencies in Figures 5(c) and 5(d). Corresponding computational details are shown in Table 3. This shows that relatively fine grid problems can be tackled, and that the geometry of the optimal structure changes when higher target frequencies are specified, with the overall volume also increasing.

Now revisiting the half wheel example, by applying the procedure proposed in this contribution a structure that satisfies both equilibrium and frequency constraints can be generated. For a target frequency of 200 Hz, the generated solution is negligibly higher in non-dimensional volume (now  $V = 3.193$ , just 0.05% greater than before); see Figure 6. Significantly, to satisfy the frequency constraint, it is evident that additional stabilizing members have been added—although in this case some of these are very thin, with some radial members below the filter cut-off (in this case area =  $6 \times 10^{-8} \text{ m}^2$ ) omitted.





**Figure 5.** Short cantilever example: results obtained using the SDP member adding method for a range of minimum frequencies. A total of  $12 \times 6$  nodal divisions are used in case (a) and  $40 \times 20$  in cases (b)–(d). (For (a)  $V = 7.134$ ,  $f_1 = 425$  Hz. (b)  $V = 7.064$ ,  $f_1 = 425$  Hz. (c)  $V = 7.129$ ,  $f_1 = 450$  Hz and (d)  $V = 7.597$ ,  $f_1 = 480$  Hz.)


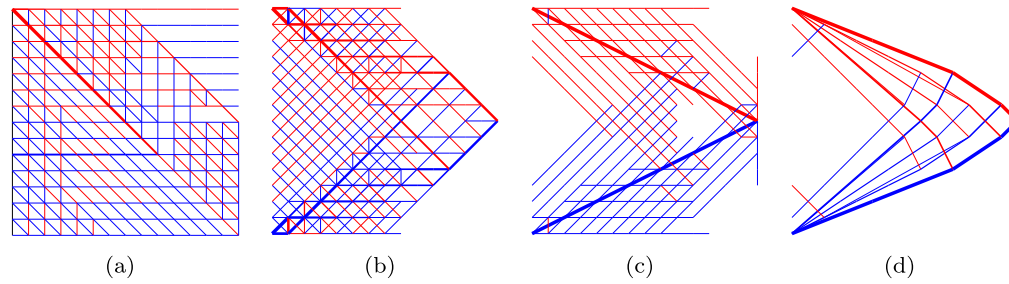


**Figure 6.** Half wheel example: structure obtained using combined equilibrium and frequency constraints for a target frequency of 200 Hz (dashed lines indicate members added to satisfy the frequency constraint, also helping to stabilize the structure).

### 3.3. Influence of initial member arrangement on computation

It has been demonstrated that the inclusion of a member adding step in the optimization reduces the memory burden and enables problems of significant size to be tackled. To understand the performance of the member adding method further, the examples originally considered by Gilbert and Tyas (2003) are used to investigate the influence of the chosen initial nodal connectivity on the solution, the computational time and the required memory footprint. A  $28 \times 28$  nodal division square domain is used; however, in this contribution overlapping connections are omitted as they can lead to instability in the frequency calculations due to multiple members coexisting in the same space. In addition, due to the significant memory requirements of the fully connected ground structure example (circa 400 GB), an additional set of results is obtained using a domain comprising a reduced number of  $14 \times 14$  nodal divisions.

Applying the same physical parameters as in the example shown in Figure 2, the original optimal truss structure from Gilbert and Tyas (2003) was assessed and found to have a first natural frequency of  $f_1 = 945$  Hz; therefore, an initial frequency target of  $f_1 = 950$  Hz was considered appropriate for the starting problem as it is close to the original yet includes an active frequency constraint. The

1414  S. J. SALT ET AL.

**Figure 7.** Influence of initial connectivity in member adding scheme: (a) adjacent nodes connected (right to left upward diagonals in all units), iteration 1; (b) minimally connected ground structure with nearest neighbour nodes connected, iteration 1; (c) minimally connected ground structure plus boundary/loaded nodes connected, iteration 1; (d) final optimized structural form common to all starting points.

target frequency was then increased by 10% to help verify the extent to which the influence of the initial member connectivity is common across a range of target frequencies.

Table 4 shows the four initial ground structures considered, (a)–(d), together with results for the two target frequencies for each of the two nodal division discretizations; note that, to maintain a basis for comparison, all presented volumes are non-dimensional. The resulting volumes for all the cases are within 1% of those provided in the original article, demonstrating that in this case the frequency constraint does not come at a high cost in terms of structural efficiency; however, CPU times are markedly increased. In contrast to the findings in the original article by Gilbert and Tyas (2003), here it is also clear that the most efficient initial ground structure in terms of CPU time comprises a ground structure with the supports directly connected to the load (case (c)); in addition, this leads to a lower number of peak LP variables, indicating a reduced memory burden. Figure 7 shows the outcome of the initial iteration for each of the three initial ground structures investigated when using the member adding scheme for the  $14 \times 14$  nodal division case. It is evident that, although the supports are in each case connected to the load, in the case of (c) this is predominantly achieved through the use of just two diagonal elements, which directly connect the load with the supports.

It should be noted that, when member adding is used, ground structure (a) has the longest associated CPU time, and also the greatest number of LP variables at the end of the optimization process. Ground structure (c) has the shortest associated CPU time, the fewest LP variables, and hence also the lowest memory consumption. However, for the sake of simplicity, initial ground structure (b) will be used for all subsequent examples in this contribution. Finally, it should also be noted that, although the optimized volume obtained when using a fully connected ground structure from the outset, (d), is marginally higher than that obtained in the other three cases, this is probably due to the contribution to the volume of a large number of elements with areas very close to zero.

#### 4. Numerical examples

A wider range of examples are now considered to investigate the efficacy of the presented SDP member adding algorithm further when used to optimize a component, considering simultaneously equilibrium, strength and first natural frequency constraints. The classical Hemp cantilever and MBB beam examples are first considered. A 3D cantilever designed to carry a point load is then considered, with different minimum specified natural frequencies used to show the resulting variation in form and associated volume. Each example begins with a minimum connectivity ground structure.

##### 4.1. Hemp cantilever example

The initial example considered was first studied by Hemp (1973) and consists of a square domain with single point load located at mid-height between two supports, as shown in Figure 8(a).



**Table 4.** Influence of initial member connectivity on efficiency of member adding scheme: (a) adjacent nodes connected (right to left upward diagonals in all cells); (b) minimally connected ground structure, comprising nearest neighbour connectivity; (c) minimally connected ground structure plus connections between boundary and loaded nodes; (d) traditional fully connected ground structure (without overlapping bars).

Grid	$f_1$ (Hz)		(a)	(b)	(c)	(d)
$28 \times 28$	950	Volume, $V$	2.432	2.432	2.432	–
		No. of iterations	9	6	7	–
		Initial no. of bars	2,408	3,192	3,221	–
		Peak no. of bars	36,151	8,000	5,881	–
		Time to 1.001 $V$ (s)	63,875.1	2,209.9	804	–
		CPU time (s)	182,738.9	3,811.6	2,102.8	–
	1,045	Volume, $V$	2.441	2.441	2.441	–
		No. of iterations	12	7	8	–
		Initial no. of bars	2,408	3,192	3,221	–
		Peak no. of bars	33,964	10,710	7,005	–
		Time to 1.001 $V$ (s)	192,161.2	4,054.9	992	–
		CPU time (s)	289,679.8	8,555.2	2,852.6	–
$14 \times 14$	950	Volume, $V$	2.435	2.435	2.435	2.437
		No. of iterations	9	6	6	–
		Initial no. of bars	616	812	827	15,556
		Peak no. of bars	4,239	1,982	1,197	15,556
		Time to 1.001 $V$ (s)	660.2	69.9	29.1	–
		CPU time (s)	1,379.1	116.7	51.2	5,501.3
	1,045	Volume, $V$	2.443	2.443	2.443	2.448
		No. of iterations	9	6	5	–
		Initial no. of bars	616	812	827	15,556
		Peak no. of bars	3,365	1,936	1,265	15,556
		Time to 1.001 $V$ (s)	346	67.4	33.8	–
		CPU time (s)	748.1	134.8	45.5	5,089.7


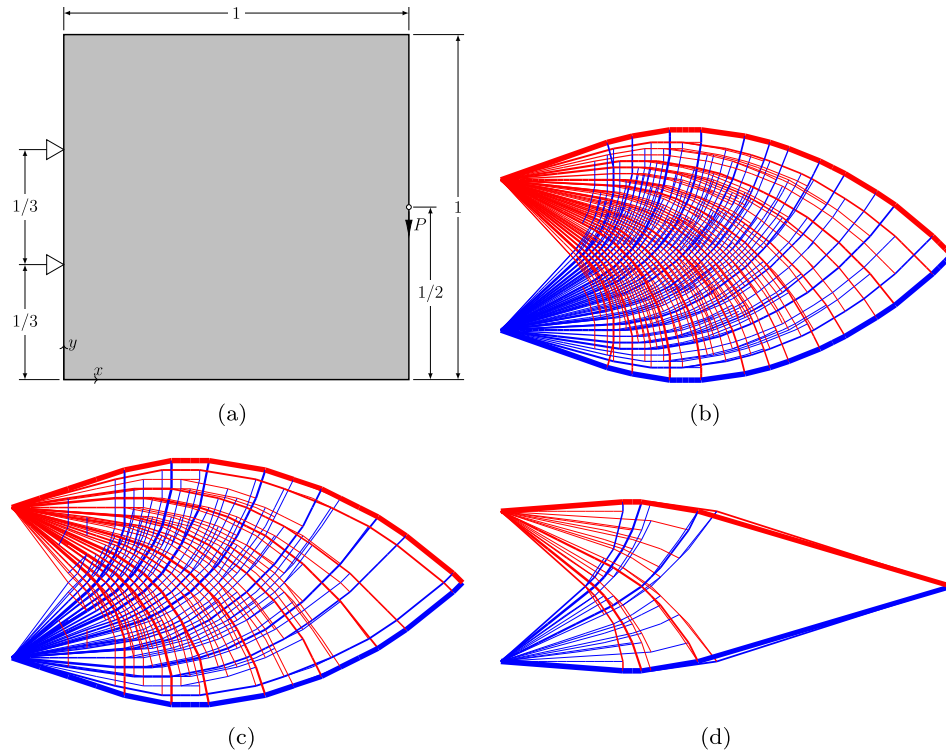
**Table 5.** Hemp cantilever example: results obtained from equilibrium optimization and with inclusion of the frequency constraints.

Figure	Model	Nodal divisions	$V$	$\Delta V$ (%)	$V(P/\sigma)$ ( $\times 10^{-5} \text{m}^3$ )	$f_1$ (Hz)	Time (s)
8(b)	REF	$72 \times 72$	4.332	...	1.238	616	194
...	LP	$48 \times 48$	4.339	+0.01	1.240	623	17
8(c)	SDP	$48 \times 48$	4.340	+0.01	1.240	700	42,676
8(d)	SDP	$48 \times 48$	4.794	+10.6	1.370	1,000	75,004

Hemp determined the non-dimensional analytical volume to be approximately 4.34; later, He and Gilbert (2015) applied more precise methods and geometry rationalization, further reducing the optimum volume to 4.3228. Here, a nodal grid comprising  $72 \times 72$  nodal divisions and the material properties  $P = 1 \times 10^3 \text{ N}$ ,  $E = 210 \times 10^9 \text{ N m}^{-2}$ ,  $\rho = 8050 \text{ kg m}^{-3}$  and the limiting tensile and compressive stresses  $\sigma = 350 \times 10^6 \text{ Pa}$  were used to obtain a reference LP solution with a volume  $V = 4.332$ , within 0.5% of the improved optimum figure. The associated structure is shown in Figure 8(b). The first natural frequency of this reference structure was computed to be  $f_1 = 616 \text{ Hz}$ .

In order to generate solutions in a reasonable timescale for the SDP analyses, the nodal density was reduced to  $48 \times 48$ . An additional LP reference was obtained at this density that has negligible impact on volume but changes the first frequency to 686 Hz. SDP analyses were conducted with target first natural frequencies of  $f_1 = 700$  and 1000 Hz to identify changes in the generated structure. Results of the associated optimization runs are presented in Table 5 and Figures 8(c) and 8(d), respectively.

In the first case, the impact on the resulting generated structure and associated volume is small, with the increase in volume being less than 1% and little difference in overall layout. In the second case,

1416  S. J. SALT ET AL.

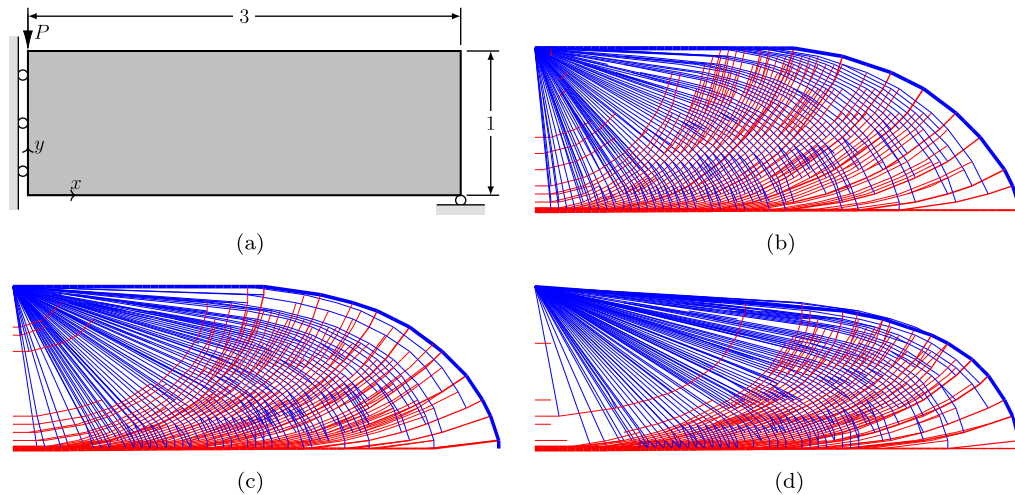
**Figure 8.** Hemp cantilever example: (a) problem definition with dimensions in metres; (b) reference LP solution, obtained with  $72 \times 72$  nodal divisions; (c) SDP member adding solution obtained for a target frequency of 700 Hz; (d) SDP member adding solution obtained for a target frequency of 1000 Hz. Note that both (c) and (d) have  $48 \times 48$  nodal divisions. (For (b)  $V = 4.332$ ,  $f_1 = 616$  Hz. (c)  $V = 4.350$ ,  $f_1 = 700$  Hz and (d)  $V = 4.794$ ,  $f_1 = 1000$  Hz.)

increasing the minimum frequency to  $f_1 = 1000$  Hz can be observed to have a much more significant impact, with the overall structural depth and complexity of the result both reduced.

#### 4.2. MBB beam example

The Messerschmidt–Bölkow–Blohm (MBB) beam is attributed to the German aircraft company of the same name, and can still be found in Airbus passenger aircraft. Though the real-world problem includes a number of design constraints, in the literature a simpler problem is normally considered, involving simple loading and boundary conditions and usually targeting minimum volume or compliance. The exact analytical layout for the MBB structure with stress constraints was derived by Rozvany (1998), with the optimal non-dimensional volume  $V = 13.597$  for a beam length of three. As the beam is symmetrical, only the right half is shown in Figure 9(a). An optimization was carried out with nodes directly along the symmetry plane free to move vertically whilst the bottom right corner was fixed in the vertical direction and free to move horizontally. The example assumes aerospace grade aluminium is used with  $P = 1 \times 10^3$  N,  $\sigma = 90 \times 10^6$  Pa,  $E = 68.9 \times 10^9$  N m $^{-2}$  and  $\rho = 2770$  kg m $^{-3}$ .

An initial LP optimization was carried out to obtain a reference volume and frequency for the structure, using  $60 \times 20$  nodal divisions to provide a balance between accuracy and computational efficiency (Figure 9(b)). SDP solutions were then sought for two minimum target frequencies; the solutions obtained (Table 6 and Figures 9(c) and 9(d)) demonstrate that the introduction of a frequency constraint has enabled minimum volume structures satisfying a given minimum frequency to be obtained, with very little impact on overall volume. However, it is evident that the time required



**Figure 9.** MBB beam example: (a) problem definition with dimensions in metres; (b) reference solution obtained for this example with the determined first natural frequency; (c) SDP member adding solution obtained for a target frequency of 400 Hz; (d) a target of 425 Hz. (For (b)  $V = 14.136$ ,  $f_1 = 374$  Hz. (c)  $V = 14.237$ ,  $f_1 = 400$  Hz and (d)  $V = 14.631$ ,  $f_1 = 425$  Hz.)

**Table 6.** MBB beam example: SDP member adding algorithm results.


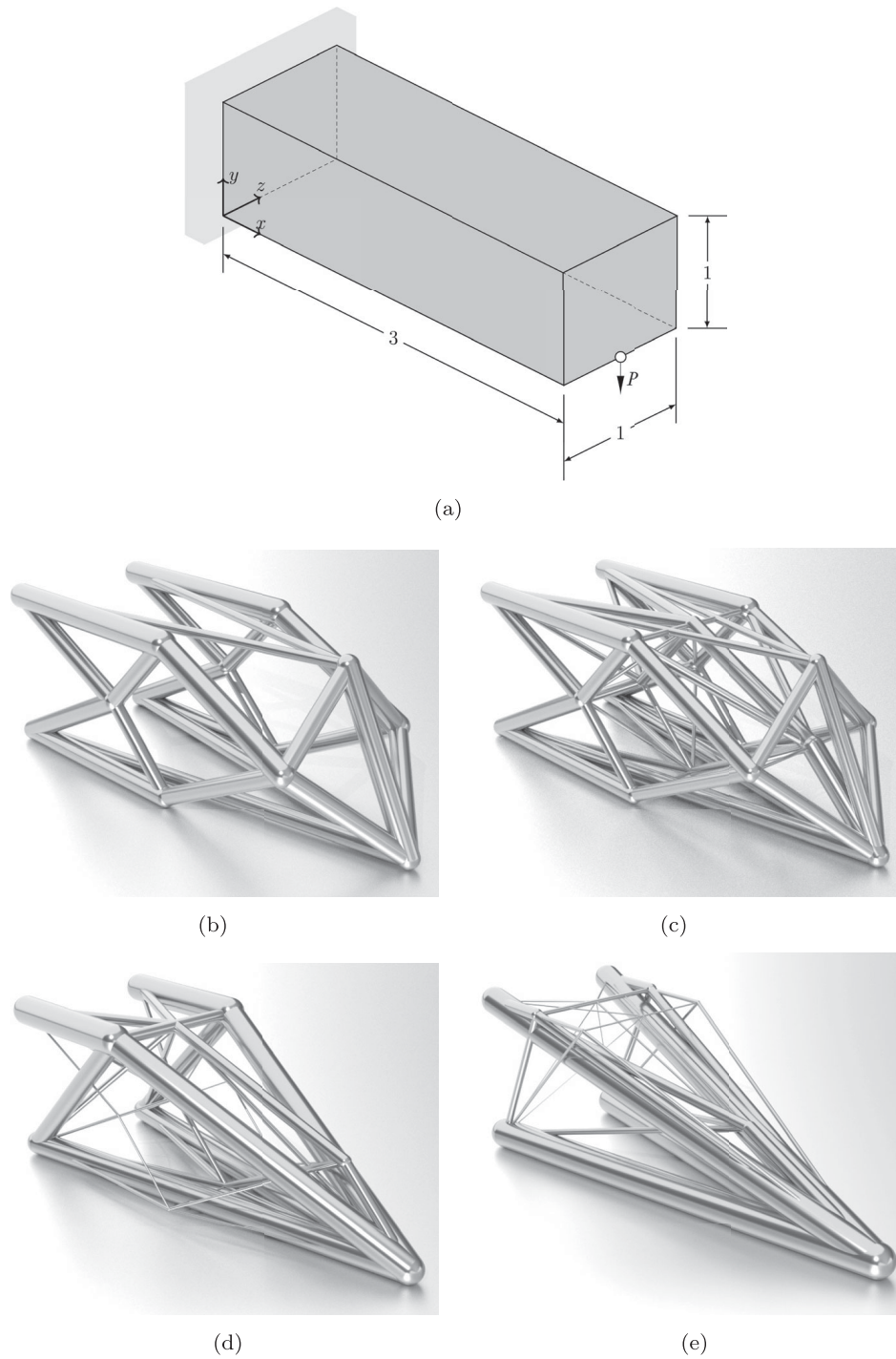
Figure	Model	Nodal divisions	$V$	$\Delta V$ (%)	$V(P/\sigma)$ ( $\times 10^{-4} \text{m}^3$ )	$f_1$ (Hz)	Time (s)
9(b)	LP	$60 \times 20$	14.136	...	1.571	374	8
9(c)	SDP	$60 \times 20$	14.238	+0.72	1.582	400	31,781
9(d)	SDP	$60 \times 20$	14.631	+3.5	1.626	425	46,317

to complete a frequency optimization is clearly considerably longer than that required for a basic LP optimization.

### 4.3. 3D cantilever example

The third example is a simple 3D cantilever beam, as shown in Figure 10(a). To improve the clarity of the results and to minimize the additional computational burden associated with solving 3D problems, the number of nodal divisions has been reduced to  $6 \times 2 \times 2$  to ensure solutions are obtained in a manageable time-frame. The properties for this example are as follows:  $P = 1 \times 10^3$  N;  $E = 210 \times 10^9$  N m $^{-2}$ ;  $\rho = 8050$  kg m $^{-3}$ ; and the maximum tensile and compressive stresses are  $\sigma = 350 \times 10^6$  Pa. Various target first natural frequencies are used to demonstrate the change in structural form that results from including a frequency constraint.

Full results for this example are shown in Table 7. Figure 10(b) shows the layout of the optimal structure based solely upon equilibrium and strength considerations, with the natural frequency of the resulting structure being found to be 57 Hz. When a frequency constraint  $f_1 = 100$  Hz is introduced (Figure 10(c)) the structure begins to change, with new members added to the structure. Similar to the 2D examples, these additional elements brace the structure, adding stiffness and therefore increasing the frequency; however, the use of member adding has allowed this to happen in a short amount of time and with limited impact on the overall volume of the structure. As the target frequency is increased further to 150 and 200 Hz as shown in Figures 10(d) and 10(e), respectively, a more dramatic change begins to take place, with the members that are primarily taking the load and providing structural stiffness becoming longer and growing in cross section.

1418  S. J. SALT ET AL.

**Figure 10.** 3D cantilever example: (a) problem definition with dimensions in metres; (b) LP solution (no frequency constraint); (c) SDP member adding solution for a target frequency of 100 Hz; (d) target of 150 Hz; (e) target of 200 Hz. All cases employ  $6 \times 2 \times 2$  nodal divisions. (For (b)  $V = 30.676$ ,  $f_1 = 57$  Hz. (c)  $V = 30.883$ ,  $f_1 = 100$  Hz. (d)  $V = 33.233$ ,  $f_1 = 150$  Hz and (e)  $V = 38.111$ ,  $f_1 = 200$  Hz.)

**Table 7.** 3D cantilever example: SDP member adding algorithm results.

Figure	Model	Cons	$V$	$\Delta V$ (%)	$V(P/\sigma)$ ( $\times 10^{-5} m^3$ )	$f_1$ (Hz)	Time (s)
10(b)	LP	474	30.676	...	8.765	57	5.8
10(c)	SDP	566	30.883	+0.6	8.824	100	9.9
10(d)	SDP	633	33.233	+8.3	9.495	150	12.6
10(e)	SDP	582	38.111	+24.2	10.889	200	13.3

## 5. Conclusions

Numerical layout optimization provides an efficient means of generating optimal truss structures for a given set of design requirements. However, traditional linear programming-based formulations are limited, and cannot for example accommodate frequency constraints. In this contribution, extended semi-definite programming-based formulations are considered that allow the minimum first natural frequency of a structure to be specified. The main conclusions are as follows.

- The use of a two phase approach, in which the traditional LP layout optimization formulation is used in the first phase and an SDP size optimization is used in the second phase, provides a computationally efficient means of generating solutions satisfying a specified frequency constraint. However, the solutions obtained are likely to be sub-optimal, with the resulting structures having higher than necessary volume.
- Alternatively, a constraint on frequency can be introduced in the optimization directly, furnishing layouts that satisfy both structural performance and first natural frequency requirements. However, when using a fully connected ground structure and a standard SDP solver, the computational cost and memory requirements have been found to be high, severely limiting the scale of problem that can be tackled.
- The use of a bespoke solver and an adaptive member adding solution strategy, which involves starting with a sparsely connected ground structure and only adding members as required until the optimal solution is found, allows solutions to be obtained in a much shorter time-frame (183 times quicker in the case of one of the examples considered), and with much lower memory consumption. This approach has been successfully applied to a range of 2D and 3D problems in this article.

In future studies, the influence of joints on vibration characteristics will be considered in more detail, with for example differences in optimal layout and volume being evaluated when rigid-joints as opposed to pin-joints are assumed. In addition, consideration will be given to limiting the number and arrangement of members within a final design, to ensure the resulting component is readily manufacturable.

## Acknowledgments

The assistance of Dr Linwei He in producing the graphics for Figures 10(b)–10(e) is gratefully acknowledged.


## Data availability statement

Details of the formulation employed are provided in the article and the supplied electronic supplementary information includes details of all inputs and the results obtained for the Hemp cantilever and MBB beam examples described. Link: <https://doi.org/10.15131/shef.data.14837913>

## Disclosure statement

No potential conflict of interest was reported by the author(s).






1420  S. J. SALT ET AL.

## Funding

The financial support provided by Rolls-Royce plc is gratefully acknowledged. The work of M. Gilbert, A.G. Weldeyesus and J. Gondzio was financially supported by EPSRC [grant references EP/N023471/1 and EP/N019652/1].

## ORCID IDs

S. J. Salt  <https://orcid.org/0000-0002-5724-1628>  
 A. G. Weldeyesus  <http://orcid.org/0000-0001-8696-8255>  
 M. Gilbert  <https://orcid.org/0000-0003-4633-2839>  
 J. Gondzio  <https://orcid.org/0000-0002-6270-4666>

## References

- Achtziger, W. 1999. "Local Stability of Trusses in the Context of Topology Optimization—Part I: Exact Modelling." *Structural Optimization* 17 (4): 235–246.
- Achtziger, W., and M. Kočvara. 2007. "On the Maximization of the Fundamental Eigenvalue in Topology Optimization." *Structural and Multidisciplinary Optimization* 34 (3): 181–195.
- Aroztegui, M., J. C. A. Costa Jr, A. Canelas, and J. Herskovits. 2011. "Maximising the Fundamental Frequency of Truss Structures." In *Proceedings of the 21st International Congress of Mechanical Engineering (COBEM 2011)*. Rio de Janeiro: Associação Brasileira de Engenharia e Ciências Mecânicas (ABCM).
- Azad, S. K., M. Bybordi, S. K. Azad, and F. Jawad. 2018. "Simultaneous Size and Geometry Optimization of Steel Trusses Under Dynamic Excitations." *Structural and Multidisciplinary Optimization* 58 (6): 2545–2563.
- Ben-Tal, A., and A. Nemirovski. 1997. "Robust Truss Topology Design Via Semidefinite Programming." *SIAM Journal on Optimization* 7 (4): 991–1016.
- Bendsøe, M. P., and O. Sigmund. 2003. *Topology Optimization: Theory, Methods and Applications*. Engineering Online Library. Berlin: Springer-Verlag. doi:10.1007/978-3-662-05086-6.
- Cooper, D. A. 1989. "Report on the Accident to Boeing 737-400 G-OBME Near Kegworth Leicestershire on 8 January 1989." Technical Report. London, UK: Department of Transport. Air Accidents Investigation Branch; 1990. <http://link.rbk.gov.uk/portal/Report-on-the-accident-to-Boeing-737-400-G-OBME/9Yld5TQuZ7o/>.
- Desrosiers, J., and M. E. Lübbecke. 2005. *A Primer in Column Generation*, 1–32. Boston, MA: Springer US.
- Dorn, W. S., R. E. Gomory, and H. J. Greenberg. 1964. "Automatic Design of Optimal Structures." *Journal de Mechanique* 3: 25–52.
- Du, J., and N. Olhoff. 2007. "Topological Design of Freely Vibrating Continuum Structures for Maximum Values of Simple and Multiple Eigenfrequencies and Frequency Gaps." *Structural and Multidisciplinary Optimization* 34 (2): 91–110.
- Fiala, J., M. Kočvara, and M. Stingl. 2013. "PENLAB: A MATLAB Solver for Nonlinear Semidefinite Optimization." ArXiv e-print, <https://arxiv.org/pdf/1311.5240.pdf>.
- Fox, R. L., and M. P. Kapoor. 1970. "Structural Optimization in the Dynamics Response Regime—A Computational Approach." *AIAA Journal* 8 (10): 1798–1804.
- Fujisawa, K., M. Fukuda, M. Kojima, and K. Nakata. 2000. *Numerical Evaluation of SDPA (Semidefinite Programming Algorithm)*, 267–301. Boston, MA: Springer US.
- Gilbert, M., and A. Tyas. 2003. "Layout Optimization of Large-Scale Pin-Jointed Frames." *Engineering Computations* 20 (8): 1044–1064.
- Giniūnaitė, R. 2015. "Application of Semidefinite Programming to Truss Design Optimization." *Science—Future of Lithuania* 7 (3): 280–284.
- Gondzio, J., P. González-Brevis, and P. Munari. 2013. "New Developments in the Primal–Dual Column Generation Technique." *European Journal of Operational Research* 224: 41–51.
- Gondzio, J., and R. Sarkissian. 1996. *Column Generation with the Primal–Dual Method*. Technical Report 1996.4. CH-1211. Geneva, Switzerland: Logilab, University of Geneva.
- Grandhi, R. V., and V. B. Venkayya. 1988. "Structural Optimization with Frequency Constraints." *AIAA Journal* 26 (7): 858–866.
- Grant, M., and S. Boyd. 2014. "CVX: Matlab Software for Disciplined Convex Programming, Version 2.1." <http://cvxr.com/cvx>.
- He, L., and M. Gilbert. 2015. "Rationalization of Trusses Generated Via Layout Optimization." *Structural and Multidisciplinary Optimization* 52 (4): 677–694.
- He, L., M. Gilbert, and X. Song. 2019. "A Python Script for Adaptive Layout Optimization of Trusses." *Structural and Multidisciplinary Optimization* 60 (2): 835–847.
- Hemp, W. S. 1973. *Optimum Structures*. Oxford, UK: Clarendon Press.

- Kanno, Y. 2018. "Robust Truss Topology Optimization Via Semidefinite Programming with Complementarity Constraints: A Difference-of-Convex Programming Approach." *Computational Optimization and Applications* 71 (2): 403–433.
- Kaveh, A., and M. Ilchi Ghazaan. 2016. "Optimal Design of Dome Truss Structures with Dynamic Frequency Constraints." *Structural and Multidisciplinary Optimization* 53 (3): 605–621.
- Khot, N. S. 1985. "Optimization of Structures with Multiple Frequency Constraints." *Computers & Structures* 20 (5): 869–876.
- Michell, A. G. M. 1904. "The Limits of Economy of Material in Frame-Structures." *Philosophical Magazine Series* 6, 8 (47): 589–597. doi:10.1080/14786440409463229.
- MOSEK ApS. 2017. *MOSEK MATLAB Documentation Release 8.1.0.24*.
- Parkes, E. W. 1975. "Joints in Optimum Frameworks." *International Journal of Solids and Structures* 11 (9): 1017–1022.
- Pritchard, T. J., M. Gilbert, and A. Tyas. 2005. "Plastic Layout Optimization of Large-Scale Frameworks Subject to Multiple Load Cases, Member Self-Weight and with Joint Length Penalties." In *Proceedings of the 6th World Congress on Structural and Multidisciplinary Optimization*, Rio de Janeiro, 1–10. <https://www.researchgate.net/publication/237133804>.
- Rozvany, G. I. N. 1998. "Exact Analytical Solutions for Some Popular Benchmark Problems in Topology Optimization." *Structural Optimization* 15 (1): 42–48.
- Smith, C. J., M. Gilbert, I. Todd, and F. Derguti. 2016. "Application of Layout Optimization to the Design of Additively Manufactured Metallic Components." *Structural and Multidisciplinary Optimization* 54 (5): 1297–1313.
- Sokoł, T. 2014. "Multi-Load Truss Topology Optimization Using the Adaptive Ground Structure Approach." In *Recent Advances in Computational Mechanics*, edited by T. Łodygowski, J. Rakowski, and P. Litewka, 9–16. Boca Raton, FL: CRC Press.
- Sokoł, T., and G. I. N. Rozvany. 2013. "On the Adaptive Ground Structure Approach for Multi-Load Truss Topology Optimization." In *Proceedings of the 10th World Congress on Structural and Multidisciplinary Optimization*, Florida, 1–10. <https://mae.ufl.edu/mdo/Papers/5428.pdf>.
- Taheri, Seyed Heja Seyed, and Shahin Jalili. 2016. "Enhanced Biogeography-Based Optimization: A New Method for Size and Shape Optimization of Truss Structures with Natural Frequency Constraints." *Latin American Journal of Solids and Structures* 13: 1406–1430.
- Tejani, Ghanshyam G., Vimal J. Savsani, Vivek K. Patel, and Seyedali Mirjalili. 2018. "Truss Optimization with Natural Frequency Bounds Using Improved Symbiotic Organisms Search." *Knowledge-Based Systems* 143: 162–178.
- Thore, C.-J. 2018. "FMINS DP—A Code for Solving Non-Linear Optimization Problems with Matrix Inequality Constraints." <https://www.mathworks.com/matlabcentral/fileexchange/43643-fminsdp>.
- Tyburec, M., and J. Zeman. 2017. "Comparison of Semidefinite Solvers for Topology Optimization of Cantilever Trusses Subject to Fundamental Eigenvalue Constraint." *Advanced Materials Research* 1144: 172–177.
- Weldeyesus, A. G., and J. Gondzio. 2018. "A Specialized Primal–Dual Interior Point Method for the Plastic Truss Layout Optimization." *Computational Optimization and Applications* 71 (3): 613–640.
- Weldeyesus, A. G., J. Gondzio, L. He, M. Gilbert, P. Shepherd, and A. Tyas. 2019. "Adaptive Solution of Truss Layout Optimization Problems with Global Stability Constraints." *Structural and Multidisciplinary Optimization* 60 (5): 2093–2111.
- Wolkowicz, H., R. Saigal, and L. Vandenberghe. 2000. *Handbook of Semidefinite Programming. Theory, Algorithms, and Applications*. Dordrecht, The Netherlands: Kluwer Academic.

# References

- N. Aage, M. Nobel-Jørgensen, C.S. Andreasen, and O. Sigmund. Interactive topology optimization on hand-held devices. *Structural and Multidisciplinary Optimization*, 47(1):1–6, 2013.
- W. Aichtziger. Local stability of trusses in the context of topology optimization part I: Exact modelling. *Structural optimization*, 17(4):235–246, 1999.
- W. Aichtziger and M. Kočvara. On the maximization of the fundamental eigenvalue in topology optimization. *Structural and Multidisciplinary Optimization*, 34(3):181–195, 2007. ISSN 1615-1488.
- Additive Manufacturing Group. Recommended guidance for certification of am components. Technical report, Aerospace Industry Group, 2020.
- G. Allaire and B. Bogosel. Optimizing supports for additive manufacturing. *Structural and Multidisciplinary Optimization*, 58(6):2493–2515, 2018.
- J. Allen. An investigation into the comparative costs of additive manufacture vs. machine from solid for aero engine parts. In *Cost Effective Manufacture via Net-Shape Processing*, pages 17–1 – 17–10. Meeting Proceedings RTO-MP-AVT-139, Paper 17. Neuilly-sur-Seine, France, 2006.
- Altair. HyperWorks Desktop, version 2022, 2022. URL <https://2022.help.altair.com/2022/hwdesktop/hwx/index.htm>.
- A. Aremu, I. Ashcroft, R.J.M. Hague, R. Wildman, and C. Tuck. Suitability of SIMP and BESO topology optimization algorithms for additive manufacture. *21st Annual International Solid Freeform Fabrication Symposium (SFF)*, pages 679–692, 2010.
- M. Aroztegui, J.C.A. Costa Junior, A. Canelas, and J. Herskovits. Maximising the fundamental frequency of truss structures. In *21st International Congress of Mechanical Engineering, Natal, RN, Brazil*. ABCM, October 2011.



- S.K. Azad, M. Bybordi, S.K. Azad, and F. Jawad. Simultaneous size and geometry optimization of steel trusses under dynamic excitations. *Structural and Multidisciplinary Optimization*, 58(6):2545–2563, 2018.
- A. Ben-Tal and A. Nemirovski. Robust truss topology design via semidefinite programming. *SIAM Journal on Optimization*, 7(4):991–1016, 1997.
- M.P. Bendsøe. Optimal shape design as a material distribution problem. *Structural Optimization*, 1(4):193–202, 1989. ISSN 0934-4373.
- M.P. Bendsøe and R.B. Haber. The Michell layout problem as a low volume fraction limit of the perforated plate topology optimization problem: An asymptotic study. *Structural optimization*, 6(4):263–267, 1993.
- M.P. Bendsøe and O. Sigmund. *Topology Optimization: Theory, Methods and Applications*. Engineering online library. Springer, 2003. ISBN 9783540429920.
- B. Blakey-Milner, P. Gradl, G. Snedden, M. Brooks, J. Pitot, E. Lopez, M. Leary, F. Berto, and A. du Plessis. Metal additive manufacturing in aerospace: A review. *Materials & Design*, 209:110008, 2021. ISSN 0264-1275.
- S. Boyd and L. Vandenberghe. *Convex Optimization*. Cambridge University Press, New York, NY, USA, 2004. ISBN 0521833787.
- D. Brackett, I. Ashcroft, and R. Hague. Topology optimization for additive manufacturing. In *22nd Annual International Solid Freeform Fabrication Symposium*, 2011.
- A. Cervantes Herrera. Optimisation driven design and additive manufacturing applied for ESA Sentinel-1 antenna. In *Altair Technology Conference*, 2015.
- D.Nha Chu, Y.M. Xie, A. Hira, and G.P. Steven. Evolutionary structural optimization for problems with stiffness constraints. *Finite Elements in Analysis and Design*, 21(4):239 – 251, 1996. ISSN 0168-874X.
- D. A. Cooper. Report on the accident to Boeing 737-400 G-OBME near Kegworth Leicestershire on 8 January 1989. Technical report, Air Accidents Investigation Branch, 1989.
- G.B. Dantzig. Programming in a linear structure. *Econometrica*, 17:73, 1949. ISSN 0012-9682.
- J. Desrosiers and M.E. Lübbecke. *A Primer in Column Generation*, pages 1–32. Springer US, Boston, MA, 2005.

- G.E. Dieter. *Engineering design : a materials and processing approach*. McGraw-Hill series in mechanical engineering. McGraw-Hill, Boston, 3rd ed. edition, 2000. ISBN 0073661368.
- W.S. Dorn, R.E. Gomory, and H.J. Greenberg. Automatic design of optimal structures. *Journal de Mechanique*, 3(25-52), 1964.
- J. Du and N. Olhoff. Topological design of freely vibrating continuum structures for maximum values of simple and multiple eigenfrequencies and frequency gaps. *Structural and multidisciplinary optimization*, 34(2):91–110, 2007. ISSN 1615-1488.
- EOS GmbH. Certified for universal success: Additive manufacturing of satellite components. URL [https://www.eos.info/01\\_parts-and-applications/case\\_studies\\_applications\\_parts/\\_case\\_studies\\_pdf/en\\_cases/cs\\_m\\_aerospace\\_ruag\\_en.pdf](https://www.eos.info/01_parts-and-applications/case_studies_applications_parts/_case_studies_pdf/en_cases/cs_m_aerospace_ruag_en.pdf).
- H.E. Fairclough, L. He, T. Pritchard, and M. Gilbert. Layopt: an educational web-app for truss layout optimization. *Structural and Multidisciplinary Optimization*, 64(4): 2805–2823, 2021.
- Anthony V. Fiacco. A general regularized sequential unconstrained minimization technique. *SIAM Journal on Applied Mathematics*, 17(6):1239–1245, 1969.
- J. Fiala, M. Kočvara, and M. Stingl. PENLAB: a MATLAB solver for nonlinear semidefinite optimization. *Mathematical Programming*, 11 2013.
- R. L. Fox and M. P. Kapoor. Structural optimization in the dynamics response regime - a computational approach. *AIAA Journal*, 8(10):1798–1804, 2017/09/21 1970.
- D. Fujii and N. Kikuchi. Improvement of numerical instabilities in topology optimization using the SLP method. *Structural and Multidisciplinary Optimization*, 19(2):113–121, 2000. ISSN 1615-147X.
- K. Fujisawa, M. Fukuda, M. Kojima, and K. Nakata. *Numerical Evaluation of SDPA (Semidefinite Programming Algorithm)*, pages 267–301. Springer US, Boston, MA, 2000.
- M. Gilbert and A. Tyas. Layout optimization of large-scale pin-jointed frames. *Engineering Computations*, 20(8):1044–1064, 2003.
- R. Giniūnaitė. Application of semidefinite programming to truss design optimization. *Science – Future of Lithuania*, 7(3):280–84, 2015.
- Global Aerospace Materials Industry. A market report by the global industry analysts (2021) id: 5797793. Technical report, 2022.

- J. Gondzio and R. Sarkissian. Column generation with the primal-dual method. Technical Report 1996.4, Logilab, University of Geneva, CH-1211 Geneva, Switzerland, June 1996.
- J. Gondzio, P. González-Brevis, and P. Munari. New developments in the primal-dual column generation technique. *European Journal of Operational Research*, 224:41–51, 2013.
- R. V. Grandhi and V. B. Venkayya. Structural optimization with frequency constraints. *AIAA Journal*, 26(7):858–866, 2017/08/11 1988.
- M. Grant and S. Boyd. CVX: MATLAB software for disciplined convex programming, version 2.1. <http://cvxr.com/cvx>, March 2014.
- W. Gu. On challenges and solutions of topology optimization for aerospace structural design. In *10th World Congress on Structural and Multidisciplinary Optimization*, 2013.
- A. Gupta, C.J. Bennett, and W. Sun. High cycle fatigue performance evaluation of a laser powder bed fusion manufactured Ti-6Al-4V bracket for aero-engine applications. *Engineering Failure Analysis*, 140:106494, 2022. ISSN 1350-6307.
- L. He and M. Gilbert. Rationalization of trusses generated via layout optimization. *Structural and Multidisciplinary Optimization*, pages 1–18, 2015. ISSN 1615-147X.
- L. He, M. Gilbert, T. Johnson, and T. Pritchard. Conceptual design of am components using layout and geometry optimization. *Computers and Mathematics with Applications*, 2019a.
- L. He, M. Gilbert, and X. Song. A python script for adaptive layout optimization of trusses. *Structural and Multidisciplinary Optimization*, 60(2):835–847, Aug 2019b. ISSN 1615-1488.
- W.S. Hemp. *Optimum Structures*. Clarendon Press, Oxford, 1973.
- Magnus R. Hestenes. Multiplier and gradient methods. *Journal of Optimization Theory and Applications*, 4(5):303–320, 1969.
- J. Hiemenz. Additive manufacturing trends in aerospace. Technical report, Stratasys Inc., 2020.
- J.H. Holland. *Adaptation in natural and artificial systems: An introductory analysis with applications to biology, control, and artificial intelligence*. MIT Press, 1992.
- R. Horst and H. Tuy. *Global optimization: Deterministic approaches*. Springer Science & Business Media, 1995.

- X. Huang and Y.M. Xie. *Evolutionary Topology Optimization of Continuum Structures*, chapter 4, pages 39–50. John Wiley & Sons, 2010.
- Y. Kanno. Robust truss topology optimization via semidefinite programming with complementarity constraints: a difference-of-convex programming approach. *Computational Optimization and Applications*, 71(2):403–433, 2018.
- Y. Kanno and M. Ohsaki. Eigenvalue optimization of structures via polynomial semidefinite programming. Technical report, Department of Mathematical Informatics, University of Tokyo, 2007.
- Hüseyin Karabiyik, Osman Eroglu, Muhammed Metin Eskimez, Berk Oncu Oncul, Muhammet Tayyip Yilmaz, İstemihan Gökdağ, and Recep M. Gorguluarslan. A Topology Optimization Methodology With Vibration Constraint for an Aerospace Bracket Design. Volume 3: Advanced Materials: Design, Processing, Characterization and Applications; Advances in Aerospace Technology, 10 2022.
- N. Karmarkar. A new polynomial-time algorithm for linear programming. *Combinatorica (Budapest. 1981)*, 4(4):373–395, 1984. ISSN 0209-9683.
- A. Kaveh and M. Ilchi Ghazaan. Optimal design of dome truss structures with dynamic frequency constraints. *Structural and Multidisciplinary Optimization*, 53(3):605–621, 2016.
- A.J. Keane and P.B. Nair. *Computational Approaches for Aerospace Design: The Pursuit of Excellence*. John Wiley & Sons, Ltd, 2005.
- J. Kennedy and R. Eberhart. Particle swarm optimization. In *Proceedings of ICNN’95 - International Conference on Neural Networks*, volume 4, pages 1942–1948 vol.4, 1995.
- N.S. Khot. Optimization of structures with multiple frequency constraints. *Computers & Structures*, 20(5):869 – 876, 1985. ISSN 0045-7949.
- A. Kirchheim, H-J Dennig, and L. Zumofen. Why education and training in the field of additive manufacturing is a necessity. pages 329–336, 01 2018. ISBN 978-3-319-66865-9.
- S. D. Larsen, O. Sigmund, and J. P. Groen. Optimal truss and frame design from projected homogenization-based topology optimization. *Structural and Multidisciplinary Optimization*, 57(4):1461–1474, 2018.
- M. Leary, L. Merli, F. Torti, M. Mazur, and M. Brandt. Optimal topology for additive manufacture: A method for enabling additive manufacture of support-free optimal structures. *Materials & Design*, 63:678 – 690, 2014. ISSN 0261-3069.

- LimitState3D. LimitState:FORM, version 3.5.0 [8043], 2019. URL <https://limitstate3d.com/limitstateform>.
- K. Liu and A. Tovar. An efficient 3D topology optimization code written in MATLAB. *Structural and Multidisciplinary Optimization*, 50(6):1175–1196, 2014. ISSN 1615-147X.
- J.C. Maxwell. On reciprocal figures and diagrams of forces. *The London, Edinburgh, and Dublin Philosophical Magazine and Journal of Science*, 27(182):250–261, 1864.
- A.G.M. Michell. The limits of economy of material in frame-structures. *Philosophical Magazine Series 6*, 8(47):589–597, 1904.
- MIL-STD-1530D. MIL-STD-1530D: Department of defense standard practice: Aircraft structural integrity program (ASIP), October 2016.
- G. E. Moore. Cramming more components onto integrated circuits. *Electronics*, 38(8):114–117, 1965. ISSN 0018-9219.
- MOSEK ApS. *MOSEK MATLAB Documentation Release 8.1.0.24*, 2017.
- MOSEK ApS. *MOSEK MATLAB Documentation Release 10.0*, 2022.
- M.P. Nielsen and L.C. Hoang. *Limit Analysis and Concrete Plasticity*. CRC Press, 2011.
- J. Nocedal and S.J. Wright. *Numerical Optimization*. Springer, New York, NY, USA, 2nd edition, 2006.
- E.W. Parkes. Joints in optimum frameworks. *International Journal of Solids and Structures*, 11(9):1017 – 1022, 1975. ISSN 0020-7683.
- C.E. Pearson. Structural design by high speed computing machines. In *Conference on Electronic Computation of the A.S.C.E.*, 1958.
- T. Pritchard, M. Gilbert, and A. Tyas. Plastic layout optimization of large-scale frameworks subject to multiple load cases, member self-weight and with joint length penalties. In *6th World Congresses of Structural and Multidisciplinary Optimization*, pages 1–10, 2005.
- O.M. Querin, G.P. Steven, and Y.M. Xie. Evolutionary structural optimisation (ESO) using a bidirectional algorithm. *Engineering Computations*, 15(8):1031–1048, 1998.
- SN. Reddy K, I. Ferguson, M. Frecker, TW. Simpson, and C.J. Dickman. Topology Optimization Software for Additive Manufacturing: A Review of Current Capabilities and a Real-World Example. volume 2A: 42nd Design Automation Conference of *International Design Engineering Technical Conferences and Computers and Information in Engineering*, 2016.

- Royal Aeronautical Society. Greener by design annual report 2021-2022, 2022.
- G.I.N. Rozvany. Exact analytical solutions for some popular benchmark problems in topology optimization. *Structural Optimization*, 15(1):42–48, 1998. ISSN 0934-4373.
- G.I.N. Rozvany. A critical review of established methods of structural topology optimization. *Structural and Multidisciplinary Optimization*, 37(3):217–237, 2009. ISSN 1615-147X.
- G.I.N. Rozvany and T. Lewiński. *Topology Optimization in Structural and Continuum Mechanics*. Springer, 2014.
- S. J. Salt, A. G. Weldeyesus, M. Gilbert, and J. Gondzio. Layout optimization of pin-jointed truss structures with minimum frequency constraints. *Engineering Optimization*, 55(8):1403–1421, 2022.
- S. Satya Hanush and M. Manjaiah. Topology optimization of aerospace part to enhance the performance by additive manufacturing process. *Materials Today: Proceedings*, 62:7373–7378, 2022. ISSN 2214-7853.
- G Shi, C Guan, D Quan, D Wu, L Tang, and T Gao. An aerospace bracket designed by thermo-elastic topology optimization and manufactured by additive manufacturing. *Chinese J. Aeronaut.*, 33:1252–1259, 2020.
- Siemens PLM Software. NX, version 1973, 2020. URL <https://docs.sw.siemens.com/en-US/documents/209349590/PL20200507135732916>.
- O. Sigmund. A 99 line topology optimization code written in MATLAB. *Structural and Multidisciplinary Optimization*, 21(2):120–127, 2001. ISSN 1615-147X.
- O. Sigmund and J. Petersson. Numerical instabilities in topology optimization: A survey on procedures dealing with checkerboards, mesh-dependencies and local minima. *Structural Optimization*, 16(1):68–75, 1998. ISSN 0934-4373.
- S. Singamneni, Y. Lv, A. Hewitt, R. Chalk, W. Thomas, and D. Jordison. Additive manufacturing for the aircraft industry: A review. 8:1, 02 2019.
- C.J. Smith, M. Gilbert, I. Todd, and F. Derguti. Application of layout optimization to the design of additively manufactured metallic components. *Structural and Multidisciplinary Optimization*, 54:1297–1313, 2016. ISSN 1615-1488.
- T. Sokół. Multi-load truss topology optimization using the adaptive ground structure approach. In T. Łodygowski, J. Rakowski, and P. Litewka, editors, *Recent Advances in Computational Mechanics*, pages 9–16. CRC Press, 2014.

- T. Sokół and G. I. N. Rozvany. On the adaptive ground structure approach for multi-load truss topology optimization. In *10th World Congresses of Structural and Multidisciplinary Optimization*, 2013.
- B. Lieu Song. Pont du gard, 2014. URL [https://en.wikipedia.org/wiki/Pont\\_du\\_Gard#/media/File:Pont\\_du\\_Gard\\_BLS.jpg](https://en.wikipedia.org/wiki/Pont_du_Gard#/media/File:Pont_du_Gard_BLS.jpg).
- S.H.S. Taheri and S. Jalili. Enhanced biogeography-based optimization: A new method for size and shape optimization of truss structures with natural frequency constraints. *Latin American Journal of Solids and Structures*, 13:1406 – 1430, 2016. ISSN 1679-7825.
- G.G. Tejani, V.J. Savsani, V.K. Patel, and S. Mirjalili. Truss optimization with natural frequency bounds using improved symbiotic organisms search. *Knowledge-Based Systems*, 143:162–178, 2018. ISSN 0950-7051.
- C-J. Thore. fminsdp - a code for solving optimization problems with matrix inequality constraints. <https://www.mathworks.com/matlabcentral/fileexchange/43643-fminsdp>, 02 2018.
- M. Tomlin and J. Meyer. Topology optimization of an additive layer manufactured (ALM) aerospace part. In *The 7th Altair The 7th Altair CAE technology conference*, 2011.
- M. Tyburec and J. Zeman. Comparison of semidefinite solvers for topology optimization of cantilever trusses subject to fundamental eigenvalue constraint. *Advanced Materials Research*, 1144:172–177, 03 2017.
- R.J. Vanderbei. *Linear Programming: Foundations and Extensions*. International Series in Operations Research & Management Science. Springer, 2001.
- S. Weber, J. Montero, M. Bleckmann, and K. Paetzold. Support-free metal additive manufacturing: A structured review on the state of the art in academia and industry. *Proceedings of the Design Society*, 1:2811–2820, 2021. doi: 10.1017/pds.2021.542.
- A. G. Weldeyesus, J. Gondzio, L. He, M. Gilbert, P. Shepherd, and A. Tyas. Truss geometry and topology optimization with global stability constraints. *Structural and Multidisciplinary Optimization*, pages 1721–1737, October 2020. ISSN 1615-147X.
- A.G. Weldeyesus. and J. Gondzio. A specialized primal-dual interior point method for the plastic truss layout optimization. *Computational Optimization and Applications*, 71(3):613–640, 2018.

- A.G. Weldeyesus, J. Gondzio, L. He, M. Gilbert, P. Shepherd, and A. Tyas. Adaptive solution of truss layout optimization problems with global stability constraints. *Structural and Multidisciplinary Optimization*, 60(5):2093–2111, 2019.
- R.B. Wilson. *A Simplicial Algorithm for Concave Programming*. PhD thesis, Harvard University, 1963.
- H. Wolkowicz, R. Saigal, and L. Vandenberghe. *Handbook of semidefinite programming. Theory, algorithms, and applications*. Kluwer Academic Publishers, 2000.
- C-Y. Wu and K-Y. Tseng. Topology optimization of structures using modified binary differential evolution. *Structural and Multidisciplinary Optimization*, 42(6):939–953, 2010. ISSN 1615-1488.
- Y.M. Xie and G.P. Steven. A simple evolutionary procedure for structural optimization. *Computers & Structures*, 49(5):885 – 896, 1993. ISSN 0045-7949.
- J. Ye, P. Shepherd, L. He, M. Gilbert, B. Davison, A. Tyas, J. Gondzio, A.G. Weldeyesus, and H. Fairclough. Computational layout design optimization of frame structures. In *Proceedings of the IASS Annual Symposium 2017*. International Association for Shell and Spatial Structures (IASS), 2017.
- P. Zakian. Design optimization of moment space frame structures based on natural frequency constraints using the adaptive charged system search algorithm. *International Journal of Optimization in Civil Engineering*, 11(4):581–597, 2021.
- M. Zhou and G.I.N. Rozvany. The {COC} algorithm, part ii: Topological, geometrical and generalized shape optimization. *Computer Methods in Applied Mechanics and Engineering*, 89(1):309 – 336, 1991. ISSN 0045-7825.
- Ji-Hong Zhu, Wei-Hong Zhang, and Liang Xia. Topology optimization in aircraft and aerospace structures design. *Archives of Computational Methods in Engineering*, 23(4):595–622, 2016.